Editorial

Foreword to the special volume on 'Field, analytical and experimental approaches to silicic magmatism in collisional orogens'

Despite more than two hundred years of vigorous scientific interest, granite plutons are still in fashion and their origin continues to be hotly debated. This special issue of the *Journal of Geosciences* is intended to be a modest contribution to the recent granite debate by collecting process-oriented research papers on a wide range of related topics. These include the significance of granitoid intrusions for reconstructing plate tectonics, pluton emplacement, and interpretation of magma sources and granite petrogenesis. Despite the fact that the papers published in this special issue mostly focus on Variscan plutons in Europe (Spain, France, Slovakia, Czech Republic) and also from other areas (Mongolia), they may hopefully provide case examples with a broad outreach.

The issue is introduced by *Bonin* who reviews the state of the art of A-type silicic magmatism in the Variscan and Alpine Europe. This paper defines varieties of A-type granites, their plutonic and volcanic associations as well as their salient petrographic, geochemical and isotopic features. Two major problems of current research on A-type igneous suites are discussed in detail: 1) uranium-thorium mobility, phase transformations of zircon and its utility for geochronological studies, and 2) preservation of A-type chemical signature during regional metamorphism. An exhaustive review of European occurrences provides background for temporal cyclicity of the A-type events. One group marks post-orogenic settings whereas the other is associated with continental break-up, rifting and formation of new oceanic basins. The European occurrences cluster at Cambrian–Ordovician and Carboniferous–Triassic boundaries, each of the events spanning approx. 60 Ma and both separated by a gap reflecting existence of the Paleotethys Ocean.

The paper by *Dietl and Koyi* addresses the formation of tabular plutons using analogue modelling. These authors set up a stratified model consisting of multiple plasticine layers and demonstrate how buoyant material develops into tabular sills, the space for which is made by floor downdrop. As the most important outcome of this study, the authors demostrate that during growth of tabular plutons, the feeder channels may become blocked as a result of subsidence of the pluton floors.

The geochemical study by *Villaseca and co-authors* is devoted to peraluminous granites of the Montes de Toledo Batholith of the Central Iberian belt. This batholith comprises a sequence of chemically distinct intrusive units, which differ in degree of peraluminosity, and calcium and phosphorus abundances. A detailed survey of neodymium and lead isotope systematics has revealed a mixed source with distinct proportions of two end-members: Neoproterozoic metasediments and lower crustal, metaigneous precursors. As an additional peculiarity, these granites contain a variety of magmatic aluminosilicate phases including coexisting andalusite and sillimanite. This mineral couple, rarely recorded elsewhere, provides independent constraints on the emplacement conditions and crystallization history of this batholith.

Leichmann and Höck provide a detailed petrographic and geochemical review of the Brno Batholith, which is a composite body located in the Brunovistulian Unit at the eastern margin of the Variscan orogenic belt. The batholith consists of two granitic complexes, which are separated by an ophiolite unit. The Eastern Granitic Complex represents an exposed, primitive magmatic arc related to the Cadomian (Pan-African) convergence. In contrast, the Western Granitic Complex is an assembly of three suites, with S-, I- and A-type affinities, which were produced by melting of lower-crustal metasedimentary lithologies underplated by mafic magmas. The geological and geochronological data point to similarities between the Brunovistulian magmatic activity and that in the Egyptian Eastern Desert and demonstrate their affiliation with the Gondwanan margin in Neoproterozoic.

The Variscan silicic activity exposed in the present-day Carpathians was investigated by *Kohút and Nabelek* using a combination of radiogenic and stable isotope methods. The Western Carpathians offer outcrops of unparalleled geochemical varieties of granitic rocks, which include potassic-magnesian, potassic-ferroan, calc-alkaline, peraluminous, subalkaline as well as alkaline-anorogenic types. Both the strontium and neodymium isotopes rule out a single-source, mantle or crustal model for their origin but require an involvement of several sources, which may have been provided by melting of a vertically zoned crustal sequence. The oxygen isotope data span a broad array as well, and this reflects significant and variable proportions of mafic to silicic igneous precursors.

Chudík and co-authors present a detailed mineralogical study of extremely evolved, highly peraluminous pegmatitic system from Považský Inovec in the Western Slovakia. The unusually high budget of high-field strength elements is stored in abundant accessory phases – columbite–tantalite, tapiolite and zircon, which are associated with garnet-sillimanite-bearing assemblage. The first two accessories do not show significant variations of divalent cations (Mn,

Fe) with distinct compatibility but oscillatory zoning in Ta and Nb, which partly overlaps with the tantalite–tapiolite miscibility gap defined by previous investigations. This pegmatitic system provides another example of Zr/Hf and Nb/Ta decoupling in magmatic reservoirs, being probably related to local extreme fractionation.

The paper by *Economos and others* combines field observations, structural data, and geochemistry from the Chandman Granite Massif, Mongolia, to resolve its geologic history and to outline implications for tectonic evolution in the nearby metamorphic terranes. The authors show that this intrusion cannot be related to Caledonian events as thought previously, but instead may reflect a subduction-related volcanic-arc magmatism of Early Carboniferous age, first reported in the western Gobi-Altay Terrane.

This issue shall provide a cross-section through various magmatic products of Variscan orogeny in time and space. We hope that the breadth and multitude of approaches presented in the following papers will stimulate new studies and applications of state-of-the-art analytical techniques to enhance our understanding of geodynamics in continental collisional zones.

We express our gratitude to all the authors who have contributed such a variety of thought-provoking articles to this Special Issue. Last but not least, we would like to acknowledge the reviewers of the above papers who volunteered their time and effort to improve the quality of this special issue.

Guest editors:
David Dolejš
Institute of Petrology and Structural Geology,
Charles University, Prague

Jiří Žák
Institute of Geology and Paleontology,
Charles University, Prague

Journal of Geosciences, 53 (2008), 237–252 DOI: 10.3190/jgeosci.036

Original paper

Death of super-continents and birth of oceans heralded by discrete A-type granite igneous events: the case of the Variscan–Alpine Europe

Bernard BONIN

UMR 8148 'IDES, Département des Sciences de la Terre, Bâtiment 504, Université de Paris-Sud, F-91405 ORSAY CEDEX, France; bernard.bonin@u-psud.fr

Granitoids occupy large areas of the Variscan–Alpine Europe. The specific group of A-type granites identifies post-collisional (post-orogenic) and anorogenic geodynamic settings. Post-orogenic igneous provinces are emplaced during the very last episodes of supercontinent amalgamation. Anorogenic igneous provinces accompany continental break-up and predate the development of new oceanic basins. Though not voluminous compared with the other granite types, A-type granites substantiate critical periods of the life of supercontinents.

Their ages of emplacement in the Variscan–Alpine Europe span the entire Cambrian–Triassic time interval. They are not random, however, and correspond to discrete episodes. Two major age groupings, both with a *c.* 60 My duration, are distinguished. The Early Cambrian–Early Ordovician period corresponds to Pannotia amalgamation, followed by its break-up and the development of the Rheic–Proto-Tethys Ocean. The Late Carboniferous–Early Triassic period corresponds to Rheic closure and Pangaea amalgamation, followed by its break-up and the development of the Neo-Tethys Ocean. Devonian–Early Carboniferous A-type igneous episodes, scarce in Europe but widespread in Central Asia, accompanied the development of the Palaeo-Tethys Ocean.

Keywords: A-type granite, geodynamic settings, Palaeozoic, Cadomian, Variscan, Triassic, Europe
Received: 14 November 2008; accepted 10 January 2009; handling editor: D. Dolejš

1. Introduction

Granitoids are extensively studied for the following reasons: (i) they are the most abundant rocks in the Earth's upper continental crust, (ii) like other igneous rocks, they represent probes into the deep planetary interiors, and (iii) they are closely connected with tectonics as well as geodynamics. Even now, the proportion of granitoids and associated volcanic rocks present on Earth is low, about 0.1 % of the Bulk Earth (Clarke 1996). Such a small proportion corresponds nevertheless to a total mass of at least 10^{22} kg and a volume of about 3.74×10^9 km^3 (Bonin et al. 2002). Roughly 86 vol. % of the upper continental crust is granitic in composition (Wedepohl 1991). Granite occurs also, albeit in smaller amounts, within lower continental crust, oceanic crust, upper mantle and meteorites (Bonin et al. 2002; Bonin and Bébien 2005, and references therein).

In this Special Issue devoted to 'Field, analytical and experimental approaches to silicic magmatism in collisional orogens', the aim of this paper is to provide an overview of the occurrences and geodynamic settings of Cambrian to Triassic A-type granites within the Variscan–Alpine Europe, i.e. the peri-Gondwanan terranes that collided with Baltica during the Palaeozoic era, before being collided by the rest of Gondwana during the Permian.

A-type granites were first named by Loiselle and Wones (1979). Further refinements (for a review, see Bonin 2007) led to a proposal of clear criteria that are commonly used to distinguish A-type granites from the other granite types worldwide (Tab. 1). They were ascribed for a long time (e.g., Billings 1945; Black et al. 1985) to the specific geodynamic settings, namely post-collisional to within-plate, which gives them the popular name of 'anorogenic'. Examples of tectonic settings of A-type igneous provinces occurring in Europe are listed in Tab. 2.

Three issues will be addressed. The first concerns the so-called "crustal signatures" yielded by radiogenic isotopes in otherwise mantle-derived rocks. The second is the problem of identifying undoubtedly A-type granites emplaced within polygenetic orogenic belts, after they suffered deformation and alteration and were converted into orthogneisses. The last one consists of a critical overview of A-type igneous provinces emplaced during the build-up of the Variscan–Alpine Europe.

2. What is A-type granite?

A-type granites constitute a well-defined type of silicic igneous rocks. The concept and usage of the term "A-type" follow closely the recommendations of the UNESCO-IGCP Project 510 "A-type granites and related

Tab.1 Major features of A-type granite igneous suites (Bonin 2007 and references therein)

A-type granites	Monzogranite – syenogranite – alkali feldspar granite		
Associated rock types IUGS nomenclature (Le Maitre, 2002)	Anorthosite – gabbro – diorite Monzogabbro – monzodiorite – monzonite Syenite – alkali feldspar syenite – nepheline syenite		
Rock-forming mineralogy	Felsic assemblage	Quartz	Purple to brown to black euhedral β-shaped crystals
		Feldspathoids in associated silica-undersaturated rocks	Anhedral crystals
		Feldspar hypersolvus type	Mesoperthite with two discrete alkali feldspar phases
		Feldspar subsolvus type	Discrete crystals of K-feldspar and plagioclase (An < 15)
		Feldspar transsolvus type	Mesoperthite cores with K-feldspar rims, K-feldspar and albite in discrete crystals
	Mafic assemblage	Liquidus assemblage	Fayalite + pyroxenes + iron oxides
		Late magmatic calcic amphibole trend	Hastingsite – ferro-edenite – ferrohornblende
		Near-solidus to subsolidus sodic-calcic – sodic – iron amphibole trend	Barroisite – winchite – richterite – arfvedsonite – riebeckite – grünerite
		Near-solidus to subsolidus mica associations	Annite – siderophyllite; Zinnwaldite – trilithionite, Montdorite; Celadonitic muscovite; Clay minerals
	Accessory mineralogy	Fe-Ti oxides	Ilmenite – ulvöspinel – magnetite
		Silicates	Zircon – thorite – elpidite – allanite – chevkinite – aenigmatite – topaz ± titanite ± tourmaline ± garnet
		Phosphates (low to very low abundances)	Apatite – monazite – xenotime
		High-tech metal ore minerals	Fergusonite – polycrase – chernovite – pyrochlore – genthelvite – ...
		Ore minerals	Cassiterite – molybdenite – wolframite – sphalerite – galena – pyrite ± pyrrhotite – chalcopyrite – mimetite – ...
		Other minerals	Fluorite – REE fluorides ± carbonates
Bulk-rock geochemistry	$FeO/(FeO + MgO) > 0.446 + 0.0046 \times$ wt. % SiO_2 $FeO^T/(FeO^T + MgO) > 0.486 + 0.0046 \times$ wt. % SiO_2		Ferroan A-type group
	For low Ga/Al and $(Zr + Nb + Ce + Y)$: $FeO^T/MgO > 16$		A-type granites
	$4 < FeO^T/MgO < 16$		Fractionated felsic granites
	$FeO^T/MgO < 4$		Unfractionated granites
	ASI = A/CNK = molar $Al_2O_3/(CaO + Na_2O + K_2O) = Al/(2\ Ca + Na + K) > 1$		Peraluminous
	ASI < 1	$NK/A = (Na + K)/Al < 1$	Metaluminous
		$NK/A > 1$	Peralkaline
	For any ASI values	$NK/A > 0.85$ $NK/A > 0.88$	Alkaline or A-type suites
	Trace-element discrimination	$Y + Nb > 50–55$ ppm $Yb + Ta > 6$ ppm	Within-Plate Granite (WPG) and Oceanic Ridge Granite (ORG)
		$10000 \times Ga/Al > 2.6$ $Zr + Nb + Ce + Y > 350$ ppm	A-type granite
		$Y/Nb < 1.2$	A1 subtype, intra-plate rifting
		$Y/Nb > 1.2$	A2 subtype, post-collisional
	REE contents and patterns	High contents in metaluminous and peralkaline types Low contents in evolved topaz-bearing peraluminous types	Gull-wing shape
		Non-mineralized types	Slightly fractionated $(La/Yb)_N < 30$ Varying Eu negative anomalies
		Mineralized types: pronounced tetrad effects	Unfractionated $(La/Yb)_N$ down to 0.3, negative Eu anomalies with Eu/Eu* down to 0.01
	Stable and radiogenic isotopes	A-type suites yield no specific values in Sr-Nd-Hf-Pb-O isotopic systems. Depleted mantle to crustal signatures are not obviously correlated with ages of emplacement and tectonic settings, thus suggesting either a mixture of various sources, complex differentiation processes, or both.	

rocks through time" discussed in its first meeting in 2005 (Bonin 2007). Clear criteria, involving specific petrological–mineralogical features and geochemical compositions (e.g., Pearce et al. 1984; Whalen et al. 1987; Eby 1990) commonly used to identify A-type granites, are listed in Tab. 1. In addition, A-type granites are not emplaced randomly in continental areas, as their tectonic settings involve always some amounts of extension (Tab. 2). Last, in agreement with their original definition (Loiselle and Wones 1979), they are associated with coeval mafic to intermediate rocks within compositionally expanded igneous suites (e.g., Bonin et al. 2008).

2.1. A-type granites and A-type granites?

No radiogenic and stable isotopic criteria (e.g., Sr, Nd, Hf, Pb, O) can define A-type granites unambiguously, thus raising the question whether we are dealing with a too vague concept. Most popular textbooks on igneous petrology usually consider granites as a specific entity genetically unrelated to other igneous, plutonic and volcanic, suites. Because they yield variable isotopic signatures, granites are also frequently regarded as entirely of crustal derivation, with or without hybridization by varying amounts of mantle-derived mafic magmas. This is, in particular, the basic scheme of the S – I – M alphabetical classification. However, A-type granites differ from the other granite types in that, though crustal sources seem to be evidenced in many cases by the isotopic record, no migmatitic terranes on Earth have yielded any leucosomes of A-type compositions, nor had experimental petrology succeeded in producing unambiguous A-type liquids from crustal materials (for a discussion, see Bonin 2007 and references therein). On the contrary, occurrences of A-type granites within oceanic islands and even on the Moon indicate they are likely to form through mineral fractionation, not partial melting, of mafic magmas, even in the absence of significant amounts of H_2O (Bonin et al. 2002).

2.2. The crustal issue

The isotopic "crustal signature" constitutes an important issue to address. Geoscientists involved in upper mantle studies are well aware of enriched compositions that can mimic crustal values. In the lack of evidence for preserved primitive mantle reservoirs, occurrences of various enriched mantle end-members are explained by subduction-induced incorporation of crustal (oceanic and continental) materials into depleted upper mantle of the overriding lithospheric plate.

Consider a depleted mantle of harzburgitic composition and add either continental upper crustal materials, or TTG-like silicic liquids produced from oceanic crust. Abundances of incompatible elements within harzburgite are exceedingly low. Addition of small volumes of products rich in incompatible elements results in harzburgite converted into re-fertilized lherzolite and/or websterite, with an overall signature strongly influenced by crustal materials. Isotopic initial ratios and Nd depleted-mantle model ages yielded by magmas originating from such a [depleted mantle + crust] mixture stand, therefore, closer to the crustal than to the depleted mantle end-member.

There is, therefore, no need for a key role played by continental wall rocks, which A-type magmas pass through, or are emplaced in. As baffling as this idea can appear at a first glance, crustal signatures have little to do with the exposed crust. They have to be searched at deeper levels within the lithospheric keels of continental plates. Evolved low-P specialized granites can be strongly contaminated by exogenous elements carried by reactive Cl- and F-rich hydrothermal fluids. Their high initial $^{87}Sr/^{86}Sr$ ratios and low $\varepsilon_{Nd}(t)$ values, totally unrelated to magma sources, constitute apparent exceptions that should be mentioned (e.g., Zinnwald–Cínovec granite).

2.3. A unified view

In the following pages, A-type granites will not be considered as a discrete entity unrelated to other coeval igneous rocks. The concept of A-type igneous suite involves not only A-type granites, but also mafic and intermediate, volcanic and plutonic, igneous rocks. Such suites include bimodal associations derived from tholeiitic and mildly alkaline basaltic magmas (Frost and Frost 2008). Though following apparently different evolutionary paths, their real unity was recognized for a long time within plu-

Tab. 2 Selected Phanerozoic A-type igneous suites in Europe (adapted from Bonin 2007)

Orogenic stages	Tectonic settings	Examples	Ages
Post-collision	Transcurrent shear zones	Assynt Igneous Province, Scotland Western Mediterranean Province Comendite, San Pietro Island, Italy	440–425 Ma 280–235 Ma 15 Ma
Rifts	Extensional regime	Midland Valley, Scotland Oslo Rift, Norway Pantellerite, Pantelleria Island, Italy	*c.* 345 Ma 280–250 Ma 0.33–0.003 Ma
Passive margins	Extensional regime	Peralkaline gneisses, Galicia, Spain Rheinisches Schiefergebirge, Germany British Tertiary Igneous Province	500–480 Ma 390–380 Ma *c.* 50 Ma

tonic–volcanic provinces, but it is still underestimated in granite studies. Keeping this idea in mind, it is not surprising that A-type granites do not have to be of only crustal derivation.

3. The A-type orthogneiss conundrum

A-type igneous suites are fairly easy to discriminate and have specific ferroan alkali-calcic to alkaline bulk-rock compositions. However, aluminous subsolvus granites do not have to yield specific features of A-type granite. In the case of post-orogenic igneous suites, in which they are abundant, it is not always straightforward to define whether they are A-type, or not. Field criteria are helpful, such as textures including euhedral shape of purple–brown–black quartz crystals and anhedral shape of biotite flakes.

3.1. Interpretation of metamorphic textures and compositions

Evidence for A-type granites highly deformed and involved within orogenic fold belts is generally not easy to decipher, because they lost partly their petrological and geochemical characteristics through mineral breakdown, leaching and/or re-crystallization. A-type orthogneisses usually carry a subsolvus feldspar assemblage, with K-feldspar only slightly to non-perthitic (Floor 1974). Alkali loss and silicification result into bulk rocks having non-igneous compositions, with less than 8 wt. % of $Na_2O + K_2O$ and more than 78 wt. % SiO_2. A-type metagranites, with primary (igneous) peraluminous and metaluminous compositions, can yield metamorphically-induced, strongly peraluminous compositions that apparently resemble evolved S-type rocks. In orthogneisses issued from strongly peralkaline granites, though (Na + K)/Al ratios can remain higher than 1.0, alkali loss is reflected by occurrence of newly formed bipyramidal zircon crystals and metamorphic riebeckite, a sodic amphibole with empty A-site, replacing igneous arfvedsonite, characterised by full occupancy of the A-site (Floor 1974). The HFSE contents can decrease through leaching by hydrothermal F-bearing fluids. In most cases, immobile elements can help, such as, e.g., fairly low (< 14–15 wt. %) Al_2O_3 contents, low MgO/FeO_T ratios and gull-wing shapes of REE patterns, diagnostic of A-type granite compositions.

The Randa orthogneiss (Thélin 1987) offers a pertinent example: this Permian (269 ± 2 Ma, Roadian, Bussy et al. 1996) A-type granite underwent Alpine tectonic episodes under greenschist-facies conditions. The slightly deformed core of the massif yields its original ferroan alkali-calcic composition, with low Fe_2O_3/FeO ratio, 40–50 ppm Y and 15–30 ppm Nb, corresponding to the Within-Plate Granite (WPG) field of Pearce et al. (1984). The still ferroan sheared margins are highly silicic, with up to 81.5 wt. % SiO_2, and calc-alkaline, due to decreasing alkali contents. They yield high Fe_2O_3/FeO ratios, low TiO_2 contents, fairly constant (20–40 ppm) Y contents and low (< 10 ppm) to very low (below detection limit by the XRF method) Nb contents. They plot no longer in the WPG, but in the Volcanic-Arc Granite (VAG) field. Positive Y–Zr correlations indicate that zircon is the main carrier of Y and that this element remains stable during the metamorphic overprint. Positive Nb–TiO_2 and negative Nb–Fe_2O_3 correlations suggest breakdown of Nb-bearing Fe–Ti oxides and Nb mobility through oxidizing fluids.

3.2. The problem of age determination of A-type orthogneiss protoliths

High LILE mobility favours partial to complete resetting of Rb-Sr isotopic systems; even Sm-Nd systems can be disturbed in the presence of F-bearing fluids. The isochron method is, therefore, unable to provide reliable emplacement ages for the igneous protoliths. In the most favourable cases of complete resetting during major metamorphic events, it can provide ages of those events. Like the Rb-Sr isotopic system, the U-Th-Pb isotopic system is also susceptible to variable amounts of resetting through Pb loss during hydrothermally mediated events. Zircon is currently in systematic use for age determination purposes, as well as other U-Th-bearing minerals, such as monazite and titanite. Abundant in non-peralkaline A-type granites, zircon precipitates either as early euhedral prismatic (100) crystals in fluid-deficient conditions, or as late euhedral to anhedral bipyramidal crystals in fluid-rich environments (Pupin et al. 1978). Early prismatic crystals are limpid, while late bipyramidal crystals are often metamict. Zircon usually cannot crystallize in Zr-rich peralkaline A-type granites, because of its high solubility in the magma, and is replaced by elpidite, a hydrous alkali zirconosilicate (Tab. 1).

Though stable under a wide range of conditions, zircon can re-crystallize during a metamorphic event forming new crystals and/or rims around igneous cores. In meta-igneous peralkaline rocks, secondary bipyramidal crystals result from alkali loss. Associated xenotime is frequent (Pan 1997). There is a range of textures between two zircon end-members. One end-member is a pristine generation of igneous crystals and/or cores, characterized by well-developed growth zoning evidenced by cathodoluminescence imaging, and the other end-member is a package of newly formed porous to skeletal metamorphic crystals and/or rims intergrown with secondary mineral inclusions, reflecting dissolution–re-precipitation processes (Tomaschek et al. 2003; Bendaoud et al. 2008).

Thus, the crystal rims are likely to yield U-Pb ages differing from the crystal cores.

The ID-TIMS technique using populations of zircon crystals is unable to provide concordant isotopic dates in the case of rocks that have undergone multiple episodes of crystallization. Zircon crystals in A-type granites are generally devoid of inherited cores. Single crystals subjected to a removal of re-crystallized and/or metamict rims by the air abrasion technique can give concordant dates that are likely to indicate the emplacement age of the protolith. If re-crystallized metamorphic rims remain, results plot along a discordia line. In the most favourable cases, the upper intercept with the concordia curve yields the age of the protolith and the lower intercept the age of the metamorphic overprint. In the more difficult cases of aluminous A-type granites containing inherited cores, multiple discordia chords can be computed and should be interpreted. The seemingly promising evaporation technique precludes direct investigations on the parts of the crystal that are removed during incremental heating steps and the results are less precise than those obtained by the ID-TIMS technique.

With modern techniques using *in situ* isotopic measurements, these difficulties could be addressed. As igneous zircon incorporates U and Th, according to zircon/liquid distribution coefficients for the two elements, Th/U ratios measured in the crystals are higher than 0.2 and frequently higher than 0.5. In the case of re-crystallization in the presence of coexisting solid phases, such as xenotime, Th/U ratios in metamorphic zircon decrease considerably, down to less than 0.05 (Williams and Claesson 1987). In zoned crystals, igneous crystals and cores, with Th/U ratios higher than 0.2, can be distinguished from low Th/U metamorphic crystals and rims, though igneous-like Th/U ratios can be preserved in some metamorphic crystals (Tomaschek et al. 2003).

3.3. Ordovician events within parts of the Iberian Peninsula

The Early to Middle Ordovician igneous episodes in the Palaeozoic orogenic belt of Western Iberia afford a pertinent example. The Ossa-Morena Zone is bordered to the north by the autochthonous units of Central Iberia and Galicia–Trás-os-Montes and the Malpica–Tuy allochthon. The terrane assemblage, deformed and amalgamated during the Variscan orogenic event, corresponds to a volcanic passive margin developed since the Ediacaran–Early Cambrian transition (Simancas et al. 2004; Etxebarria et al. 2006). A-type orthogneisses are exposed within all units and their zircon crystals have been analysed for U-Pb dating (e.g., Lancelot et al. 1985; Santo Zalduegui et al. 1995; Valverde-Vaquero et al. 2005; Bea et al. 2006; Cordani et al. 2006; Montero et al. 2008).

Ion microprobe and LA-ICPMS techniques allowed to obtain trace-element and isotopic data on zircon crystals of orthogneisses from Portalegre and Alcóçavas, Ossa-Morena Zone (Cordani et al. 2006), Galiñeiro, Galicia (Montero et al. 2008), and Miranda do Douro, Central Iberian Zone (Bea et al. 2006). The evolution of Th/U ratios with time (Fig. 1) constitutes a good marker of the origin of zircon crystals. The 370–340 Ma (Variscan) crystals and rims yield consistently low Th contents and Th/U ratios, from 0.12 to 0.03, substantiating metamorphic crystallization.

In the Portalegre orthogneiss, a single population of crystals yields a concordant age of 497 ± 10 Ma, with no obvious inherited cores (Fig. 1). Igneous crystals yield 109 to 363 ppm U and igneous Th/U ratios from 0.15 to 1.43, suggesting that they crystallized at various stages from liquidus to solidus. One non-igneous U-rich (682 ppm), low-Th/U (0.09), yet concordant crystal is likely to have precipitated in subsolidus conditions from late-stage fluids.

In the Alcóçavas orthogneiss, two populations of crystals yield concordant ages of 539 ± 20 Ma and 464 ± 14 Ma, with one 2.5 Ga inherited core and one 620 Ma highly discordant crystal. The Th/U ratios are higher than 0.22 in the 464 Ma crystals and 0.18 in the 539 Ma crystals, implying that both populations grew from magmas (Fig. 1). Rounded shapes displayed by some crystals suggest that all 539 Ma crystals are inherited from Early Cambrian igneous formations. The emplacement age of the protolith to the Alcóçavas orthogneiss is, therefore, Middle Ordovician.

In the Galiñeiro peralkaline orthogneiss, abundant zircon crystals are brown, turbid, totally or partially metamict, thus apparently not suitable for U-Pb dating. However, SIMS analyses yield a mean common Pb-corrected age of 482 ± 2 Ma, considered as the age of emplacement. U and Th contents, 265–5827 ppm and 30–641 ppm, respectively, and Th/U ratios ranging from 0.64–0.17 (igneous, 50 % spots) to 0.14–0.01 (secondary) show that zircon crystallized under magmatic to subsolidus conditions and that late-stage fluids were coeval to the emplacement of the peralkaline protolith (Fig. 1).

Like other metavolcanic and metagranitic rocks of the Ollo de Sapo Formation of the Central Iberian Zone (Parga-Pondal et al. 1964; Montero et al. 2007), the magnesian calc-alkaline Miranda do Douro orthogneiss does not display A-type characteristics. Its age of emplacement is currently a matter of controversy. Based on upper intercept in U-Pb concordia diagram, a 618 ± 9 Ma age was reported by Lancelot et al. (1985), while Bea et al. (2006) claimed that the dominant population of 483 ± 3 Ma crystals reveals the true age of a granitoid produced by melting of Panafrican source. Using the U-Th data of Bea et al. (2006), it appears that the 483 ± 3 Ma concor-

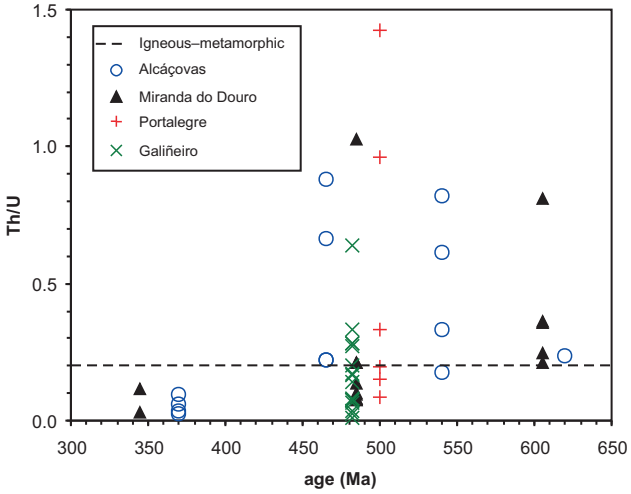

Fig. 1. Th/U ratios vs. radiometric ages in Iberian orthogneisses. Dashed line: boundary line separating disturbed metamorphic compositions (Th/U < 0.2) from undisturbed igneous compositions (Th/U > 0.2). Zircon crystals of Portalegre and Galiñeiro orthogneisses, though yielding varying Th/U ratios, give the same ages, implying that ages of emplacement and of hydrothermal disturbance are identical within analytical uncertainties. Zircon crystals of Alcóçavas and Miranda do Douro orthogneisses yield igneous compositions and ages of emplacement that differ largely from disturbed compositions and ages of metamorphic overprint. In addition, the distribution of igneous ages in the Alcóçavas orthogneiss reveals an occurrence of older inherited cores.

dant crystals yield non-igneous Th/U ratios lower than 0.21 (down to 0.07), with only one crystal having high U and Th contents (808 ppm and 828 ppm, respectively) and Th/U ratio as high as 1.02. On the contrary, the 605 ± 13 Ma concordant crystals yield igneous Th/U ratios consistently higher than 0.21 (Fig. 1). It is suggested here that the Miranda do Douro orthogneiss was derived from an Ediacaran protolith, which underwent hydrothermal alteration by fluids issued from Early Ordovician A-type dykes and sills that are known throughout the Ollo de Sapo domain and are related to the Galiñeiro igneous episode (Floor 1974; Lancelot et al. 1985).

3.4. Relevance of A-type orthogneisses in geodynamic reconstructions

A-type igneous suites can be recognized fairly well, if, after their emplacement and cooling, they were not subsequently deformed and metamorphosed. The A-type orthogneiss issue is critical for two reasons: (i) the original bulk-rock and mineral compositions can be obscured by hydrothermal alteration promoted by fluids percolating within the shear zones, (ii) the exact age of igneous emplacement can be erased within the isotopic clocks.

The geological record can provide some help. Within-plate settings can be recognized from sedimentary formations evidencing rifting or passive margin regimes during their deposition. Associated orthogneisses are ascribed to A-type igneous episodes, even if their compositions do not fulfil the required criteria. Accurate radiometric age determinations are necessary, as both inheritance and isotopic resetting may result in dates that are difficult to interpret correctly.

Granitoids and orthogneisses occupy large areas of the basement of the Variscan–Alpine Europe. Careful examination of chemical and isotopic data on undeformed granitoids as well as on orthogneisses provides an evidence of discrete A-type igneous events. Though pieces of older A-type igneous provinces can be preserved, major igneous events took place frequently since the Neoproterozoic and are still going on in the Mediterranean area (Tab. 1).

4. Periodic A-type granite events within the Variscan–Alpine Europe: an overview

Though not voluminous compared with the other granite types, A-type granites substantiate post-collisional (post-orogenic) and anorogenic geodynamic settings. Their emplacement ages span a large time interval, from Neoproterozoic (*c.* 600 Ma) to Triassic (*c.* 230 Ma). The intrusive ages are not randomly distributed, however, and correspond to discrete critical episodes. This will be illustrated by a roughly N–S geotraverse. The occurrences described hereafter are listed in Tab. 3.

4.1. The Central Europe geotraverse

The Variscan–Alpine Europe is essentially made up of slices of continental and oceanic terranes that were squeezed between the big old continents of Laurentia, Baltica and Gondwana during the Palaeozoic. The terminology used hereafter is extracted from Stampfli and Borel (2004)[1]. The geotraverse considered here comprises the southern margin of Laurentia, the Eastern Avalonia Superterrane and the Hunic Superterrane, which includes the Armorican Terrane Assemblage (ATA). Names of stages, epochs and periods follow hereafter the very last definitions of the IUGS International Commission of Stratigraphy (Ogg et al. 2008).

[1] Constantly updated versions of paleogeographic maps are available at:
http://www.unil.ch/igp/page22636.html
Other useful world-scale maps can be consulted at:
http://www.scotese.com/earth.htm and *http://jan.ucc.nau.edu/rcb7/RCB.html*

4.2. The Laurentian margin

The southern margin of Laurentia in Scotland is composed of a Lewisian foreland, or Hebridean Terrane, bordered by a collage of narrow (*c.* 50 km wide) terranes (Oliver et al. 2008 and references therein). The Northern Highland and Grampian terranes, delimited by the Moine Thrust, the Great Glen Fault and the Highland Boundary Fault, yield Proterozoic basements. The Midland Valley and Southern Upland terranes, bordered by the Highland Boundary Fault, the Southern Upland Fault and the Iapetus Suture, represent Early Palaeozoic island arcs and accretionary prisms including remnants of oceanic crust (Ballantrae ophiolite). Ediacaran, Ordovician and Silurian A-type granites occur within the northern continental terranes (Oliver et al. 2008). Early Carboniferous A-type basalt–rhyolite–trachyte igneous suites are mostly exposed within the southern island arc terranes.

The Ediacaran massifs (Older Granites, according to the terminology of Barrow 1893) yield U-Pb zircon ages ranging from 601 ± 4 Ma to 588 ± 8 Ma, substantiating a fairly short-lived event. Metagranite augen gneisses include riebeckite-bearing peralkaline types and constitute, with coeval 601 ± 4 Ma metabasalt–keratophyre formations, a bimodal igneous suite. Isotopic ratios (summary in Steinhoefel et al. 2008) are variable, with $\varepsilon_{Nd}(t)$ ranging from -6.3 to -4.3 in A-type metagranite and to +4 in metavolcanic rocks, precluding a single homogeneous source, $\delta^{18}O$ of 8–9 ‰ and high initial $^{87}Sr/^{86}Sr$ (> 0.710), due to Rb-Sr disturbance during metamorphism and deformation. The 601–588 Ma old bimodal rift-related igneous suite was classically assigned to Rodinia break-up (Soper 1994). This interpretation is at odds with the recent synthesis issued from IGCP 440 (Li et al. 2008), in which the Rodinia supercontinent was subjected to discrete rifting events, prior to the onset of continental disruption at 740 Ma. From the 600 Ma period of time onwards, Rodinia was already broken-up, whereas Scottish Laurentia was bordered by a passive margin created by Iapetus Ocean drifting (see Fig. 9j in Li et al. 2008).

The Ediacaran A-type massifs were metamorphosed and deformed during two discrete episodes forming the Caledonian orogeny, namely the *c.* 470 Ma Grampian and the *c.* 430 Ma Scandian events (Oliver 2001). The Grampian event is related to 'hard' collision (Oliver et al. 2008) of Laurentia with the southern island arc terranes and its age is bracketed between the Floian (Mid Arenig), based on 473 ± 2 Ma emplacement age of a S-type Newer Granite, and the Darriwilian (Late Arenig), based on 466 ± 3 Ma cooling ages. No A-type granites are known from that period of time.

Between the Grampian and Scandian events, after a 12 My pause, S-type granites were emplaced between 457 ± 1 Ma and 451 ± 4 Ma in the Grampian Terrane, under extensional regime inducing crustal thinning and erosion rate of about 1.4 $mm.a^{-1}$. In the Northern Highland Terrane, only one alkaline igneous event is displayed by the 456 ± 5 Ma (Sandbian-Katian boundary) Glen Dessary syenite (van Breemen et al. 1979). Isotopic characteristics ($\varepsilon_{Nd}(t)$ varying from +1 to +4, $^{87}Sr/^{86}Sr_i$ = 0.7041 ± 0.0001, $\delta^{18}O$ of 5.5–7.5 ‰), fractionated concave-upward REE patterns and Nb–Ti troughs require an amphibole-bearing upper mantle source of probable lithospheric origin (Halliday et al. 1987).

After a 20 My gap, the Scandian event corresponds to flat thrusting of the Northern Highland Terrane onto the Hebridean Terrane to the north and 'soft' collision of the extended Laurentian margin, comprising the Grampian to Southern Upland terranes, with Avalonia to the south (Oliver et al. 2008). It is marked by the emplacement of numerous and voluminous Newer Granite massifs from the Middle Silurian to the Middle Devonian. A-type igneous suites were emplaced coevally with the Newer Granites in the continental terranes.

Within the Northern Highland Terrane, syenite complexes aligned along the Moine Thrust Zone yield emplacement ages from 439 ± 4 Ma (Loch Ailsh) to 426 ± 9 Ma (Loch Loyal), indicating a Llandovery–Wenlock short-lived magmatic episode (Halliday et al. 1987). Their ages constrain the timing of the ductile to brittle transition along the Moine Thrust Zone. Independently acquired phengite-feldspar Rb-Sr data indicate a long-lasting episode of brittle deformation from 437 ± 5 Ma to 408 ± 6 Ma, covering the Silurian and the Early Devonian (Freeman et al. 1998). Syenites are either slightly older than, or roughly coeval with, the famous high-Ba-Sr ("HiBaSr") alkali-calcic granites. The igneous suite comprises mafic rocks, silica-saturated to undersaturated syenites and felsic peralkaline (grorudite) dykes. Isotopic data, i.e. $\varepsilon_{Nd}(t)$ varying from 0 to -8, $^{87}Sr/^{86}Sr_i$ of 0.7045–0.7065 and $\delta^{18}O$ of 8.1–10.0 ‰, plot along the Caledonian Parental Magma Array (CPMA) defined by two, depleted and enriched, mantle end-members (Fowler et al. 2008 and references therein).

Within the Grampian Terrane, scarce A-type granite massifs and dykes include biotite ± amphibole-bearing subsolvus and hypersolvus types. Published ages (Oliver et al. 2008) ranging from 408 ± 5 Ma to 406 ± 5 Ma indicate a short-lived Early Devonian episode. They are younger than the 415 ± 3 Ma (Lochkovian) ultimate stage displayed by the Etive dyke swarm within the famous Glen Coe Complex (Morris et al. 2005). Geochemical features (Steinhoefel et al. 2008) include high LILE and HFSE contents, low Ba, Sr and Eu contents, poorly fractionated REE patterns, with unfractionated patterns showing the tetrad effect. The $\varepsilon_{Nd}(t)$ vary from -2.1 to -6.9, in the same range as the Caledonian array defined in the Northern Highland Terrane.

No Ordovician–Silurian A-type igneous suites are exposed in the southern Midland Valley and Southern Upland island arc terranes that are located close to the Iapetus Suture. By contrast, they occur as large lava sheets erupted during the Early Carboniferous and filling the Midland Valley (Francis 1983). The greatest volume, up to 6000 km^3, was produced during the Tournaisian–Visean in the form of lava flows, of which *c.* 85 % were mildly silica-undersaturated basalts. The other formations consist of silica-undersaturated and saturated trachytic and rhyolitic differentiates, which were mostly erupted at *c.* 345 Ma (Tournaisian–Visean boundary). After the Visean, only basalts and basanites were emitted with no felsic differentiates.

4.3. Eastern Avalonia

Avalonian terranes constitute a long ribbon extending from eastern North America to southeastern Europe. They are commonly subdivided into Western Avalonia, located now in the North American continent, and Eastern Avalonia, covering in Europe a large area from Ireland–England to north-central Europe to Eastern Carpathians–Moesia. The Proterozoic continental basement crops out in Poland and Czech Republic, whereas the Early to Middle Palaeozoic sedimentary cover is developed in Belgium and Germany.

The Proterozoic continental basement is exposed in Poland and Czech Republic or known from boreholes (Jelínek and Dudek 1993). Despite a great complexity due to numerous boundary faults, terranes of Avalonian affinities, i.e. made up of Neoproterozoic high-grade metamorphic rocks unconformably overlain by a Devonian–Carboniferous envelope, can be recognized (Oliver et al. 1993). Among them, the Brunovistulian Terrane, including its Moravo–Silesian metamorphic counterparts (Kalvoda et al. 2008 and references therein) occupies the eastern Bohemian Massif and the Eastern Sudetes. The timing of collage of these terranes onto Baltica is still debated (for contrasting views, see Mazur et al. 2006; Nawrocki and Poprawa 2006). Orthogneisses interleaved with paragneisses and amphibolites yield Ediacaran to Cambrian ages (Oliver et al. 1993). Non-A-type Strzelin–Nowolesie orthogneisses, SW Poland, have zircon crystals with older inherited cores, igneous rims at 600 ± 7 Ma and metamorphic overgrowths at 568 ± 7 Ma (Oberc-Dziedzic et al. 2003). The latter age is reminiscent of the 567 ± 5 Ma igneous age of A-type metagranite exposed as small massifs within the *c.* 600–580 Ma Thaya Batholith, Austria (Friedl et al. 2004). These Ediacaran ages correspond to post-orogenic processes occurring after the Cadomian orogeny. A-type Gosciecice and Stachów–Henryków orthogneisses, SW Poland, yield, respectively, igneous ages of 504 ± 1 Ma and 500 ± 5 Ma (Drumian–Guzhangian) (Oberc-Dziedzic et al. 2005), coeval to the beginning of Rheic Ocean drifting. A-type metagranites, carrying both hypersolvus (Rudná-type) and subsolvus (Polanka-type) alkali feldspar assemblages, occur as yet undated small masses within the Desná Unit, Czech Republic. A Carboniferous age was assumed on the basis of too low $^{87}Sr/^{86}Sr$ ratios corrected to Ediacaran times (Hanžl et al. 2007), but this is questionable for low-grade cataclastic rocks (see above). In any case, high Nd isotopic ratios indicate juvenile magmas.

Early Paleozoic rocks are rare, only one basalt vein was dated by K-Ar at 438 ±16 Ma (Llandovery), substantiating Silurian igneous activity. Cooling ages of 487–420 Ma recorded by detrital white mica and monazite occurring within Devonian–Carboniferous sedimentary formations document, however, an important igneous and/or thermal activity in the source area during the Ordovician–Silurian period (Kalvoda et al. 2008). The Devonian Moravo–Silesian Basin is filled up with Emsian–Famennian shallow marine sedimentary formations and submarine to subaerial volcanic formations. Two discrete belts are distinguished (Janoušek et al. 2006). The western belt is characterised by abundant metasediments accompanied by submarine basic–intermediate calc-alkaline volcanites, with subordinate felsic types, suggesting a volcanic-arc setting above a subduction zone. The eastern belt displays abundant, partly subaerial, alkali basalt–A-type rhyolite volcanic suite, with a high proportion of Frasnian felsic products and dykes (rhyolite–comendite–pantellerite) crosscutting the Proterozoic basement. Late tholeiitic dolerite dykes and sills complete the igneous association. The within-plate settings indicate a continental passive margin subjected to extensional regime, perhaps under the influence of a nearby subduction zone (Patočka and Valenta 1996). As the Devonian basins within the Brunovistulian Terrane seem to have rotated *c.* 90° clockwise at the Devonian–Carboniferous boundary, the original orientation of the volcanic belts and the sedimentary basins should have been E–W, but their exact configuration remains unclear.

In Germany, Eastern Avalonia consists of inliers covered by the Mesozoic–Cenozoic sedimentary cover. It comprises the Rheno-Hercynian Zone (Kossmat 1927) and exotic terranes, including the Harz Mountains. From contradictory statements in etymological dictionaries, it appears that the classical term "Hercynian" could either come from, or be the origin for, the name of Harz, which formed a part of the larger Hercynian Forest described in the Antiquity. The Rheno-Hercynian Zone in Belgium and Germany is characterized by plateaux dissected by river valleys, among which the "Rheinisches Schiefergebirge" exposes autochthonous folded–faulted Palaeozoic sedimentary series, overthrusted by Giessen–Harz Nappe and other allochthonous slices. Autochthonous units rep-

resent the sedimentary cover of the former southern passive margin of Avalonia facing the Rheic Ocean, whereas allochthonous units are composed of dismembered oceanic flysch basins formed during the progressive Rheic oceanic closure (Huckriede et al. 2004).

No basement formations older than Devonian are exposed within the "Rheinisches Schiefergebirge". The autochthonous sedimentary series comprises Devonian deltaic, shallow and deep marine sequences, with local development of reefs, and Lower Carboniferous turbidites. Within-plate igneous activity is documented by Devonian (Flick et al. 2008) and Carboniferous (Salamon et al. 2008) volcanic events. The first Givetian–Frasnian event consists of 389–384 Ma episodes dated by conodont zones. It involved submarine eruptions of basanite–alkali basalt–trachyandesite pillow lavas and hyaloclastites forming large seamounts. Emerged islands display additional trachyte and A-type rhyolite lava flows, pyroclastites and domes. Subsequent events erupted only submarine mafic products, i.e. Famennian primitive basanites–alkali basalts, Tournaisian–Visean tholeiitic picrites–basalts and, ultimately, Visean primitive alkali basalts crowded with xenoliths of possible upper mantle origin, and no felsic differentiates.

Numerous boreholes through the Mesozoic–Cenozoic Northeast German Basin have reached or even perforated a *c.* 2000 m-thick Late Carboniferous–Early Permian volcanic succession (Benek et al. 1996). Based largely on lithostratigraphic correlations, five episodes, yet undated by radiometric techniques, are documented from the Ghzelian, i.e. slightly before the Carboniferous–Permian boundary, to the Sakmarian–Artinskian boundary. They accompanied extensional settings within the Pangaea super-continent. East Brandenburg yields an enigmatic, presumably Asselian, (trachy-) andesite–(trachy-) dacite magnesian suite that straddles the alkaline–subalkaline boundary in the total alkali–silica diagram (Rickwood 1989 and references therein). Ghzelian–Sakmarian tholeiitic dolerites–basalts, with depleted to enriched MORB-like compositions, are coeval to basalt–trachyandesite–trachyte–A-type rhyolite ferroan alkaline suites and were postdated by Late Sakmarian basanites–trachybasalts. A-type rhyolites, forming up to 70 % of the *c.* 48 000 km^3 volume of the Northeast German Basin volcanics, occur as ignimbrites (Benek et al. 1996) or lava domes (Paulick and Breitkreuz 2005). The U-Pb zircon igneous ages, bracketed between 300 and 297 ± 3 Ma, substantiate a very short-lived episode close to the Carboniferous–Permian boundary, though dated samples do not cover the entire range of volcanic activity in the Northeast German Basin. The mean extrusion rate was estimated at about 0.01 $km^3.a^{-1}$, corresponding to a magma production rate in the order of 0.1 $km^3.a^{-1}$ (Breikreutz and Kennedy 1999). Thermal subsidence in the Northeast German Basin, slow during the Permian, increased abruptly at the Permian–Triassic boundary. The complete absence of post-Permian igneous activity was related to cooling and thickening of the continental lithosphere (Benek et al. 1996).

Allochthonous units display neither Proterozoic nor Early Paleozoic basements. They are essentially made up of metamorphosed Devonian–Carboniferous sedimentary units, with very few occurrences of metabasalts. Detrital zircon grains yield dominant Precambrian and rare Silurian–Early Devonian igneous, not metamorphic ages, implying that the sedimentation never took place before 410 ± 10 Ma (Geisler et al. 2005). Pelagic sediments are associated with turbidites, like the non-metamorphosed successions observed in autochthonous units. The Giessen–Harz Nappe contains N-MORB tectonic slices overlain by extremely condensed Devonian radiolarian cherts and pelagic shales, implying an oceanic provenance (Huckriede et al. 2004). A-type granite complexes and the coeval Harzburg layered igneous body, which the term "harzburgite" comes from, are exposed in the Harz Mountains, or were drilled near Flechtingen (Baumann et al. 1991, Förster and Tischendorf 1996). In the Flechtingen inlier, a bimodal trachyandesite–rhyolite igneous suite was emplaced as sills and ignimbritic sheets (Breitkreuz and Kennedy 1999). The U-Pb zircon igneous ages of 302 ± 3 Ma (ignimbrite), 295 ± 1 Ma (Oker granite), 294 ± 1 Ma (Harzburg gabbronorite) and 293 ± 3 Ma (Brocken granite) with K-Ar biotite cooling ages of 298 ± 5 Ma (Flechtingen granite) and 296 ± 10 Ma (Ramberg granite) document again a short-lived episode close to the Carboniferous–Permian boundary, in agreement with the U-Pb zircon 296 ± 1 Ma and titanite 295 ± 1 Ma cooling ages recorded in hornfels aureoles. Major- and trace-element compositions indicate A-type post-orogenic settings (for a review, see Förster and Tischendorf 1996).

4.4. The Armorican Terrane Assemblage

The Armorican Terrane Assemblage (ATA) is a part of the Hunic Superterrane (Stampfli et al. 2004). It occupies a nearly 1000 km-wide area throughout central and southern Europe and is bordered to the south by tectonic units (Rif, Kabylies) overthrusted onto the North African Gondwana shelf during Neogene times (Jolivet and Faccenna 2000). The current configuration differs strongly from the original setting, because the Armorican Terrane Assemblage was dismembered and recomposed by wrench and transcurrent shear zones.

A-type igneous suites exposed in Alpine-related realms have been reviewed elsewhere (Bonin et al. 1998 and references therein). The most voluminous suites were emplaced well after Pangaea welding and predate continental break-up and Neo-Tethys Ocean development

during the Mesozoic. Corsica provides a unique example yielding two discrete igneous episodes separated by a period of quiescence. The first was Permian at 275 ± 10 Ma (Artinskian–Wordian) and the second Triassic at 245 ± 10 Ma (Induan–Anisian), followed ultimately by a thermal event at *c.* 200 Ma (Triassic–Liassic boundary) (Bonin et al. 2008, and references therein). Silica-oversaturated to undersaturated complexes, e.g., Monzoni–Predazzo and Karavanken in Southern Alps, Ditrău in Eastern Carpathians, yield Ladinian (*c.* 237–232 Ma) ages.

Such a sequence is unknown in the ATA that was unaffected by Alpine tectonics. The Mid-German Crystalline Zone and the Saxo-Thuringian Zone will be reviewed hereafter. The Mid-German Crystalline Zone (MGCZ) constitutes a SW–NE trending belt of crystalline rocks that are exposed in various inliers in Pfalz and form the massifs of Odenwald, Spessart, Ruhla and Kyffhäuser. The MGCZ was penetrated by drill holes in the Saar–Nahe Basin and other sedimentary troughs to the NE and could extend southwestwards to Cornwall (Dörr et al. 1999) and even Spain. It is currently considered as a part of the Rheic suture zone between the Eastern Avalonia and the Saxo-Thuringian Zone, which belongs to the ATA.

Post-Cambrian metasedimentary units yield both Gondwana and Baltica affinities (Gerdes and Zeh 2006). Intercalated metabasalts are mainly calc-alkaline with an island-arc signature, whereas MORB signatures are scarce. Such features suggest that the composite terrane could correspond to an accretionary prism close to the suture zone. Early Devonian orthogneisses intercalated with IAB-like metabasalts yield volcanic arc signatures, such as the 413 ± 5 and 398 ± 3 Ma members of the Central Gneiss Unit, Ruhla (Brätz 2000). From the Devonian–Carboniferous boundary onward, all orthogneissic and metasedimentary formations followed a clockwise P-T-t metamorphic evolution associated to ductile deformation before and during emplacement of post-collisional 360–325 Ma (Tournaisian–Serpukhovian) high-K calc-alkaline suites (Reischmann and Anthes 1996; Altherr et al. 1999; Zeh et al. 2005).

A-type igneous suites span the entire Cambrian–Permian range of time. The 489 ± 1 Ma (Cambrian–Ordovician boundary) Volkach syenite, revealed by drilling east of Spessart, yields the oldest age (Anthes and Reischmann 2001) and a Bulk Silicate Earth (BSE) isotopic signature (Anthes 1998); it was coeval to Rheic Ocean development. Late Silurian alkali-calcic orthogneisses of A-type affinities include the 426 ± 4 Ma Silbergrund gneiss and the 423 ± 6 Ma Erbstrom gneiss, Ruhla (Brätz 2000), the 418 ± 18 Ma Rotgneiss (Okrusch and Richter 1986) and the 410 ± 18 Ma Haibach gneiss, Spessart (Dombrowski et al. 1995). Early Devonian alkali-calcic A-type orthogneisses comprise the 405 ± 3 Ma Böllstein orthogneiss, Odenwald (Reischmann et al. 2001), and the 400 ± 4 Ma Steinbach augen gneiss, Ruhla (Brätz 2000). All igneous suites were emplaced in a continental area experiencing tensional regimes and located far from the active margin of the ATA. The *c.* 344 Ma (Visean) Darmstadt albite granite, Odenwald, is unique during the Early Carboniferous, with its A-type composition and a BSE isotopic signature (Anthes 1998).

A short-lived within-plate igneous episode at the Carboniferous–Permian boundary is documented by trachybasalt–trachydacite–A-type rhyolite igneous suites of the Halle Volcanic Complex (Romer et al. 2001) and the Saar–Nahe Basin as well as by the plutonic suite of the Ruhla inlier (Zeh and Brätz 2002). A-type rhyolite occurs as laccolith units (Breitkreuz and Mock 2004) emplaced in discrete pulses from the Middle Pennsylvanian to the Sakmarian at 307 ± 3 Ma, 301–298 ± 3 Ma and 294 ± 3 Ma (Breitkreuz and Kennedy 1999). Intense volcanic activity, with magmas ranging from basalt to trachyte and A-type rhyolite, took place in the Saar–Nahe Basin during the 296–293 Ma (Asselian–Sakmarian) period of time. Intrusions, extrusions, diatremes, lava flows and ignimbrites are exposed in a half-graben bounded to the north by a detachment fault parallel to the Avalonia–Armorica plate boundary (for a review, see Lorenz and Haneke 2004). As shown by major- and trace-element whole-rock chemical data (Brätz 2000), the Ruhla plutonic suite, emplaced under a transcurrent ductile–brittle shear regime, includes a monzonite–syenite feldspar cumulate body (the so-called Trusetal granite), monzodiorite (Brotterode diorite), A-type granites (Ruhla and Eselsprung granites) and granite porphyry dykes. Intrusive episodes yield mean ages of *c.* 305 Ma (Eselsprung granite, Brätz 2000), 301 ± 5 Ma (Trusetal granite), 295 ± 5 Ma (Ruhla granite and granite porphyry dykes), 289 ± 5 Ma (Brotterode diorite) and 285 ± 5 Ma to 277 ± 7 Ma (late granite porphyry dykes), in agreement with field evidence and Ar-Ar cooling ages in the metamorphic country rocks (Zeh et al. 2000).

The Saxo-Thuringian Zone represents a continental part of the ATA. In Saxony and Thuringia, each of them representing a *locus typicus* defining the Saxo-Thuringian Zone, A-type granite suites are fairly well represented during the Paleozoic. In the external domain, the Vesser MOR-related complex comprises a basalt (508 ± 2 Ma) – dacite (497 ± 2 Ma) – rhyolite volcanic suite, associated with a 502 ± 2 Ma tholeiitic gabbro–dolerite. The nearby Ediacaran sedimentary assemblages were intruded by a *c.* 490 Ma (Furongian) granite (Linnemann et al. 2007). In the internal domain, they are cut by 490 ± 3 Ma (Furongian) to 485 ± 6 Ma (Tremadocian) granites and covered unconformably by two episodes of 487 ± 5 Ma (Cambrian–Ordovician boundary) rhyolitic pyroclastic units and 479 ± 5 Ma (Tremadocian–Floian) porphyroid (Linnemann et al. 2007). During the Carboniferous,

contrasting igneous suites emplaced under shear stress regimes that changed abruptly from the 340–330 Ma (Visean) high-K Meissen granite association, related to dextral strike-slip movement of the Elbe Fault Zone, to the 327 ± 4 Ma (Visean–Serpukhovian boundary) Markersbach A-type granite, showing no strike-slip influence (Hofmann et al. 2008). This A-type Li-mica-bearing granite (Förster and Tischendorf 1996; Förster 2001) shares the same A-type affinities with the Sudetic 319–314 ± 4 Ma Karkonosze and 309 ± 2 Ma Strzegom-Sobotka granite massifs, as well as bimodal trachybasalt–trachyandesite–trachydacite–rhyolite volcanic suite (Mazur et al. 2007). Younger volcanic activity took place at the Carboniferous–Permian boundary, as shown by the 308 ± 1 Ma Teplice–Altenberg rhyolitic caldera (Förster et al. 1995), the younger, yet undated, Zinnwald–Cínovec zinnwaldite-albite granite and the 297 ± 8 Ma rhyolite dykes within the Eibenstock Pluton (Kempe et al. 2004). Later on, two eruptive episodes are documented in the Lower Rotliegend molasse of the Saxonian Sub-Erzgebirge Basin. A pyroxene quartz porphyry yielded an age of 296 ± 2 Ma (Förster and Tischendorf 1996), and "lower series" rhyolites 278 ± 5 Ma (Nasdala et al. 1998), substantiating diachronous activity throughout the large intermontane basin.

5. Summary and conclusions

A-type granite igneous complexes are fairly abundant within the Variscan–Alpine Europe (Tab. 3). However, discrete ages of emplacement document geodynamic settings varying from post-orogenic, through intra-continental rifting to passive margin tectonic regimes. They thus illustrate a repeated history of continental breakup and oceanic basin development followed by oceanic closure and post-collisional transcurrent displacement.

At the end of the Neoproterozoic, Laurentia developed a passive margin toward the Iapetus Ocean, whereas the Cadomian–Pan-African orogenic episode had its climax within Gondwana at about 600 Ma (Ediacaran). Ediacaran to Early Cambrian A-type granites, occupying pieces of consolidated Gondwana basement, display early anorogenic features associated with the birth of the Rheic Ocean.

The incipient drifting of the Rheic Ocean was followed within the Armorican Terrane Assemblage by a major 485 Ma (Tremadocian) rifting and igneous event characterized by A-type suites now converted into orthogneisses (metagranites), amphibolites (metabasalts) and leptynites (metatrachytes–metarhyolites) in the internal parts of the Variscan belt. The further development of the Rheic

Tab. 3 Representative A-type igneous episodes within the Variscan–Alpine Europe

Period	Stage	Age (Ma)	Laurentian margin	Eastern Avalonia	Armorican Terrane Assemblage
Triassic	Induan–Anisian	250–230			Corsica Monzoni–Predazzo Ditrău, Romania — Intra-continental rift
Permian	Artinskian–Wordian	285–265			Saar–Nahe Basin, W Mediterranean Province — Intra-continental rift
	Asselian–Sakmarian	302–293		NE German Basin, Harz — Intra-continental rift	Halle, Saar–Nahe basins, Ruhla — Intra-continental rift
	Serpukhovian–Moscovian	327–309			Saxo-Thuringian — Intra-continental rift
Carboniferous	Tournaisian	345	Midland Valley — Intra-continental rift		
Devonian	Givetian–Frasnian	389–384		Rheinisches Schiefergebirge — Rheic Ocean passive margin	
	Pragian	408–400	Grampian — Post-Scandian episode		Mid-German Crystalline Rise — Intra-continental rift
Silurian	Telychian–Lochkovian	426–410			Mid-German Crystalline Rise — Intra-continental rift
	Llandovery–Wenlock	440–426	Moine Thrust — Scandian episode		
Ordovician	Sandbian–Katian	456	Northern Highland — Post-Grampian episode		
	Furongian–Tremadocian	490–480			Mid-German Crystalline Rise, Saxo-Thuringian — Rheic Ocean passive margin
Cambrian	Epoch 3	508–497		SW Poland — Rheic Ocean drifting	Saxo -Thuringian — Rheic Ocean drifting
Neoproterozoic	Ediacaran	570–560		Thaya, Austria — Post-Cadomian episode	
		601–588	Older Granites — Iapetus passive margin		

Ocean led to Avalonia–Laurentia collision postdated by A-type igneous episodes in Scotland. In addition, the Late Ordovician to Early Carboniferous period was marked by alkaline igneous episodes at the passive margin of Avalonia, whereas the active margin of the Armorican Terrane Assemblage was devoid of any A-type igneous events.

The Variscan collision was followed in the Armorican Terrane Assemblage by discrete post-orogenic episodes, namely 350–340 Ma (Tournaisian), 320 Ma (Serpukhovian) and 300 Ma (Ghzelian) igneous events. The 300 Ma event, widespread throughout the Variscan–Alpine Europe, constituted a climactic igneous event affecting both Avalonia and Armorican Terrane Assemblage.

Early to Middle Permian (280–260 Ma) and Late Permian to Early Triassic (250–230 Ma) A-type provinces were emplaced in the southernmost parts of the Variscan–Alpine Europe. They accompanied incipient Pangaea breakup and heralded the future birth of the Neo-Tethys Ocean, which started by the 200 Ma Central Atlantic Large Igneous Province.

A-type granite events provide space and time clues to discrete Ediacaran to Triassic episodes, during which Pannotia broke up, Gondwanan terranes were amalgamated onto Baltica and, ultimately, Pangaea broke up. They identify waning orogenic stages, corresponding to orogenic belt collapse, transcurrent movements along transform fault zones and subsequent peneplanation, as well as pre- to early oceanic stages, corresponding to extensional reactivation of shear zones, incipient rifting and passive margin development. Their occurrences are, therefore, especially helpful for recognition of terrane boundaries and palinspatic reconstructions.

Acknowledgements. This is a contribution to the UNESCO-IGCP Project 510 "A-type granites and related rocks through time", chaired by Roberto Dall'Agnol and led jointly by Carol Frost, Tapani Rämö and Laurence Robb. Vojtěch Janoušek prompted me to submit this paper to the Special Issue of the *Journal of Geosciences* on "Field, analytical and experimental approaches to silicic magmatism in collisional orogens" and I am indebted to him for his patience. The considerations presented here on the evolution of Variscan Germany stem from observations and discussions made during the field trip Frankfurt–Dresden, managed by Peter Königshof, Ulf Linnemann and Armin Zeh, following the UNESCO-IGCP Projects 497–499 Joint Conference held at Frankfurt in October 2008. The whole party is thanked for judicious remarks and information, but should not be held responsible for any misconceptions and prejudices that remain my own. Many thanks are due to the anonymous reviewer and David Dolejš, the handling editor, who both gave quick critical assessments of the first version and were of great help in improving the paper.

References

Altherr R, Henes-Klaiber U, Hegner E, Satir M, Langer C (1999) Plutonism in the Variscan Odenwald (Germany): from subduction to collision. Int J Earth Sci 88: 422–443

Anthes G (1998) Geodynamische Entwicklung der Mitteldeutschen Kristallinschwelle: Geochronologie und Isotopengeochemie. Unpublished Ph.D. Thesis, Johannes Gutenberg-Universität Mainz, pp 1–154

Anthes G, Reischmann T (2001) Timing of granitoid magmatism in the eastern mid-German crystalline rise. J Geodyn 31: 119–143

Baumann A, Grauert B, Mecklenburg S, Vinx R (1991) Isotopic age determinations of crystalline rocks of the Upper Harz Mountains, Germany. Geol Rundsch 80: 669–690

Bea F, Montero P, Talavera C, Zinger T (2006) A revised Ordovician age for the Miranda do Douro orthogneiss, Portugal. Zircon U-Pb ion-microprobe and LA-ICPMS dating. Geol Acta 4: 395–401

Bendaoud A, Ouzegane K, Godard G, Liégeois JP, Kienast JR, Bruguier O, Drareni A (2008) Geochronology and metamorphic P-T-X evolution of the Eburnian granulite-facies metapelites of Tidjenouine (Central Hoggar, Algeria): witness of the LATEA metacratonic evolution. In: Ennih N, Liégeois JP (eds) The Boundaries of the West African Craton. Geol Soc London Spec Pub 297: pp 111–146

Benek R, Kramer W, McCann T, Scheck M, Negendank JFW, Korich D, Huebscher HD, Bayer U (1996) Permo-Carboniferous magmatism in the Northeast German Basin. Tectonophysics 266: 379–404

Billings MP (1945) Mechanics of igneous intrusion in New Hampshire. Amer J Sci 243-A: 40–68

Black R, Lameyre J, Bonin B (1985) The structural setting of alkaline complexes. J Afr Earth Sci 3: 5–16

Bonin B (2007) A-type granites and related rocks: evolution of a concept, problems and prospects. Lithos 97: 1–29

Bonin B, Bebien J (2005) The granite-upper mantle connection in terrestrial planetary bodies: an anomaly to the current granite paradigm? Lithos 80: 131–145

Bonin B, Azzouni-Sekkal A, Bussy F, Ferrag S (1998) Alkali-calcic and alkaline post-orogenic (PO) granite magmatism: petrologic constraints and geodynamic settings. Lithos 45: 45–70

Bonin B, Bebien J, Masson P (2002) Granite: a planetary point of view. Gondwana Res 5: 261–273

Bonin B, Platevoet B, Poitrasson F, Renna MR (2008) The Permian–Triassic A-type volcanic-plutonic igneous suite of Corsica. Eurogranites – IGCP 510 2008 Joint Field-Meeting, field guide, pp 1–54

Bowen NL (1928) The Evolution of Igneous Rocks. Princeton University Press, Princeton, pp 1–334

Brätz H (2000) Radiometrische Altersdatierungen und geochemische Untersuchungen von Orthogneisen, Graniten und Granitporphyren aus dem Ruhlaer Kristallin, Mitteldeutsche Kristallinzone. Unpublished Ph.D. Thesis, Bayerische Julius-Maximilians-Universität Würzburg, pp 1–151

Breitkreuz C, Kennedy A (1999) Magmatic flare-up at the Carboniferous/Permian boundary in the NE German Basin revealed by SHRIMP zircon ages. Tectonophysics 302: 307–326

Breitkreuz C, Mock A (2004) Are laccolith complexes characteristic of transtensional basin systems? Examples from the Permo-Carboniferous of Central Europe. In: Breitkreuz C, Petford N (eds) Physical Geology of High-level Magmatic Systems. Geol Soc London Spec Pub 234: pp 13–31

Bussy F, Sartori M, Thelin P (1996) U-Pb zircon dating in the middle Penninic basement of the Western Alps (Valais, Switzerland). Schweiz Mineral Petrogr Mitt 76: 81–84

Clarke DB (1996) Two centuries after Hutton's 'Theory of the Earth': the status of granite science. Trans Roy Soc Edinb, Earth Sci 87: 353–359

Cordani UG, Nutman AP, Andrade AS, Santos JF, Azevedo MDR, Mendes MH, Pinto MS (2006) New U-Pb SHRIMP zircon ages for pre-Variscan orthogneisses from Portugal and their bearing on the evolution of the Ossa-Morena Tectonic Zone. Anais Acad Brasil Ciências 78: 133–149

Dombrowski A, Henjes-Kunst F, Höhndorf A, Kröner A, Okrusch M, Richter P (1995) Orthogneisses in the Spessart Crystalline Complex, north-west Bavaria: Silurian granitoid magmatism at an active continental margin. Geol Rundsch 84: 399–411

Dörr W, Floyd PA, Leveridge BE (1999) U-Pb ages and geochemistry of granite pebbles from the Devonian Menaver Conglomerate, Lizard Peninsula: provenance of Rhenohercynian flysch of SW England. Sedim Geol 124: 131–147

Eby GN (1990) The A-type granitoids: a review of their occurrence and chemical characteristics and speculations on their petrogenesis. Lithos 26: 115–134

Etxebarria M, Chalot-Prat F, Apraiz A, Eguíluz L (2006) Birth of a volcanic passive margin in Cambrian time: rift paleogeography of the Ossa-Morena Zone, SW Spain. Precambr Res 147: 366–386

Flick H, Nesbor D, Königshof P (2008) Volcanism and reef development in the Devonian: a case study from the Rheinisches Schiefergebirge (Lahn syncline, Germany). In: Königshof P, Linnemann U (eds) The Rheno-Hercynian, Mid-German Crystalline and Saxo-Thuringian Zones (Central European Variscides). Final meeting of IGCP 497 and IGCP 499 Excursion Guide, pp 55–78

Floor P (1974) Alkaline gneisses. In: Sørensen H (ed) The Alkaline Rocks. John Wiley & Sons, London, pp 124–142

Förster HJ (2001) Synchysite-(Y) – synchysite-(Ce) solid solutions from Markersbach, Erzgebirge, Germany: REE and Th mobility during high-T alteration of highly fractionated A-type granites. Mineral Petrol 72: 259–280

Förster HJ, Seltmann R, Tischendorf G (1995) High-fluorine, low-phosphorous A-type (post collision) silicic magmatism in the Erzgebirge. Terra Nostra 7: 32–34

Förster HJ, Tischendorf G (1996) Compositional heterogeneity of silicic magmatic rocks from the German Variscides. Z geol Wiss 24: 467–482

Fowler MB, Kocks H, Darbyshire DPF, Greenwood PB (2008) Petrogenesis of high Ba-Sr plutons from the Northern Highlands Terrane of the British Caledonian Province. Lithos 105: 129–148

Francis EH (1983) Carboniferous–Permian igneous rocks. In: Craig GY (ed) Geology of Scotland, 2nd edition. Scottish Academy Press, Edinburgh, pp 297–324

Freeman SR, Butler RWH, Cliff RA, Rex DC (1998) Direct dating of mylonite evolution: a multi-disciplinary geochronological study from the Moine Thrust Zone, NW Scotland. J Geol Soc, London 155: 745–758

Friedl G, Finger F, Paquette JL, von Quadt A, McNaughton NJ, Fletcher IR (2004) Pre-Variscan geological events in the Austrian part of the Bohemian Massif deduced from U-Pb zircon ages. Int J Earth Sci 93: 802–823

Frost BR, Frost CD (2008) A geochemical classification for feldspathic igneous rocks. J Petrol 49: 1955–1969

Geisler T, Vinx R, Martin-Gombajov N, Pidgeon RT (2005) Ion microprobe (SHRIMP) dating of detrital zircon grains from quartzites of the Eckergneiss Complex, Harz Mountains (Germany): implications for the provenance and the geological history. Int J Earth Sci 94: 369–384

Gerdes A, Zeh A (2006) Combined U-Pb and Hf isotope LA-(MC-)ICP-MS analyses of detrital zircons: comparison with SHRIMP and new constraints for the provenance and age of an Armorican metasediment in Central Germany. Earth Planet Sci Lett 249: 47–61

Halliday AN, Aftalion M, Parsons I, Dickin AP, Johnson MRW (1987) Syn-orogenic alkaline magmatism and its relationship to the Moine Thrust Zone and the thermal state of the lithosphere in NW Scotland. J Geol Soc, London 144: 611–617

Hanžl P, Janoušek V, Žáček V, Wilimský D, Aichler J, Erban V, Pudilová M, Chlupáčová M, Buriánková K, Mixa P, Pecina V (2007) Magmatic history of granite-derived mylonites from the southern Desná Unit (Silesicum, Czech Republic). Mineral Petrol 89: 45–75

Hofmann M, Linnemann U, Gerdes A, Ullrich B (2008) Closure of the Rheic Ocean and the final pulse of the Variscan orogeny in the Bohemian Massif – timing of large-scale strike-slip processes and basement exhumation by LA-ICP-MS U-Pb zircon dating from the Elbe Zone (Saxo-Thuringian Zone, Germany). In: Königshof

P, Linnemann U (eds) From Gondwana and Laurussia to Pangaea: Dynamics of Oceans and Supercontinents. Final Meeting of IGCP 497 and IGCP 499, 20th International Senckenberg-Conference & 2nd Geinitz-Conference, Abstracts and Programme, pp 53

Janoušek V, Hanžl P, Aichler J, Pecina V, Erban V, Wilimský D, Žáček V, Mixa P, Buriánková K, Pudilová M, Chlupáčová M (2006) Contrasting petrogenesis of two volcanic suites in the Devonian Vrbno Group (Hrubý Jeseník Mts., Czech Republic). Geolines 20: 57–59

Jelínek E, Dudek A (1993) Geochemistry of subsurface Precambrian plutonic rocks from the Brunovistulian Complex in the Bohemian Massif, Czechoslovakia. Precambr Res 62: 103–125

Jolivet L, Faccenna C (2000) Mediterranean extension and the Africa-Eurasia collision. Tectonics 19: 1095–1106

Kalvoda J, Bábek O, Fatka O, Leichmann J, Melichar R, Nehyba S, Špaček P (2008) Brunovistulian Terrane (Bohemian Massif, Central Europe) from Late Proterozoic to Late Paleozoic: a review. Int J Earth Sci 97: 497–518

Kempe U, Bombach K, Matukov D, Schlothauer Y, Hutschenreuter J, Wolf D, Sergeev S (2004) Pb/Pb and U/Pb zircon dating of subvolcanic rhyolite as a time marker for Hercynian granite magmatism and Sn mineralisation in the Eibenstock granite, Erzgebirge, Germany: considering effects of zircon alteration. Miner Depos 39: 646–669

Kossmat F (1927) Gliederung des varistischen Gebirgsbaues. Abhandl Sächs Geol Landesamts 1: 1–39

Lancelot JR, Allegret A, Iglesias Ponce de Leon M (1985) Outline of Upper Precambrian and Lower Paleozoic evolution of the Iberian Peninsula according to U-Pb dating of zircons. Earth Planet Sci Lett 74: 325–337

Le Maitre RW (2002) A Classification of Igneous Rocks and Glossary of Terms. Cambridge University Press, Cambridge, pp 1–236

Li ZX, Bogdanova SV, Collins AS, Davidson A, de Waele B, Ernst RE, Fitzsimons ICW, Fuck RA, Gladkochub DP, Jacobs J, Karlstrom KE, Lu S, Natapov LM, Pease V, Pisarevsky SA, Thrane K, Vernikovsky V (2008) Assembly, configuration, and break-up history of Rodinia: a synthesis. Precambr Res 160: 179–210

Linnemann U, Gerdes A, Drost K, Buschmann B (2007) The continuum between Cadomian orogenesis and opening of the Rheic Ocean: constraints from LA-ICP-MS U-Pb zircon dating and analysis of plate-tectonic setting (Saxo-Thuringian Zone, northeastern Bohemian Massif, Germany). In: Linnemann U, Nance RD, Kraft P, Zulauf G (eds) The Evolution of the Rheic Ocean: From Avalonian-Cadomian Active Margin to Alleghanian–Variscan Collision. Geol Soc Am Spec Paper 423: pp 61–96

Loiselle MC, Wones DR (1979) Characteristics and origin of anorogenic granites. Geological Society of America, Abstracts with Programs 11: pp 468

Lorenz V, Haneke J (2004) Relationship between diatremes, dykes, sills, laccoliths intrusive-extrusive domes, lava flows, and tephra deposits with unconsolidated water-saturated sediments in the late Variscan intermontane Saar–Nahe Basin, SW Germany. In: Breitkreuz C, Petford N (eds) Physical Geology of High-Level Magmatic Systems. Geol Soc London Spec Pub 234: London, pp 75–124

Mazur S, Aleksandrowski P, Kryza R, Oberc-Dziedzic T (2006) The Variscan orogen in Poland. Geol Quart 50: 89–118

Mazur S, Aleksandrowski P, Turniak K, Awdankiewicz M (2007) Geology, tectonic evolution and Late Paleozoic magmatism of Sudetes – an overview. In: Kozlowski A, Wiszniewska J (eds) Granitoids in Poland. Arch Miner Monogr 1, Warszawa, pp 59–87

Montero P, Bea F, González-Lodeiro F, Talavera C, Whitehouse MJ (2007) Zircon ages of the metavolcanic rocks and metagranites of the Ollo de Sapo Domain in central Spain: implications for the Neoproterozoic to Early Paleozoic evolution of Iberia. Geol Mag 144: 963–976

Montero P, Bea F, Corretgé LG, Floor P, Whitehouse MJ (2008) U-Pb ion microprobe dating and Sr and Nd isotope geology of the Galiñeiro Igneous Complex. A model for the peraluminous/peralkaline duality of the Cambro–Ordovician magmatism of Iberia. Lithos, doi:10.1016/j.lithos.2008.10.009

Morris GA, Page L, Martinez V (2005) New dates (415 Ma) for the Etive Dyke Swarm and the end of the Caledonian Orogeny in the SW Grampian Highlands of Scotland. J Geol Soc, London 162: 741–744

Nasdala L, Götze J, Pidgeon RT, Kempe U, Seifert T (1998) Constraining a SHRIMP U-Pb age: micro-scale characterization of zircons from Saxonian Rotliegend rhyolites. Contrib Mineral Petrol 132: 300–306

Nawrocki J, Poprawa P (2006) Development of Trans-European Suture Zone in Poland: from Ediacaran to Early Paleozoic accretion. Geol Quart 50: 59–76

Oberc-Dziedzic T, Klimas K, Kryza R, Fanning CM (2003) SHRIMP U-Pb zircon geochronology of the Strzelin gneiss, SW Poland: evidence for a Neoproterozoic thermal event in the Fore-Sudetic Block, Central European Variscides. Int J Earth Sci 92: 701–711

Oberc-Dziedzic T, Kryza R, Klimas K, Fanning MC, Madej S (2005) Gneiss protolith ages and tectonic boundaries in the NE part of the Bohemian Massif (Fore-Sudetic Block, SW Poland). Geol Quart 49: 363–378

Ogg JG, Ogg G, Gradstein FM (2008) The Concise Geologic Time Scale. Cambridge University Press, Cambridge, UK, pp 1–177

Okrusch M, Richter P (1986) Orthogneisses of the Spessart Crystalline Complex, Northwest Bavaria: indicators of the geotectonic environment? Geol Rundsch 75: 555–568

Oliver GJH, Corfu F, Krogh TE (1993) U-Pb ages from SW Poland: evidence for a Caledonian suture zone between Baltica and Gondwana. J Geol Soc, London 150: 355–369

Oliver GJH (2001) Reconstruction of the Grampian episode in Scotland: its place in the Caledonian Orogeny. Tectonophysics 332: 23–49

Oliver GJH, Wilde SA, Wan Y (2008) Geochronology and geodynamics of Scottish granitoids from the late Neoproterozoic break-up of Rodinia to Palaeozoic collision. J Geol Soc, London 165: 661–674

Pan Y (1997) Zircon- and monazite-forming metamorphic reactions at Manitouwadge, Ontario. Canad Mineral 35:105–118

Parga-Pondal I, Matte P, Capdevila R (1964) Introduction à la géologie de l'« Ollo de Sapo ». Formation porphyroïde antésilurienne du nord ouest de l'Espagne. Notas Comun Instit Geol Minero España 76: 19–154

Patočka F, Valenta J (1996) Geochemistry of the late Devonian intermediate to acid metavolcanic rocks from the southern part of the Vrbno Group, the Jeseníky Mts. (Moravo-Silesian Belt, Bohemian Massif, Czech Republic): paleotectonic implications. Geolines 4: 42–54

Paulick H, Breitkreuz C (2005) The Late Paleozoic felsic lava-dominated large igneous province in northeast Germany: volcanic facies analysis based on drill cores. Int J Earth Sci 94: 834–850

Pearce JA, Harris NBW, Tindle AG (1984) Trace element discrimination diagrams for the tectonic interpretation of granitic rocks. J Petrol 25: 956–983

Pupin JP, Bonin B, Tessier M, Turco G (1978) Rôle de l'eau sur les caractères morphologiques et la cristallisation du zircon dans les granitoïdes. Bull Soc Géol France 7: 721–725

Reischmann T, Anthes G (1996) Geochronology of the Mid-German Crystalline Rise west of the River Rhine. Geol Rundsch 85: 761–774

Rickwood PC (1989) Boundary lines within petrologic diagrams which use oxides of major and minor elements. Lithos 22: 247–263

Romer RL, Förster HJ, Breitkreuz C (2001) Intracontinental extensional magmatism with a subduction fingerprint: the late Carboniferous Halle Volcanic Complex (Germany). Contrib Mineral Petrol 141: 201–221

Reischmann T, Anthes G, Jaeckel P, Altenberger U (2001) Age and origin of the Böllsteiner Odenwald. Mineral Petrol 72: 29–44

Salamon M, Flick H, Nesbor D, Königshof P, Schindler E, Brocke R (2008) Volcanism in the Lower Carboniferous and characteristic basinal settings in the Devonian. In: Königshof P, Linnemann U (eds) The Rheno-Hercynian, Mid-German Crystalline and Saxo-Thuringian Zones (Central European Variscides). Final meeting of IGCP 497 and IGCP 499 Excursion Guide, pp 79–88

Santos Zalduegui JF, Schärer U, Gil Ibarguchi JI (1995) Isotope constraints on the age and origin of magmatism and metamorphism in the Malpica–Tuy allochthon, Galicia, NW Spain. Chem Geol 121: 91–103

Simancas F, Expósito I, Azor, A, Martínez Poyatos D, González Lodeiro F (2004) From the Cadomian orogenesis to the Early Paleozoic Variscan rifting in southwest Iberia. J Iberian Geol 30: 53–71

Soper NJ (1994) Was Scotland a Vendian RRR junction? J Geol Soc, London 151: 579–582

Stampfli GM, Borel GD (2004) The TRANSMED transects in space and time: Constraints on the paleotectonic evolution of the Mediterranean Domain. In: Cavazza W, Roure F, Spakman W, Stampfli GM, Ziegler P (eds) The TRANSMED Atlas: the Mediterranean Region from Crust to Mantle. Springer-Verlag, Berlin, pp 53–80 and CD ROM

Steinhoefel G, Hegner E, Oliver GJH (2008) Chemical and Nd isotope constraints on granitoid sources involved in the Caledonian Orogeny in Scotland. J Geol Soc, London 165: 817–827

Thelin P (1987) Nature originelle des gneiss œillés de Randa (Nappe de Siviez-Mischabel, Valais). Mémoires Soc vaudoise Sci Natur 18: 1–75

Tomaschek F, Kennedy AK, Villa IM, Lagos M, Ballhaus C (2003) Zircons from Syros, Cyclades, Greece – Recrystallization and mobilization of zircon during high-pressure metamorphism. J Petrol 44: 1997–2002

Valverde-Vaquero P, Marcos A, Farias P, Gallastegui G (2005) U-Pb dating of Ordovician felsic volcanism in the Schistose Domain of the Galicia–Trás-os-Montes Zone near Cabo Ortegal (NW Spain). Geol Acta 3: 27–37

van Breemen O, Aftalion M, Johnson MRW (1979) Age of the Loch Borrolan Complex, Assynt, and late movements along the Moine Thrust Zone. J Geol Soc, London 136: 489–495

Wedepohl KH (1991) Chemical composition and fractionation of the continental crust. Geol Rundsch 80: 207–223

Whalen JB, Currie KL, Chappell BW (1987) A-type granites: geochemical characteristics, discrimination and petrogenesis. Contrib Mineral Petrol 95: 407–419

Williams IS, Claesson S (1987) Isotopic evidence for the Precambrian provenance and Caledonian metamorphism of high grade paragneisses from the Seve Nappes, Scandinavian Caledonides. II. Ion microprobe zircon U–Th–Pb. Contrib Mineral Petrol 97: 205–217

Zeh A, Brätz H (2002) Timing of Late Carboniferous-Permian granite and granite porphyry intrusions in the Ruhla Crystalline Complex (Central Germany), new constraints from SHRIMP and $^{207}Pb/^{206}Pb$ single zircon dating. Chem Erde 62: 303–316

Zeh A, Cosca AM, Brätz H, Okrusch M, Tichomirowa M (2000) Simultaneous horst-basin formation and magmatism during Late Variscan transtension: evidence from

$^{40}Ar/^{39}Ar$ and $^{207}Pb/^{206}Pb$ geochronology in the Ruhla Crystalline Complex. Int J Earth Sci 89: 52–71

Zeh A, Gerdes A, Will TM, Millar IL (2005) Provenance and magmatic-metamorphic evolution of a Variscan island-arc complex: constraints from U-Pb dating, petrology, and geospeedometry of the Kyffhäuser Crystalline Complex, Central Germany. J Petrol 46: 1393–1420

Journal of Geosciences, 53 (2008), 253–261 DOI: 10.3190/jgeosci.032

Original paper

Formation of tabular plutons – results and implications of centrifuge modelling

Carlo DIETL[1,*], Hemin KOYI[2]

[1] *Institut für Geowissenschaften, Goethe-Universität, Altenhöferallee 1, D-60438 Frankfurt am Main, Germany; c.dietl@em.uni-frankfurt.de*
[2] *Hans Ramberg Tectonic Laboratory, Department of Earth Sciences, Uppsala University, Villavägen 16, S-75236 Uppsala, Sweden*
[*] *Corresponding author*

Geophysical investigations reveal that many granitoid plutons possess a tabular shape: either laccolithic, lopolithic or phacolithic. In this study, the results of a centrifuge experiment are used to understand the formation mechanisms of these features. The model was build of a sequence of 14 differently coloured plasticine layers. Two buoyant layers – with a volume of *c.* 40 cm^3 each – were incorporated into the model stratigraphy at different depths to investigate, whether the rise and emplacement of buoyant material at different levels results in different intrusion structures.

After centrifuging for 30 min at 700 G, both the buoyant layers had formed two lenticular sills (phacoliths) with aspect ratios (length/thickness) of 6 and 3.4 for the upper and lower phacoliths, respectively, directly above both pre-existing perturbations in the buoyant layers. During their movement, the buoyant phacoliths had pushed their roof plasticine upward. Simultaneously, their floor plasticine had subsided (bottom sinking). Subsidence of the floor material had choked the inflow of further buoyant material into the feeder channel of the developing sills and inhibited their further lateral growth.

The observed forced downward movement of the plasticine floor of the forming PDMS (polydimethylsiloxane) phacoliths resembles the so-called "floor depression" of host rock material around an emplacing tabular pluton. Floor depression is supposed to be a very important vertical material transfer process, which provides space for the construction of lopo- and phacoliths. The subsidence of host material made space for the developing buoyant phacoliths, but also restricted their growth to a certain time slot before the influx of new buoyant material into the feeder dyke of the tabular intrusive body was shut off. Similarly, in nature, the growth of a tabular pluton might be limited not only by the rate of magma ascent and its physical properties, but also by the emplacement processes of the evolving pluton.

Keywords: phacoliths, laccoliths, tabular plutons, ascent, emplacement, centrifuge modelling
Received: 16 September 2008; accepted 17 December 2008; handling editor: J. Žák

1. Introduction

Field geological as well as geophysical investigations on numerous large plutons (encompassing areas in the range of several hundred up to more than thousand km^2) during the last 20 years have revealed that many of them are of tabular, either laccolithic (convex roof and straight floor) or lopolithic (straight roof and concave floor) or phacolithic (biconvex) shape. Despite their differences in emplacement level and tectonic setting, the development of the lensoidal shapes of all these plutons can be described as a three-stage process (e.g. Corry 1988; Cruden 1998). In a first stage a vertical dyke is established, where magma is transported upward until it reaches a horizontal unconformity along which the magma then – in the second stage – spreads laterally to form a sill. In the third stage additional magma ascends through the feeder dyke to be emplaced into the sill, which inflates due to the magma overpressure by doming of the roof and/or depression of the floor of the growing pluton. These three stages are incremental processes and intimately entangled with each other, in particular in the case of composite plutons which consist of several magma batches. Magma ascent generated by dyking as well as roof uplift and floor depression of the developing pluton take advantage of shear zones and faults; either as magma pathways (magma ascent) or as planes of movement along which individual blocks of the roof and floor of the evolving pluton are shifted upward or downward (magma emplacement). The lateral spreading of magma prior to magma chamber inflation benefits from horizontal anisotropy planes in the host rock, such as bedding and foliation planes, fractures or shear zones. According to Cruden (1998) the roof uplift plays a major role as a space-making process only for laccoliths emplaced in the uppermost crust at around 3 km depth, while floor depression seems to be responsible for most of the – then lopolithic – tabular plutons being emplaced deeper within the Earth's crust below *c.* 4–5 km depth.

Based on dimensional data from several hundred plutons McCaffrey and Petford (1997) and Petford and Clemens (2000) showed that the proportions of intrusive

bodies (length vs. thickness) can be described by the following power law:

$$T = c \times L^{a} \qquad (1.1)$$

with pluton thickness T, its length L, a constant c and the power-law exponent a.

McCaffrey and Petford (1997) based their calculations on field data from 135 laccoliths and 21 plutonic intrusions. According to their data base power law (1.1) for laccoliths only can be formulated as:

$$T = 0.12 \times L^{0.88} \qquad (1.2)$$

while power law (1.1) applied to plutons is

$$T = 0.29 \times L^{0.80} \qquad (1.3).$$

Cruden (1998) ended up with a value of 0.29 for constant c when calculating the power law relationship between the length and thickness of tabular plutons. Petford and Clemens (2000) found – based on the dimensional data from more than 100 plutons and batholiths – that the power law exponent a in formula (1.1) equals 0.6 ± 0.1. According to Petford et al. (2000), tabular plutons, which are established mainly by downward directed material transfer (e.g. floor depression) can be distinguished from laccoliths from the power-law regression lines they follow in a $\log_{length}$ vs. $\log_{thickness}$ plot. Laccoliths plot along a power-law regression line with a = 0.88 ± 0.1, while plutons appear in this diagram along regression line with a = 0.60 ± 0.1 (Fig. 1).

The differences in numbers for a and c reflect the differing data sets the individual power law formulas

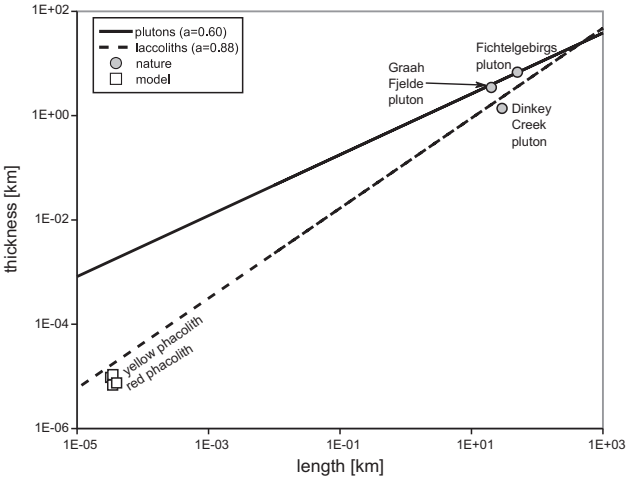

Fig. 1 Length vs. thickness plot for plutons and laccoliths, showing their differing dimensional ratios as expressed by the two regression lines (Petford et al. 2000). Grey dots indicate length-thickness ratios of the three real plutons discussed in text, open squares show the dimensions of the model phacoliths.

are based on and the quality of these data. Moreover, for the formulation of the individual equations only two – thickness and length – of the three available dimensional data (thickness, length and width) are taken into account. However, in particular the thickness data for the individual intrusions are not well constrained, because until today no major intrusive body with exposed roof *and* floor was observed. In particular descriptions of outcropping intrusion floors lack almost entirely in literature. One exception is the Bergell pluton in the Central Alps, the floor of which is exposed, together with its root zone (Rosenberg et al. 1995). Consequently, information about

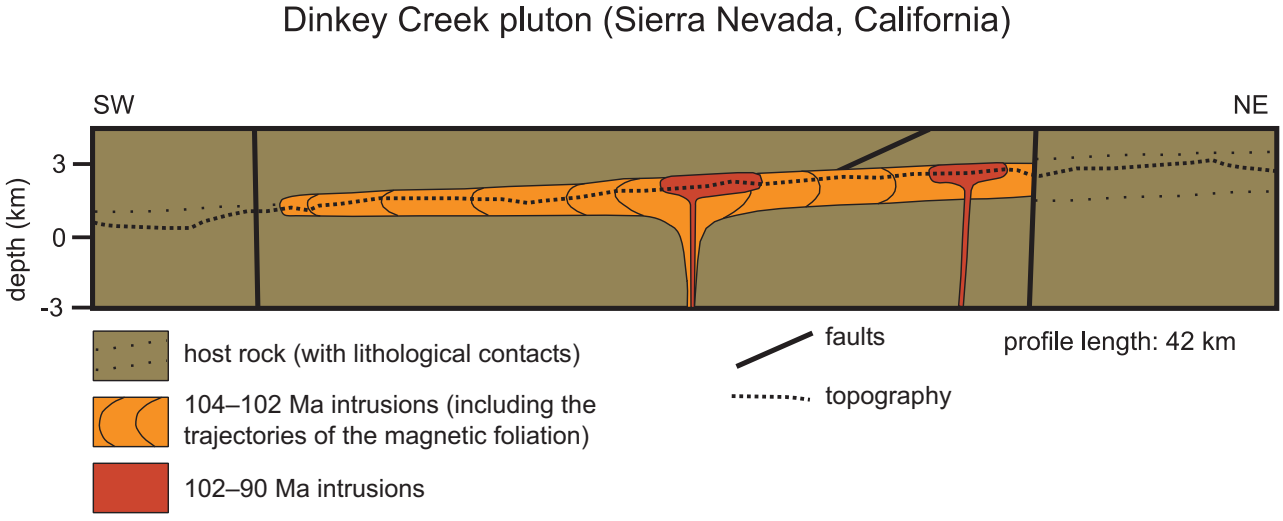

Fig. 2 Cross section through the Cretaceous Dinkey Creek pluton (Sierra Nevada, redrawn from Cruden et al. 1999).

intrusion floors stem mainly from indirect, geophysical methods, such as gravimetry and seismic investigations. Nevertheless, all these six power laws for laccoliths and plutons have one thing in common: the power law exponent *a* is always < 1, indicating the tabular shape of the granitoid bodies. However, the power law behaviour of these tabular intrusives does not only describe their shape, but also their growth: they start as thin, horizontal sills, which only after some lateral growth expand also vertically, giving them their final tabular shape.

2. Natural examples for tabular plutons

Typical tabular plutons include the upper-crustal, syn-orogenic Cretaceous Dinkey Creek pluton in the Sierra Nevada (California; Cruden et al. 1999; Hammarstrom and Zen 1986; Fig. 2), the mid-crustal, late-orogenic Carboniferous Fichtelgebirge pluton (Bohemian Massif; Hecht and Vigneresse 1999; O'Brien 2000; Fig. 3), and the upper-crustal, late- to post-orogenic Proterozoic Graah Fjelde Rapakivi Granite (Greenland – Grocott et

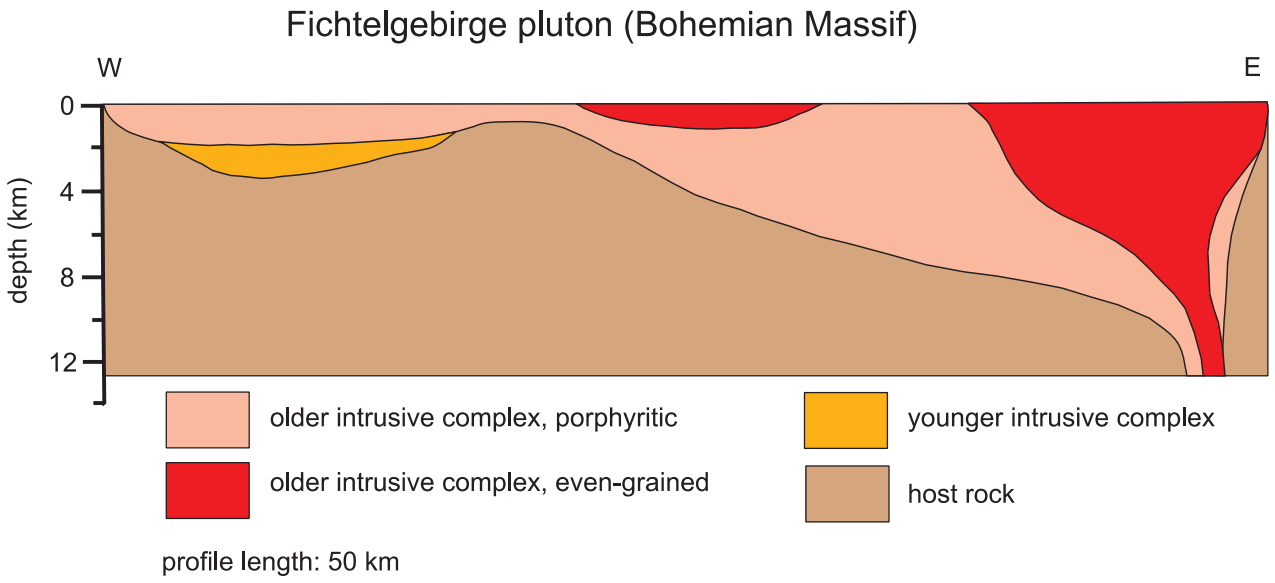

Fig. 3 Cross section through the Variscan Fichtelgebirge pluton (Bohemian Massif, redrawn from Hecht and Vigneresse 1999). The older and younger intrusive complexes are genetically not related to each other (J.L. Vigneresse, pers. comm.).

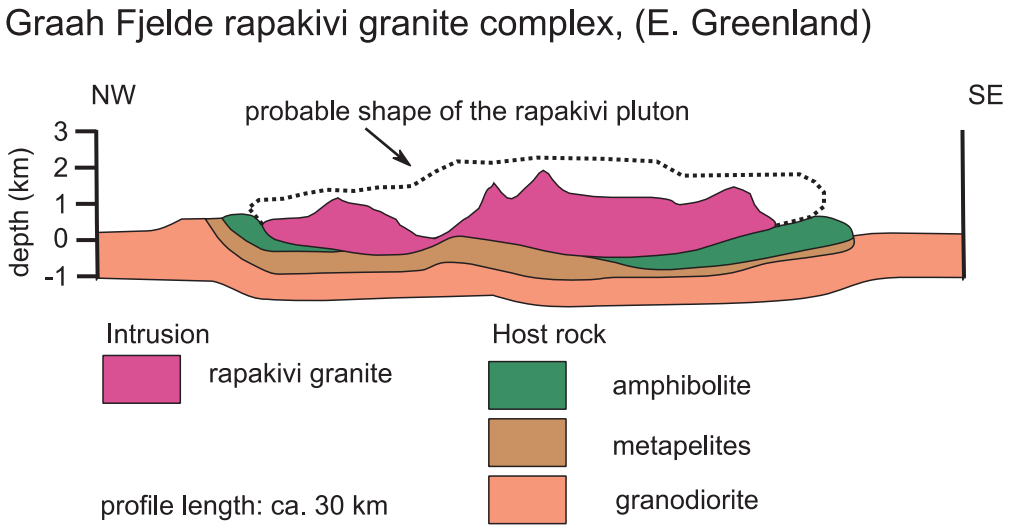

Fig. 4 Cross section through the Precambrian Graah Fjelde Rapakivi Granite (Greenland, redrawn from Garde et al. 2002).

al. 1999; Garde et al. 2002; Fig. 4). Grocott et al. (1999), Hecht and Vigneresse (1999) and Cruden et al. (1999) suggested floor depression by the inflowing magma due to its overpressure as the main emplacement mechanism for the Graah Fjelde, Fichtelgebirge and Dinkey Creek plutons, respectively. All three tabular intrusions named here follow the power-law for pluton proportions developed by McCaffrey and Petford (1997) and Petford and Clemens (2000). Plotting the thickness-length ratios of the Graah Fjelde, Fichtelgebirge and Dinkey Creek plutons, respectively (calculated based on the cross sections shown in Figs 2–4; see also Tab. 1) reveals that the Graah Fjelde and Fichtelgebirge plutons occur close to the "pluton" regression line and the Dinkey Creek pluton slightly below the "laccolith" regression line (Fig. 1). According to the interpretation of Petford et al. (2000) the Graah Fjelde and Fichtelgebirge plutons should be regarded as lopoliths emplaced by floor depression; and the Dinkey Creek pluton should then be interpreted as a laccolith emplaced by roof-uplift, although all three intrusive bodies plot quite close to the intersection of both the regression lines.

Tab. 1 Dimensions of the three presented plutons as taken from Figs 2–4, as well as of the two PDMS intrusions in the centrifuge model.

Natural examples	Thickness [km]	Length [km]
Dinkey Creek pluton	1.38	29.22
Fichtelgebirgs pluton	6.82	50.00
Graah Fjelde pluton	3.47	20.06
PDMS intrusions	Thickness [cm]	Length [cm]
Yellow phacolith, section 1	0.96	3.24
Yellow phacolith, section 2	1.08	3.50
Red phacolith, section 1	0.68	3.48
Red phacolith, section 3	0.75	4.00

3. The experiment

3.1 Motivation of the experiment

The three examples presented briefly above are only a small selection of tabular plutons, which are common features of the continental crust. They develop independently of their temporal, tectonic or rheological context, usually according to the same ascent and emplacement style, i.e. dyking, followed by sill formation and magma chamber inflation. According to McCaffrey and Petford (1997), their growth during emplacement is ruled by the power law (1.1). Consequently, also the dimensions of a growing pluton follow the power law (1.1): it lengthens more rapidly than it thickens.

Analogue modeling has proven to be an effective tool in studying geologic structures and processes (Koyi 1997). Here we present the results of an analogue centrifuge experiment, to test the viability of the proposed emplacement mechanisms for tabular plutons, in particular:

- how roof uplift and floor depression are linked to each other;
- whether floor depression is more typical of deep-seated and roof uplift more common of shallowly intruding tabular plutons;
- whether floor depression might hinder the filling and inflation of the magma chamber due to chocking of the magma source (provided the magma source is a horizontal layer of partially molten rock).

Moreover, we test the validity of the assumptions made by Petford et al. (2000) concerning the discrimination between (lopolithic) plutons and laccoliths based on power-law regression lines in length-thickness diagrams for intrusive bodies.

3.2 Setup of the experiment

The overall shape of the model was cylindrical with a diameter of 10 cm and 6.75 cm thick. The scaling factor for distances is 10^{-5} ($length_{model}$ / $length_{nature}$), i.e. 1 cm in the model corresponds to 1 km in nature (Tab. 2). As overburden material a semi-brittle plasticine (density $\rho = 1.71$ g/cm^3, viscosity $\mu = 4.2\times10^7$ Pa·s at a strain rate of 10^{-3} s^{-1}) was used, representing upper to middle crustal siliciclastic rocks ($\rho \approx 2.6$ g/cm^3 and $\mu \approx 10^{21}$ Pa·s). Polydimethylsiloxane (PDMS; $\rho = 0.964$ g/cm^3, $\mu = 4\times10^4$ Pa·s; Koyi 1991) played the role of the buoyant material, corresponding to a partially molten granitic magma ($\rho \approx 1.5$ g/cm^3, $\mu \approx 10^{18}$ Pa·s). The assumed crustal viscosity of 10^{21} Pa·s is quite low, but falls within the range of presumed viscosity values for crustal rocks of 10^{20} to 10^{23} Pa·s (Koyi et al. 1999). These estimated viscosity values for the upper and middle crust are based

Tab. 2 Dimensions and physical parameters of both the model and its natural counterpart as well as their ratios (t = thickness, ρ = density, μ = viscosity).

Scaling	**Model**	**Nature**	**Ratio (model/ nature)**
$t_{overburden}$ (red PDMS source layer)	3.2 cm	3.2 km	10^{-5}
$t_{overburden}$ (yellow PDMS source layer)	6.05 cm	6.05 km	10^{-5}
$t_{buoyant}$	0.5 cm	500 m	10^{-5}
$\rho_{overburden}$	1.71 g/cm^3	2.63 g/cm^3	6.5×10^{-1}
$\rho_{buoyant}$	0.964 g/cm^3	1.48 g/cm^3	6.5×10^{-1}
$\mu_{overburden}$	4×10^7 Pa•s	10^{21} Pa•s	4.2×10^{-14}
$\mu_{buoyant}$	4×10^4 Pa•s	10^{18} Pa•s	4.2×10^{-14}
g	6.87×10^3 m/s^2	9.81 m/s^2	7×10^2

on experimental determinations of effective viscosities for dry and wet quartzites at a temperature between 300 °C and 700 °C and at a geologically relevant strain rate of 10^{-14} s^{-1} (Weyermars 1997 and references therein), which gave effective viscosities between 10^{21} Pa·s (wet and hot quartzite) and 10^{23} Pa·s (dry and cold quartzite). On the other hand, the assumed viscosity of the partially molten granitic magma – calculated on the basis of the PDMS viscosity – is much too high compared to experimentally determined viscosity values of granitic magmas, which range between 10^{3} and 10^{12} Pa·s (Dingwell et al. 2000). However, applying proper scaling and using consequently fluids with very low viscosities, such as water ($\mu \approx 10^{-3}$ Pa·s) or olive oil ($\mu \approx 10^{-1}$ Pa·s) as magma analogues would lead to ascent and emplacement structures which are of unrealistic shape for granitic intrusive bodies (Ramberg 1981). As such, the presented model is only partially scaled to nature. However, the model is a first approximation to nature and focuses on the formation of tabular intrusions and the effects of floor depression and roof uplift on their ascent and emplacement in general.

Model stratigraphy included two buoyant layers of PDMS (5 mm thick each and with a volume of *c.* 40 cm^3 each) at the base and in the middle (3 cm high in the model stratigraphy) of the model. At the upper boundary of each buoyant layer a perturbation (1 cm × 1 cm × 0.7 cm) was introduced to trigger the formation of two intrusions. Of course, it is impossible to model with these two single intrusions exactly the incremental growth of a tabular pluton due to the continuous influx of magma. However, the presented model serves as a good proxy for the role roof uplift and floor depression play during the ascent into and the construction of a tabular granitoid body due to the rise of a single magma batch. The perturbation of the lower buoyant layer was placed in the centre of the model (5 cm from its rim), while the perturbation of the middle buoyant layer was shifted from the model's centre by 2.3 cm (Fig. 5). Both the perturbations were intended to act as pathways for the ascending buoyant material during centrifuging, in correspondence to the feeder dykes of tabular plutons. The horizontal offset between both the perturbations was designed to prevent the developing intrusive bodies to interact too much with each other. The overburden of both the buoyant layers was stratified consisting of five (above the lower buoyant layer) and eight (above the upper buoyant layer) differently coloured plasticine layers of 0.25 to 0.7 cm thick (Fig. 5).

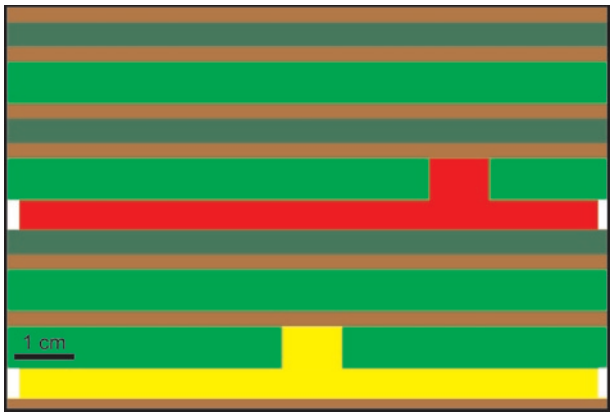

Fig. 5 Setup of the experiment. The yellow and red layers represent the buoyant PDMS, the light and dark green as well brown layers are the plasticine overburden.

3.3 Run of the experiment

The model was centrifuged in the small centrifuge of the Hans Ramberg Tectonic Laboratory (Uppsala University, Sweden) for *c.* 5 minutes at 700 G when a small bulge formed on top of the model directly above the perturbation of the middle buoyant layer. After photographing the top view with the small bulge on the model's surface (Fig. 6), the model was centrifuged for 20 more minutes at 700 G in order to see, whether in the current configuration the bulge on top of the model would increase or a second bulge would form. When no major changes happened after 25 minutes of centrifuging, the uppermost three plasticine layers – in total 0.9 cm of the overburden – were removed to thin the overburden and assist the rise of the buoyant material. The model was then centrifuged for further 5 minutes at 700 G. No major changes in the top view of the model occurred and the model was then sectioned in order to study it in detail.

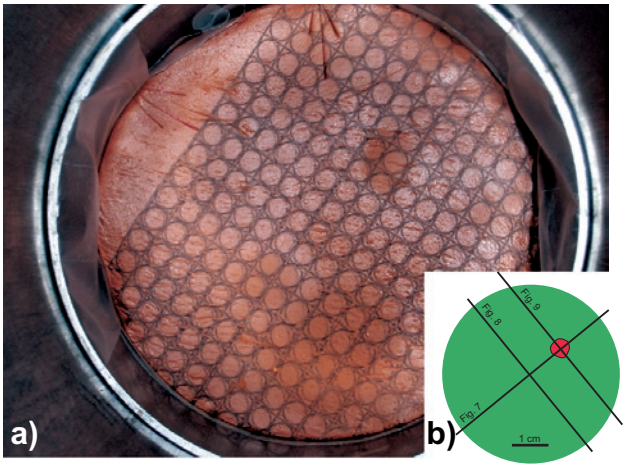

Fig. 6a – Top view of the model after 5 minutes of centrifuging at 700 G. The slight bulge northeast (with north at the top of the image) of the centre marks the location of the upper phacolith. The diameter of the model is 10 cm. **Inset b –** sketch of the photograph in Fig. 6a with the location of the red phacolith indicated by the red circular area above and to the right of the centre of the model (model surface in green); the lines indicate the positions of the sections presented in Figs 7–9.

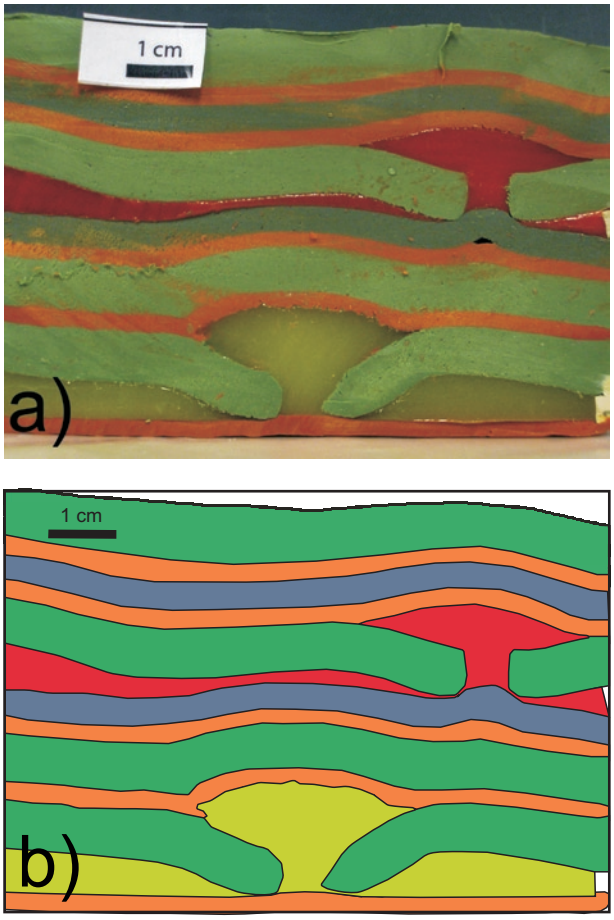

Fig. 7a – Section 1 through the model after 30 minutes of centrifuging at 700 G cutting both phacoliths: the red one in the upper part of the model and the yellow one in its lower part. **b –** line drawing of the section shown in Fig. 7a.

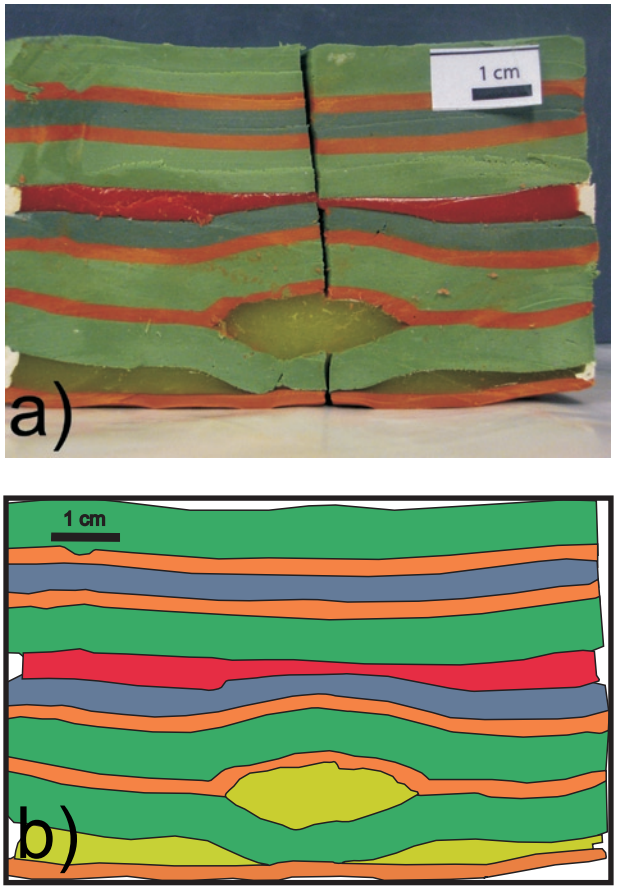

Fig. 8a – Section 2 – perpendicular to section 1 – through the model after 30 minutes of centrifuging at 700 G proofs the lensoidal shape of the yellow intrusive PDMS body. **b –** line drawing of the section shown in Fig. 8a.

3.4 Results of the experiment

A first vertical section in the middle of the model showed two tabular intrusive bodies that had formed directly above the perturbations along the interface between the buoyant layers and the overburden layers immediately overlying them (Fig. 7). Both the intrusions are characterized by a domed-up roof and a depressed floor, which is typical of phacoliths. The subsided floors of both PDMS bodies cut off the influx of the buoyant material from the source layers. The overburden units above the lower phacolith bulge into the middle buoyant layer, which accommodates the deformation by thinning (Fig. 7). The plasticine layers initially located directly above the buoyant layers, partly detach from the overlying overburden layers and subside in the immediate vicinity of the perturbations (Fig. 7). Moreover, the plasticine layer immediately beneath the perturbation of the upper buoyant layer is detached from its pad to form a small bulge (Fig. 7).

Two additional profiles (Figs 8 and 9), both perpendicular to the first one and carving each through one of the two buoyant intrusions, verified the phacolith nature of both bodies and helped to measure their dimensions and, in addition, calculate their volumes. The lower phacolith is between 3.24 and 3.5 cm in diameter, depending on which section is considered. Its maximum thickness lies between 0.96 and 1.08 cm. The upper phacolith is 3.48 to 4.00 cm long and 0.68 to 0.75 cm thick (Tab. 1). The volume of the tabular buoyant bodies was calculated according to the following equation (Bronstein and Semendjajew 1987):

$$V = 2\times(1/6)\pi\times h(3a^2+h^2) \qquad (2)$$

where h is half the height and a is half the diameter of the respective phacoliths.

Accordingly, the volume of the lower intrusion is between 4.06 and 5.34 cm^3 and the volume of the middle intrusion ranges between 3.29 and 4.77 cm^3.

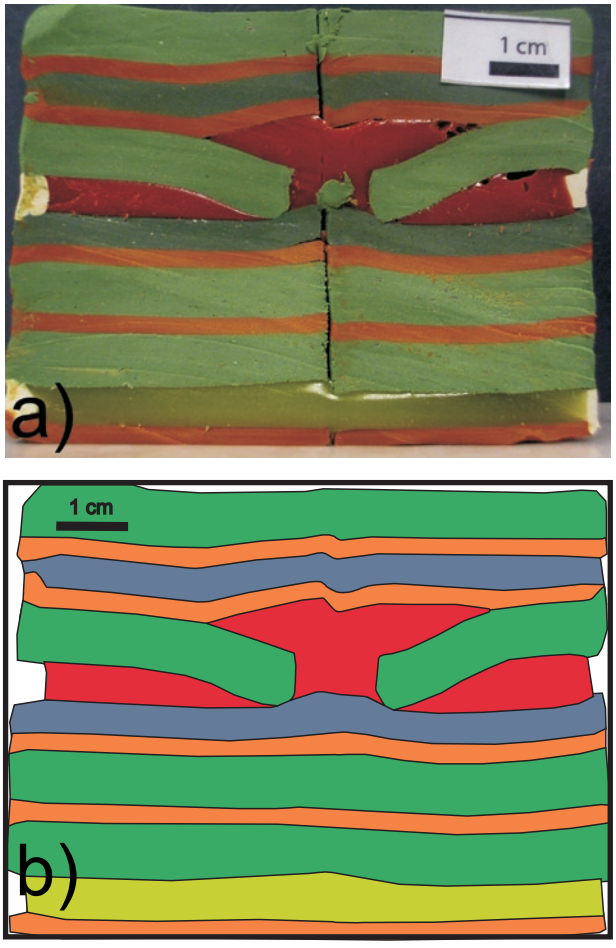

Fig. 9a – Section 3 – perpendicular to section 1 and parallel to section 2 – through the model after 30 minutes of centrifuging at 700 G proofs the lensoidal shape also of the red intrusive PDMS body. **b –** line drawing of the section shown in Fig. 9a.

4. Formation of both the phacoliths

As planned, the perturbation in the buoyant layers acted as pathways (or feeder dykes) for the buoyant material during centrifuging of the model. However, the buoyant material did not manage to rise through the plasticine overburden and instead spread laterally as sills along the interfaces between the two plasticine layers directly above the buoyant layers. With further centrifuging, additional material was transported buoyantly from the PDMS layer through the feeder dykes into the sills. The influx of new material led to inflation of the sills by vertical displacement of their roofs and floors. Thereby the plasticine above the developing phacoliths was deformed plastically within a distance of 1.5 to 2 cm, while the floors of the inflated intrusions were depressed by *c.* 0.5 cm. Additionally, the thin plasticine layer beneath the upper buoyant layer was sucked up into the conduit of the buoyant body by the upward moving buoyant material. On the other hand, subsidence of the bottom of the inflating sills choked the flow of further buoyant material into the feeder dykes and inhibited the further growth of the two phacoliths. Inflation of the lensoidal intrusives terminated after *c.* 5 min centrifuging when no increase of the bulge on the surface of the model was observed. Until then about 4 to 5 cm^3 of the buoyant material had been emplaced into the tabular intrusive bodies, i.e. the buoyant reservoirs had been depleted by 10 to 12.5 vol. %.

It can be excluded that the formation of both intrusive PDMS bodies through roof uplift and floor depression were influenced by boundary effects such as the relatively small volume of the sample box, because both lensoidal intrusions and their structural aureoles look very much alike irrespective from their relative position within the model and the sample box. Moreover, the total volume of the intrusions is only *c.* 10 cm^3, i.e. less than 2 % of the entire model volume (*c.* 530 cm^3).

5. Implications of the experiment for the emplacement of tabular plutons

Scaling the model to nature the lensoidal intrusive buoyant bodies would represent 1 km thick and 3 to 4 km long granitoid phacoliths (Tabs 1 and 2) that were emplaced at 3.2 km and 6.05 km depths, respectively, i.e. at different levels within the upper continental crust.

Both tabular intrusions formed – similar to what is known from their natural counterparts – along anisotropies within the model, i.e. along the interfaces between individual overburden layers. Corresponding anisotropies in nature are horizontal lithological contacts, foliation and fracture planes or shear zones.

The phacolithic shape of the intrusions suggests that space for their emplacement was made by both roof uplift and floor depression, independent of their intrusion depth. This observation contradicts the hypothesis of Cruden (1998) who suggested roof uplift to be only an important space-making process for plutons in the uppermost crust, while floor depression is responsible for the emplacement of all other, deeper-seated tabular plutons. We have to point out that the reason behind achieving roof uplift by the lower intrusion is because of the presence of another weak buoyant layer in the middle of the model stratigraphy. This weak layer enabled and accommodated the roof uplift at deeper level. In other words, in our model, similar to a shallow intrusive body, even the deeper intrusive body uplifted its roof. This was possible because the roof uplift of the deeper intrusion was accommodated by flow of the upper buoyant (viscous) layer. In practice, the mechanical thickness of the overburden units above the lower buoyant layer is relatively thin. The presence of the upper buoyant weak layer enables and accom-

modates roof uplift by the deeper intrusion. Absence of this shallow buoyant weak horizon would have resulted in a thicker overburden unit, which might not have been uplifted by a deep intrusion. Presence of layered intrusions may assist roof uplift even at deeper levels. The same is in principle true for floor depression which was facilitated by the presence of the two relatively low-viscous PDMS source layers beneath the two developing lensoidal PDMS intrusions.

Plotting the length and thickness data of the PDMS laccolith in the $\log_{length}$ vs. $\log_{thickness}$ diagram of Petford et al. (2000) with the regression lines for laccolith and tabular plutons (Fig. 1) the data pairs of both sections of the model appear close to the regression line for laccoliths. The model intrusions are definitely not laccolithic in shape and were, consequently, not only emplaced by roof uplift – as typical of laccoliths (Figs 7–9 and Tab. 1). On the contrary, they are biconvex in shape and were intruded by a combination of roof uplift and floor depression – as it is typical of phacoliths. Obviously, more data from nature and models – in particular reliable thickness data for granitoid bodies – are necessary to improve the regression lines which could then describe better the shape of different types of intrusions.

Displacement of the top and bottom sides of both the experimental tabular intrusions took place plastically. No brittle deformation or concentration of deformation along discrete fractures, faults or shear zones was observed as it might be the case for most natural lacco- lopo- or phacoliths (e.g. Bussel 1976; Dehls et al. 1998; Zimmerman 2005; Hacker et al. 2007).

The most prominent feature within the emplacement scenario of the model is the choking of the influx of buoyant material into the feeder dykes of both the phacoliths due to the floor depression of the inflating intrusive bodies. The source layer of the buoyant material was segmented by the subsiding overburden units and further flow into the intrusive body was inhibited. As such, the scenario presented by Cruden (1998), where the depression of the floor of an inflating tabular pluton will force the magma within its source region towards the conduit(s) of the growing pluton, does not apply to our model. We argue therefore that Cruden's (1998) idea depends on the initial geometry of the feeding magma source; a horizontal magma source, possibly a migmatitic layer within the Earth's crust would face the fate as the PDMS source layers of our model, whereas a magma source with an irregular geometry would most likely behave as Cruden (1998) proposed. Nevertheless, the "strangulation" of the buoyant-material supply in the model did not prevent the formation of the intrusive bodies, but restricted their growth to a volume of 4 to 5 cm^3 (reached within *c.* 5 minutes) and limited the depletion of the buoyant reservoir to *c.* 10 vol. %. Transferring these model observations to nature could mean that the size of tabular plutons and their growth rate are not only controlled by the volume of the reservoir and the rate of magma ascent and the magma's physical properties (T, μ, ρ), but also by the shape of the magma source region and, moreover, by the effectiveness of vertical, downward-directed material transfer to create space for the build-up of the pluton. Time of the model phacoliths (t_m) is scaled to nature (t_n) as follows (Ramberg 1981):

$$t_n = (t_m \times l_r \times \rho_r \times g_r) / \mu_r \qquad (3)$$

where l_r is the length ratio, ρ_r is the density ratio, g_r is the gravitational acceleration ratio and μ_r is the viscosity ratio between model and nature (for numbers see Tab. 2).

Even if the model is dynamically not properly scaled, because of the too high viscosity of the buoyant material compared to its overburden, time scaling based on the available numbers (Tab. 2) gives a rough estimate of the time span for the formation of a natural phacolith before its growth is stopped due to choking of the influx of more magma by floor depression.

In the model, it took *c.* 5 minutes to form a lensoidal intrusion of 4 to 5 cm^3 0.7 cm above the buoyant source layer. Accordingly, in nature a phacolith of 4 to 5 km^3, being emplaced 700 m above its source layer, would have formed within *c.* 1 Ma. This time span would be sufficient to emplace such small tabular plutons. Assuming a lower and more realistic viscosity of the magma (10^9 to 10^3 Pa·s, e.g. Clemens and Petford 1999) than that used in the model (10^{18} Pa·s) more voluminous tabular intrusive bodies could be built in a greater distance from the magma source layer within the same or even a shorter time. Ascent rates of magma through dykes are in the range of 10^6 to 10^7 metres/year (Delaney and Pollard 1981) and the lateral growth rate of a laccolith is assumed by Corry (1988) to be 200–300 metres/year in maximum. According to other authors (e.g. Scaillet et al. 1995; Hogan and Gilbert 1995; Cruden 1998; Petford and Clemens 2000) the construction of plutons of 10^2 to 10^4 km^3 takes 10^2 to 10^6 years. All these figures for rates of magma ascent through dykes and the formation of lensoidal, tabular plutons are in good agreement with the model results presented here.

In conclusion it can be stated that our model shows that roof uplift and floor depression are viable processes to form tabular plutons, but that floor depression might choke a horizontal and layered magma source, thus narrowing the time span for the build-up of a granitoid lopolith or phacolith.

Acknowledgements. The experiment described here was carried out during an international graduate course about pluton emplacement at Uppsala University in September

2006 with participants from Germany, Greece, Finland and Sweden. Therefore we would like to thank the students of this class – Z. Chemia, M. Dümmler, D. Geis, R. Kraus, T. Kravtsov, T. Laurila, M. Mertineit, R. Nyman, H. Oksanen, E. Piispa, M.D. Tranos, R. Unverricht, J. Woodard, K. Zarins – for building, running and discussing the model with us. Thanks are also due to J.L. Vigneresse and P. Závada for their helpful reviews which greatly improved the manuscript. HAK was funded by the Swedish Research Council. We are grateful to O. Jungmann for improving the figures.

References

Bussels MA (1976) Fracture control of high-level plutonic contacts in the Coastal Batholith of Peru. Proceed Geol Assoc 87: 237–246

Bronstein IN, Semendjajew KA (1987) Taschenbuch der Mathematik. Teubner, Leipzig, pp 1–840

Clemens JD, Petford N (1999) Granitic melt viscosity and silicic magma dynamics in contrasting tectonic settings. J Geol Soc, London 156: 1057–1060

Corry CE (1988) Laccoliths: Mechanics of Emplacement and Growth. GSA Spec Paper 220, Boulder, Colorado, pp 1–110

Cruden AR (1998) On the emplacement of tabular granites. J Geol Soc, London 155: 853–862

Cruden AR, Tobisch OT, Launeau P (1999) Magnetic fabric evidence for conduit-fed emplacement of a tabular intrusion: Dinkey Creek pluton, central Sierra Nevada batholith, California. J Geophys Res 104: 10 511–10 530

Dehls JF, Cruden AR, Vigneresse JL (1998) Fracture control of late Archean pluton emplacement in the northern Slave Province, Canada. J Struct Geol 20: 1145–1154

Delaney PT, Pollard, DD (1981) Deformation of host rocks and flow of magma during growth of minette dikes and breccia bearing intrusions near Ship Rock, New Mexico. USGS Prof Paper 1202, pp 1–61

Dingwell, DB, Hess, KU, Romano, C (2000) Viscosities of granitic (sensu lato) melts: influence of the anorthite component. Amer Miner 85: 1342–1348

Garde AA, Hamilton MA, Chadwick B, Grocott J, McCaffrey KJW (2002) The Ketilidian orogen of South Greenland: geochronology, tectonics, magmatism and fore-arc accretion during Palaeoproterozoic oblique convergence. Can J Earth Sci 39: 765–793

Grocott J, Garde AA, Chadwick B, Cruden AR, Swager C (1999) Emplacement of rapakivi granite and syenite by floor depression and roof uplift in the Palaeoproterozoic Ketilidian orogen, South Greenland. J Geol Soc, London 156: 15–24

Hacker DB, Petronis MS, Holm DK, Geissman JW (2007) Shallow level emplacement mechanisms of the Miocene Iron Axis Laccolith Group, Southwest Utah. GSA Rocky Mountain Section Annual Meeting Field Guide, pp 1–49

Hammarstrom JM, Zen E (1986): Aluminium in hornblende: an empirical igneous geobarometer. Amer Miner 71: 1297–1313

Hecht L, Vigneresse JL (1999) A multidisciplinary approach combining geochemical, gravity and structural data: implications for pluton emplacement and zonation. In: Castro A, Fernandez C, Vigneresse JL (eds) Understanding Granites: Integrating New and Classical Techniques. Geol Soc London Spec Publ 168: pp 95–110

Hogan JP, Gilbert MC (1995) The A-type Mount Scott Granite sheet: importance of crustal magma traps. J Geophys Res 100: 15 779–15 792

Koyi HA (1991) Mushroom diapirs penetrating into high viscous overburden. Geology 19: 1229–1232

Koyi HA (1997) Analogue modelling; from a qualitative to a quantitative technique, a historical outline. J Petrol Geol 20: 223–238

Koyi HA, Milnes AG, Schmeling H, Talbot CJ, Juhlin C, Zeyen H (1999) Numerical models of ductile rebound of crustal roots beneath mountain belts. Geophys J Int 139: 556–562

McCaffrey KJW, Petford N (1997) Are granitic intrusions scale invariant? J Geol Soc, London 154: 1–4

O'Brien P (2000) The fundamental Variscan problem: high-temperature metamorphism at different depths and high-pressure metamorphism at different temperatures. In: Franke W, Haak V, Oncken O, Tanner D (eds) Orogenic Processes: Quantification and Modelling in the Variscan Belt. Geol Soc London Spec Publ 179: 369–386

Petford N, Clemens JD (2000) Granites are not diapiric! Geol Today 16: 180–184

Petford N, Cruden AR, McCaffrey KJW, Vigneresse JL (2000) Granite magma formation, transport and emplacement in the Earth's crust. Nature 408: 669–673

Ramberg, H (1981) Gravity, Deformation and the Earth's crust. 2nd edition. Academic Press, London, pp 1–452

Rosenberg CL, Berger A, Schmid SM (1995) Observations from the floor of a granitoid pluton: inferences on the driving force of final emplacement. Geology 23: 443–446

Scaillet B, Pecher A, Rochette P, Champenois M (1995) The Gangotri granite (Garhwal Himalaya): laccolithic emplacement in an extending collisional belt. J Geophys Res 100: 585–608

Weyermars, R (1997) Principles of Rock Mechanics. Alboran Science Publishing, Amsterdam, pp 1–360

Zimmerman, NM (2005) Host rock fracture analysis: applying the deformation mechanics associated with shallow igneous intrusion to the fracture bridging theory, McKinney Hills Laccolith, Big Bend National Park. Master's thesis, Texas Tech University, Lubbock. Available electronically from http://hdl.handle.net/2346/1286

Journal of Geosciences, 53 (2008), 263–280 DOI: 10.3190/jgeosci.035

Original paper

Contrasting crustal sources for peraluminous granites of the segmented Montes de Toledo Batholith (Iberian Variscan Belt)

Carlos VILLASECA[1*], Cecilia PÉREZ-SOBA[1], Enrique MERINO[1], David OREJANA[1], José A. LÓPEZ-GARCÍA[2], Kjell BILLSTROM[3]

[1] *Department of Petrology and Geochemistry, Centro mixto UCM-CSIC, Faculty of Geological Sciences, Complutense University, 28040 Madrid, Spain; granito@geo.ucm.es*

[2] *Department of Crystallography and Mineralogy, Faculty of Geological Sciences, Complutense University, 28040 Madrid, Spain*

[3] *Swedish Museum of Natural History, Box 50007, 104 05 Stockholm, Sweden*

[*] *Corresponding author*

The Variscan Montes de Toledo Batholith (MTB) is an E–W linear array of peraluminous granite plutons which is chemically segmented. The study is focused on the western segment of the MTB (W-MTB), mainly composed of granites with slightly lower CaO and higher P_2O_5 contents than associated eastern plutonic units and nearby S-type granites, giving them a more pronounced peraluminous nature. The chemical contrast is also observed in isotopic composition, especially in radiogenic Nd and Pb ratios. The W-MTB granites have higher initial ε_{Nd} (–5.0 to –5.9) and lower $^{206}Pb/^{204}Pb$ and $^{208}Pb/^{204}Pb$ ratios than peraluminous types from the E-MTB segment. A mixed pelitic–greywackeous derivation from regional Neoproterozoic formations is suggested, whereas lower crustal and meta-igneous sources were involved in the origin of the easternmost MTB granites. The presence of igneous muscovite together with coexisting andalusite and sillimanite in some of the studied granites suggests that solidus was reached at 650–700 ºC and depth corresponding to the pressure of 2–3 kbar.

Keywords: peraluminous granites, andalusite, sillimanite, Sr-Nd-Pb isotopes, Iberian Variscan Belt
Received: 19 September 2008; accepted 22 December 2008; handling editor: D. Dolejš

1. Introduction

The petrogenesis of strongly peraluminous granitoids has attracted attention of petrologists since early demonstration that granitic melts from which aluminium silicates can crystallize have been experimentally produced (e.g. Green 1976; Clemens and Wall 1981). Additionally, aluminium silicates have been found as unambiguous magmatic phenocrysts in volcanic rocks (e.g. Pichavant et al. 1988). The main problems in deciphering origin of peraluminous granites include: i) nature of the protolith, ii) incorporation of restites and presence of inherited components, iii) contamination during magma transport and emplacement, iv) superimposed magma differentiation processes (crystal fractionation, magma mixing, volatile exsolution, etc.), and v) pressure and temperature conditions during magma generation and crystallization.

The Variscan Iberian Belt is a sector of the European Variscides which is mainly composed of large granitic batholiths, particularly in its innermost area, that is, in the Central Iberian Zone (Fig. 1). Granitoids in this area constitute more than one third of the outcrops, and form one of the largest batholithic masses in the World. These granite plutons are predominantly peraluminous; metaaluminous varieties and related basic rocks are extremely scarce (e.g. Capdevila et al. 1973; Villaseca et al. 1998a; Bea et al. 1999). Most of these Variscan batholiths are complex assemblages where peraluminous and the more scarce metaluminous granite varieties appear together (e.g. Villaseca and Herreros 2000). The studied Montes de Toledo Batholith (MTB) is a large batholithic array (around 200 km long) exclusively composed of peraluminous plutonic units (Fig. 1). Nevertheless, distinct compositional differences between the western and eastern plutonic units suggest contrasting granite sources that gave rise to a chemically segmented granite batholith.

The existence of such a huge volume of peraluminous granitoids in the Variscan Iberian Belt has triggered extensive discussion about its genesis. Petrogenetic theories vary from i) important mantle input to its present-day composition, either by mixing (e.g. Dias and Leterrier 1994; Moreno Ventas et al. 1995) or by assimilation (e.g. Castro et al. 1999), to ii) mainly crustal recycling either by melting at mid-crustal levels (Bea et al. 2003) or by lower crustal derivation (Villaseca et al. 1999). Furthermore, it is difficult to assign S-type, I-type or transitional affinity to plutons with different degree of peraluminosity (e.g. Villaseca et al. 1998a).

In this paper we focus on the strongly peraluminous western segment of the Montes de Toledo Batholith,

which has a clear S-type affinity. Most of the studied granites contain peraluminous minerals (andalusite, sillimanite, cordierite, muscovite, Al-rich biotite, tourmaline, etc.). The abundance of restite enclaves poses the problem of restite fractionation vs. other petrogenetic scenarios. This work provides mineralogical, geochemical and, for the first time, Sr-Nd-Pb isotopic information to motivate discussion on granite sources in this compositionally segmented peraluminous batholith.

2. Geological setting

The Montes de Toledo Batholith (MTB) is a linear array of approximately twenty granite plutons that is ~200 km long and 20 km wide (in a W–E direction) from Belvís de Monroy (Cáceres) to Madridejos (Toledo), and occupies an area of about 2000 km^2 (Fig. 1). The best outcrop areas of this elongate granite batholith are their western and eastern segments, respectively, because its central part only crops out in deeply eroded river valleys. There the MTB is covered by Triassic sediments of the Tajo Basin and by coarse-grained alluvial fans from the Montes de Toledo Heights.

This plutonic array intruded into low-grade Neoproterozoic and Lower Palaeozoic metasedimentary rocks and generated remarkable contact metamorphic aureoles (IGME 1985, 1987, 1989). These units consist of alternating sandstone and shale, more than 4000 m thick, with interbedded conglomerate, calcareous mudstone and limestone of the so called "Schist–Greywacke Formation", which is of Cambrian age in its upper part (Valdelacasa or Pusa Group – Valladares et al. 2002; Liñán et al. 2002). It is important to note the high phosphorous content of some metasediments in either Neoproterozoic or Lower Cambrian series (IGME 1987, 1989). The MTB cross-cuts a set of open antiforms and synforms with NW–SE trending axes, related to the Variscan D_1 compressional event (Ábalos et al. 2002). D_2 and D_3 structures are rare in the area although a conjugate system of NW–SE to NNW–SSE trending strike-slip dextral shear zones (D_3 phase) has been described (Ábalos et al. 2002).

The granitic MTB has been studied in detail in its eastern sector, that is, the Mora-Las Ventas Plutonic Complex, where an exhaustive petrological study (mineral chemistry, whole-rock geochemistry and Sr-Nd isotopes) has been performed (Andonaegui 1990; Villaseca et al. 1998a; Andonaegui and Villaseca 1998). The post-tectonic peraluminous S-type granites from the eastern MTB sector have been interpreted as derived from felsic meta-igneous sources (mainly from lower crustal levels), because outcropping metamorphic rocks and metasedimentary protoliths from low to middle and upper crust have a clearly different isotopic composition (Villaseca et al. 1998a; 1999). A preliminary Rb-Sr geochronological study gave an intrusion age of 320 ± 8 Ma (Andonaegui 1990). This age has to be considered with caution as the Variscan D_3 phase has been dated to 313 to 325 Ma elsewhere in the Central Iberian Zone (CIZ) (Dias et al. 1998; Fernández-Suárez et al. 2000).

The western MTB segment studied in the present work comprises seven granitic plutons (Fig. 1) which were only incompletely described in the literature (IGME 1985, 1987, 1989). Nevertheless, some preliminary petrological studies on the Aldeanueva de Barbarroya Pluton have been performed (Andonaegui and Barrera 1984), and the presence of two aluminium silicates (andalusite and sillimanite) in granites of this western segment of the MTB has been previously noted (Andonaegui and Barrera 1984; Fernández-Catuxo et al. 1995).

3. Analytical techniques

The major-element mineral compositions have been analysed at the Centro de Microscopía Electrónica "Luis Bru" (Complutense University of Madrid) using a Jeol JXA-8900 M electron microprobe with four wavelength dispersive spectrometers. Analytical conditions were an accelerating voltage of 15 kV, an electron beam current of 20 nA, and a beam diameter of 5 μm. Elements were counted for 10 s on the peak and 5 s on each background position. Corrections were made using the ZAF method. Representative major-element compositions of granite minerals are listed in Tables 1 to 3.

The whole-rock major- and trace-element compositions were analysed at Actlabs (Ancaster, Ontario, Canada). The powdered samples were melted using $LiBO_2$ and dissolved in HNO_3. The solutions were analysed by inductively coupled plasma atomic emission spectrometry (ICP-AES) for major elements whereas trace elements were determined by ICP mass spectrometry (ICP-MS). Uncertainties in major elements are bracketed between 1 and 3 %, except for MnO (5–10 %). The precision of ICP-MS analyses at low concentration levels has been evaluated from repeated analyses of the international standards BR, DR-N, UB-N, AN-G and GH. The precision for Rb, Sr, Zr, Y, V, Hf and most of the REE is in

⇨

Fig. 1a – Sketch map of the Variscan Iberian Belt showing the location of the major granitic batholiths. Granite batholiths mentioned in the text are: Al = Albalá, A = Alburquerque, CA = Cabeza de Araya, G = Gata, J = Jálama, MV = Mora-Ventas, TD = Tormes Dome; granite cupolas are: P = Pedroso de Acim, T = Trujillo, Tr = El Trasquilón. **b** – Granite plutons of the western segment of the Montes de Toledo Batholith (W-MTB) with sample locations.

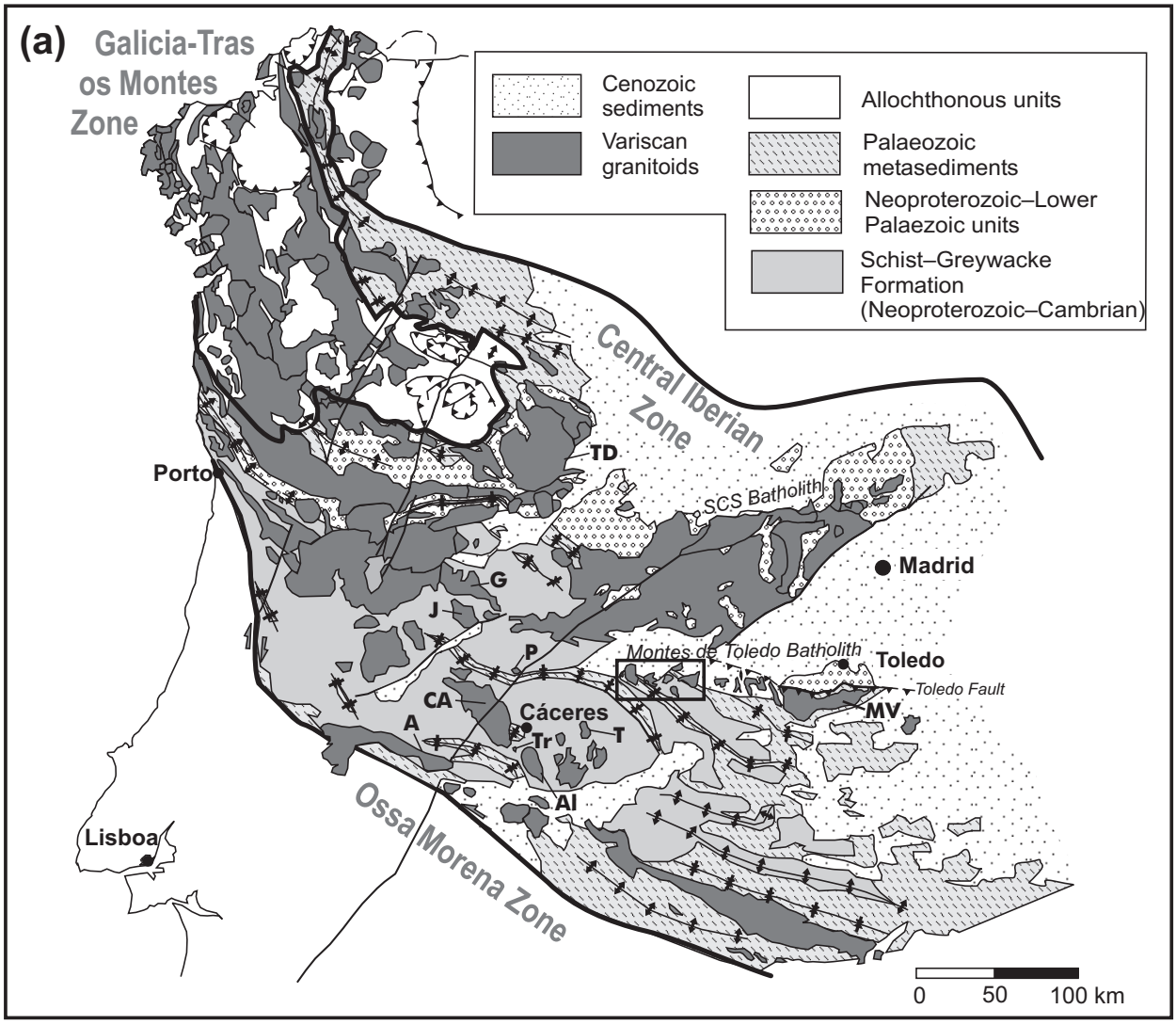
(a)
Galicia-Tras os Montes Zone
Cenozoic sediments
Variscan granitoids
Allochthonous units
Palaeozoic metasediments
Neoproterozoic–Lower Palaeozoic units
Schist–Greywacke Formation (Neoproterozoic–Cambrian)
Central Iberian Zone
Ossa Morena Zone
Porto
Lisboa
Madrid
Toledo
Toledo Fault
Montes de Toledo Batholith
SCS Batholith
TD
G
J
P
CA
A
Cáceres
Tr
T
MV
Al
0
50
100 km

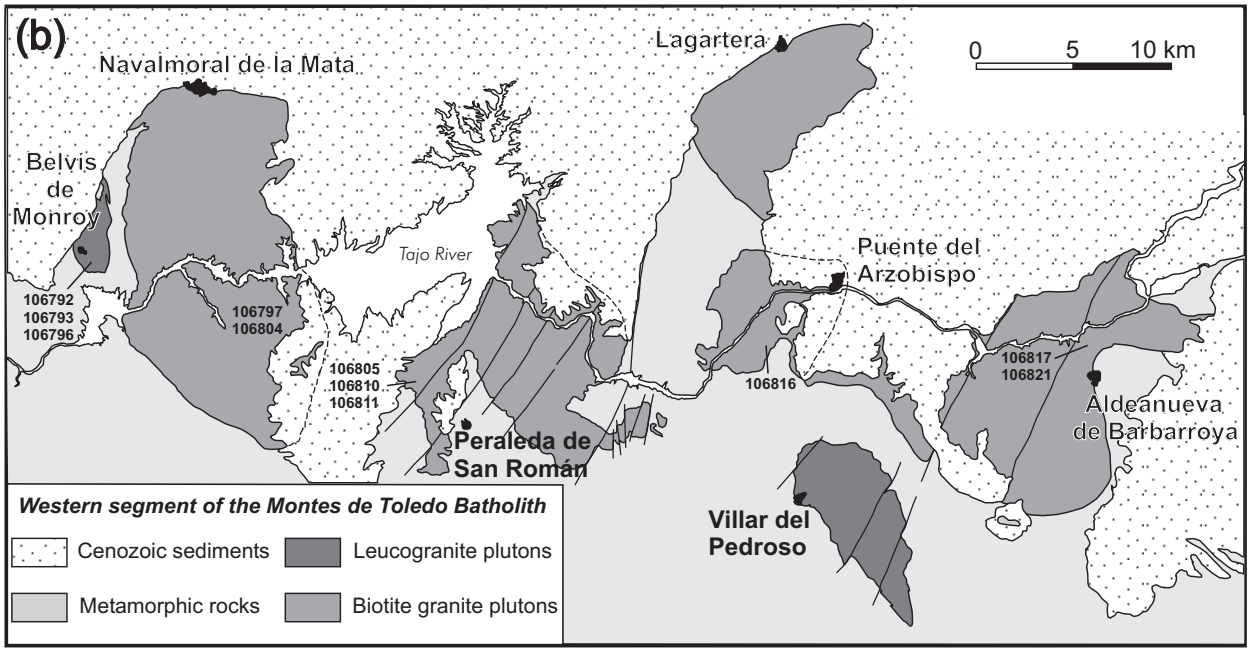
(b)
Navalmoral de la Mata
Lagartera
0
5
10 km
Belvis de Monroy
Tajo River
Puente del Arzobispo
106792
106793
106796
106797
106804
106805
106810
106811
106816
106817
106821
Aldeanueva de Barbarroya
Peraleda de San Román
Villar del Pedroso
Western segment of the Montes de Toledo Batholith
Cenozoic sediments
Leucogranite plutons
Metamorphic rocks
Biotite granite plutons

the range 1 to 5 % whereas it varies from 5 to 10 % for other trace elements including Tm. Some samples have concentrations of several elements below detection limits (V: 5, Cr: 20, Sc: 1 ppm) and all the granites have Ni < 20 ppm. More information on the procedure, precision and accuracy of the Actlabs ICP-MS analyses can be found at *http://www.actlabs.com*.

The Sr-Nd isotopic analyses were carried out at the CAI de Geocronología y Geoquímica Isotópica, at the Complutense University of Madrid, using an automated VG Sector 54 multicollector thermal ionisation mass spectrometer. Analytical data were acquired in multidynamic mode. The analytical procedures used in this laboratory have been described elsewhere (Reyes et al. 1997). Repeated analyses of the NBS 987 standard gave $^{87}Sr/^{86}Sr$ = 0.710234 ± 30 (2σ, n = 12) and for the JM Nd standard the values of $^{143}Nd/^{144}Nd$ = 0.511854 ± 3 (2σ, n = 63) were obtained. The 2σ error on ε_{Nd} calculation is ± 0.3.

One whole-rock granite (from the eastern MTB) and K-feldspar separates from three peraluminous granites (one from the western MTB and two from the Spanish Central System) were selected for Pb isotopic analyses at the Swedish Museum of Natural History (Stockholm) using a Finnigan MAT 261 TIMS with multicollector detection. The samples were dissolved with HF and HNO_3 and a ^{205}Pb spike was added to each of them. Lead was separated using cation exchange columns. The NBS 981 and 982 standards were used to evaluate instrumental fractionation and precision, the latter being about 0.1 % for the isotopic ratios shown. Repeated analyses of international standard BCR-1 were used to monitor the accuracy.

4. Petrography

This study is mainly focused on five granite plutons cropping out from W to E in the following order: Belvís de Monroy, Navalmoral de la Mata, Peraleda de San Román, Puente del Arzobispo and Aldeanueva de Barbarroya (Fig. 1). Sample locations are shown in Fig. 1. Three samples of two-mica leucogranite were taken from the Belvís de Monroy Pluton, and they represent the most fractionated granite in this study. Samples from the Navalmoral de la Mata Pluton are biotite granites with variable amounts of K-feldspar megacrysts, whereas biotite granites from the Puente del Arzobispo Pluton are more equigranular and include leucocratic varieties. The granites sampled from the Peraleda Pluton are slightly more mafic and have Al-rich minerals such as pinnitized cordierite and two aluminium silicates (andalusite and sillimanite). The fine-grained granodioritic facies of the Aldeanueva Pluton (also with Al-rich mineral phases) was only sampled for mineral chemistry, but the whole-rock major-element chemical data from Andonaegui and Barrera (1984) have been considered in the geochemistry section for comparison.

All studied granites are peraluminous in composition and most of them have quartz, plagioclase, K-feldspar and biotite as major rock-forming minerals. Biotite is the main mafic mineral in the studied granites; its amount varies from approx. 20 vol. % (Aldeanueva granodioritic facies) to 1–5 vol. % (Belvís leucogranite). In the last mentioned two-mica leucogranite pluton, muscovite dominates over biotite.

Accessory amounts of cordierite, aluminium silicates, muscovite, tourmaline, apatite, zircon, monazite, ilmenite and xenotime appear in the MTB granites. It is interesting to note the presence of two polymorphs of the Al_2SiO_5 in two granite plutons, Peraleda and Aldeanueva, in which a clear textural evolution from andalusite to sillimanite is observed, rarely described in the literature.

The studied granites host different amounts of metasedimentary and restitic xenoliths, and locally some igneous felsic microgranular enclaves of cognate appearance, but they never contain mafic microgranular enclaves. The crustal xenoliths could be described as: i) metapsammitic xenoliths, ii) refractory metapelitic xenoliths, iii) surmicaceous enclaves, iv) globular quartz, and v) K-feldspar-rich lumps. Such a suite of metasedimentary lithologies is typical of S-type granites (Chappell et al. 1987; Barbero and Villaseca 1992). These inclusions are rarely larger than 25 cm in size, usually around 2–10 cm, and could locally define enclave-rich sectors or contaminated facies.

5. Mineral chemistry

Plagioclase composition in studied granites ranges between An_{35} and An_{05}, reaching albite in the leucogranites from the Belvís de Monroy Pluton (Fig. 2a). Zoning is poorly developed, but the most An-rich analyses are usually found in core zones. The P_2O_5 contents increase with the Na contents of the plagioclase, those from Belvís leucogranites show the highest concentrations (up to 0.91 wt. %) (Fig. 2b). Plagioclase from granites of this MTB western sector is richer in P than that from other peraluminous S-type granites of central Spain (Fig. 2b).

K-feldspar is weakly perthitic. Its composition varies between Or_{100} and Or_{78}, being more Ab-rich in the Peraleda Pluton (Tab. 1). The P_2O_5 content is also high in the Belvís leucogranites (up to 0.92 wt. %), exceeding concentrations in the perphosphorous Pedrobernardo granite from the Spanish Central System (SCS) (Bea et al. 1994) (Fig. 2c).

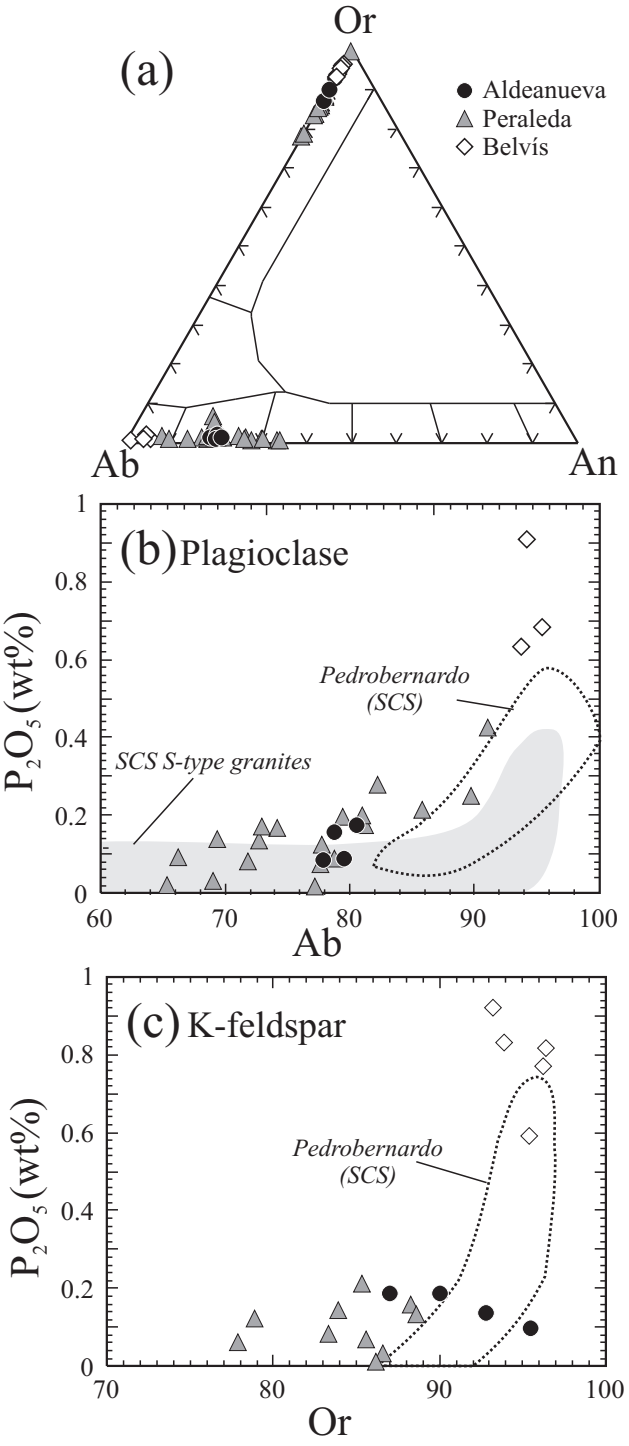

Fig. 2 Composition of feldspars from the W-MTB granites. **a** – Ternary Ab-Or-An diagram. **b** – Plagioclase composition: P_2O_5 *vs* Ab. **c** – K-feldspar composition: P_2O_5 *vs* Or. Fields for feldspars from the perphosphorous SCS Pedrobernardo Pluton are from Bea et al. (1994), whereas plagioclase from SCS S-type granites are from Villaseca et al. (unpublished data).

Biotite appears as subhedral crystals rich in mineral inclusions, usually accessory phases (Fig. 3a). It has Al-rich composition, and plots in peraluminous fields in biotite classification diagrams (e.g. Nachit et al. 1985; Abdel-Rahman 1994) similarly to other biotites from the SCS S-type granites (Fig. 4a). Biotite from the most felsic pluton of the MTB (the Belvís leucogranite) shows the highest Al and F contents (and, concomitantly, the lowest Mg and Ti contents) (Tab. 2).

Muscovite appears in most of the granites as late-magmatic anhedral crystals, sometimes rimming aluminium silicate grains, and usually in accessory amounts only. Nevertheless, in the Belvís leucogranites muscovite is the main mica, with larger size than associated biotite (Fig. 3b). In this two-mica leucogranite, muscovite crystals are remarkably euhedral (Fig. 3b). In granites where biotite dominates over muscovite, the larger muscovite crystals are those forming monocrystalline rims around andalusite, and are interpreted as magmatic according to the textural criteria reviewed by Clarke et al. (2005). There are no significant chemical differences between different textural types of muscovite and they all plot within igneous muscovite fields (Fig. 4b), including the fine-grained and flaky crystals of late-to-postmagmatic appearance. Similarly to biotite, muscovite of the Belvís leucogranites shows the highest F contents in the MTB (up to 0.86 wt. %) (Tab. 2).

Cordierite is usually strongly transformed to secondary pinnite aggregates. Only in the fine-grained granodiorites of the Aldeanueva Pluton it appears as unaltered euhedral crystals of medium to coarse grain size (up to 2 cm), hosting inclusions of quartz, biotite and scarce sillimanite. This suggests a non-cotectic growth but rather reaction with restitic or xenocrystic minerals immersed in the granite magma (similar to the CG1 type of Erdmann et al. 2004). Cordierite from the Aldeanueva Pluton has an X_{Mg} of *c.* 0.57 with relatively low Mn and Na contents, although high enough to plot within the igneous field defined by the SCS cordierite-bearing granites (Fig. 5).

Andalusite appears as inclusions-free euhedral crystals of medium size in the Peraleda and Aldeanueva granites (Fig. 3c–d). It is of late-magmatic origin, occasionally closely associated with Ab-rich margins of plagioclase crystals. It seems to have crystallized close to magma solidus conditions as is the case of many andalusite-bearing granites (Clarke et al. 2005). Andalusite has a thin rim of muscovite, but it maintains its original shape. Occasionally it shows a thin rim of fibrolitic sillimanite (always less than 100 μm) and an outer muscovite rim (Fig. 3c–d). Andalusite may show chemical zoning characterized by outward decreasing FeO content, in the range of 0.58 to 0.23 wt. % (Fig. 6). This chemical zoning is less pronounced than in andalusites from other felsic

Tab. 1 Selected representative EMP analyses of feldspars from the W-MTB granites

Sample	106795	106795	106795	106795	106795	106809	106809	106810	106809	106814	106814	106821	106821	106817	106821
Analysis	45	55	77	79	82	57	61	92	60	35	24	38	43	70	86
Pluton	Belvís					Peraleda						Aldeanueva			
Mineral	Pl	Pl	Pl	Kfs	Kfs	Pl	Pl	Pl	Kfs	Kfs	Kfs	Pl	Pl	Kfs	Kfs
SiO_2	65.66	64.98	65.57	62.53	62.34	66.47	62.31	58.75	64.50	64.63	65.91	62.64	62.84	63.46	63.93
TiO_2	0.02	0.35	0.00	0.01	0.03	0.00	0.00	0.04	0.00	0.00	0.00	0.01	0.00	0.01	0.03
Al_2O_3	20.60	20.94	21.17	18.92	19.60	20.87	24.31	26.17	18.78	18.92	19.34	23.46	23.33	19.07	19.15
FeO	0.03	0.00	0.00	0.00	0.03	0.03	0.05	0.00	0.01	0.00	0.09	0.00	0.04	0.00	0.01
MnO	0.00	0.04	0.00	0.00	0.01	0.04	0.08	0.00	0.04	0.03	0.00	0.00	0.00	0.00	0.02
MgO	0.00	0.00	0.04	0.00	0.00	0.02	0.01	0.00	0.00	0.01	0.00	0.01	0.00	0.00	0.01
CaO	1.08	0.71	0.74	0.00	0.00	1.55	5.55	6.96	0.00	0.04	0.00	4.08	4.20	0.02	0.06
Na_2O	10.59	10.05	11.00	0.42	0.76	10.70	8.53	7.73	1.27	1.83	2.53	9.19	8.75	0.79	1.41
K_2O	0.16	0.35	0.20	16.13	15.85	0.29	0.21	0.15	14.67	14.02	13.58	0.33	0.24	15.88	14.67
P_2O_5	0.64	0.91	0.69	0.77	0.92	0.43	0.14	0.10	0.16	0.08	0.06	0.16	0.09	0.14	0.19
Total	98.00	98.41	99.48	98.78	99.55	100.42	101.31	99.95	99.53	99.75	101.59	99.96	99.52	99.43	99.51
Ab	93.80	94.20	95.40	3.80	6.80	91.10	72.70	66.20	11.70	16.50	22.10	78.80	77.90	7.00	12.70
An	5.30	3.70	3.50	0.00	0.00	7.30	26.10	33.00	0.00	0.20	0.00	19.30	20.70	0.10	0.30
Or	0.90	2.20	1.10	96.20	93.20	1.60	1.20	0.80	88.30	83.30	77.90	1.90	1.40	92.80	87.00

Tab. 2 Selected representative EMP analyses of micas from the W-MTB granites

Sample	106795	106795	106795	106795	106795	106809	106809	106809	106809	106809	106809	106817	106817	106821	106821
Analysis	52	75	47	49	50	68	12	4	11	3	5	66	74	34	89
Pluton	Belvís					Peraleda						Aldeanueva			
Mineral	Bt	Bt	Ms	Ms	Ms	Bt	Bt	Bt	Ms	Ms	Ms	Bt	Bt	Ms	Ms
SiO_2	35.84	35.63	46.02	45.63	46.23	35.17	35.50	36.25	45.66	46.03	44.50	34.65	34.85	46.66	45.83
TiO_2	2.01	1.89	0.50	0.43	0.35	2.98	2.56	2.52	1.11	0.29	0.56	2.63	2.93	0.09	0.17
Al_2O_3	22.53	22.28	35.88	35.65	36.00	19.05	19.47	19.20	35.30	35.52	38.32	19.80	19.61	37.07	36.73
FeO	19.10	20.30	1.51	1.41	1.38	20.66	18.05	18.19	0.73	1.03	0.54	19.96	18.43	1.13	0.79
MnO	0.23	0.14	0.00	0.02	0.00	0.25	0.13	0.16	0.03	0.01	0.00	0.24	0.24	0.00	0.01
MgO	4.10	3.02	0.65	0.77	0.64	7.54	8.21	8.62	0.65	0.69	0.51	7.44	7.83	0.83	0.67
CaO	0.01	0.00	0.01	0.00	0.01	0.02	0.00	0.00	0.00	0.07	0.03	0.00	0.00	0.01	0.01
Na_2O	0.07	0.08	0.58	0.72	0.74	0.13	0.19	0.13	0.57	0.70	0.52	0.11	0.19	0.59	0.55
K_2O	9.55	9.42	9.59	9.80	9.45	9.50	9.59	9.57	10.62	10.76	9.91	9.61	9.55	9.90	10.06
F	1.17	0.81	0.73	0.72	0.76	0.00	0.25	0.28	0.16	0.19	0.12	0.40	0.48	0.11	0.12
Total	94.66	93.65	95.56	95.21	95.67	95.43	94.08	95.08	94.92	95.30	95.05	94.95	94.19	96.40	94.98
Mg/(Fe+Mg)	0.28	0.21	0.48	0.53	0.49	0.39	0.45	0.46	0.65	0.58	0.66	0.40	0.43	0.61	0.64

granites of the Central Iberian Zone (CIZ) or from the granite pegmatites (Fernández-Catuxo et al. 1995; Clarke et al. 2005) (Fig. 6).

Sillimanite only appears in andalusite-bearing granites, and mostly forms thin rims surrounding andalusite. Nevertheless, a second textural sillimanite type in these granites is the one associated with mica-rich enclaves or aggregates or even included in cordierite crystals as described previously (restites?). Sillimanite formed by andalusite transformation is invariably fibrolitic. Chemi-

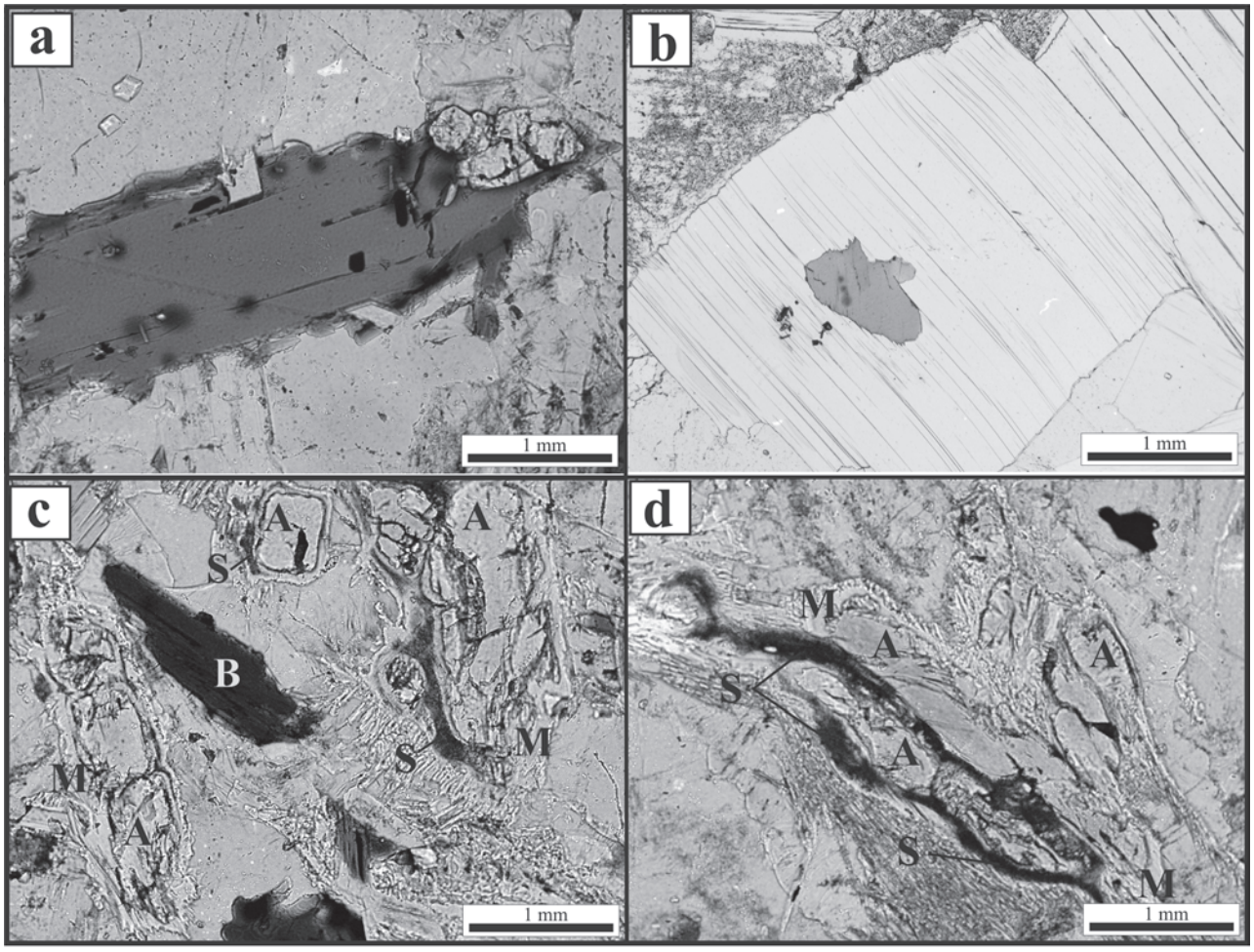

Fig. 3 Photomicrographs of granites from the W-MTB. **a** – Inclusion-rich subhedral biotite crystal (106810 Peraleda granite). **b** – Large euhedral muscovite crystal enclosing biotite (106795 Belvís leucogranite). **c–d** – Andalusite crystals (A) rimmed by fibrolitic sillimanite (S) and muscovite (M) (106809 and 106810 Peraleda granites, respectively).

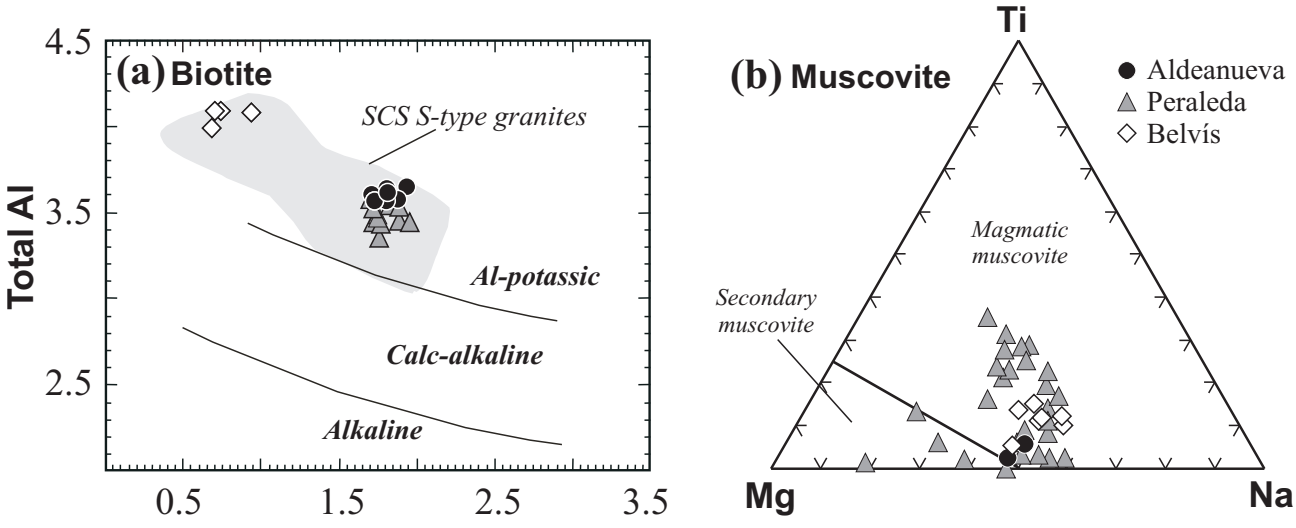

Fig. 4 Composition of micas from the W-MTB granites. **a** – Al_T *vs* Mg (atoms per 22 O) diagram for biotite. Biotite compositional fields from different magmatic series are taken from Nachit et al. (1985). Biotite compositional field of peraluminous S-type granites from the Sierra de Guadarrama (SCS granites) is taken from Villaseca and Barbero (1994). **b** – Mg-Ti-Na (atoms per 22 O) diagram for muscovite. Magmatic and secondary muscovite fields are taken from Miller et al. (1981).

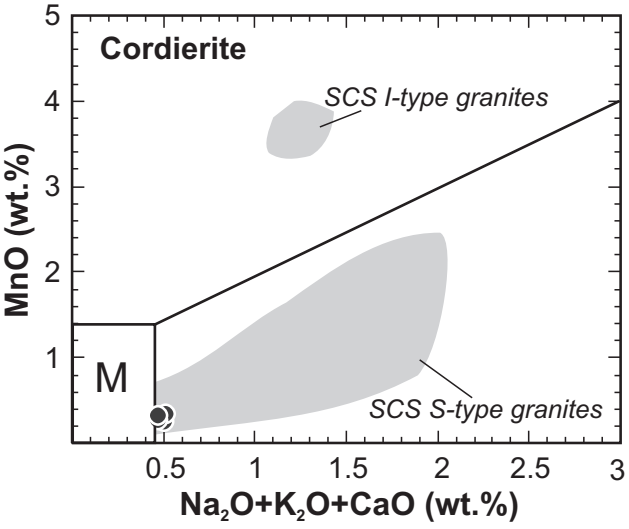

Fig. 5 Composition of cordierite in the discriminant diagram (Na_2O + K_2O + CaO) *vs* MnO. Compositional fields for metamorphic (M field) and igneous (S- and I-type granites) cordierite come from data of Barbero and Villaseca (1992) and Villaseca and Barbero (1994). Within the M field are also included cordierites from anatectic leucogranites and restite-rich granites of migmatite–granulite terranes (Barbero and Villaseca 1992).

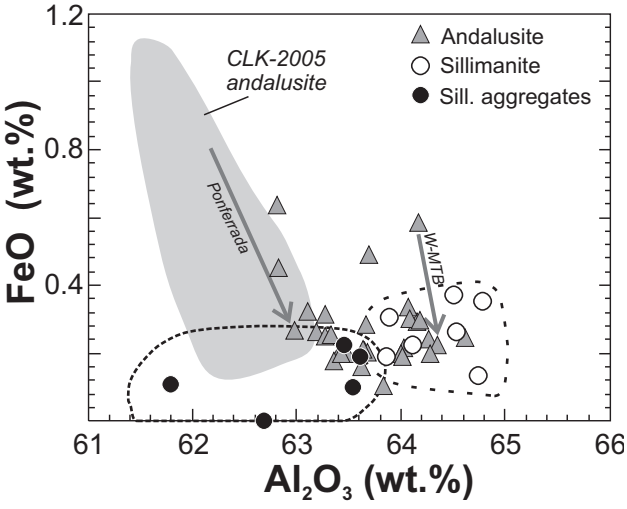

Fig. 6 Composition of aluminium silicates from the W-MTB granites in the Al_2O_3 *vs* FeO diagram. Arrows show core to rim zoning of an andalusite crystal from a W-MTB granite (Peraleda), together with andalusite zoning in another CIZ granite – the Ponferrada granite (Fernández-Catuxo et al. 1995). Andalusite compositional field from Clarke et al. (2005) (CLK-2005) is also included.

Tab. 3 Selected representative EMP analyses of minerals from the W-MTB granites

Sample	106821	106821	106821	106814	106814	106814	106814	106809	106817	106817	106809	106810	106817
Analysis	35	36	83	4	11	24	28	55	73	58	59	96	59
Pluton	Aldeanueva			Peraleda					Aldeanueva		Peraleda		Aldeanueva
Mineral	Crd	Crd	Crd	And	And	And	Sil	Sil	And	Sil	Ap	Ap	Ap
SiO_2	47.44	47.39	46.64	36.63	37.05	36.63	35.82	36.80	36.23	36.25	0.00	0.03	0.03
TiO_2	0.00	0.00	0.00	0.00	0.11	0.15	0.05	0.00	0.07	0.01	0.00	0.00	0.00
Al_2O_3	33.13	33.31	33.48	62.82	62.81	64.16	64.46	62.67	64.17	63.85	0.00	0.00	0.00
FeO	9.40	9.07	8.88	0.45	0.64	0.58	0.39	0.00	0.30	0.19	0.39	0.33	0.34
MnO	0.25	0.34	0.27	0.00	0.00	0.00	0.04	0.00	0.01	0.00	0.61	0.56	0.47
MgO	6.74	7.15	6.91	0.00	0.14	0.12	0.10	0.00	0.04	0.01	0.00	0.01	0.06
CaO	0.00	0.01	0.01	0.01	0.00	0.00	0.05	0.00	0.00	0.01	53.33	53.73	56.35
Na_2O	0.5	0.49	0.48	0.00	0.04	0.00	0.03	0.02	0.02	0.04	0.20	0.23	0.12
K_2O	0.00	0.02	0.00	0.00	0.00	0.00	0.16	0.06	0.00	0.00	0.02	0.00	0.01
P_2O_5	–	–	–	–	–	–	–	–	–	–	41.64	41.39	42.00
F	–	–	–	–	–	–	–	–	–	–	4.04	4.38	4.11
Total	97.49	97.79	96.68	100.05	100.81	101.77	101.14	99.93	100.85	100.38	100.23	100.66	101.80

cally it is slightly richer in Al than that from restitic environments (aggregates, enclaves, inclusions) (Fig. 6).

Apatite is very common (except in the Belvís leucogranites), forming euhedral crystals. Its F content (up to 4.8 wt. %) is noteworthy as it is higher than that from the SCS S-type granites (2.6 to 4.0 wt. % F; Clarke et al. 2005) (Tab. 3).

6. Geochemistry

6.1 Major and trace elements

Major- and trace-element compositions of the studied granites are listed in Tab. 4. Major-element contents

Tab. 4 Whole-rock major (wt. %) and trace-element (ppm) compositions of the western MTB granites

Sample	106811	106810	106805	106797	106804	106815	106816	106792	106796	106793
Pluton	Peraleda			N. Mata		P. Arzobispo		Belvís		
SiO_2	68.67	69.96	70.21	71.52	71.33	72.45	74.05	73.34	74.08	74.51
TiO_2	0.58	0.53	0.44	0.55	0.39	0.27	0.27	0.04	0.10	0.03
Al_2O_3	15.69	15.41	15.47	13.71	15.11	14.38	14.29	15.17	14.87	14.85
Fe_2O_3	3.57	3.01	2.58	3.40	2.36	1.68	1.88	0.50	0.90	0.37
MnO	0.05	0.04	0.03	0.04	0.03	0.02	0.03	0.05	0.02	0.02
MgO	1.25	1.04	0.93	0.84	0.67	0.50	0.56	0.09	0.19	0.06
CaO	1.67	1.40	1.06	1.34	0.85	0.61	0.57	0.39	0.46	0.41
Na_2O	3.47	3.08	3.04	2.57	3.07	3.07	2.98	4.11	3.77	4.30
K_2O	3.84	4.56	4.79	4.63	5.43	4.75	4.61	3.84	3.96	3.68
P_2O_5	0.39	0.41	0.47	0.29	0.38	0.27	0.39	0.85	0.63	0.76
LOI	0.83	0.84	1.27	0.71	0.78	1.05	1.02	0.99	1.19	0.94
Total	100.00	100.30	100.30	99.62	100.40	99.29	100.70	99.37	100.20	99.92
A/CNK	1.22	1.23	1.28	1.17	1.21	1.27	1.31	1.30	1.31	1.26
Ba	496	549	441	493	474	254	243	16	63	16
Rb	270	277	255	260	263	414	393	569	459	430
Sr	177	170	126	105	94	63	49	48	97	123
Pb	24	25	30	29	33	26	27	10	18	10
Th	17.8	18.4	12.1	17.9	13.2	14.2	15.2	0.73	1.9	0.59
U	9.67	8.64	7.13	4.83	6.28	11.4	3.28	13.5	6.82	11.5
Zr	198	165	150	175	128	104	104	28	44	20
Nb	10.9	10.1	9.8	12.4	10.4	8.5	14.0	14.4	13.5	11.7
Y	19.9	17.5	15.6	22.9	15.3	9.2	13.5	2.1	7.3	2.9
Sc	7	5	5	7	5	3	4	1	2	<1
V	43	34	35	32	27	15	18	<5	<5	<5
Cr	140	80	30	30	40	30	60	<20	30	<20
Ga	26	23	22	21	20	25	25	21	21	20
Ta	1.10	1.23	1.42	1.67	1.67	1.83	2.52	4.98	5.34	5.29
Hf	5.3	4.5	4.1	5.3	3.4	3	3.3	1.4	1.6	1.3
Cs	19.4	18.6	20.6	14.5	19.3	45.9	29.2	13.7	70.6	16.9
Sn	7	7	9	9	11	34	24	34	50	23
La	43.20	37.80	26.40	35.60	26.20	19.20	21.10	1.73	4.91	1.46
Ce	100.00	85.50	60.50	83.50	60.00	48.70	53.00	3.84	11.30	3.23
Pr	11.10	9.63	6.86	9.43	6.81	5.73	6.03	0.42	1.30	0.35
Nd	44.90	39.10	27.90	37.10	27.60	23.00	23.60	1.62	5.38	1.47
Sm	7.68	7.15	5.62	7.30	5.18	5.13	5.41	0.37	1.34	0.38
Eu	0.99	0.96	0.86	0.97	0.84	0.50	0.45	0.03	0.15	0.03
Gd	5.64	5.47	4.97	5.95	4.26	3.66	4.20	0.38	1.45	0.41
Tb	0.80	0.76	0.73	0.87	0.63	0.49	0.62	0.07	0.28	0.09
Dy	4.01	3.47	3.29	4.42	3.02	2.19	2.90	0.38	1.47	0.51
Ho	0.64	0.57	0.49	0.74	0.50	0.31	0.44	0.06	0.20	0.08
Er	1.70	1.48	1.19	2.01	1.33	0.77	1.10	0.15	0.48	0.21
Tm	0.24	0.20	0.17	0.27	0.18	0.10	0.15	0.02	0.07	0.03
Yb	1.52	1.23	1.01	1.69	1.12	0.64	0.94	0.13	0.39	0.18
Lu	0.22	0.18	0.13	0.24	0.15	0.09	0.13	0.02	0.05	0.02

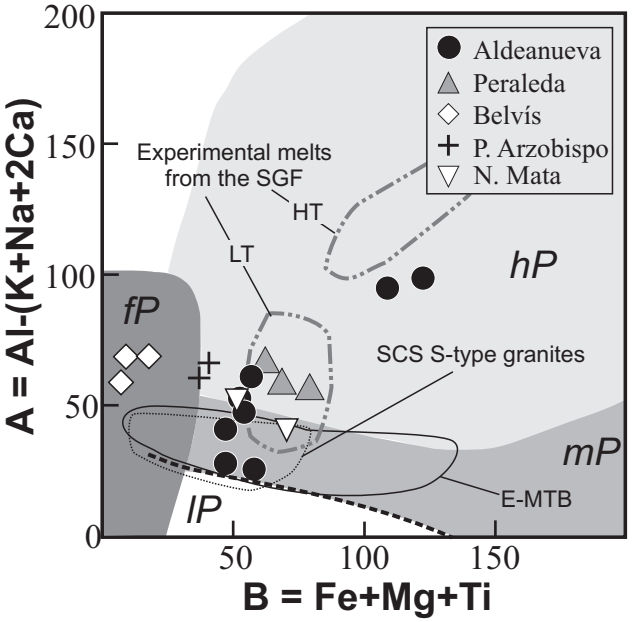

of granitoids from the Aldeanueva Pluton (taken from Andonaegui and Barrera 1984) have only been included in Fig. 7. The MTB granites range in SiO_2 from 68.3 to 74.5 wt. %. They all plot in subalkaline fields in the SiO_2 versus $Na_2O + K_2O$ diagram and are peraluminous. In the A–B diagram (Debon and Le Fort 1983; modified by Villaseca et al. 1998b; Fig. 7) samples from the most felsic pluton (Belvís de Monroy) fall in the *fP* field, whereas other samples plot between the highly and

⇦

Fig. 7 Composition of the W-MTB granites in the A–B diagram of Debon and Le Fort (1983), modified by Villaseca et al. (1998b). Compositional fields of the Mora-Ventas Batholith (E-MTB) and the SCS S-type granites are taken from Andonaegui (1990) and Villaseca et al. (1998b), respectively. In this diagram are also plotted chemical data from the Aldeanueva Pluton (Andonaegui and Barrera 1984). Fields of partial melting experiments at low (1000–1100 ºC) and high temperature (1200 ºC) of schist–greywacke mixtures from the SGF are taken from Fernández et al. (2008).

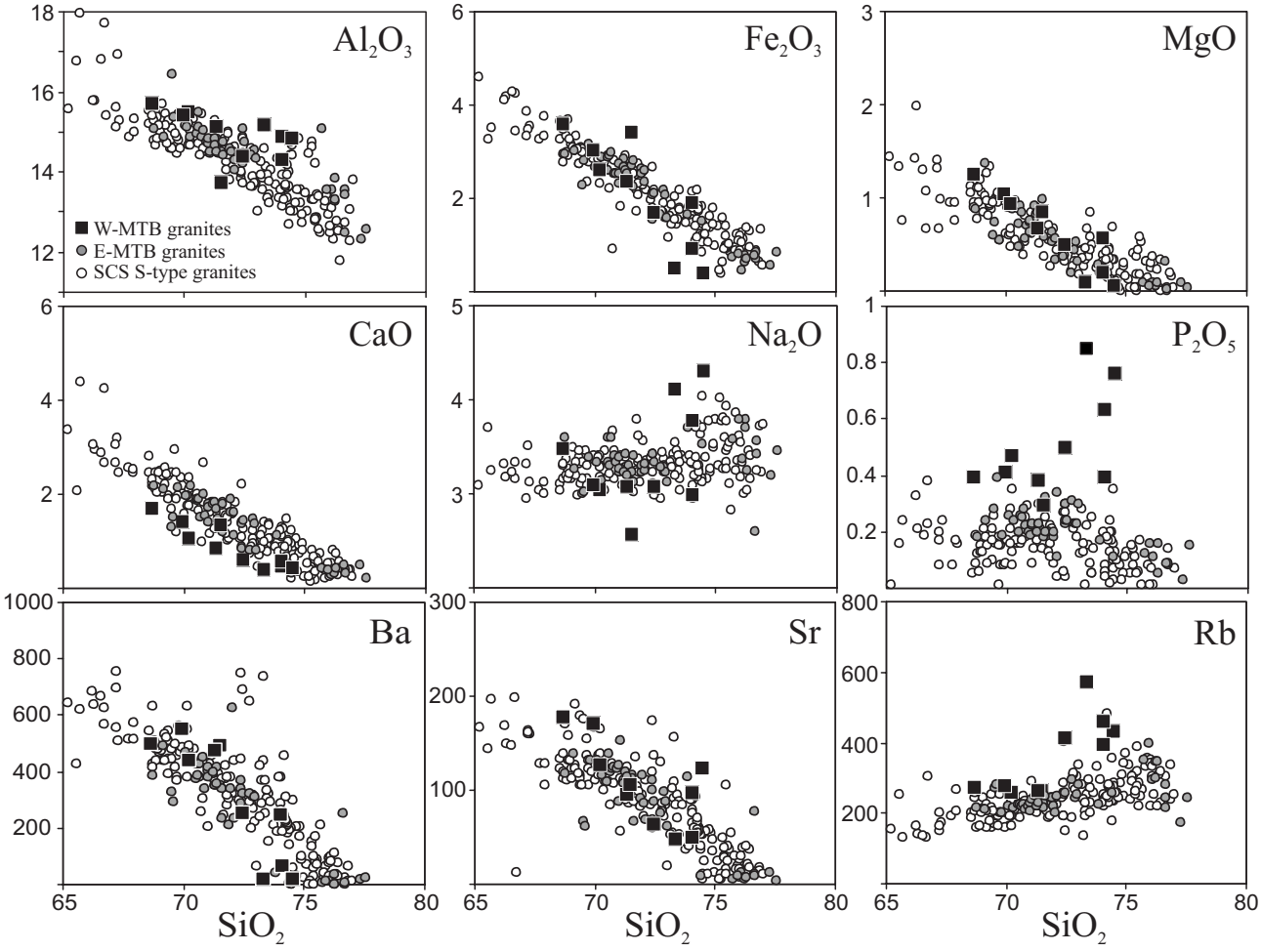

Fig. 8 Selected major (wt. %) and trace (ppm) element variation diagrams for the W-MTB granites (Tab. 4). Data for S-type granites from the Mora-Ventas Batholith (E-MTB) and the SCS are taken from Andonaegui (1990) and Villaseca et al. (1998b), respectively.

moderately peraluminous fields (Peraleda granites plot in the *hP* field) with a higher peraluminosity than S-type granites either from the eastern MTB or from the SCS. In variation diagrams using SiO_2 (Fig. 8), the studied MTB granites define a nearly continuous trend of decreasing Fe_2O_3, MgO, Al_2O_3, TiO_2, CaO values and increasing P_2O_5 contents. It is remarkable that the CaO and P_2O_5 contents are lower and higher, respectively, in the western MTB granites when compared with S-type granites from central Spain (eastern MTB and SCS) (Fig. 8). This is in agreement with the higher peraluminosity of the western MTB granites and this suggests different crustal sources for the segmented batholith. Moreover, the Belvís leucogranites show a marked perphosphorous trend, with P mainly hosted in feldspars, which is typical of some peraluminous granites of the south-western Central-Iberian Zone (Cabeza de Araya Batholith: Bea et al. 1992; Gata Plutonic Complex: Hassan Mohamud et al. 2002; Jálama and Alburquerque batholiths: Ramírez and Menéndez 1999) (for locations see Fig. 1).

There are no major differences in trace-element contents with respect to other S-type granite suites from central Spain (except for slightly higher Rb contents, Fig. 8). The studied MTB granites define a trend of decreasing Ba, Sr, Zr, and, to a lesser degree, Y and HREE with silica concentration suggesting feldspar, biotite and accessory minerals fractionation. The lowest Ba, Sr, Cr, V, Sc, Zr, Hf, Y, HREE and Th contents are those observed in the Belvís leucogranites, which, by contrast, show the highest P and Rb values. The lack of increase in Th, Y and HREE contents with SiO_2 is a feature typical of S-type granite suites (e.g. Villaseca et al. 1998a).

Chondrite-normalized REE patterns for the western MTB granites are very similar to each other without significant degree of REE fractionation with increasing SiO_2 contents (Fig. 9a), although the magnitude of the negative Eu anomaly (expressed as the Eu/Eu* ratios) increases from 0.33 (biotite granites of the Navalmoral and Peraleda plutons) to 0.15 (Belvís leucogranites). The relatively flat HREE patterns of all these MTB granites, with $(Gd/Yb)_N$ values in the range of 4.6 to 1.8, suggest an absence of garnet in the source and, therefore, middle crustal levels of partial melting. This feature is common to many strongly peraluminous granites (e.g. Rossi et al. 2002).

Multi-element patterns for the different MTB granites normalized by Bulk Continental Crust vary between flat crust-like compositions (biotite granites) and more spiky and depleted behaviour (leucogranites) (Fig. 9b). These patterns are very similar to the Lachlan Fold Belt cordierite-bearing S-type granites and to the Himalayan leucogranites, respectively (Kemp and Hawkesworth 2003). In addition, differences appear between individual leucogranite types (the Belvís leucogranites are much more fractionated and markedly richer in phosphorous and depleted in lead than Himalayan types).

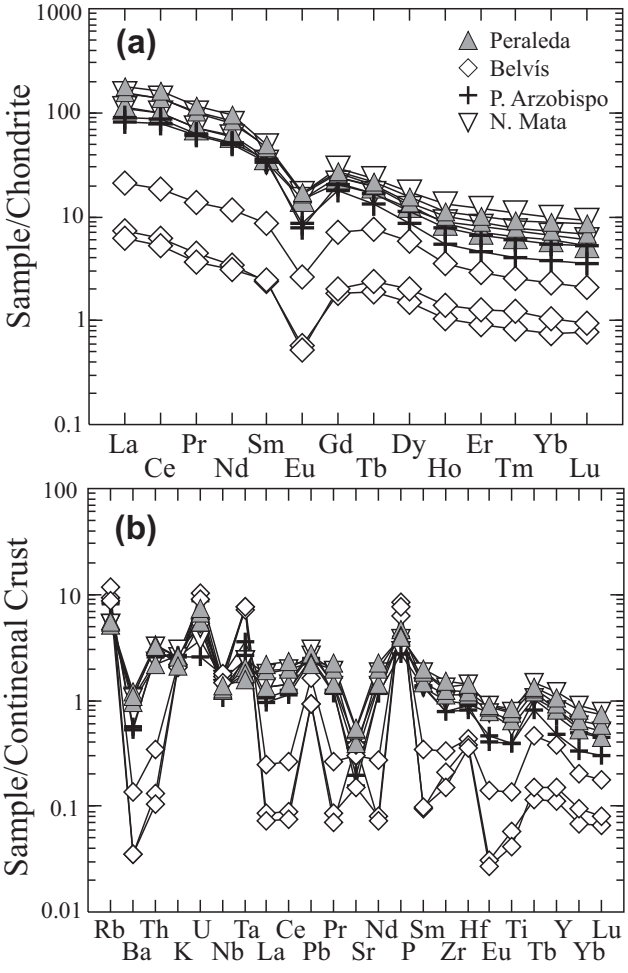

Fig. 9 Trace-element composition of the W-MTB granites. **a** – Chondrite-normalized REE patterns for the W-MTB granites. Normalizing values from Sun and McDonough (1989). **b** – Trace-element patterns for the W-MTB granites normalized by the Bulk Continental Crust (Rudnick and Gao 2003).

6.2 Sr-Nd-Pb isotopes

The Sr and Nd isotopic ratios were corrected to a representative Variscan age of 300 Ma. Analysed granites from the western MTB show a large variation in initial $^{87}Sr/^{86}Sr$ ratios (0.7060 to 0.7133) whereas initial ε_{Nd} values are much less variable between –5.0 and –5.9 (Tab. 5; Fig. 10). The granites from the eastern MTB show slightly lower ε_{Nd} values, from –5.7 to –6.6, similar to values for the SCS S-type granites (Villaseca et al. 1998a) (Fig. 10). The only Sr-Nd isotopic data for other perphosphorous granites intruding the Schist–Greywacke Formation are those from the Alburquerque Batholith,

Tab. 5 Sr and Nd isotope data and concentrations (ppm) of the W-MTB granites

Sample	Pluton	Rb	Sr	$^{87}Rb/^{86}Sr$	$^{87}Sr/^{86}Sr$	$(^{87}Sr/^{86}Sr)_{300}$	Sm	Nd	Sm/Nd	$^{147}Sm/^{144}Nd$	$^{143}Nd/^{144}Nd$	$\varepsilon(Nd)_{300}$
106792		569	48	34.808	0.856018 ± 06	0.707421	0.37	1.62	0.2284			
106793	Belvís	430	123	10.171	0.760438 ± 05	0.717019	0.38	1.47	0.2585			
106796		459	97	13.788	0.776847 ± 05	0.717983	1.34	5.38	0.2491	0.1506	0.512266 ± 04	-5.49
106797	N. Mata	260	105	7.189	0.739902 ± 06	0.709209	7.30	37.10	0.1968	0.1189	0.512212 ± 03	-5.34
106804		263	94	8.129	0.747152 ± 04	0.712447	5.18	27.60	0.1877	0.1135	0.512191 ± 03	-5.53
106805		255	126	5.873	0.735012 ± 05	0.709939	5.62	27.90	0.2014	0.1218	0.512221 ± 03	-5.27
106810	Peraleda	277	170	4.726	0.729482 ± 05	0.709306	7.15	39.10	0.1829	0.1105	0.512205 ± 03	-5.15
106811		270	177	4.424	0.727392 ± 06	0.708507	7.68	44.90	0.1710	0.1034	0.512201 ± 03	-4.95
106815	P. Arzobispo	414	63	19.183	0.795180 ± 06	0.713288	5.13	23.00	0.2230	0.1348	0.512212 ± 03	-5.94
106816		393	49	23.437	0.806042 ± 05	0.705988	5.41	23.60	0.2292	0.1386	0.512229 ± 03	-5.75

Uncertainties for the $^{87}Sr/^{86}Sr$ and $^{143}Nd/^{144}Nd$ ratios are 2 sigma errors in the last two digits.

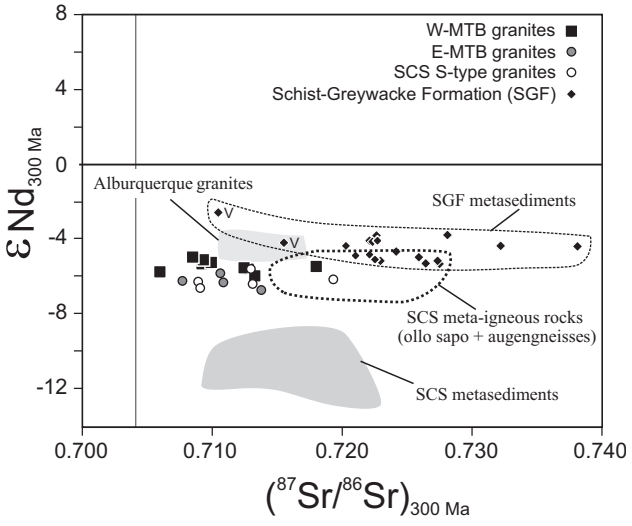

Fig. 10 Sr-Nd isotopic ratios at 300 Ma for the W-MTB granites and related rocks. Fields for S-type granites from the Mora-Ventas Batholith (E-MTB) and the SCS are taken from Andonaegui (1990) and Villaseca et al. (1998b). Compositional field of the SGF is from Beetsma (1995), Ugidos et al. (1997) (shales), and Rodríguez-Alonso et al. (2004) (meta-volcaniclastic rocks) (V). Isotopic field for the SCS meta-igneous rocks comprises: "ollo de sapo" (meta-volcanic) samples (Castro et al. 1999) and granite-derived orthogneisses (Villaseca et al. 1998a). Isotopic field for Alburquerque granites is taken from Menéndez and Bea (2004).

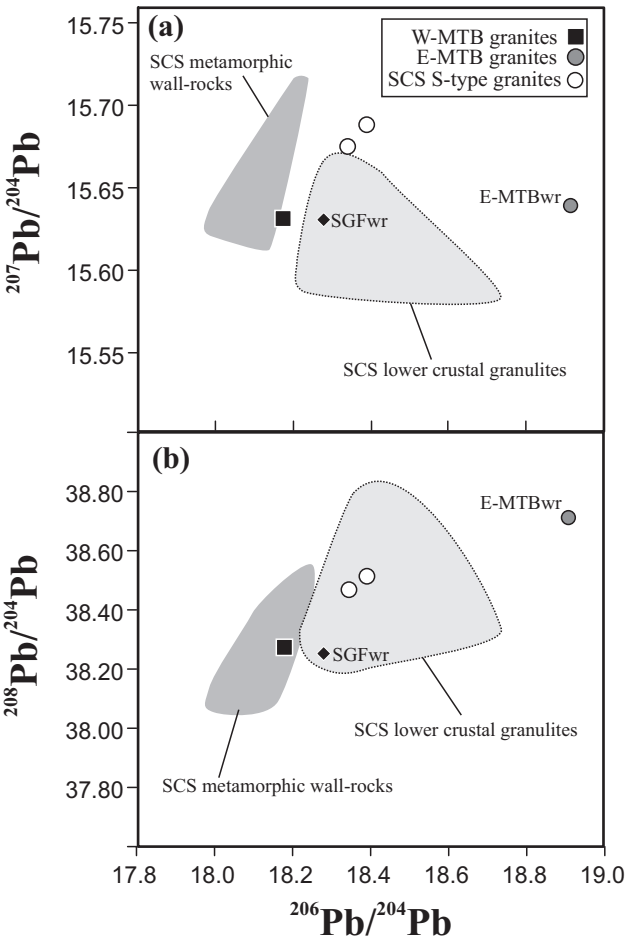

Fig. 11 Lead isotopic ratios of K-feldspars from S-type granites of central Spain: **a** – $^{206}Pb/^{204}Pb$ *vs* $^{207}Pb/^{204}Pb$. **b** – $^{206}Pb/^{204}Pb$ *vs* $^{208}Pb/^{204}Pb$. Also shown is the field for the SCS lower crustal granulites (Villaseca et al. 2007) and the outcropping SCS metamorphic rocks (Villaseca et al. unpublished data). Age-corrected radiogenic Pb ratios for whole-rock analyses are also included (*SGFwr* and *E-MTBwr*). See text for further explanation.

which have even higher initial ε_{Nd} values (–3.4 to –5.2; Menéndez and Bea 2004).

Metasediments from the Neoproterozoic Schist-Greywacke Formation (SGF) have significantly higher ε_{Nd} values when compared to other metasedimentary sequences in the Central Iberian Zone (Beetsma 1995; Rodríguez-Alonso et al. 2004). For example, metasediments from the SCS have ε_{Nd} values mainly from –9.1 to –12.5 at 300 Ma (Villaseca et al. 1998a) whereas those from the SGF have ε_{Nd} mainly in the range of –3.9 to –5.2

Tab. 6 Pb isotope data for S-type granites from central Spain

Sample	Pluton	Material	U	Th	Pb	$^{206}Pb/^{204}Pb$	$^{207}Pb/^{204}Pb$	$^{208}Pb/^{204}Pb$
106804	N. Mata (W-MTB)	Kfsp				18.180	15.630	38.269
80910	Mora (E-MTB)	whole rock	2.92	10	24	18.857*	15.637*	38.715*
95916	Alpedrete (SCS)	Kfsp				18.393	15.688	38.513
Y-82	Hoyo Manz. (SCS)	Kfsp				18.345	15.674	38.465

* Whole-rock data calculated at 300 Ma. Trace element contents in ppm.

(Beetsma 1995; Ugidos et al. 1997), which is much closer to reported values for western MTB granites (Fig. 10).

The only Pb isotopic analysis of a granite from the western MTB segment obtained in course of the present study (Tab. 6) shows the lowest isotopic ratios when compared to other peraluminous S-type granites from adjacent areas (Fig. 11). These low Pb isotopic ratios overlap with the field of outcropping metamorphic rocks from the CIZ, and are in contrast to the peraluminous granites from the SCS or from eastern MTB, which display radiogenic values more alike meta-igneous granulites from lower crustal levels to which they have been genetically related (Villaseca et al. 1999, 2007).

7. Discussion

7.1 Conditions for magmatic andalusite-sillimanite crystallization

The coexistence of andalusite and sillimanite in igneous felsic rocks is relatively uncommon and their origin remains controversial (e.g. Clarke et al. 2005). In some cases sillimanite is older than andalusite and the latter forms as crystallization proceeds during cooling (e.g. Macusani rhyolites, Pichavant et al. 1988) or as a consequence of nucleation around residual (xenolithic) sillimanite (D'Amico et al. 1981). However, as described for the studied MTB granites, it is more common to find the formation of sillimanite from andalusite. This polymorphic transformation has been interpreted in a number of ways: i) increasing temperature during progressive partial melting (e.g. Himalayan granites, Visonà and Lombardo 2002), ii) thermal metamorphism induced by younger granitic intrusions (e.g. Barrera et al. 1985), or iii) post-magmatic hydrothermal fibrolitic sillimanite transformation (e.g. Hassan Mohamud et al. 2002). Neither of these interpretations can be applied to the MTB granites. They are isolated plutonic massifs in which andalusite–sillimanite transformation appears in many samples within the pluton and it is unrelated to secondary processes or thermally metamorphosed areas. A late magmatic origin for both aluminium silicates is suggested by their euhedral appearance, chemical zoning and wide regional distribution, although unequivocal textural and chemical criteria to determine their origin are not straightforward (e.g. Clarke et al. 2005). However, these authors stated that chemical equilibrium with other granite minerals (e.g. biotite, muscovite) should reinforce the magmatic origin of aluminium silicates. In this respect, the correlation of TiO_2 and FeO + MgO contents with similar slopes of the tie lines between coexisting mica pairs suggests attainment of chemical equilibrium. The magmatic origin of muscovite is also consistent with the high Na/(Na + K) ratios and projection in the Mg-Ti-Na diagram (Miller et al. 1981), shown by most of the analyzed muscovites (Fig. 4b), including the crystals surrounding andalusite.

Minor chemical impurities in andalusite structure enlarge its stability field towards higher temperatures (Kerrich and Speer 1988). Incorporation of Fe, Ti, Mg and Mn is higher in andalusite than in sillimanite which suggests a divariant rather than univariant equilibrium between both polymorphs (see also Kerrich 1990). Calculated *Kd* values ($X^{sil}_{Al2SiO5}/X^{and}_{Al2SiO5}$) in coexisting andalusite and sillimanite in the MTB granites are in the range of 1.00 to 1.02, which points to a shift of their equilibrium boundary

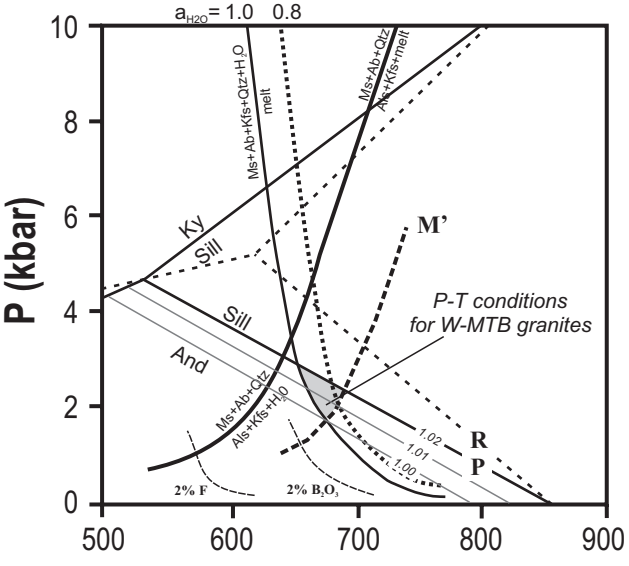

Fig. 12 A *P-T* diagram showing the estimated crystallization conditions for the studied W-MTB granites. Isopleths of K_{eq} (= $X^{sill}_{Al2SiO5}/X^{and}_{Al2SiO5}$) for the andalusite–sillimanite equilibrium after Kerrick and Speer (1988). Andalusite–sillimanite–kyanite equilibria after (P) Pattison (1992) and (R) Richardson et al. (1969). Melting curves and reaction involving muscovite are taken from Johannes and Holtz (1996). M' muscovite reaction from D'Amico et al. (1981). Solidus curves for water-saturated haplogranitic systems with F and B are after Manning and Pichavant (1983).

by 50 ºC upward (Kerrich 1990 drew this isopleth close to the Pattison 1992 equilibria) (Fig. 12). Moreover, the frequently observed andalusite chemical zoning towards rims poorer in minor elements indicates lowering of *Kd* values as crystallization proceeds (see also Fernández-Catuxo et al. 1995). The incorporation of Fe, Ti and Mg in andalusite and their progressive decrease in the felsic granitic magma, close to solidus conditions, makes andalusite unstable and sillimanite precipitates instead, or in combination with magmatic muscovite, depending on the water activity during crystallization. Thus, the transition from andalusite to sillimanite could be explained by changing local chemical conditions in residual granite melts rather than involving significant changes or reversals in magmatic *P-T* conditions.

The possible equilibrium between andalusite–sillimanite and muscovite is rather restricted in a *P-T* space (Fig. 12). This was discussed by D'Amico et al. (1981) who suggested that a deviation from the muscovite ideal formula (due to Ti-F-Na substitutions) would enlarge its stability field towards slightly lower *P* conditions (M' curve in Fig. 12). The restricted *P-T* locus for late-magmatic crystallization of the proposed mineral assemblage in the western MTB granites remains around 2–3 kbar and 650–700 ºC.

7.2 Granite sources

The high peraluminosity of the western MTB granites and their remarkably low CaO contents when compared to the closely related S-type granites from the eastern MTB or the SCS suggest a major contribution from a metapelitic source (Chappell et al. 1991). This is in agreement with the suggestion of Sylvester (1998) who stated that S-type peraluminous melts derived from pelites have lower CaO/Na_2O ratios (< 0.3) than melts produced from clay-poor (greywackeous) sources. The western MTB granites show CaO/Na_2O ratios between 0.19 and 0.52 (except for the Belvís leucogranites which are fractionated magmas), and this suggests mixed pelitic–greywackeous sources.

The high phosphorous content of the studied granites could be a consequence of their high peraluminosity as apatite dissolves more in such melts (Bea et al. 1992; Pichavant et al., 1992; Wolf and London 1994) or, alternatively, it can reflect inheritance from a P-rich source. Crustal sources with the highest phosphorous enrichments are pelitic shales (e.g. Gromet et al. 1984). The initially high phosphorous contents of metapelitic protoliths are reflected in the granitic melts that they produce, because phosphorous is more soluble in peraluminous compositions. The early crystallization of plagioclase, which removes calcium that would consume phosphorous in the form of apatite, contributes to a perphosphorous granite trend (London 2008).

Most of the P-rich granites of the CIZ are confined to the region where the Schist–Greywacke Formation occurs (Albalá, Alburquerque, Cabeza de Araya, Gata, Jálama, Trujillo, the western MTB) (Fig. 1). At the same time, the SGF is the CIZ metasedimentary formation richest in dispersed phosphate nodules and shows elevated P levels (IGME, 1989; Rodríguez-Alonso et al. 2004). Other isolated P-rich plutons in the CIZ include the Pedrobernardo Pluton from the SCS described as a classical perphosphorous granite (Bea et al. 1994) and similar bodies were studied in central Portugal (Neiva 1998). In the Tormes Dome area a large P-rich leucogranite batholith also occurs (López Plaza and López Moro 2003) but the more fractionated leucogranites show neither a marked perphosphorous trend nor any associated P-rich pegmatite fields as in the southern areas of the CIZ (e.g. P-rich granite pegmatites emplaced in the Pedroso de Acim and El Trasquilón granite cupolas, Gallego 1992; and also in the Alburqerque and Belvís de Monroy plutons: London et al. 1999; IGME 1983, respectively) (see Fig. 1 for locations). According to the current data, the strongly peraluminous granites of the southern half of the CIZ form the main P-rich pluton concentration in the whole Iberian Variscan Belt.

Isotope geochemistry of western MTB granites is consistent with a metasedimentary derivation from Neoproterozoic SGF rocks. The initial Nd ratios of the western MTB granites are similar to the isotopic ratios shown by mixed pelitic, greywackeous and metavolcaniclastic sources from the SGF (Fig. 10). The scarce Pb isotope data for the SGF metasediments (Beetsma 1995), and their age-corrected Pb isotope ratios (to 300 Ma: $^{206}Pb/^{204}Pb = 18.28$, $^{207}Pb/^{204}Pb = 15.63$, $^{208}Pb/^{204}Pb = 38.26$) are close to those obtained for the western MTB granite (Fig. 11). Isotopic data for Lower Palaeozoic felsic meta-igneous formations in the SCS (metavolcanics and metagranitic augen gneisses: Villaseca et al. 1998a; Castro et al. 1999 and references therein) have been also included in Fig. 10 for comparison, but their compositional field does not overlap with most of the studied W-MTB granites. Moreover, the absence of these meta-igneous formations in the southern part of the Central Iberian Zone makes the presence of meta-igneous rocks at depth difficult to imagine, especially when considering the eastern vergency of the whole SG metamorphic area (Fig. 1).

In Fig. 7 the compositional data of experimental melts derived from pelite–greywacke mixtures of the SGF (Fernández et al. 2008) are shown. Most of the biotite granites (Peraleda, N. Mata and Aldeanueva samples) have composition close to melts in low temperature experiments (1000–1100 ºC) or produced at low melt

fractions. By contrast, the more mafic granodiorites from Aldeanueva Pluton plot near the high-temperature experimental melts (1200 ºC) (Fig. 7). As such extremely high-T conditions are difficult to attain in continental collision areas, an alternative is that granodiorites, rich in surmicaceous and restitic enclaves, can contain a significant fraction of residual metasedimentary material. In any case, geochemical signatures of the studied W-MTB granites agree with their derivation by melting of SGF sources at crustal depths.

Most of the previous works on these P-rich plutons also support granite derivation from pelitic or pelitic-greywackeous sources (Ramírez and Menéndez 1999; Menéndez and Bea 2004). Nevertheless, more recent studies suggest that mafic mantle-derived materials participated in the genesis of some of these plutons (e.g. the Cabeza de Araya Pluton – Castro and Corretgé 2002; García-Moreno et al. 2007), because the most mafic granite facies are less aluminous in composition and enclose hybrid mafic microgranular enclaves. In the studied W-MTB granites the more mafic granites are, however, more peraluminous, plotting in the *hP* fields of Villaseca et al. (1998b) (Fig. 7), thus supporting that metasedimentary sources were mainly involved in their origin.

7.3 A segmented peraluminous granite batholith

The MTB is a large peraluminous batholith which shows two contrasting S-type granites. The western segment includes the most peraluminous plutons with markedly higher P contents giving rise to strongly fractionated perphosphorous granites. The eastern segment of the MTB is built by peraluminous granites very close in composition to those of the SCS (Villaseca et al. 1998a) (Figs 7, 8 and 10).

The major differences in isotopic composition between the granites of the MTB are related to Nd and Pb ratios (Figs 10 and 11). The slightly higher initial Nd and the lower $^{206}Pb/^{204}Pb$ ratios in the western MTB granites suggest mainly metasedimentary sources, probably similar to the SGF, which presumably contains a greater proportion of juvenile magmatic components (Ugidos et al. 1997; Rodriguez-Alonso et al. 2004). On the contrary, the eastern MTB granites are closer in isotopic composition to meta-igneous granulites of lower crustal derivation, as stated in previous works (Villaseca et al. 1998a, 1999). However, this discussion should be considered as preliminary because the current isotopic Pb data are very scarce and the SGF and E-MTB (Mora-Ventas granite) samples were analyzed as whole-rock aliquots, which yield less accurate age-corrected ratios. Further analytical work is needed to constrain the isotopic composition of the MTB granites and associated metamorphic country rocks.

We propose that distinct crustal sources may have been involved in the origin of the peraluminous MTB and this implies that the S-type assignment is weakened. The combined use of chemical diagrams showing different peraluminosity and perphosphorous degrees could contribute to discrimination of different parental materials in the genesis of peraluminous granites (Fig. 13). In the A–B diagram the western MTB granites spread from *hP* towards *fP* fields. On the other hand, the eastern MTB granites plot mostly in the *mP* and *fP* fields, but close to the proposed I–S boundary line of Villaseca et al. (1998b) (Fig. 7). The more mafic granites of the western MTB show a higher peraluminosity indicating more pelitic metasedimentary contribution, or alternatively, a higher melt fraction. In contrast, peraluminous granites with clear negative trends in the A–B plot suggest meta-igneous derivation or mixed crustal-mantle sources (Villaseca et al. 1998b).

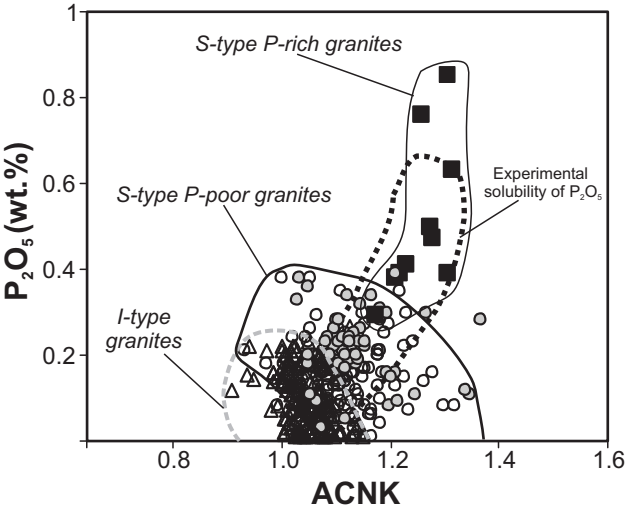

Fig. 13 – A/CNK (molar $Al_2O_3/(CaO + Na_2O + K_2O)$) *vs* P_2O_5 (in wt. %) of the CIZ granitic rocks. The three discriminant fields are: i) I-type granites from the SCS (Villaseca et al. 1998a), ii) S-type granites from the SCS and E-MTB (Andonaegui 1990; Villaseca et al. 1998a), iii) S-type P-rich granites from W-MTB. Field of experimental solubility of P_2O_5 in low-Ca peraluminous melts after Wolf and London (1994).

The MTB data demonstrate that there are different series of S-type granites. In this respect, the similarity in P enrichment of these peraluminous granites with the experimental solubility of P_2O_5 as a function of the alumina saturation index of the melt (Fig. 13) supports the distinction of perphosphorous S-type granite series as the one that has other sinks for phosphate in the fractionation sequence (e.g. feldspars, Wolf and London 1994).

The western MTB granites intruded into the SGF region whereas eastern plutons are more allochthonous, and penetrated the Lower Palaeozoic series. The Mora-Ventas Batholith (E-MTB) intruded along the Toledo listric fault (Fig. 1), a late Variscan E–W shear band which gave rise to a core complex-like structure, separating a large anatectic complex to the north (the ACT, Barbero and Villaseca 1992) from epizonal metamorphic series to the south. The ACT metasedimentary series displays the same geochemical signature as the SCS Neoproterozoic series (Villaseca et al. 1998a). Furthermore, the late-Variscan Toledo shear band is coincident with the general E–W granitic array of the MTB, suggesting tectonic control of granite generation and emplacement within the Montes de Toledo region. Shallower metasedimentary sources played a role in the genesis of granites of the western MTB, whereas deeper meta-igneous lithotypes (lower crustal felsic granulites) could have been involved in the granite genesis of its eastern segment. Still, an evidence for a minor contribution of some mantle-derived mafic magmas can be postulated (presence of mafic bodies smaller than 20 m in length, and conspicuous mafic microgranular enclaves within the Mora-Ventas granites; Andonaegui 1990). The change from a ductile to brittle E–W faulting, from east to west across the MTB is perceptible, but the tectonic control and the main mechanism triggering partial melting and giving rise to this segmented batholith remains to be evaluated.

Acknowledgements. We acknowledge Alfredo Fernández Larios and José González del Tánago for their assistance with the electron microprobe analyses in the CAI of Microscopía Electrónica (UCM). Also José Manuel Fuenlabrada Pérez and José Antonio Hernández Jiménez from the CAI of Geocronología y Geoquímica (UCM) for their help in analysing samples by TIMS. We appreciate critical comments and suggestions by Antonio Castro, Miguel López Plaza and David Dolejš, which greatly improved the quality of the manuscript. This work is included in the objectives of, and supported by, the CGL2004-02515/BTE and CGL2008-05952-CO2-01/BTE projects of the Ministerio de Educación y Ciencia of Spain, and the CCG07-UCM project.

References

Ábalos B, Carreras J, Druguet E, Escuder J, Gómez-Pugnaire MT, Lorenzo Álvarez S, Quesada C, Rodríguez-Fernández R, Gil-Ibarguchi JI (2002) Variscan and Pre-Variscan tectonics. In: Gibbons W, Moreno T (eds) The Geology of Spain. Geol Soc London, pp 155–183

Abdel-Rahman A-F M (1994) Nature of biotites from alkaline, calc-alkaline and peraluminous magmas. J Petrol 35: 525–541

Andonaegui P (1990) Geochemistry and Geochronology of the Granitoids South of Toledo. Unpublished PhD. Thesis, Complutense University, Madrid, pp 1–357 (in Spanish)

Andonaegui P, Barrera JL (1984) Petrology of two peraluminous granite series from Valdeverdeja-Aldeanueva de Barbarroya (Toledo). Bol Geol Min España 95: 165–183 (in Spanish)

Andonaegui P, Villaseca C (1998) Granites from the Mora-Gálvez Pluton (Toledo): an example of evolution by crystal fractionation. Bol R Soc Española Hist Nat 94: 17–31 (in Spanish)

Barbero L, Villaseca C (1992) The Layos granite, Hercynian complex of Toledo (Spain): an example of parautochthonous restite-rich granite in a granulitic area. Trans Roy Soc Edinb, Earth Sci 83: 127–138

Barrera JL, Bellido F, Klein E (1985) Contact metamorphism in synkinematic two-mica granites produced by younger granitic intrusions. Geol Mijnbouw 64: 413–422

Bea F, Fershtater G, Corretgé LG (1992) The geochemistry of phosphorus in granite rocks and the effect of aluminium. Lithos 29: 43–56

Bea F, Pereira MD, Corretgé LG, Fershtater GB (1994) Differentiation of strongly peraluminous, perphosphorous granites: the Pedrobernardo Pluton, central Spain. Geochim Cosmochim Acta 58: 2609–2627

Bea F, Montero P, Molina JF (1999) Mafic precursors, peraluminous granitoids, and late lamprophyres in the Avila batholith: a model for the generation of Variscan batholiths in Iberia. J Geol 107: 399–419

Bea F, Montero P, Zinger T (2003) The nature, origin, and thermal influence of the granite source layer of Central Iberia. J Geol 111: 579–595

Beetsma JJ (1995) The late Proterozoic/Paleozoic and Hercynian crustal evolution of the Iberian Massif, N Portugal, as traced by geochemistry and Sr-Nd-Pb isotope systematics of pre-Hercynian terrigenous sediments and Hercynian granitoids. Unpublished PhD.Thesis, Vrije Universiteit, Amsterdam, the Netherlands, pp 1–223

Capdevila R, Corretgé LG, Floor P (1973) Les granitoides Varisques de la Meseta Ibérique. Bull Soc Géol France 15: 209–228

Castro A, Patiño-Douce A, Corretgé LG, De la Rosa J, El-Biad M, El-Hmidi H (1999) Origin of peraluminous granites and granodiorites, Iberian Massif, Spain: an experimental test of granite petrogenesis. Contrib Mineral Petrol 135: 255–276

Castro A, Corretgé LG (2002) Variscan granites. In: Gibbons W, Moreno T (eds) The Geology of Spain. Geol Soc London, pp 129–136

Chappell BW, White AJR, Wyborn D (1987) The importance of residual material (restite) in granite petrogenesis. J Petrol 28: 1111–1138

Chappell BW, White AJR, Williams IS (1991) A transverse section through granites of the Lachlan Fold Belt. Second Hutton Symposium Excursion Guide. ABMR Record 1991/22, Canberra, pp 1–125

Clarke DB, Dorais M, Barbarin B, Barker D, Cesare B, Clarke G, El Baghdadi M, Erdmann S, Förster H-J, Gaeta M, Gottesmann B, Jamieson RA, Kontak DJ, Koller F, Gomes CL, London D, Morgan VI GB, Neves LJPF, Pattison DRM, Pereira AJSC, Pichavant M, Rapela CW, Renno AD, Richards S, Roberts M, Rottura A, Saavedra J, Sial AN, Toselli AJ, Ugidos JM, Uher P, Villaseca C, Visonà D, Whitney DL, Williamson B, Woodard HH (2005) Occurrence and origin of andalusite in peraluminous felsic igneous rocks. J Petrol 46: 441–472

Clemens JD, Wall VJ (1981) Origin and crystallization of some peraluminous (S-type) granitic magmas. Canad Mineral 10: 111–131

D'Amico C, Rottura A, Bargossi GM, Nannetti MC (1981) Magmatic genesis of andalusite in peraluminous granites. Examples from Eisgarn type granites in Moldanubicum. Rend Soc Italiana Mineral Petrol 38: 15–25

Debon F, Le Fort P (1983) A chemical-mineralogical classification of common plutonic rocks associations. Trans Roy Soc Edinb, Earth Sci 73: 135–149

Dias G, Leterrier J (1994) The genesis of felsic–mafic plutonic associations: a Sr and Nd isotopic study of the Hercynian Braga Granitoids Massif (Northern Portugal). Lithos 32: 207–223

Dias G, Leterrier J, Mendes A, Simões PP, Bertrand JM (1998) U-Pb zircon and monazite geochronology of syn- to post-tectonic Hercynian granitoids from the Central Iberian Zone (Northern Portugal). Lithos 45: 349–369

Erdmann S, Clarke DB, MacDonald MA (2004) Origin of chemically zoned and unzoned cordierites from the South Mountain and Musquodoboit batholiths. Trans Roy Soc Edinb, Earth Sci 95: 99–110

Fernández-Catuxo J, Corretgé LG, Suárez O (1995) Influence of minor elements on the stability of andalusite in granitic rocks from the Iberian Massif. Bol Soc Española Mineral 18: 55–71 (in Spanish)

Fernández-Suárez J, Dunning GR, Jenner GA, Gutiérrez-Alonso G (2000) Variscan collisional magmatism and deformation in NW Iberia: constraints from U-Pb geochronology of granitoids. J Geol Soc, London 157: 565–576

Fernández C, Becchio R, Castro A, Viramonte JM, Moreno-Ventas I, Corretgé LG (2008) Massive generation of atypical ferrosilicic magmas along the Gondwana active margin: implications for cold plumes and back-arc magma generation. Gondwana Res 14: 451–473

Gallego M (1992) Las mineralizaciones de litio asociadas a magmatismo ácido en Extremadura y su encuadre en la zona Centro-Ibérica. Unpublished PhD. Thesis, Complutense University, Madrid, pp 1–323 (in Spanish)

García-Moreno O, Corretgé LG, Castro C (2007) Processes of assimilation in the genesis of cordierite leucomonzogranites from the Iberian Massif: a short review. Canad Mineral 45: 71–85

Green TH (1976) Experimental generation of cordierite- or garnet-bearing liquids from a pelitic starting composition. Geology 4: 85–88

Gromet LP, Dymek RF, Haskin LA, Korotev RL (1984) The "North American shale composite": its compilation, major and trace element characteristics. Geochim Cosmochim Acta 48: 2469–2482

Hassan Mohamud A, Casquet C, Pérez del Villar L, Cozar J, Pellicer MJ (2002) High temperature hydrothermal fibrolite in "El Payo granite" Cadalso-Casillas de Flores granitic complex (Salamanca-Cáceres, Spain). Geogaceta 32: 23–26

IGME (1985) Spanish Geological Map, Sheet nº 653, Valdeverdeja. Serv Publ Minist Industria, Madrid.

IGME (1987) Spanish Geological Map, Sheet nº 652, Jaraicejo. Serv Publ Minist Industria, Madrid.

IGME (1989) Spanish Geological Map, Sheet nº 654, El Puente del Arzobispo. Serv Publ ITGE, Madrid.

Johannes W, Holtz F (1996) Petrogenesis and Experimental Petrology of Granitic Rocks. Springer-Verlag, Berlin, pp 1–335

Kemp AIS, Hawkesworth CJ (2003) Granitic perspectives on the generation and secular variation of the continental crust. In: Rudnick RL (ed) The Crust, vol. 3 Treatise of Geochemistry. Elsevier-Pergamon, Oxford, pp 349–410

Kerrick DM (1990) The Al_2SiO_5 polymorphs. Mineralogical Society of America Reviews in Mineralogy 22, pp 1–406

Kerrick DM, Speer JA (1988) The role of minor element solid solution on the andalusite-sillimanite equilibrium in metapelites and peraluminous granitoids. Amer J Sci 288: 152–192

Liñán E, Gozalo R, Palacios T, Gámez-Vintaned JA, Ugidos JM, Mayoral E (2002) Cambrian. In: Gibbons W, Moreno T (eds) The Geology of Spain. Geol Soc London, pp 17–29

London D (2008) Pegmatites. Canad Mineral Spec Publ 10, pp 1–347

London D, Wolf MB, Morgan GB-VI, Gallego M (1999) Experimental silicate–phosphate equilibria in peraluminous granitic magmas, with a case study of the Alburquerque batholith at Tres Arroyos, Badajoz, Spain. J Petrol 40: 215–240

López Plaza M, López Moro FJ (2003) The Tormes Dome. Eurogranites in western Castilla y León. Guide Book, pp 1–192

Manning DAL, Pichavant M (1983) The role of fluorine and boron in the generation of granitic melts. In: Atherton MP, Gribble CD (eds) Migmatites, Melting and Metamorphism, Shiva, Nantwich, pp 94–109

Menéndez LG, Bea F (2004) The Nisa-Alburquerque Batholith. In: Vera JA (ed) Geology of Spain, IGME-SGE, Madrid, pp 120–122 (in Spanish)

Miller CF, Stoddar EF, Bradfish LJ, Dollase WA (1981) Composition of plutonic muscovite: genetic implications. Canad Mineral 19: 25–34

Moreno Ventas I, Rogers G, Castro A (1995) The role of hybridization in the genesis of Hercynian granitoids in the Gredos Massif, Spain: inferences from Sr-Nd isotopes. Contrib Mineral Petrol 120: 137–149

Nachit H, Razafimahefa N, Stussi JM, Carron JP (1985) Composition chimique des muscovites et feldspaths potassiques dans les leucogranite du massif de Millesvaches (Massif Central Français). Comptes Rendus Acad Sci Paris 301: 813–818

Neiva AMR (1998) Geochemistry of highly peraluminous granites and their minerals between Douro and Tamega valleys, northern Portugal. Chem Erde 58: 161–184

Pattison DRM (1992) Stability of andalusite and sillimanite and the Al_2SiO_5 triple point: constraints from the Ballachulish aureole, Scotland. Amer Miner 86: 1414–1422

Pichavant M, Kontak DJ, Herrera JV, Clark AH (1988) The Miocene–Pliocene Macusani Volcanics, SE Peru. I. Mineralogy and magmatic evolution of a two-mica aluminosilicate-bearing ignimbrite suite. Contrib Mineral Petrol 100: 300–324

Pichavant M, Montel JM, Richard LR (1992) Apatite solubility in peraluminous liquids: experimental data and extension of the Harrison–Watson model. Geochim Cosmochim Acta 56: 3855–3861

Ramírez JA, Menéndez LG (1999) A geochemical study of two peraluminous granites from south-central Iberia: the Nisa-Alburquerque and Jalama batholiths. Canad Mineral 63: 85–104

Reyes J, Villaseca C, Barbero L, Quejido AJ, Santos Zalduegui JF (1997) Description of a Rb, Sr, Sm and Nd separation method for silicate rocks in isotopic studies. I Congr Iber Geoquim Abstract Vol, pp 46–55 (in Spanish)

Richardson SW, Gilbert MC, Bell PM (1969) Experimental determination of kyanite–andalusite and andalusite–sillimanite equilibria: the aluminium silicate triple point. Amer J Sci 267, 259–272

Rodríguez-Alonso MD, Peinado M, López-Plaza M, Franco P, Carnicero A, Gonzalo JC (2004) Neoproterozoic–Cambrian synsedimentary magmatism in the Central Iberian Zone (Spain): geology, petrology and geodynamic significance. Int J Earth Sci 93: 897–920

Rossi JN, Toselli AJ, Saavedra J, Sial AN, Pellitero E, Ferreira VP (2002) Common crustal sources for contrasting peraluminous facies in the early Paleozoic Capillitas Batholith, NW Argentina. Gondwana Res 5: 325–337

Rudnick RL, Gao S (2003) Composition of the continental crust. In: Rudnick RL (ed) The Crust, vol. 3 Treatise of Geochemistry. Elsevier-Pergamon, Oxford, pp 1–64

Sun SS, McDonough WF (1989) Chemical and isotopic systematics of oceanic basalts; implications for mantle composition and processes. In: Saunders AD, Norry MJ (ed) Magmatism in the Ocean Basins. Geol Soc London Spec Publ 42: 313–345

Sylvester PJ (1998) Post-collisional strongly peraluminous granites. Lithos 45: 29–44

Ugidos JM, Valladares MI, Recio C, Rogers G, Fallick AE, Stephens WE (1997) Provenance of Upper Precambrian–Lower Cambrian shales in the Central Iberian Zone, Spain: evidence from a chemical and isotopic study. Chem Geol 136: 55–70

Valladares MI, Barba P, Ugidos JM (2002) Precambrian. In: Gibbons W, Moreno T (eds) The Geology of Spain. Geol Soc London, pp 7–16

Villaseca C, Barbero L (1994) Chemical variability of Al-Ti-Fe-Mg minerals in peraluminous granitoid rocks from central Spain. Eur J Mineral 6: 691–710

Villaseca C, Herreros V (2000) A sustained felsic magmatic system: the Hercynian granitic batholith of the Spanish Central System. Trans Roy Soc Edinb, Earth Sci 91: 207–219

Villaseca C, Barbero L, Rogers G (1998a) Crustal origin of Hercynian peraluminous granitic batholiths of central Spain: petrological, geochemical and isotopic (Sr, Nd) constraints. Lithos 43: 55–79

Villaseca C, Barbero L, Herreros V (1998b) A re-examination of the typology of peraluminous granite types in intracontinental orogenic belts. Trans R Soc Edinb, Earth Sci 89: 113–119

Villaseca C, Downes H, Pin C, Barbero L (1999) Nature and composition of the lower continental crust in central Spain and the granulite-granite linkage: inferences from granulite xenoliths. J Petrol 40: 1465–1496

Villaseca C, Orejana D, Paterson BA, Billstrom K, Pérez-Soba C (2007) Metaluminous pyroxene-bearing granulite xenoliths from the lower continental crust in central Spain: their role in the genesis of Hercynian I-type granites. Eur J Mineral 19: 463–477

Visonà D, Lombardo B (2002) Two-mica and tourmaline leucogranites from the Everest–Makalu region (Nepal–Tibet). Himalayan leucogranite genesis by isobaric heating? Lithos 62: 125–150

Wolf MB, London D (1994) Apatite dissolution into peraluminous haplogranitic melts: an experimental study of solubilities and mechanisms. Geochim Cosmochim Acta 58: 4127–4145

Journal of Geosciences, 53 (2008), 281–305 DOI: 10.3190/jgeosci.037

Original paper

The Brno Batholith: an insight into the magmatic and metamorphic evolution of the Cadomian Brunovistulian Unit, eastern margin of the Bohemian Massif

Jaromír LEICHMANN[1,*], Volker HÖCK[2]

[1] *Department of Geological Sciences, Faculty of Science, Masaryk University Brno, Kotlářská 2, 611 37 Brno; leichman@sci.muni.cz*
[2] *Fachbereich Geographie, Geologie und Mineralogie der Universität Salzburg, Hellbrunnerstrasse 34/III, A-5020 Salzburg, Austria*
[*] *Corresponding author*

The Brno Batholith, a part of the larger Brunovistulian Unit, consists of three genetically independent complexes – Western Granitoid Complex (part of the Thaya Terrane), Ophiolite Belt (formerly Metabasite Zone or Central Basic Belt), and Eastern Granitoid Complex (part of the Slavkov Terrane). The field with geochronological evidence indicate younger age of both granitoid complexes compared with the ophiolite.

The composition of the *Eastern Granitoid Complex* (not newly studied in this paper) points to a relatively primitive Cadomian volcanic-arc environment. The *Ophiolite Belt* comprises a tilted segment of an almost complete metamorphosed ophiolite sequence with lithologically and geochemically obvious suprasubduction signature. Three main granite suites, with distinct S-, I-, and A-type affinities, are exposed in the *Western Granitoid Complex*. Abundance of crustal xenoliths, complex morphological zircon population, overall S-type chemistry, as well as geophysical and petrological evidence for basalt underplating, all point to the origin of the Tetčice suite via melting of the older metasedimentary crust. The Rena suite consists of I-type volcanic-arc granodiorites to granites, whereas small intrusions of granites with certain A-type affinity are characteristic of the Hlína suite. Equivalents of all three suits were recognized in the northern part of the Dyje Batholith, which represents the direct continuation of the western branch of the Brno Batholith.

The geological structure and geochronological data from both the Brno and Dyje batholiths exhibit some similarities with those documented in the Eastern Desert in Egypt. This may indicate a probable Gondwana affinity to the whole Brunovistulian assembly.

Keywords: Brno Batholith, Brunovistulicum, granites, ophiolites, Gondwana, petrology
Received: 22 October 2008; accepted 9 January 2009; handling editor: E. Jelínek

1. Introduction

The aim of this paper is new petrologic characterization and geological interpretation of the Brno Batholith. This paper deals mainly with mafic rocks from the Metabasite Zone, and granites from the Western Granitoid. The position of Brno Batholith in the Brunovistulian Complex Unit as well as its relation to the southern Dyje Massif, and magmatic evolution of the whole Brunovistulicum are discussed.

The easternmost margin of the Bohemian Massif on the Austrian, Czech, and Polish territories, approximately between the Danube and the Odra rivers, is built up of a complex of metamorphic and magmatic rocks called Brunovistulicum by Dudek (1980) or the Brunovistulian Complex by Jelínek and Dudek (1993). The most important outcrops of Brunovistulicum are the Dyje (Thaya) Batholith (Finger et al. 1995, 2000a) or Dyje Massif in the Czech literature (e.g. Štelcl and Weiss 1986), between Krems and Znojmo at the Czech–Austrian border; the Brno Batholith (Leichmann 1996; Hanžl and Melichar 1997; Kalvoda et al. 2008), or Brno Massif (Štelcl and Weiss 1986) in the vicinity of Brno (Fig. 1); and the Desná Gneiss (Fišera and Patočka 1989) in the Jeseníky Mountains (N Moravia). The term 'batholith' is preferred here, as the term 'massif' has not been used in the English publications for large granitic bodies recently (see Best and Christiansen 2001). The eastern part of the Brunovistulicum, which was not reactivated during the Variscan orogeny, acted as a stable foreland for both the Variscan and the Alpine fold belts. In the west, the Moravicum as the western Variscan mobile part was thrust onto non-mobilized part of the Brunovistulicum, and in turn concealed under the Moldanubian nappes. In the East, the Brunovistulicum, together with its sedimentary cover, is covered by the Carpathian nappes. The buried eastern part is known from deep drillings, and was described by Dirnhofer (1996) with Riegler (2000) in Austria, Jelínek and Dudek (1993) with Finger et al. (2000a) in the Czech Republic, and by Żelaźniewicz et al. (1997, 2001 and citations therein) in Poland. The Brunovistulicum consists of low- to high-grade metamorphic rocks (Höck 1975; Dudek 1980; Štelcl and Weiss 1986; Finger et al 2000a) and several types of magmatic rocks, rang-

ing from ultramafic to very acid rhyolites (Leichmann 1996). Jelínek and Dudek (1993) interpreted the whole magmatic Brunovistulian assembly, based mostly on the geochemical data from the covered part of this unit, as being comagmatic. The most widespread, well-preserved, and remarkable surface exposure of the Brunovistulian Complex is the Brno Batholith. A comparison with the other exposed and covered parts of Brunovistulicum shows that the composition and architecture in the Brno Batholith is of crucial importance for the whole of Brunovistulicum and its correct interpretation.

2. Geological setting

The Brno Batholith exhibits a complex internal structure and evolutionary history. It extends over 70 km in the S–N direction between Miroslav in the South and Boskovice in the North. Brno is situated in central part towards the E (Fig. 2). In the West the Brno Batholith is off cut by the eastern marginal fault of the Boskovice Furrow. In the East it is covered partly by Tertiary and Quaternary, and partly in contact with Devonian and Carboniferous sediments. It can be subdivided into three parts (com-

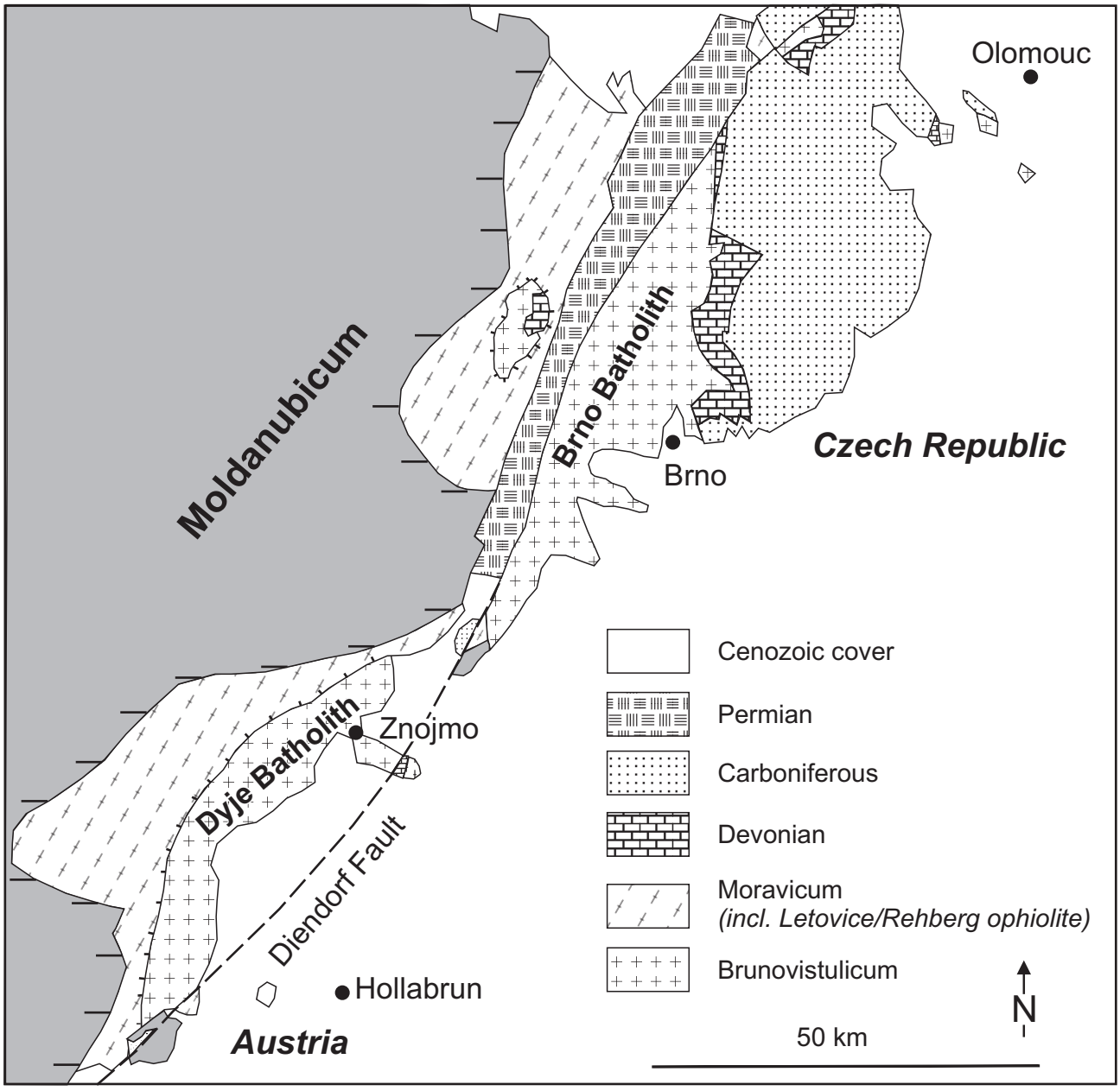

Fig. 1 Simplified map of the eastern margin of the Bohemian Massif.

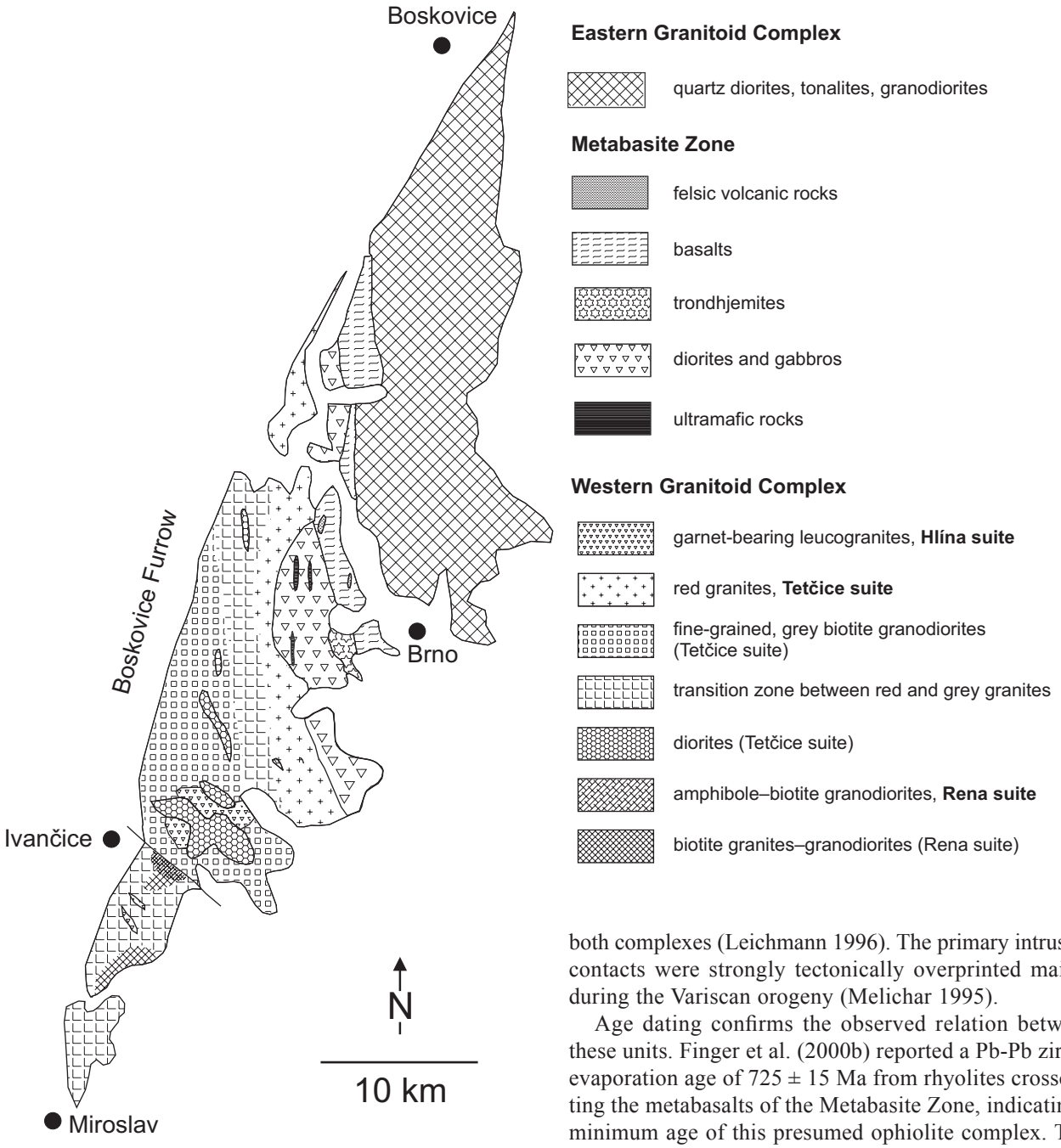

Fig. 2 Geological sketch map of the Brno Batholith.

plexes) separated by steep boundaries (Štelcl and Weiss 1986, Fig. 2). The Western Granitoid Complex consists of granites, granodiorites, and diorites, which intruded highly metamorphosed gneisses, amphibolites, and calc silicates schists. The central part, Metabasite Zone in the older Czech literature, is chiefly an assemblage of mafic plutonic and volcanic rocks; and the Eastern Granitoid Complex is built by granodiorites, tonalites, and quartz diorites. The Metabasite Zone is cut by granitoids of the both complexes (Leichmann 1996). The primary intrusion contacts were strongly tectonically overprinted mainly during the Variscan orogeny (Melichar 1995).

Age dating confirms the observed relation between these units. Finger et al. (2000b) reported a Pb-Pb zircon evaporation age of 725 ± 15 Ma from rhyolites crosscutting the metabasalts of the Metabasite Zone, indicating a minimum age of this presumed ophiolite complex. This age contrasts with these reported from granitoids of the western and eastern complexes. Several geochronological data were reported from both granitoid complexes. An $^{40}Ar/^{39}Ar$ amphibole dating from the eastern part yielded an age of 596.1 ± 2.1 Ma (Dallmeyer et al. 1994). From the western part are known two ages for the diorites; a U-Pb zircon age of 584 ± 5 Ma (van Breemen et al. 1982) is very close to an $^{40}Ar/^{39}Ar$ age determination on amphibole of 586.9 ± 0.5 Ma (Dallmeyer et al. 1994).

In the following chapters we will concentrate on the Metabasite Zone and the granites of the Western Granitoid Complex. Regarding the Eastern Granitoid Complex

we will refer only to published data (Štelcl and Weiss 1986; Jelínek and Dudek 1993; Hanžl 1994; Hanžl and Melichar 1997; Finger et al. 2000a).

3. Methods

Whole-rock major-element and mineral analyses were carried out by means of an electron microprobe (EMP, type JEOL 8600, at University of Salzburg). The glass pellets (for EMP) and polished thin-sections were measured at 15 kV and 50 nA. Glass pellets were prepared from melted rocks with addition of lithium borate; five points were measured on each pellet. Major elements were corrected according to the ZAF method.

Trace elements were determined on powder pellets using Philips PW 1400 XRF (University of Salzburg) at 45kV/60 mA. Zircons were separated according to the method described by Frasl (1963), their morphology was evaluated according to Pupin (1980). The REE were determined at the Acme Chemical Laboratories Ltd, Vancouver, by ICP-MS. See *http://www.acmelab.com* for analytical details.

4. Results

4.1. Metabasite Zone

The Metabasite Zone (Štelcl and Weiss 1986) or Central Basic Belt (Finger et al. 2000a) is situated between the two granitoid parts, and constitutes a 27 km long and maximally 8 km wide belt. This zone is divided, based on the lithology, in two sequences – (a) plutonic and (b) volcanic. The former consists of four rock types (ultramafic rocks, amphibole-bearing diorites, gabbros, and trondhjemites – Leichmann 1994), and the later of two rock assemblages – basalts and bimodal association of dolerites with rhyolites.

The whole complex dips to the east. Therefore the plutonic rocks crop out preferentially in the West, while the volcanic sequence is found in the East, of the Metabasite Zone. The Zone is marked by a distinct positive gravity anomaly (Geofyzika 2000).

Apart from the rock types listed above, younger discordant intrusions of fine-grained granites to rhyolites belonging of the granitoid complexes, Silurian basaltic (Přichystal 1999), and Variscan lamprophyric dykes (Šmejkal 1964), were mapped in this belt.

4.1.1. Plutonic sequence

The ultramafic rocks form small – max. 50 m thick and 400 m long – elongated lenses and layers in the gabbros and diorites. Their present-day mineralogy is of metamorphic origin. The ultramafic rocks are not homogenous; several types could be distinguished based on their mineralogical and chemical compositions (Sulovský 1975; Gregerová 1982; Leichmann 1996). The rocks could be classified, based on CIPW normative compositions, as dunites and harzburgites consisting mainly of serpentine, talk, chlorite and iron oxides, whereas green amphibole, chlorite, and iron oxides are major components in the olivine websterites.

Diorites and gabbros are the most widespread rocks in the plutonic sequence. Diorites strongly prevail over gabbros. Cumulate- as well as pegmatite-like structures (with up to 12 cm long amphiboles) are observed within the gabbros, partly alternating with layers of former websterites.

The modal composition with variably zoned plagioclase (Tab. 1), amphibole (Tab. 2, Fig. 3), zoisite, chlorite, epidote, carbonate, white mica, Fe/Ti oxides, and rarely quartz imply a complex metamorphic overprinting (see below for details). Due to the metamorphic overprinting, the original composition of plagioclases, necessary to distinguish between gabbros and diorites, is only rarely preserved. Tentatively we used instead the whole-rock geochemistry (Tab. 3). Two groups can be distinguished: one with higher SiO_2 (51–53 wt. %) and low MgO (~5 %), and another more basic (SiO_2 ~ 49 %) with high MgO (~20 %) corresponding by their normative Ab/An ratios to diorites and gabbros, respectively. Low concentrations of HFSE (TiO_2 = 0.72–0.84 wt. %; Zr = 7–24 ppm; Nb = 3–4 ppm and Y = 8–11 ppm), as well as of LILE (Rb = 13–19 ppm; Sr = 438–558 ppm and Ba = 95–106) are typical of both diorites and gabbros. However, the concentrations of LILE, mainly Rb, as well as K (0.44–0.69 wt. % K_2O) might be elevated as a consequence of the later alteration (sericitization) of plagioclases.

Trondhjemites (Baker 1979) crop out at the boundary between the plutonic and volcanic sequences. They consist of plagioclase (52–66 vol. %), ranging from An_1 at the rims to the An_{30} in the cores (Tab. 1; points 26–29), quartz (25–43 vol. %), relics of clinopyroxene, rarely K-feldspar (less than 1 %), secondary white mica, and chlorite (up to 9 %). The younger albite and white mica replace the original oscillatory-zoned plagioclase almost entirely. The clinopyroxene is nearly completely replaced by chlorite and Fe–Ti oxides. The chemical composition (Tab. 3), with high SiO_2 (72.8–74.5 wt. %), Na_2O (4.4–4.5 %), and low CaO (0.95–1.5 %), with FeO_{tot} (1.4–2 %) is in accord with their mineralogy. The unusually high concentration of K_2O (0.83–1.3 %), not typical of trondhjemites, is caused by later sericitization of plagioclase. Table 4 (analyses 7–10) shows four EMP analyses of the fine-grained muscovites replacing the

Tab. 1 Electron microprobe analyses from plagioclase (wt. % and apfu based on 8 O)

Sample	1	2	3	4	5	6	7	8	9	10	11	12	13	14	15
SiO_2	57.69	62.11	60.54	66.88	64.87	62.99	62.25	67.63	55.53	55.68	58.20	57.53	68.19	67.79	66.56
Al_2O_3	26.01	23.46	24.09	20.48	21.86	23.16	23.	19.68	28.06	27.96	26.19	26.99	19.61	19.60	19.99
FeO	0.00	0.00	0.10	0.16	0.00	0.00	0.00	0.06	0.07	0.00	0.06	0.12	0.00	0.14	0.07
CaO	8.17	4.74	4.93	1.18	2.81	4.45	4.93	0.60	10.38	10.20	8.26	8.82	0.14	0.30	0.88
Na_2O	6.58	8.70	7.94	10.47	9.85	8.69	8.61	11.18	5.66	5.83	6.82	6.49	11.35	11.05	10.82
K_2O	0.23	0.13	0.35	0.40	0.07	0.14	0.25	0.12	0.09	0.10	0.12	0.12	0.09	0.09	0.11
Total	98.68	99.14	97.95	99.57	99.46	99.43	99.52	99.27	99.79	100.07	99.65	100.08	99.38	98.97	98.43
Si	2.613	2.771	2.737	2.994	2.867	2.796	2.770	2.978	2.504	2.516	2.612	2.575	2.993	2.989	2.958
Al	1.388	1.234	1.284	1.062	1.139	1.212	1.231	1.021	1.491	1.481	1.385	1.424	1.014	1.019	1.047
Ca	0.396	0.277	0.239	0.056	0.133	0.212	0.235	0.028	0.502	0.491	0.397	0.423	0.007	0.014	0.042
Na	0.578	0.753	0.696	0.893	0.844	0.748	0.743	0.955	0.495	0.508	0.593	0.563	0.966	0.945	0.932
K	0.013	0.007	0.020	0.022	0.004	0.008	0.014	0.007	0.005	0.006	0.007	0.007	0.005	0.005	0.006
An	0.401	0.230	0.250	0.057	0.136	0.219	0.237	0.029	0.501	0.489	0.398	0.426	0.007	0.015	0.043
Ab	0.585	0.763	0.729	0.920	0.860	0.773	0.749	0.965	0.494	0.505	0.595	0.567	0.988	0.980	0.951
Or	0.013	0.008	0.021	0.023	0.004	0.008	0.014	0.007	0.005	0.006	0.007	0.007	0.005	0.005	0.006

Sample	16	17	18	19	20	21	22	23	24	25	26	27	28	29
SiO_2	66.19	63.90	64.30	65.40	65.40	50.45	49.72	65.42	61.77	59.67	60.43	60.62	68.87	68.10
Al_2O_3	21.14	21.80	22	20.70	21	30.77	31.58	21.51	24.36	25.39	24.08	24.40	19.39	19.35
FeO	0.15	0.06	0.08	0.00	0.00	0.27	0.12	0.09	0.07	0.00	0.13	0.13	0.00	0.00
CaO	1.69	3.04	3.06	1.73	2.20	14.32	14.65	2.58	3.78	7.39	6.22	6.14	0.08	0.18
Na_2O	10.06	9.40	9.80	10.40	10.10	3.65	3.22	10.16	8.40	7.40	7.99	7.83	11.64	11.43
K_2O	0.41	0.40	0.29	0.12	0.06	0.04	0	0.08	0.94	0.06	0.24	0.31	0.05	0.07
Total	99.64	98.60	99.53	98.35	98.76	99.51	99.29	99.84	99.31	99.89	99.09	99.44	100.00	99.13
Si	2.914	2.856	2.849	2.916	2.905	2.314	2.283	2.882	2.754	2.662	2.715	2.711	3.004	2.998
Al	1.097	1.148	1.149	1.088	1.099	1.663	1.709	1.117	1.280	1.335	1.275	1.286	0.997	1.004
Ca	0.080	0.146	0.145	0.083	0.105	0.704	0.721	0.122	0.180	0.353	0.299	0.294	0.004	0.009
Na	0.859	0.814	0.842	0.899	0.870	0.325	0.287	0.868	0.726	0.640	0.696	0.679	0.985	0.975
K	0.023	0.023	0.016	0.007	0.003	0.003	0	0.004	0.054	0.004	0.014	0.018	0.003	0.004
An	0.083	0.148	0.145	0.084	0.107	0.683	0.715	0.122	0.188	0.354	0.297	0.297	0.004	0.009
Ab	0.893	0.829	0.839	0.909	0.889	0.315	0.285	0.873	0.756	0.642	0.690	0.685	0.994	0.987
Or	0.024	0.023	0.016	0.007	0.003	0.002	0	0.005	0.056	0.004	0.014	0.018	0.003	0.004

Nr. 1–4; J/10/93 amphibole-biotite granodiorite (Rena suite): 1 core; 2 medium zone; 3 rim; 4 albitic rim
Nr. 5–8; J/5/93 fine-grained, grey biotite granodiorite (Tetčice suite): 5 altered core; 6–7 medium zone; 8 albitic rim
Nr. 9–12; J/14b/93 biotite-amphibole diorites: 9–10 core; 11–12 rim
Nr. 13–16; J/23/93 red granites (Tetčice suite): 13–14 albite appearing together with white mica; 15–16 irregular layers of slightly more calcic albite in previous type
Nr. 17–20; J/21/93 garnet-bearing leucogranites: 17–18 core; 19–20 rim
Nr. 21–25; diorites, plutonic complex (Ophiolite Belt): 21–22 core; 23–24 rim; 25 transition core–rim
Nr. 26–29; trondhjemites, plutonic complex (Ophiolite Belt): 26–27 core; 28–29 rim

plagioclase. They are rich in K_2O (10.3–10.4 wt. %) and Al_2O_3 (31–31.6 %), but poor in CaO (max. 0.08 wt. %) and Na_2O (up to 0.20 wt. %). As the later crystallization of white mica is affecting the whole area, the potassium enrichment is probably a secondary feature, possibly connected to the intrusion of younger granites. Apart from disturbed K contents, the low concentrations of LILE (Rb = 15–25 ppm, Sr = 264–295 ppm), as well as those of the HFSE (Nb = 5–7 ppm, Zr = 80–295 ppm, Y = 9–10 ppm, Ti = 840–1619 ppm, Tab. 3) are noticeable.

4.1.2. Volcanic sequence

In the volcanic sequence were recognized dolerites, pillow lavas, massive lava flows as well as tuffs. Petrological and geochemical studies indicate a bimodal volcanism.

Tab. 2 Electron microprobe analyses from amphibole (wt. % and apfu based on 23 O)

Sample	1	2	3	4	5	6	7	8	9	10	11
SiO_2	43.81	44.40	41.89	42.68	53.40	54.84	48.99	46.38	49.58	51.31	54.16
TiO_2	1.11	1.47	0.37	0.32	0.11	0.10	0.86	0.25	0.24	0.74	0.83
Al_2O_3	9.69	9.28	13.98	13.72	2.15	1.38	6.15	8.85	5.13	4.10	2.05
Cr_2O_3	n.d.	n.d.	n.d.	n.d.	n.d.	n.d.	n.d.	n.d.	n.d.	0.22	0.28
FeO	18.43	18.77	17.50	17.41	12.30	10.97	14.15	18.27	17.41	14.59	10.66
MnO	0.36	0.34	0.32	0.35	0.21	0.24	0.26	0.27	0.36	0.32	0.25
MgO	9.54	9.44	8.71	8.91	15.70	16.98	13.19	9.79	11.64	13.70	16.56
CaO	11.99	11.77	11.30	11.82	12.51	12.45	11.92	11.90	12.30	12.32	12.78
Na_2O	0.89	1.04	1.25	1.17	0.15	0.12	0.51	0.83	0.56	0.41	0.18
K_2O	0.76	0.74	0.24	0.28	n.d.	n.d.	0.25	0.20	0.17	0.08	0.03
Total	96.57	97.24	95.56	96.67	96.53	97.08	96.27	96.57	97.39	97.78	97.77
Si	6.693	6.737	6.406	6.449	7.765	7.862	7.256	6.991	7.374	7.480	7.726
Al^{IV}	1.307	1.263	1.594	1.551	0.235	0.138	0.744	1.009	0.626	0.520	0.274
Al^{VI}	0.438	0.397	0.925	0.892	0.133	0.096	0.329	0.564	0.273	0.184	0.071
Ti	0.127	0.168	0.043	0.036	0.012	0.011	0.095	0.029	0.027	0.081	0.090
Cr	0.000	0.000	0.000	0.000	0.000	0.000	0.000	0.000	0.000	0.026	0.031
Mn	0.046	0.043	0.041	0.045	0.026	0.029	0.033	0.035	0.046	0.039	0.030
Mg	2.172	2.137	1.986	2.008	3.402	3.630	2.914	2.20	2.581	2.977	3.521
Fe^{2+}	2.216	2.255	2.006	2.018	1.426	1.233	1.629	2.172	2.073	1.694	1.256
Fe^{2+}	0.139	0.126	0.233	0.182	0.069	0.081	0.124	0.131	0.092	0.085	0.015
Ca	1.963	1.914	1.852	1.914	1.949	1.912	1.891	1.922	1.960	1.924	1.953
Na	0.365	0.346	0.454	0.438	0.060	0.026	0.162	0.297	0.215	0.125	0.018
K	0.147	0.143	0.046	0.053	0.000	0.000	0.047	0.038	0.033	0.014	0.005
XMg (mol)	0.480	0.473	0.470	0.477	0.695	0.734	0.624	0.489	0.544	0.626	0.735

Nr. 1–2, J/14b/93; biotite-amphibole diorites (Tetčice suite)
Nr. 3–7; diorites, plutonic complex (Ophiolite Belt): 3–4 rim; 5–6 core; 7 transition core–rim
Nr.8–11 metabasalts, volcanic complex (Ophiolite Belt): 8–9 rim; 10–11 core
n.d. – nit determined

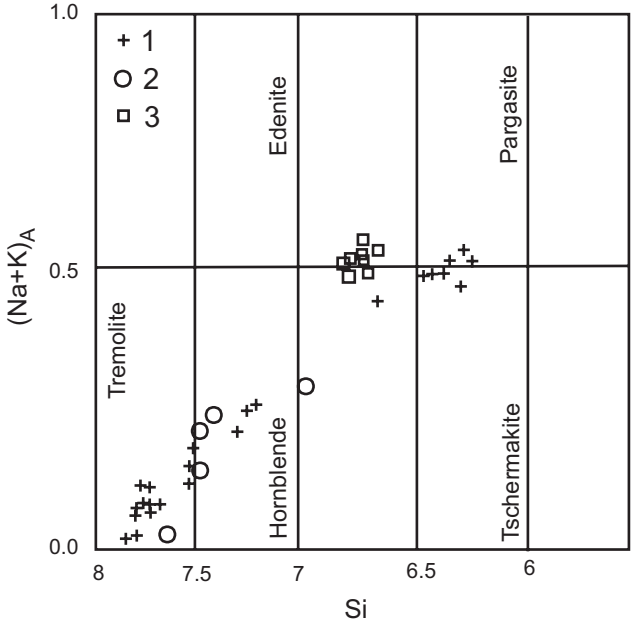

As in the plutonic sequence, the original mineralogy was overprinted by a metamorphic assemblage. The mafic metavolcanics consist mainly of amphibole and plagioclase ($An_{5–15}$). Other important phases are chlorite, epidote, zoisite, carbonate and white mica. Increasing content of secondary white mica is accompanied by an increase in alkalis in the whole-rock geochemical analyses. Thus, the geochemical classification of the volcanic products based on the TAS diagram (Fig. 4) has to be considered with caution. This is particularly important for the analyses plotting in, or close to, the field of the

Fig. 3 Classification of the Ca-rich amphiboles according to Deer et al. (1992) in the binary plot Si vs. Na + K in the A position (atoms per formula unit).
1 – amphiboles from diorites, magmatic complex, Metabasite Zone
2 – amphiboles from basalts, volcanic complex, Metabasite Zone
3 – amphiboles from diorites, Tetčice suite, Western Granitoid Complex

Tab. 3a Whole-rock major- and trace-element analyses from the Western Granitoid Complex and the Ophiolite Belt (wt. % and ppm)

Sample	1	2	3	4	5	6	7	8	9	10	11	12	13	14	15
	J/8	J/9	J/10	J/22	J/3	J/19	J/4	J/5	J/6	J/1c	J/14b	J/15	J/16	J/20	J/23
SiO_2	71.97	73.35	69.43	70.14	71.86	71.86	72.19	73.43	72.33	51.67	51.42	64.55	74.04	73.46	74.21
TiO_2	0.26	0.16	0.37	0.35	0.27	0.21	0.21	0.13	0.27	1.46	1.39	0.32	0.15	0.11	0.21
Al_2O_3	14.59	14.28	15.11	15.38	14.67	15.17	14.96	15.11	15.64	18.16	18.75	18.33	13.92	13.74	13.74
FeO	2.05	1.46	2.83	2.54	2.04	1.55	1.81	1.24	2.09	8.80	9.04	2.80	1.25	1.41	1.57
MnO	0.01	0.07	0.43	0.09	0.10	0.04	0.04	0.00	0.00	0.13	0.15	0.09	0.00	0.00	0.00
MgO	0.74	0.46	1.25	0.97	0.54	0.38	0.67	0.53	0.40	4.62	4.56	0.95	0.36	0.23	0.51
CaO	2.22	1.95	2.73	2.69	2.05	2.29	1.41	1.84	1.56	7.79	8.08	4.25	1.24	1.35	0.62
Na_2O	3.25	3.24	3.29	3.64	3.64	3.87	4.34	4.23	4.66	3.71	3.65	4.51	3.13	3.25	3.39
K_2O	3.83	3.82	3.36	2.88	3.46	3.15	2.55	3.37	2.82	2.32	1.74	2.18	4.61	4.68	5.13
P_2O_5	0.05	0.00	0.09	0.11	0.09	0.03	0.05	0.00	0.02	0.64	0.44	0.10	0.00	0.07	0.07
LOI	0.90	0.75	1.15	1.45	1.05	0.80	1.10	0.75	0.40	1.40	1.40	1.00	0.95	0.85	0.60
Sum	99.87	99.53	99.65	100.23	99.76	99.35	99.32	100.62	100.20	100.71	100.62	99.06	99.66	99.47	100.08
Nb	10	11	11	12	15	11	9	7	15	22	23	10	17	7	15
Zr	92	71	121	120	92	125	147	80	324	220	182	227	155	109	166
Y	19	10	22	17	25	14	16	10	17	34	31	10	18	13	17
Sr	211	169	268	303	266	356	384	427	197	793	823	684	270	307	196
Rb	150	163	134	114	120	94	87	104	79	75	53	57	123	100	133
Pb	19	18	22	18	16	20	16	24	14	18	17	16	15	14	17
Ga	16	15	17	17	18	18	15	16	18	22	23	20	17	15	15
Zn	48	31	51	48	42	42	20	45	38	99	91	42	17	19	24
Cu	9	4	7	7	9	6	7	12	4	24	17	13	19	10	10
Ni	11	7	9	9	8	9	8	9	6	23	18	9	6	7	9
Co	11	6	6	4	4	2	6	8	8	22	22	6	8	3	4
Ba	462	322	525	473	444	622	849	1284	1554	1364	648	767	1185	779	796
Sc	4	2	5	4	4	1	2	0	4	27	24	3	2	1	0
Cr	8	7	8	3	4	0	1	4	7	137	96	2	3	0	0
V	20	11	31	20	12	6	15	8	3	192	156	23	5	3	7
K/Rb	211	195	208	210	239	278	243	269	296	256	272	317	311	388	320
K/Ba	67	98	53	50	64	42	24.9	18	17.2	14	22	24	32	49.9	53
mg#	27	24	31	28	21	28	27	30	16	34	34	25	22	14	25

Nr. 1–6 Rena suite: 1–4 amphibole-biotite granodiorites; 5–6 biotite granodiorites–granites
Nr. 7–12 Tetčice suite: 7–9 biotite granodiorites; 10–11 biotite-amphibole diorites; 12 biotite tonalite
Nr. 13–15 red granites

trachybasalts (S1), basaltic trachyandesites (S2) and trachytes (T). Despite of possibly affected alkalis, the TAS diagram indicates a bimodal distribution. The basaltic rocks cluster in one area, but can be separated into two groups based on their trace-element contents (Tab. 3). In the first group, the NMORB-normalized (Pearce and

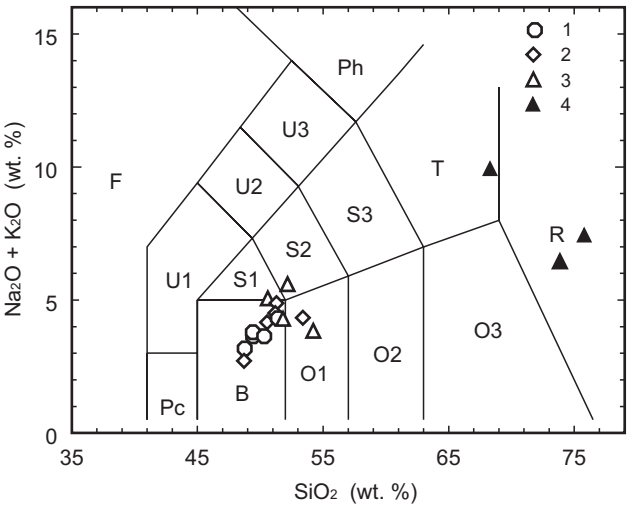

Fig. 4 Total alkalis–silica (TAS) diagram (Le Maitre 1989). 1 – basalts with MORB character, 2 – enriched basalts, 3 – transitional basalts, 4 – felsic volcanic rocks.
The basalts with MORB character plot in the field of basalts (B), the enriched basalts in the field of basaltic andesites (O1) and basaltic trachyandesites (S2), The felsic volcanic rocks fall into the field of rhyolites (R) and trachytes (T).

Tab. 3a Continued

Sample	16	17	18	19	20	21	22	23	24	25	26	27	28	29
	J/29	J/21b	J/21c	J Re	J Iv	J/7	J/11	J/24	J/70	J/126	J/79	J/31	J/32	J/33
SiO_2	74.11	75.79	75.86	74.92	75.46	72.95	74.47	72.83	52.73	51.78	49.66	47.25	50.81	47.43
TiO_2	0.20	0.03	0.04	0.04	0.04	0.27	0.14	0.22	0.72	0.84	0.44	1.15	2.46	1.72
Al_2O_3	13.62	13.64	13.60	13.48	13.27	15.40	14.27	15.07	19.15	19.57	7.98	16.37	14.79	14.89
FeO	1.68	0.9	0.71	0.79	0.84	2.02	1.38	1.74	8.12	8.07	8.07	9.21	12.32	11.75
MnO	0.00	0.1	0.09	0.04	0.9	0.05	0.09	0.00	0.14	0.16	0.16	0.16	0.23	0.19
MgO	0.44	0.03	0.03	0.03	0.02	1.13	0.68	0.88	5.13	5.44	20.76	9.50	4.61	6.57
CaO	0.36	0.96	1.02	1.16	0.61	0.96	0.95	1.53	8.12	9.77	8.83	10.02	6.00	11.92
Na_2O	3.80	3.85	3.85	3.93	4.18	4.52	4.51	4.44	3.46	3.44	1.00	2.23	4.73	2.50
K_2O	4.89	4.21	4.29	4.15	4.11	1.26	1.28	0.83	0.69	0.44	0.14	0.85	0.72	0.14
P_2O_5	0.04	0.02	0.01	0.01	0.01	0.06	0.07	0.00	0.19	0.16	0.00	0.16	0.75	0.25
LOI	1.10	0.30	0.30	0.70	0.50	1.75	1.50	1.70	2.40	1.40	2.95	3.15	2.30	2.70
Sum	100.21	99.71	99.8	99.25	99.13	100.34	99.33	99.24	100.86	101.07	100.00	100.02	99.72	100.04
Nb	9	51	45.5	19	23	5	7	6	3	4	2	3	12	5
Zr	147	79	74	76	72	80	100	91	7	24	10	76	285	120
Y	16	56	47	23	14	9	10	9	8	11	7	23	72	35
Sr	384	22	21	30	16	264	300	295	438	558	69	198	152	286
Rb	87	174	156	174	311	25	20	15	19	13	3	20	17	3
Pb	16	11	6	8	24	14	9	10	10	11	9	4	11	7
Ga	15	24	21	20	19	15	14	15	18	18	9	17	26	22
Zn	20	9	7	12	12	62	45	61	89	95	60	81	151	97
Cu	7	1	b.d.l.	4	13	51	7	18	80	131	43	70	27	120
Ni	8	b.d.l.	b.d.l.	b.d.l.	b.d.l.	9	6	6	43	47	597	172	50	71
Co	6	1	b.d.l.	b.d.l.	1	7	2	8	35	36	78	43	24	37
Ba	849	18	14	17	46	488	517	329	106	95	37	213	192	41
Sc	2	2	2	2	1	2	2	3	32	33	27	30	33	39
Cr	1	b.d.l	b.d.l.	b.d.l.	b.d.l.	6	0	3	157	163	2111	320	98	126
V	15	5	b.d.l.	b.d.l.	b.d.l.	35	6	22	364	311	188	213	252	292
K/Rb	466	201	228	198	110	418	531	459	301	281	387	352	351	387
K/Ba	48	1941	2544	2026	742	21	21	21	54	38	31	31	31	28
mg#	21	5	7	6	5	36	33	34	39	40	72	51	27	36

Nr. 16 red granites
Nr. 17–20 Hlína suite: garnet-bearing granites
Nr. 21–26 magmatic complex, Ophiolite Belt: 21–23 trondhjemites; 24–25 diorites; 26 gabbro
Nr. 27–29 volcanic complex, Ophiolite Belt: mafic volcanics

Cann 1973) concentrations (Fig. 5a) for Sr, Nb, P, Zr, Ti, Sc and Cr, resemble closely typical MOR basalts (Pearce and Cann 1973). The enrichment in K, Rb, and Ba is probably connected with the alteration processes. In contrast, the second group of mafic volcanic rocks is enriched in elements such as P, Ti, Nb, Y, Zr, combined with low concentrations of Cr and Sc. As evidenced by the NMORB-normalized multi-element plot (Fig. 5b), they show a strong within-plate affinity. Both groups are connected by basalts, which are only moderately enriched in HFSE and depleted in Cr and Sc. The basalts with a MORB-like signature prevail in the southern part of the Metabasite Zone, whereas the enriched basalts are more widespread in the North.

The acid volcanic rocks form concordant layers, or discordant dykes, in the metabasalts. Their thickness ranges from few decimetres to several metres, but does not exceed 100 m. They are usually very fine grained and are, therefore, microscopically undistinguishable from each other.

Two acidic layers, each from geochemically contrasting basalt group, were studied in the detail for this reason only. The first one, a rhyolite layer within the basalts with a MORB-like signature shows elevated Nb, Zr, and Y contents (Tab. 3), thus resembling geochemically a "Hypothetical Ocean Ridge Granite" (HORG) according to Pearce et al. (1984). The second represents a trachyte layer within basalts with the intraplate signature. It re-

Tab. 3a Continued

Sample	30	31	32	33	34	35	36	37	38	39	40	41	42	43
	J/34	J/35	J/38	J/40	J/41	J/42	J/44	J/45	J/46	J/47	J/49	J/43	J/36	J/27
SiO_2	50.01	50.40	52.62	46.92	49.83	49.40	52.39	48.46	50.76	49.21	50.76	78.60	67.84	74.36
TiO_2	2.64	1.66	1.92	1.44	1.50	1.84	2.32	1.51	1.63	1.49	1.93	0.16	0.37	0.00
Al_2O_3	13.17	14.85	14.99	16.54	15.45	14.72	13.98	16.41	15.06	15.12	14.80	11.10	17.26	13.97
FeO	14.14	10.78	10.74	11.74	10.06	11.49	12.45	10.17	10.86	10.64	9.59	1.27	2.11	0.60
MnO	0.20	0.27	0.25	0.17	0.21	0.21	0.21	0.20	0.23	0.21	0.22	0.00	0.00	0.00
MgO	5.48	7.23	5.12	9.47	7.45	7.00	4.94	7.37	7.26	7.60	5.69	0.09	0.97	0.09
CaO	7.80	8.04	7.02	5.01	8.91	8.79	7.18	10.02	8.56	9.77	10.15	1.02	1.01	1.23
Na_2O	3.82	4.16	3.46	3.14	4.15	3.78	3.81	2.43	3.78	3.14	3.69	3.77	5.60	3.12
K_2O	1.18	0.64	0.27	0.31	0.24	0.29	0.44	1.15	0.48	0.42	0.52	2.88	3.73	4.50
P_2O_5	0.38	0.25	0.66	0.16	0.26	0.21	0.39	0.24	0.16	0.19	0.64	0.00	0.20	0.00
LOI	1.45	2.25	2.20	5.90	2.55	2.20	2.15	2.70	1.80	1.45	1.20	0.65	1.20	1.85
Sum	100.28	100.53	99.27	100.8	99.89	99.93	100.25	100.66	100.61	99.24	99.19	99.54	100.29	99.72
Nb	8	7	11	3	9	4	12	4	4	4	11	21	12	25
Zr	222	131	245	81	170	116	237	102	91	85	186	292	197	74
Y	54	32	64	24	39	34	49	31	28	27	50	54	14	19
Sr	151	222	222	90	222	175	232	198	232	234	208	88	67	78
Rb	41	18	6	8	7	6	13	34	9	13	14	44	69	195
Pb	9	17	33	3	13	6	16	11	8	15	25	9	11	14
Ga	23	18	22	18	18	19	22	17	19	18	20	14	16	16
Zn	131	121	385	18	115	115	107	112	109	88	176	12	34	26
Cu	40	78	34	48	58	120	80	88	84	42	45	5	6	7
Ni	39	94	56	128	115	58	47	124	79	98	59	10	9	6
Co	18	40	21	59	43	39	34	34	37	41	32	6	8	4
Ba	187	205	121	119	63	121	285	200	127	101	127	393	1153	214
Sc	6	34	30	30	30	39	40	35	39	33	32	5	0	1
Cr	17	229	105	289	204	159	77	226	197	192	126	19	28	1
V	392	258	169	287	241	308	430	259	301	304	243	8	301	1
K/Rb	238	295	373	321	284	401	281	281	442	298	308	543	462	191
K/Ba	59	26	19	22	32	20	13	47	31	35	34	60	26	174
mg#	28	40	25	45	42	38	28	42	40	42	37	7	31	13

Nr. 30–43 volcanic complex, Ophiolite Belt: 30–40 mafic volcanics, 41–43 rhyolites

Tab 3b Concentration of Rare Earth elements, Hlína suite, garnet-bearing granites

Sample	La	Ce	Pr	Nd	Sm	Eu	Gd	Tb	Dy	Ho	Er	Tm	Yb	Lu	U	Th
J/21b	2.00	5.00	0.87	4.30	2.20	0.21	3.44	0.74	6.51	1.64	6.30	1.23	9.18	1.74	12.30	13.90
J/21c	3.00	6.60	1.16	5.00	2.80	0.19	3.26	0.71	5.53	1.45	5.08	1.02	7.08	1.44	17.00	12.40
J Re	3.50	6.70	1.25	5.10	2.30	0.27	2.34	0.44	2.94	0.81	2.58	0.46	4.43	0.76	7.10	13.10
J Iv	1.90	5.20	0.53	2.40	1.40	0.10	2.97	0.79	6.48	1.80	6.26	1.09	10.03	1.74	16.10	21.50

sembles by its lower contents of HFSE and a higher LILE rather volcanic-arc granitoids (VAG).

4.1.3. Metamorphic evolution

The Metabasite Zone underwent several stages of metamorphic evolution, which are still under investigation. Nevertheless, some qualitative observations can be presented here.

As already stressed, the metamorphic overprint in the plutonic and volcanic sequences is pervasive. Magmatic relics are extremely rare, and could be only observed in some samples of diorites. The core of some large plagioclase crystals is still composed of homogenous bytownite

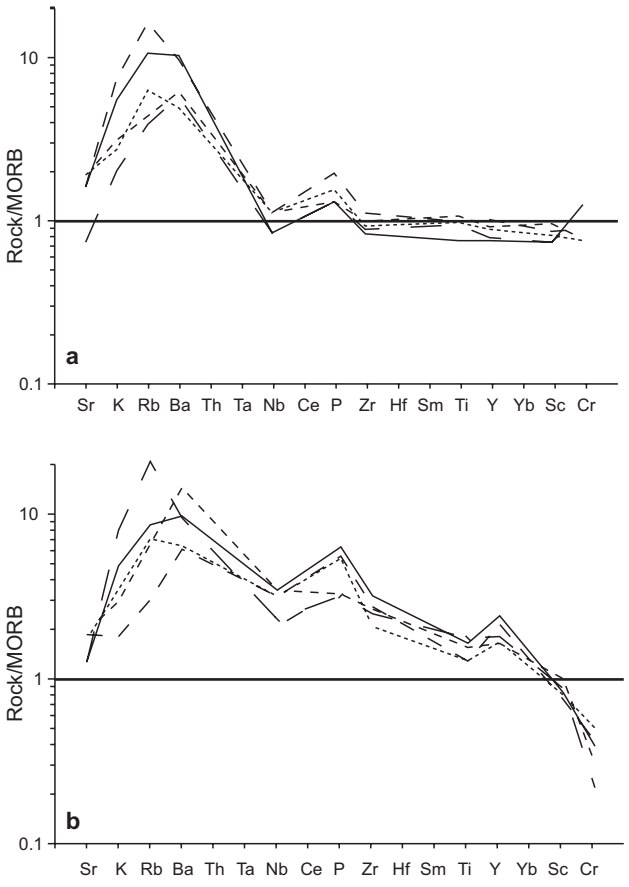

Fig. 5 The MORB-normalized (Pearce and Cann 1973) diagrams. **a –** MORB-like basalts from the volcanic complex, Metabasite Zone. The content of relatively immobile elements such as Nb, P, Zr, Ti, Y, Sc and Cr correspond well with the MORB characteristics. The enrichment in K, Rb and Ba is connected with later alteration of the rock. **b –** enriched basalts, volcanic complex, Metabasite Zone.

($An_{70,}$ Tab. 1), reflecting the magmatic stage. Albite/oligoclase rims surrounding the relicts of magmatic plagioclase document the first metamorphic event. The cores of smaller plagioclases from metabasalts were completely replaced by albite/oligoclase. Magmatic pyroxenes were transformed to actinolites in the diorites as well as in the basalts. The mineral assemblage characteristic of the first stage is albite/oligoclase + actinolite.

The second metamorphic phase is documented by an increase in Al, Na, K, and decreasing Si towards the amphibole rims. This process ultimately leads to tschermakite–pargasite rims around actinolite in the diorites, and hornblende rims in the metabasalts (Tab. 2, Fig. 3). Similarly, andesine develops around the albite/oligoclase zones in the metadiorites, whereas oligoclase commonly rims the albite/oligoclase cores in the metabasalts. This medium-grade overprint affected both the plutonic and volcanic complexes of the Metabasite Zone. However its effects can be identified only rarely, where no penetrative deformation occurred, and the magmatic textures are well preserved. Based on the still incomplete data set, the degree of the metamorphic overprinting seems to have been slightly higher within the plutonic complex.

The third metamorphic stage was retrogression. Plagioclases are often partly replaced by white mica, albite, zoisite and epidote. Effects of carbonatization are developed as well, but only locally. Chlorite and epidote replace the amphiboles. In the final stage, only chlorite pseudomorphs after amphibole are seen. The tourmaline veins and pods observed in the strongly altered diorites, along the contact with the Western Granite Complex (Novák and Filip 2002), suggest a circulation of probably granitoid-derived fluids rich in boron, through the rocks of the Metabasite Zone. Circulation of these fluids could have lead to a regional enrichment in K and probably also Rb with Ba, i.e. the elements responsible for the common muscovitization developed within the Metabasite Zone.

4.2. Granitoids

As already noted, the Metabasic Zone splits the granitoids of the Brno Batholith into two different parts, the eastern and the western complexes. Regarding the Eastern Granitoid Complex we will refer shortly only to available literature data in the following section. The Western Granitoid Complex was recently investigated by the authors and will be described and discussed in more detail.

4.2.1. Eastern Granitoid Complex

The database for the Eastern Granitoid Complex is rather variable as far as geochemical and isotopic data concerns. However the unit is petrographically rather homogenous, being built by amphibole- to amphibole-biotite quartz diorites to granodiorites. Some biotite-bearing leucotonalites and granodiorites belong to this sequence as well. The modal mineralogy includes, apart from quartz, plagioclase and K-feldspar, magmatic biotite with, or without, amphibole. Secondary alteration of rock-forming minerals is widespread (Štelcl and Weiss 1986; Hanžl 1994). The geochemistry is characterized by low contents of K and Rb, but the granodiorites are rich in MgO, Na_2O, CaO and Sr (Jelínek and Dudek 1993; Hanžl 1994). In addition few low Sr initial ratios of 0.704–0.705 and high ε_{Nd} values of 0 to +3 are available (Finger et al. 2000a). All these data suggest that the rocks can be interpreted as I-type, volcanic-arc derived granitoids (Pearce et al 1984; Chappell and White 1992).

4.2.2. Western Granitoid Complex

The original divisions of the Western Granitoid Complex were based mostly on petrographic descriptions. Thus

Tab. 4 Electron microprobe analyses from white micas (wt. % and apfu based on 22 O)

Sample	1	2	3	4	5	6	7	8	9	10
SiO_2	51.52	46.88	46.53	46.86	45.72	45.95	46.44	46.11	48.51	48.28
TiO_2	0.00	0.00	0.00	0.00	0.06	0.00	0.00	0.00	0.00	0.00
Al_2O_3	30.60	37.63	29.62	29.71	30.75	30.24	29.28	29.65	31.63	30.95
BaO	0.00	0.00	0.00	0.13	0.00	0.00	0.61	0.43	0.20	0.23
FeO	0.81	0.39	4.41	3.47	6.43	5.67	4.84	4.14	1.50	1.67
MnO	0.05	0.07	0.05	0.00	0.09	0.08	0.00	0.00	0.00	0.05
MgO	0.51	0.18	1.65	1.38	0.04	0.41	1.61	1.72	1.57	1.73
CaO	0.46	0.00	0.00	0.00	0.09	0.00	0.00	0.03	0.06	0.08
Na_2O	2.02	0.12	0.13	0.46	0.22	0.22	0.19	0.20	0.17	0.14
K_2O	9.60	11.09	11.11	10.75	10.87	11.00	10.81	10.83	10.27	10.41
Total	95.57	96.36	93.50	92.76	94.27	93.57	93.79	93.11	93.91	93.54
Si	6.779	6.134	6.445	6.504	6.340	6.398	6.456	6.429	6.535	6.550
Al^{IV}	1.221	1.866	1.555	1.498	1.660	1.602	1.541	1.571	1.495	1.450
Al^{VI}	3.525	3.938	3.281	3.364	3.366	3.360	3.259	3.300	3.556	3.499
Ti	0.000	0.000	0.000	0.000	0.006	0.000	0.000	0.000	0.000	0.000
Fe	0.089	0.043	0.511	0.403	0.746	0.660	0.563	0.483	0.169	0.190
Mn	0.006	0.008	0.006	0.000	0.011	0.009	0.000	0.000	0.000	0.006
Mg	0.100	0.035	0.341	0.286	0.008	0.085	0.333	0.357	0.316	0.350
Ca	0.065	0.000	0.000	0.000	0.013	0.000	0.000	0.005	0.009	0.011
Na	0.515	0.030	0.035	0.124	0.059	0.059	0.052	0.055	0.044	0.038
K	1.612	1.851	1.963	1.903	1.923	1.954	1.919	1.927	1.766	1.801
XMg (mol)	0.529	0.451	0.40	0.415	0.011	0.114	0.372	0.425	0.652	0.648
Mu	0.735	0.984	0.983	0.939	0.964	0.971	0.973	0.970	0.971	0.974
Pg	0.235	0.016	0.017	0.061	0.030	0.029	0.027	0.028	0.024	0.020
Ma	0.030	0.000	0.000	0.000	0.007	0.000	0.000	0.002	0.005	0.006

Nr. 1–2, J/5/93; fine-grained, grey biotite granodiorites (Tetčice suite)
Nr. 3–4, J/23/93; red granites (Tetčice suite)
Nr. 5–6, J/21/93; garnet-bearing leucogranites (Hlína suite)
Nr. 7–10, J/24/93; trondhjemites, magmatic complex of the Ophiolite Belt

Štelcl and Weiss (1986) mapped 8 granitoid types, while Mittrenga and Rejl (1993) proposed a different subdivision to 7 petrographic types. Recent study nevertheless implies that some types are genetically related, and can be therefore grouped into fewer granitic suites.

Three principal magmatic suites, Rena, Tetčice, and Hlína, have been identified in the Western Granitoid Complex (Fig. 2). The first two, Rena and Tetčice, are widespread on the surface. The rocks of the third, Hlína suite, form only discrete veins or small intrusive bodies cutting both the previous suites.

The Rena suite, named after a hill southeast of Ivančice, forms the southernmost part of the Brno Batholith. The northern Tetčice suite, termed after small village 15 km W of Brno, is separated from the Rena suite by an approximately W–E trending Ivančice Fault (Mittrenga et al. 1976; Leichmann 1996). The Jihlava river valley between villages Ivančice and Moravské Bránice is a remarkable geomorphological manifestation of this tectonic zone. It is also recognizable in the steep gravimetric gradient up to ~20 mGal (Skácelová and Weiss 1978). Geologically the Ivančice Fault separates the relatively light granitoids of the Rena suite in the South, from the more dense Tetčice suite rocks in the North. The direct contact between the two suites cannot be observed because of the younger, Tertiary–Quaternary, sedimentary cover in the Jihlava river valley.

Rena suite is represented by two types of intrusive rocks: (1) felsic (SiO_2 > 69 %), coarse-grained amphibole-biotite granodiorites, which grade into (2) biotite granites. The rocks of the suite contain almost no enclaves; some amphibole-cumulate structures (up to 1 m long layers with elevated coarse-grained amphibole contents) appear rarely. The modal composition (Tab. 5) includes oscillatory-zoned, often altered, euhedral plagioclase (Tab. 1, $An_{40–6,}$ 36–55 vol. %), anhedral quartz (23–29 %), euhedral to subhedral K-feldspar (10–26 %), pseudohexagonal biotite (0.5–8 %), euhedral amphibole (up to 7 %) and secondary chlorite (up to 10 %). Titanite, zircon, and apatite are the common accessories. The K-

Tab. 5 Modal compositions of granitoids from the Western Granitoid Complex (vol. %)

Sample	Qtz	Pl	Kfs	Bt	Amp	Grt	Ms	Chl	Opaque	Rest
1 J/22	27	46	15	8	3	–	–	1	–	×
2 J/10	29	42	13	8	7	–	–	1	×	×
3 J/140	26	44	11	1	7	–	–	9	×	×
4 J/130	25	55	10	×	–	–	–	10	×	×
5 J/139	23	50	20	×	–	–	–	6	×	×
6 J/19	26	36	26	4	–	–	–	6	–	2
7 J/3	28	41	23	5	–	–	×	2	×	×
8 J/23	22	25	46	×	–	–	×	5	2	×
9 J/23a	38	22	35	×	–	–	×	3	×	2
10 J/101	39	27	30	×	–	–	×	3	×	1
11 J/102	39	15	44	×	–	–	×	2	×	×
12 J/29	38	28	32	×	–	–	×	1	×	×
13 J/29a	30	28	37	×	–	–	×	4	×	×
14 J/12	35	25	35	5	–	–	1	1	–	×
15 J/21	26	29	41	×	–	1	2	×	1	×
16 J/13	29	30	38	1	–	1	1	×	×	×

× concentration of mineral is lower than 1 %
– mineral was not found in the sample
Nr. 1–5: amphibole-biotite granodiorites (Rena suite)
Nr. 6–7: fine-grained grey biotite granodiorites (Tetčice suite)
Nr. 8–13: red granites (Tetčice suite)
Nr. 14–16: garnet-bearing leucogranites (Hlína suite)

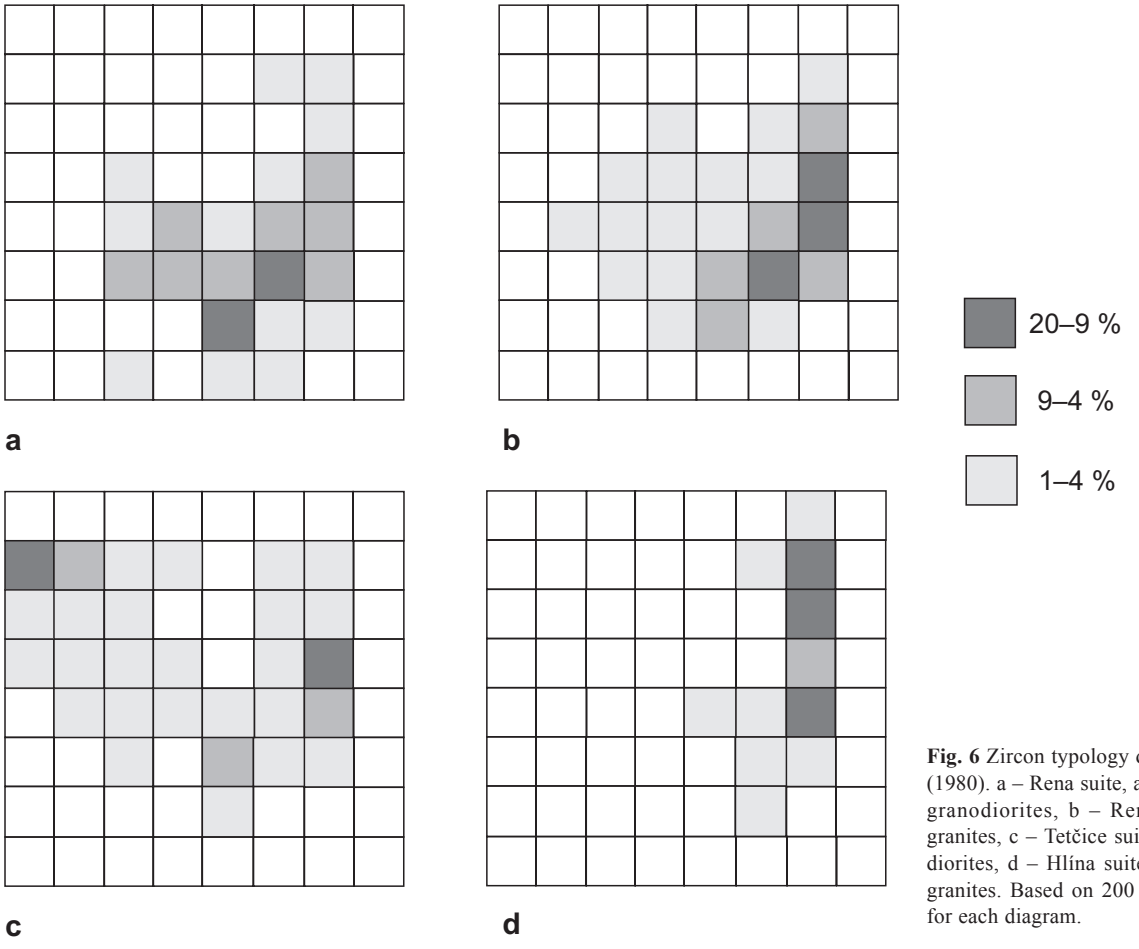

Fig. 6 Zircon typology diagram of Pupin (1980). a – Rena suite, amphibole-biotite granodiorites, b – Rena suite, biotite granites, c – Tetčice suite, biotite granodiorites, d – Hlína suite, garnet-bearing granites. Based on 200 grains examined for each diagram.

Tab. 6 Electron microprobe analyses from K-feldspar (wt. %)

Sample	SiO_2	Al_2O_3	Na_2O	K_2O	CaO	BaO	FeO	Total
1	64.6	18.3	0.46	16.5	0.00	0.27	0.00	100.16
2	64.2	18.2	0.50	16.6	0.00	0.19	0.00	99.66
3	63.9	18.2	0.51	16.2	0.00	0.29	0.00	99.12
4	64.4	18.2	0.43	16.5	0.00	0.25	0.00	99.78
5	63.9	18.4	0.56	16.0	0.08	0.87	0.00	99.79
6	64.1	18.5	0.58	15.9	0.04	0.74	0.00	99.85
7	63.8	18.4	0.42	16.4	0.09	0.88	0.00	100.01
8	63.9	18.5	0.68	15.8	0.13	0.89	0.00	99.92
9	64.0	18.3	0.54	15.9	0.00	0.26	0.06	99.03
10	64.4	18.3	0.78	15.8	0.00	0.27	0.07	99.62
11	64.1	18.3	0.32	16.8	0.00	0.00	0.00	99.55
12	64.2	18.4	0.27	16.8	0.03	0.00	0.00	99.68

Nr. 1–4, J/10/93: amphibole-biotite granodiorites (Rena Suite)
Nr. 5–8, J/5/93: fine-grained, grey biotite granodiorite, (Tetčice suite),
Nr. 9, 10; J/23/93 red granites, Tetčice suite
Nr.11 rim, 12 core; J/21/93 garnet-bearing leucogranites (Hlína suite)

feldspar (Tab. 6) typically contains small amounts of Na_2O (0.43–0.51 wt. %) and BaO (0.19–0.27 wt. %). Biotite appears in two forms: large (1 cm), often pseudo-hexagonal crystals differ slightly in their chemistry from the tiny biotite that often overgrows the amphibole grains (Tab. 7). The large grains (points 1, 2) differ from the smaller (points 3, 4) mainly in their TiO_2 and BaO contents. In the large grains the TiO_2 varies from 3.6 to 3.69 wt. % and BaO from 0.37 to 0.56 wt. %, whereas the TiO_2 in the small grains is slightly lower (3.36–3.41 %), and no BaO was detected.

The zircons from the amphibole-biotite granodiorites plot in the lower right corner of the Pupin`s (1980) typology diagram (S24, S20, Fig. 6). Zircons from the biotite granite fall in the centre of the right side in the same (P3, S20, P2). Electron microprobe analyses of common titanite are listed in Tab. 8. In the whole rock analysis, the SiO_2 (69.4–73.35 wt. %) contents correlate negatively with MgO (0.46–1.25 %), FeO_{tot} (1.46–2.83 %), CaO (1.95–2.69 %), and TiO_2 (0.16–0.37 %), as well as positively with K_2O (2.88–3.83 %) (Fig. 7, Tab. 3). Only a weak, or no correlation whatever was found between SiO_2 and Al_2O_3 (14.28–15.38 %), Na_2O (3.24–3.64 %), Ba (322–622 ppm), Rb (94–163), and Sr (169–356). The low contents of HFSE (Zr = 71–125, Nb = 10–15, and Y = 10–25 ppm) correspond well to the concentrations typical of volcanic-arc granites (Fig. 8, Pearce et al. 1984).

Tab. 7 Electron microprobe analyses from biotite (wt. % and apfu based on 22 O)

Sample	1	2	3	4	5	6	7
SiO_2	35.97	35.52	35.86	35.52	36.58	36.26	36.04
TiO_2	3.60	3.69	3.36	3.41	3.23	3.44	3.38
Al_2O_3	14.41	14.40	14.39	14.57	15.05	14.74	14.58
BaO	0.37	0.56	0.00	0.00	0.16	0.00	0.13
FeO	23.97	23.96	24.07	23.88	22.75	23.05	23.11
MnO	0.39	0.46	0.36	0.40	0.41	0.40	0.38
MgO	8.34	8.28	8.29	8.31	8.77	8.70	8.63
CaO	0.00	0.05	0.13	0.06	0.06	0.08	0.00
Na_2O	0.07	0.06	0.04	0.00	0.05	0.04	0.06
K_2O	9.62	9.49	9.26	9.53	9.73	9.71	9.38
Total	96.74	96.37	95.76	95.68	96.79	96.42	95.69
Si	5.579	5.543	5.592	5.551	5.612	5.592	5.604
Al^{IV}	2.421	2.457	2.408	2.449	2.388	2.408	2.396
Al^{VI}	0.213	0.191	0.236	0.235	0.334	0.271	0.275
Ti	0.420	0.433	0.394	0.401	0.373	0.399	0.395
Fe	3.109	3.127	3.139	3.121	2.919	2.973	3.005
Mn	0.051	0.061	0.048	0.053	0.053	0.052	0.050
Mg	1.928	1.926	1.927	1.936	2.006	2.000	2.000
Ca	0.000	0.008	0.022	0.010	0.100	0.013	0.000
Na	0.021	0.018	0.012	0.000	0.015	0.012	0.018
K	1.903	1.889	1.842	1.900	1.904	1.910	1.861
Z	8	8	8	8	8	8	8
Y	5.722	5.738	5.743	5.746	5.685	5.695	5.726
X	1.925	1.916	1.876	1.910	1.929	1.936	1.879
XMg	0.383	0.381	0.380	0.383	0.407	0.402	0.400

Nr. 1–5, J/10/93: amphibole-biotite granodiorite (Rena suite): 1–2 large grains – core; 3–4 biotite associated with amphibole –core
Nr. 5–7, J/5/93: fine-grained, grey biotite granodiorite (Tetčice suite)

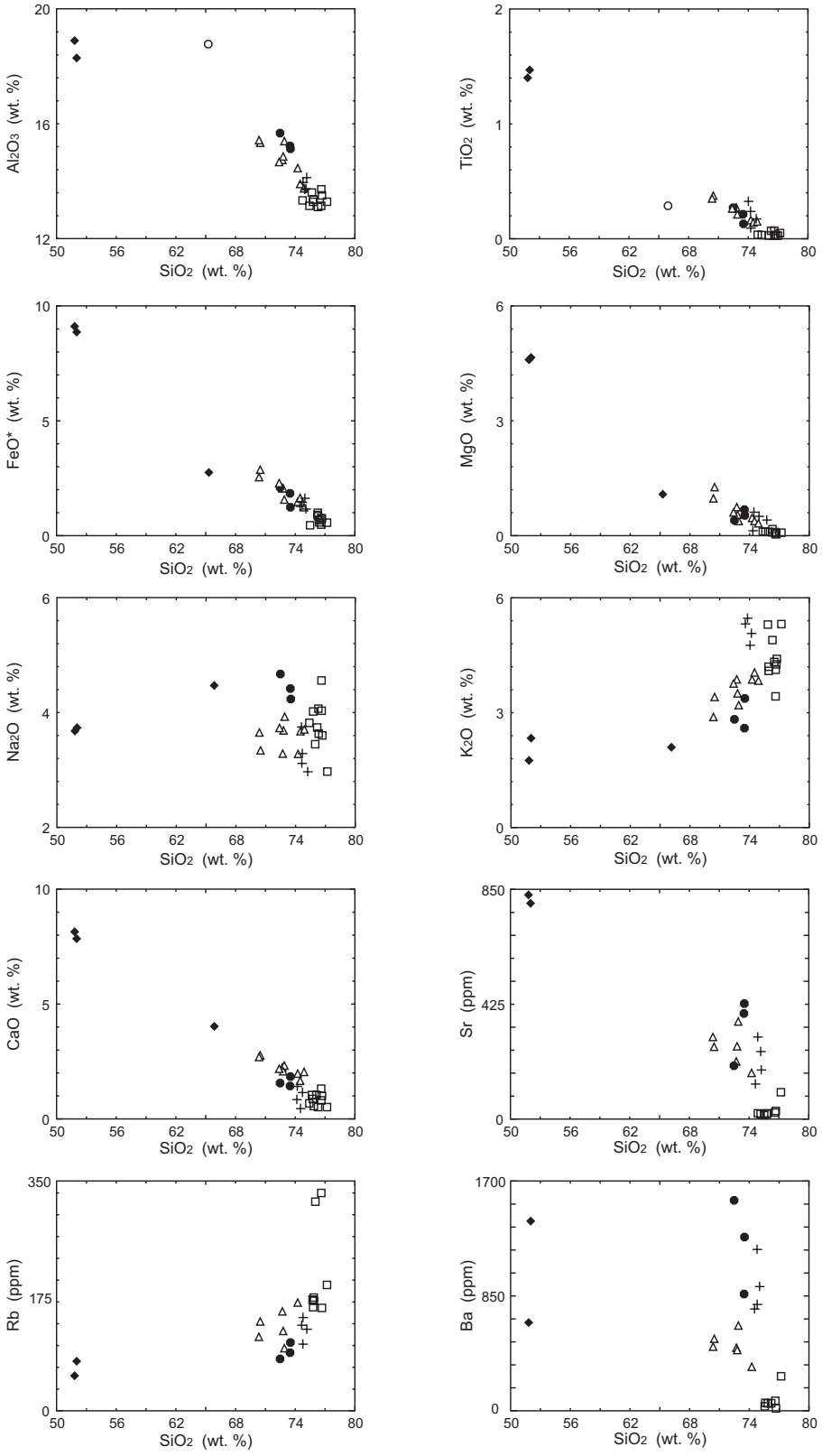

Fig. 7 Variation diagrams of SiO_2 vs. selected major- and trace-elements for granitoids from the Western Granitoid Complex.

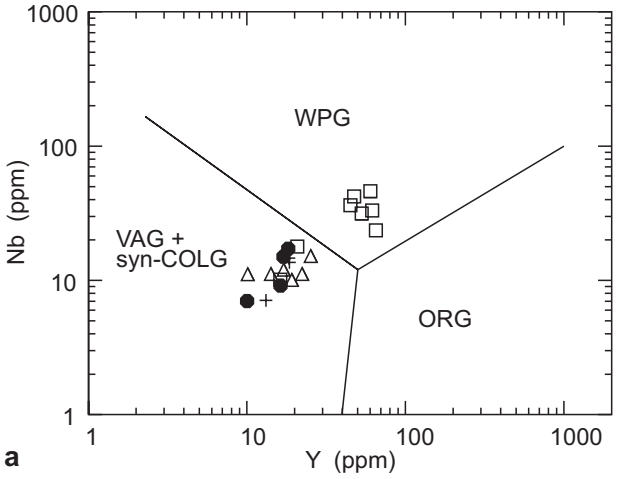

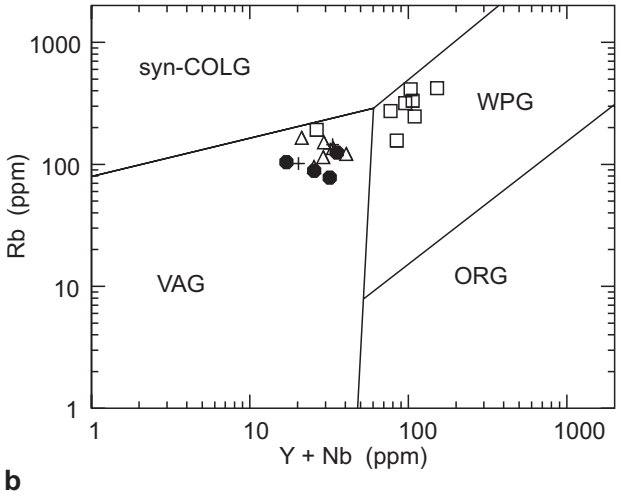

Fig. 8 Nb – Y and Rb – Nb + Y diagrams after Pearce et al. (1984), for granitoids from the Western Granitoid Complex, symbols as in Fig. 7. The granitoids from the Rena and Tetčice suites plot in the field of Volcanic Arc Granites, the garnet-bearing granites from the Hlína suite in the field of Within Plate Granites.

Tetčice suite consists of three main types of plutonic rocks: (1) biotite-bearing, fine-grained granodiorites, which are, close to the contact with Metabasite Zone, rimmed by (2) coarse-grained red granites. Lastly, (3) biotite-amphibole diorites form xenoliths in both granite types. Normally the contacts between granites and diorites are transitional; occasionally tonalites appear at the contact between diorites and granites as a product of their mutual interaction. Sharp contacts between both rock types are more seldom. The dioritic enclaves with a sharp contact to the host granite do not exceed 2 m in size, and are usually partly rounded, which indicates some transport of the already solidified diorite by the granitic magma (Didier 1987). Apart from dioritic enclaves, the granites host a broad spectrum of metasedimentary xenoliths, e.g. gneisses, migmatites, and calc silicates. The size of xenoliths varies greatly. The smallest can be observed only microscopically as biotite + plagioclase spots several millimetres across set in the light-coloured granites. The maximum size of roof pendants ranges up to 3 km. The large metasedimentary xenoliths are often surrounded by a zone of intense migmatitization. The presence of numerous enclaves and hybrids developing around them induces a strong inhomogeneity of the host rocks, first noted by Suess (1903).

The **diorites** are amphibole- or biotite-amphibole-bearing, medium- to coarse-grained, dark-grey to green-grey rocks. They consist of simply zoned plagioclase (An_{50} core, An_{40} rim, Tab. 1), unzoned amphibole (hornblende–edenite; Tab. 2, Fig. 3), biotite, quartz, ilmenite with titanite overgrowths, zircon and apatite. The cores of plagioclase are usually strongly altered. The alteration products include white mica, epidote and sodic plagioclase. Since no relics of pyroxene were found in the amphibole, and amphibole is enriched in both TiO_2 (1.06–1.48 wt. %) and K_2O (0.69–0.76 %), its origin is probably magmatic. Some amphibole grains are rimed by biotite. Titanites replacing ilmenite differ chemically from those from granodiorites. They are enriched in TiO_2 (38.4 wt. %) and depleted in Al_2O_3 (1.44 %, Tab. 8). Apatite appears in two morphologically different forms. It forms generally long prismatic crystals (L:W > 20); the small diorite enclaves in the granodiorites contain short prismatic (L:W = 4) apatite generation in addition. The latter, short prismatic crystals are typical of the host Tetčice granitoids. The common occurrence of both apatite types in the dioritic enclaves indicates magma mixing between diorite and granodiorite (Didier

Tab. 8 Electron microprobe analyses from titanite (1–5) and ilmenite (6)

Sample	SiO_2	Al_2O_3	MgO	TiO_2	CaO	FeO	MnO	Total
1	30.7	5.01	0.00	32.9	28.4	0.66	0.06	97.71
2	30.3	4.21	0.00	33.7	28.2	0.70	0.08	97.16
3	30.2	3.04	0.00	35.1	27.9	0.55	0.12	96.87
4	30.6	4.39	0.03	33.4	28.0	0.71	0.06	97.48
5	30.0	1.44	0.00	38.4	28.4	0.57	0.06	98.79
6	0.00	0.00	0.16	52.7	0.05	45.70	2.37	101.01

Nr. 1–2, J/10/93: amphibole-biotite granodiorites (Rena suite)
Nr. 3–4, J/5/93: fine-grained, grey biotite granodiorites (Tetčice suite)
Nr. 5–6, J/14b/93: biotite-amphibole diorites (Tetčice suite)

1987). The diorites are relatively basic (SiO_2 = 51.5 wt. %) but alumina rich (18.5 %). The MgO (4.6 %), Cr (*c.* 115 ppm), and V (*c.* 170 ppm) contents are rather low. The TiO_2 (1.4 wt. %), P_2O_5 (0.44–0.64 %), K_2O (2%), Rb (64 ppm), Zr (200 ppm), Nb (23 ppm) and Y (33 ppm) are comparatively high (Tab. 3).

The **granitoids** of the Tetčice suite are extremely inhomogeneous. Two principal types of granites were recognized within this suite – (1) grey, fine-grained biotite-bearing granodiorites, (2) red, coarse-grained granites. The contact between both types could not be observed directly in the field. Locally mapped zone between both types, several hundred meters thick, of pink porphyritic biotite-bearing granodiorites–granites renders the transitional contact more likely. The grey granodiorites consist of subhedral plagioclase (33–52 vol. %), subhedral to anhedral K-feldspar (9–22 %), anhedral quartz (30–43 %), biotite (3–7 %), with accessoric zircon, apatite, and titanite (Tab. 5). White mica, chlorite, and epidote are the secondary phases. The smaller size with generally sub- to anhedral habit of the rock-forming minerals and the absence of amphibole are the main differences compared to the Rena suite granodiorites.

Plagioclases are typically oscillatory-zoned (Tab. 1). The central zone is usually altered. It consists mostly of oligoclase (An_{14}), white mica (muscovite with 2–24 % of paragonite molecule, Tab. 4), epidote and zoisite (Tab. 9). The unaltered zone between core and rim consists mostly of oligoclase ($An_{22–24}$). Albite (An_3) was found as a very thin zone at the rim. The K_2O content in the plagioclase (0.07–0.25 wt. %) is low compared with the Rena suite (0.13–0.40 %).

Tab. 9 Electron microprobe analyses from epidote (1–2) and zoisite (3)

Sample	1	2	3
SiO_2	38.10	37.90	39.50
Al_2O_3	26.10	25.80	32.80
FeO	8.60	9.00	0.91
MnO	0.38	0.31	0.10
CaO	23.10	23.10	24.50
Total	96.34	96.08	97.74

J/5/93 fine-grained, grey biotite granodiorite (Tetčice suite)

The perthitic K-feldspar frequently exhibits cross-hatched twinning and hosts strongly altered plagioclases, biotite, chlorite and quartz. Myrmekite appears along the contact between plagioclase and K-feldspar locally. The results of the EMP analyses are listed in Tab. 6. The major differences in contrast to the Rena suite are a higher BaO (0.74–0.89 wt. %) and CaO (0.04–0.13 %) concentration.

Biotite forms small subhedral grains, which are often replaced by chlorite. The alteration is usually stronger at the rim. The fresh biotite is not zoned (Tab. 7). Compared with biotite from the Rena suite it is enriched in Al_2O_3 (14.58–15.05 wt. %) and depleted in $FeO_{tot.}$ (22.75–23.11 %) with BaO (0–0.16 %). The chloritization is accompanied by a decrease in SiO_2, K_2O, TiO_2 and by an increase in Al_2O_3, MgO, FeO, and H_2O.

The zircon morphology reflects the inhomogeneous nature of the rock once more (Fig. 6). The presence of rounded zircon grains reveals an assimilation of metasedimentary rocks. The igneous zircons with a crystal habit display three maxima if plotted in a typology diagram (Pupin 1980). The maximum in the upper left corner (H, L1) is typical of S-type granites. These zircons probably originated during crystallization of the granitic melt. The maxima approximately in the centre (S19) and on the right side of the diagram (P2, P3), may indicate a contamination of the granitic magma by a diorite, because zircons with P2, P3 forms are typical of dioritic xenoliths.

The granodiorites of the Tetčice suite are, from the geochemical point of view (Tab. 3), enriched in Al_2O_3 (14.96–15.64 wt. %), Na_2O (4.23–4.66 %) and Ba (849–1554 ppm), as well as depleted in CaO (1.24–1.84 %) and Sr (197–427 ppm) when compared with similar granodiorites of the Rena suite. The alumina saturation index (ASI) higher than 1.1 (1.14–1.20) indicates a S-type affinity for these granodiorites. The major elements do not exhibit clear trends in the variation diagrams (Fig. 7). The Mg–Fe and K–Rb pairs do not show any systematic variation either. The concentrations of the HFSE (mostly Nb, Zr, and, to a lesser degree, Ti) are variable and depend directly on the biotite contents. The biotite-rich samples exhibit elevated concentrations of Nb (15 ppm), Zr (324 ppm), and TiO_2 (0.27 wt. %). The lower values (Nb = 9 ppm, Zr = 80–147 ppm, TiO_2 = 0.13–0.21) are typical of biotite-poor members.

The red granites form mostly continuous rim along the western margin of the Metabasite Zone (Fig. 2). These granites are usually coarser grained than the grey granodiorites. Dykes of this granite penetrated the Metabasite Zone locally; some of these have a subvolcanic character with corroded quartz phenocrysts in a very fine-grained matrix. Remarkable attributes are, apart from the red colour, higher modal contents of K-feldspar (32–46 % vs. 23–26 % in the grey granodiorites) and mostly a complete alteration of biotite to chlorite.

Their modal composition is – K-feldspar (32–46 vol. %), plagioclase (15–28 %), quartz (22–39 %), chlorite (1–5 %), magnetite–haematite (up to 2 %), remnants of biotite, white mica, zircon, and apatite (Tab. 5). The anhedral to subhedral, perthitic K-feldspars are up to 2 cm long. The finely dispersed hematite gives the reddish colour to the feldspar. The perthites occupy up to 40 % of the individual crystals. Plagioclases from coarse perthites are

usually strongly altered. K-feldspars from red granites are depleted in BaO (0.26–0.27 wt. %) and enriched in FeO (0.06–0.07 wt. %) if compared with grey granodiorites.

Plagioclases are significantly smaller than K-feldspars. Their size is about 8 mm. Plagioclase inclusions in K-feldspar are abundant, and sometimes represent the most common form of plagioclase in the rock. Rapakivi texture (K-feldspar rimmed by plagioclase) was observed locally. Plagioclase ($An_{4–8}$) is commonly replaced by Fe-rich muscovite (Tab. 4), and pure albite ($An_{0.7–1.5}$). The Ca and Al released by decomposition of plagioclase are accommodated in epidote, forming veins cutting the rock. Chlorite originated from biotite, and reasonably fresh biotite could be found as relics in chlorite only.

The red granites are, compared with the grey granodiorites from Tetčice suite, highly enriched in SiO_2 (73.45–74.21 wt. %), and K_2O (4.68–5.13 %), but only slightly in Rb (87–144 ppm), and depleted in MgO (0.23–0.51 %), Al_2O_3 (13.62–13.92 %), CaO (0.36–1.35 %), with BaO (779–846 ppm). The concentrations of HFSE – Zr (109–171), Y (13–18 ppm) and Nb (13–18 ppm) are similar (Tab. 3, Fig 8).

Hlína suite is represented by irregular intrusions and dykes of felsic (SiO_2 > 75 wt. %), K-rich, fine-grained, garnet- and/or biotite-bearing granites. Some dykes grade into a coarse-grained facies in their central parts. Relatively large intrusions were found only within the Tetčice suite; dykes however cut both the Tetčice and Rena suites. Several metres wide alteration zones, marked by reddish haloes, are developed along the contact between dykes and surrounding rocks.

This granite consists of anhedral quartz (26–35 vol. %), subhedral, zoned (core – An_{15}, rim – An_8) plagioclase (25–30 %), and subhedral to anhedral K-feldspar (35–41%, Tab. 5). Some plagioclases are rimmed by granophyre. Minor to accessory minerals include garnet (1 %), biotite (0.5–5 %), magnetite, epidote, Nb, Y-rich zircon (≤ 6.60 Nb_2O_5), cheralite, Nb, Ta, Al-rich titanite, plumbopyrochlore and karnarsurtite (Leichmann et al. 1999). White mica (1–2 %), and chlorite (< 1 %, Tab. 5) are of secondary origin. Compared with the other granites from the Brno Batholith, K-feldspars of the Hlína suite (Tab. 6) are depleted in Na_2O (0.27–0.32 wt. %) and devoid of Ba (whole-rock analyses yielded 14–46 ppm Ba only). K-feldspars exhibit sector zoning if observed in cathodoluminescence. Oscillatory-zoned spessartite–almandine is a typical accessory mineral ($Sps_{48–46}$, $Alm_{36–35}$, $And_{12–11}$, $Grs_{7–4}$, $Prp_{4–1}$; Tab. 10). Its most prominent feature is a high concentration of yttrium (2.16 wt. % Y_2O_3) at the rim.

The felsic nature of the rock is reflected in the high SiO_2 (74.9–75.9 wt. %; Tab. 3), K_2O (4.11–4.29 %), Na_2O (3.73–4.18 %), and low FeO (0.79–0.90%), MgO (0.02–0.03 %), CaO (0.61–1.02 %), and TiO_2 (0.02–0.04 %).

Tab. 10 Electron microprobe analyses from garnet (wt. % and apfu based on 12 O)

Sample	1	2	3
SiO_2	36.09	35.83	34.88
TiO_2	0.22	0.09	0.26
Al_2O_3	18.21	18.43	17.62
Cr_2O_3	0.00	0.00	0.00
Y_2O_3	0.73	0.31	2.16
FeO	18.05	17.94	18.12
MnO	19.40	19.27	19.95
MgO	0.28	0.29	0.85
CaO	5.87	6.12	3.88
Total	98.83	98.27	95.56
Alm	0.355	0.352	0.362
Sps	0.458	0.454	0.483
Prp	0.012	0.012	0.036
Grs	0.070	0.082	0.004
Adr	0.106	0.100	0.115

Nr. 1–3, J/21/93: garnet-bearing leucogranites (Hlína suite)

The low ASI (1.02–1.07), disregarding the high SiO_2 contents, indicates an I-type affinity of the Hlína suite. A high degree of fractionation is indicated by fairly low mg# (2–7), K/Rb (228–103), and very high K/Ba (742–2544) ratios. The elevated amount of MnO (0.04–0.11 %) and high content of Y (23–58 ppm) correspond with their high concentrations in garnet. The Nb (19–51 ppm) and Rb (156–311 ppm) concentrations are elevated; Zr (72–79 ppm), Sr (16–30 ppm), and Ba (14–46 ppm) contents are lower than in the other Brno Batholith granitoids. The concentration of LREE is very low, whereas concentration of HREE is unusually high (Fig. 9, Tab. 3). The granites plot, based on their high concentrations of Y, Nb, and Rb, in the field of WPG (Within-Plate Granites) of Pearce et al. (1984) (Fig. 8).

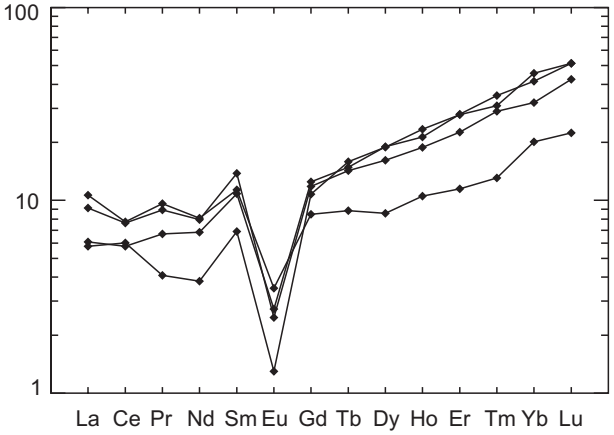

Fig. 9 Chondrite-normalized REE patterns (Sun 1980) for garnet-bearing granites, Hlína suite.

5. Discussion

5.1. Interpretation of individual rock units

5.1.1. Metabasite Zone

The sequence of ultramafic, plutonic and volcanic rocks from the Metabasite Zone resembles most likely an ophiolite succession (Best and Christiansen 2001). Even though the sheeted-dyke complex has not been observed yet, the sequence is rather complete ranging from ultramafic rocks (cumulates) to NMORB-like volcanic rocks. All members of the ophiolite suite underwent a similar metamorphic evolution, starting with greenschist-, passing to lower amphibolite- and ending with retrograde, lower greenschist-facies conditions. This style of metamorphic evolution could be compared with ocean-floor metamorphism. On the other hand, no relics of high-pressure overprinting, which could indicate subduction processes, were recognised in the Metabasite Zone. This metamorphic evolution markedly differs from typical simple lower greenschist-facies overprinting of surrounding granites and diorites. Many plutonic rocks from the Western Granitoid Zone are even fresh, without any traces of alteration or metamorphic overprinting. This fact argues strongly for a genetic relationship between the plutonic and volcanic sequences of the ophiolite, indicating their common origin.

Even though the lithology and metamorphic evolution of the Metabasite Zone is reasonably well known and comparable with modern ophiolite complexes, the tectonic interpretation of this ophiolite complex is less well constrained. Its tilted position, metamorphic evolution and relative small regional extent indicate that the Metabasite Zone represents only a small piece of an ophiolite complex, which could have been obducted onto an ancient continental or arc crust. However, the nature and character of this ancient crust, its relation to the granites surrounding the Metabasite Zone at the present-day erosion level, which are at least 150 Ma younger, as well as many other features that influenced the post-magmatic evolution of the ophiolites remain unknown. The same is valid for the petrotectonic interpretation of this zone. The metabasalts range, apart from post-magmatic alteration affecting certainly LILE, from typical depleted MORB compositions to enriched types. The high positive initial ε_{Nd} values (+6.7 to +7.4 – Finger et al 2000b; +5.2 to +8.4 – Janoušek and Hanžl 2000) confirm a depleted-mantle source for the NMORB-like basalts.

While the more depleted rocks seem to prevail in the South, the more enriched metabasic rocks occur in the North (see also Janoušek and Hanžl 2000). This distribution argues for a possible systematic change in the mantle source composition, becoming less depleted northwards. An alternative view is an assumption that the intraplate basalts may overlay locally the depleted MORB. The rhyolites, given to the small size of the available dataset, are difficult to interpret. They might represent strongly fractionated members of the ophiolite suite or may be interpreted as volcanic equivalents of the plutonic trondhjemites. The later model is supported by their chemistry, resembling trondhjemites, as well as by high ε_{Nd} (+6.8, Finger et al 2000b). Anyhow, apparently not all rhyolites from the Metabasite Zone belong to the ophiolite sequence. Some rhyolite dykes, especially those enriched in potassium, were probably associated with the intrusion of the later granites.

The chemistry of the basalts, rhyolites and trondhjemites indicates three possible environments – ocean floor, volcanic arc, and within-plate setting. At least three arguments make the interpretation of geochemical data relative. (1) It is not clear, to which extent were their trace-element signatures influenced by postmagmatic processes. This concerns even concentrations of HFSE, which are the main argument for the petrotectonic interpretations. The age of the ophiolites is very high (> 725 Ma, Finger et al 2000). The studied ophiolite complex was formed just close in time to the beginning of the modern plate tectonics (Goodwin 1996). Thus the simplistic extrapolation of geochemical data, which were obtained from recent or at least Phanerozoic settings, may be problematic for such old complexes. (2) Fragment only, from probably much larger ophiolite complex, is accessible for the study today. It is not clear, how representative this fragment is, and why just this fragment survived. (3) Anyhow, even the lithology and chemistry of the studied ophiolite complex – the Metabasite Zone – indicate that it did not originate on the typical ocean ridge. Its genesis could be rather envisaged in an environment, which would resemble a modern back-arc basin or a supra-subduction zone environment.

5.2. Granites

5.2.1. Rena suite

A close relation between the geochemistry, mineralogy and zircon typology was observed within this suite. The amphibole-rich granodiorites are enriched in MgO, TiO_2, and depleted in Na_2O. Moreover, they exhibit higher Mg/Fe ratios (0.32–0.44) compared with the biotite-rich granites of the same suite (Mg/Fe = 0.24–0.26). The decrease in Mg/Fe from granodiorites to granites, accompanied by a decrease in V, Cr, and Ni, indicates an important role for the amphibole fractionation in the evolution of the Rena suite. The assessment of the role for both feldspars in the fractionation process remains much more uncertain. The decreasing Ba contents and increasing K/Rb ratios

during the evolution of a granitic magma are commonly used as a fingerprint of the K-feldspar fractionation (Best and Christiansen 2001). However, in the present case no systematic variation in Ba contents or K/Rb ratios was observed in the whole-rock chemistry between the amphibole-biotite granodiorites and biotite granites. This is probably due to the fact that biotite contains even more BaO (0.37–0.56 %) than K-feldspar (0.19–0.27 %), and Ba, together with potassium, disappeared almost completely from biotite during chloritization. This later chloritization affected the biotites from the Rena suite to various degrees (10–100 %). Therefore, it is very likely, that the concentrations of the LILE (especially Ba and K) are affected by a late-stage alteration, mainly by chloritization of biotite.

The evolutionary trend from granodiorites to granites is reflected in switch in zircon typology approximately from S24 to P3 (Fig. 6). Taken together, the mineral composition of the amphibole-biotite granodiorites and biotite granites, the occurrence of oscillatory zoned plagioclases, mostly linear differentiation trends, decreasing Mg/Fe ratios from granodiorites to granites, an aluminum saturation index below 1.1, a low content of HFSE, as well as the evolutionary trend of zircon morphology (Pupin 1985) are indicative for I-type granitoids (Champion and Chappell 1992), and suggest that both granite types may be connected by fractional crystallization processes. The concentration of trace elements is comparable to granites derived at volcanic arcs. However, the lack of precise geochronological and isotopic data makes a more detailed genetic interpretation for this suite speculative.

5.2.2. Tetčice suite

From the geophysical point of view, the Tetčice suite is accompanied by a positive gravity anomaly. The difference, compared to the Rena suite, is + 20 mGal. This observation does not agree with the surface situation, as the granites from the Rena suite are denser (2.66–2.67 g/cm^3) when compared with the Tetčice suite (2.62 g/cm^3; Skácelová and Weiss 1978). The Rena suite should exhibit a positive gravimetrical anomaly, but this is not the case. This discrepancy indicates that the diorites, which are dense enough (2.86 g/ cm^3) to account for such an anomaly, are widespread under the current exposure level, and are covered only by a thin layer of granitoids.

The geochemical features of the granitoids of the Tetčice suite, such as the peraluminous nature (ASI = 1.14–1.20), Ca-poor character, as well as the mineral composition, especially the presence of Al-rich biotite as a dominant dark mineral, allow us to interpret the Tetčice granitoids as being of S-type character (Clarke 1981; Chappell and White 1992). Barbarin (1996) distinguished two main groups among the S-type granitoids. The first are muscovite-bearing granitoids generated through wet anatexis of crustal rocks. The second, formed by biotite-cordierite or biotite-bearing granitoids, originated as a consequence of a fairly dry anatexis of crustal material caused by an intrusion of a hot basic melt into the metasedimentary crust. Similar processes were invoked by Williamson at al. (1992), with Barton and Sidle (1993) to explain the origin of biotite-bearing peraluminous granitoids. Many features like (1) shared occurrence of metasedimentary and mafic inclusions in the granodiorites (Didier 1987); (2) presence of several types of zircon and apatite; (3) large extent of migmatitization and anatexis of enclosed metasedimentary rocks; (4) magma mixing phenomena indicative of an interaction between acid and basic magmas; and (5) gravimetric evidence, suggest the presence of more dense basic rocks at depth, below the granitoids. Especially the last feature indicates that the origin of the Tetčice suite granitoids can be best explained by an intrusion of hot basic magma into the metasedimentary crust, triggering a large-scale melting. Nevertheless it is necessary to take into account that the late-stage alteration – invoking mineralogical changes, like decomposition of biotite and calcic plagioclase accompanied by the formation of new K- (white mica), and Ca- (epidote, zoisite, titanite) phases, may have slightly changed the primary whole-rock chemical compositions. The decomposition of biotite was recognized as the initial reaction, accompanied by the release of potassium. It caused a succession of following reactions and, consequently, a redistribution of Ca, K, and Na (decomposition of Ca-rich cores of plagioclases, formation of white mica, K-feldspar, albite, zoisite, etc.). Realistic seems to assume that these reactions were initiated by an influx of aqueous fluids with only limited changes of the whole-rock chemistry. An intense redistribution of elements like K, Na, and Ca may explain the occurrence and origin of copious myrmekites (Garcia et al. 1996) observed in the Tetčice granitoids.

The red granites could probably represent more fractionated, marginal facies, strongly influenced by the fluid migration. Disturbed concentrations of mainly LILE, induced by alteration, as well as the absence of isotopic data, do not allow the verification of this scenario by precise geochemical data.

5.2.3. Hlína suite

Some accessory (primary to secondary) minerals found in this felsic granite correspond to peralkaline or hyperalkaline rocks: e.g., Y, Na-rich spessartine–almandine (≤ 2.16 Y_2O_3, ≤ 0.25 Na_2O), Nb, Y-rich zircon, Nb, Ta, Al-rich titanite, plumbopyrochlore and karnarsurtite are in a contrast with the relatively high ASI (1.02–1.07). This may be a result of anhydrous crystallization of felsic, REE-,

Nb-, F-rich and Fe-, Mg-, Ca-, Ti-, P-poor, probably even highly fractionated magma, which prevented early precipitation of alkali pyroxenes and amphiboles, allanite or REE-phosphates (Leichmann et al. 1999). This type of granite strongly differs, by its mineralogy and geochemistry, from all other S- or I-type granites known from Brunovistulicum. The rocks are evidently anhydrous, anorogenic and, at least accessory minerals, indicate their alkaline affinity. Clearly, a distinct A-type component (Pitcher 1997) is apparent in this type of granite.

5.3. Geotectonic development

The rock association exposed in Brno Batholith is fairly variegated. The oldest member is evidently the Ophiolite Belt. Our petrological and geochemical data indicate, in accordance with Finger et al. (2000a) that it originated in supra-subduction zone environment. This, at least 725 old, already metamorphosed ophiolite was intruded by variable granite complexes at approximately 600 Ma. The Eastern Granitoid Complex (part of the Slavkov Terrane *sensu* Finger et al. 2000a) intruded the ophiolite in the hanging-wall. It represents monotonous, I-type, amphibole- to biotite-bearing suite of quartz diorites–tonalites–granodiorites. Petrologic (Štelcl and Weiss 1986; Hanžl and Melichar 1997) as well as isotopic data (Finger et al. 2000b) indicate an origin in a primitive volcanic-arc environment. The Western Granitoid Complex (part of the Thaya Terrane) intruded the base of the ophiolite sequence and has a much complex structure. Common relics of gneisses and calc silicates bring a strong evidence for an existence of an older continental crust. The age of this crust, as well as its possible relation to the ophiolites, is unknown, due to the intrusions of later granites. This probably mainly metasedimentary crust was intruded by mafic magma of dioritic composition. The Sr-Nd isotopic composition ($^{87}Sr/^{86}Sr = 0.705–0.707$, $\varepsilon_{Nd} = -1$ to -2; Finger et al. 2000b) as well as petrologic and geochemical data indicate most likely a lower crustal origin for the parental mafic magma, or a strong interaction between an ascending magma and the crust. This intrusion could have lead to a large-scale melting of the pre-existing crust and gave rise to a large S-type granite pluton of the Tetčice suite. Due to the presence of concealed diorite bodies, this type of crust is nowadays associated with a positive gravity anomaly. Another type of crust is characterized by negative gravity anomaly from geophysical point of view. Geologically it is formed by felsic, highly evolved I-type, VAG granites of the Rena suite. The protolith of this suite is unknown, because of the lack of isotopic data and absence of any geological evidence, such as enclaves.

Even less clear is the origin and tectonic position of the Hlína suite. The rocks are evidently strongly fractionated, but enriched in elements such as Y, Nb, Ta, U, and Th. Low ASI, very high SiO_2, and anhydrous character would make it difficult to derive these rocks from Rena or Tetčice granites.

5.4. Relation between the western part of the Brno Batholith and the Dyje Batholith

Already Suess (1912) recognized some similarities between the Thaya (Dyje) and Brno batholiths. The close relation between the two was noticed more recently by Höck and Leichmann (1994), as well as Finger et al. (1995, 2000a). The correlation between these two batholiths is not simple because of strong deformation in the western part of the Dyje Batholith. However, petrological data presented here enable us to correlate individual rock types from both batholiths.

Finger et al. (1989) distinguished four main granitoid types – Hauptgranit, Gumping, Passendorf and Gaudendorf – in the Austrian part of the Dyje Batholith.

The most widespread variety of medium-grained, light-coloured granites and granodiorites is called Hauptgranit. This type occupies more than two thirds of the batholith's area. Finger et al. (1995) divided the Hauptgranit into two subtypes in addition. The light grey to pink biotite-bearing granites of the Eggenburg/Maissau type occupy the southern part of the Batholith. The biotite-bearing, light-grey granodiorites to granites of the Pulkau/Zellendorf type are widespread in the northern part. The Gumping type corresponds to biotite-rich granodiorites to quartz monzodiorites with K-feldspar phenocrysts 2–3 cm across. This type is restricted to the south-western part of the Batholith. The Passendorf type, cropping out in the area between the Pulkau and Dyje valleys, is built by biotite-bearing tonalites. The term Gaudendorf type refers to fine-grained granites to granodiorites cropping out north of Eggenburg.

The division of the Dyje Batholith on the Czech territory is slightly different. The granites in the western part, approximately west of the city Znojmo, correspond mostly to the Pulkau type (Finger and Friedl 1993). The amphibole-biotite diorites and reddish leucogranites of the so-called Tasovice type (Batík 1984) crop out east of Znojmo. Diorites are often enclosed in the fine-grained biotite granodiorites, which differ from the common Pulkau type macroscopically by their finer grain and slightly higher biotite content. Likewise, the biotite-bearing gneisses were found as inclusions in these fine-grained granodiorites. The fine-grained granodiorites pass to the east into the coarse-grained granites of the Tasovice type.

The biotite granites to granodiorites from the Rena suite in the Brno Batholith can be well compared with

the Pulkau/Zellendorf type from the Dyje Batholith. The common traits are leucocratic and biotite-bearing character, granitic to granodioritic composition, as well as pseudohexagonal development of the biotite crystals. Apart form petrology, similarities could be documented in whole-rock chemistry (Finger et al. 1995). The Pulkau granite is associated with the Passendorf tonalite. Tonalites were not found in the Rena suite in the Brno Batholith, however the amphibole-biotite granodiorites are characterised by relatively low modal contents of K-feldspar. Even though the tonalites from the Dyje Batholith are more mafic compared with the granodiorites from the Brno Batholith, their gradational, spatial relation to the prevailing granites in both batholiths, and some textural traits (e.g. up to 1 cm long pseudohexagonal columnar biotite) suggest a close relation.

The Tetčice suite has an equivalent in the northeastern part of the Dyje Batholith in the form of inhomogeneous granodiorites with diorite and gneiss enclaves, which occur northeast of Znojmo. The abundance of enclaves, together with the petrological character (biotite granodiorites) and structural similarities (fine-grained types) support such a correlation. The diorites from the Tetčice suite are almost identical to those from the Dyje Batholith. Both are amphibole- and biotite-bearing, being enriched in P, Ti, and K_2O. Titanite with an ilmenite core is a typical accessory. Tonalites commonly appear at the contact with granodiorites. The whole suite cropping out northeast of Znojmo, is similar to the Tetčice suite, accompanied by a distinctive, positive gravimetric anomaly. The light, garnet-bearing, fine-grained granites which form dykes in the northern part of the Dyje Batholith (Batík and Čtyroký 1983; Leichmann 1987) could be compared, from the petrological point of view, with garnet-bearing leucogranites of the Hlina suite in the Brno Batholith.

Correlation of other two granitoid types from the Dyje Batholith is less certain. The Gaudendorf granodiorite is, according to description by Finger et al. (1989, 1995), similar to the granodiorites from the Tetčice suite in the Brno Batholith. Unfortunately, the published data from the Gaudendorf area do not suffice for a really detailed correlation of both types. Similarly the red Tasovice granite seems petrologically close to the red granites from the Tetčice suite.

The occurrence of the Gumping type is restricted to the Dyje Batholith. Likewise, the Sr-poor and Zr-rich Maissau type has no equivalent in the Brno Batholith. Some pink to reddish biotite granites from the Rena suite are petrologically very close to the Maissau type. But the granites from the Rena suite are enriched in Sr and depleted in Zr compared to those from the Maissau area.

Taken together, the rocks which crop out in the northern part of the Dyje Batholith – approximately north of Pulkau river – have their equivalents in the Brno Batholith. Some types from the southern extremity of the Dyje Batholith (Gumping and Maissau) are not known from the Brno Batholith. At least the northern Dyje Batholith represents the direct southern continuation of the Western Granitoid Complex of the Brno Batholith. This Complex and Dyje Batholith differ principally from the Eastern Granitoid Complex of the Brno Batholith, though.

The Brunovistulian magmatism could be therefore classified by two principles. The petrological observations presented in this paper strongly support the division of the Brunovistulicum into two different terranes with an ophiolite belt in-between, as firstly published by Finger et al. (2000a). In this case, Thaya Terrane comprises the Brunovistulian magmatic and metamorphic rocks cropping out west of the ophiolite belt (Western Granitoid Complex of the Brno Batholith, Dyje Batholith and the concealed parts). Slavkov Terrane then contains the Brunovistulian rocks located east of the Metabasite Zone (Eastern Granitoid Complex of the Brno Batholith and concealed parts).

The second division arises more from geomorphological aspects that reflect post-Miocene erosion processes, and classify Brunovistulicum conventionally according the outcrop areas into Brno Batholith, Dyje Batholith etc.

5.5. The position of Brunovistulicum during the Cadomian orogeny

The discussion about the position of Brunovistulicum during the Cadomian orogeny was recently summarized by Kalvoda et al. (2008). Three different models have already been published. Pharaoh (1999) with Żelaźniewicz et al. (1997, 2001) argued, based on geochronological and lithological data (Glassmacher et al 1999; Gee 2001; Scarrow et al 2001), for Baltica affinity of the Brunovistulicum.

More recently, Friedl et al. (2000, 2004) interpreted Brunovistulicum as a terrane derived from the South American part of Gondwana. Their main argument were SHRIMP zircon ages spectra with peaks at 1.2 Ga, 1.5 Ga and 1.65–1.8 Ga indicating affinity to the Grenvillian orogeny. However, these high ages were found in the so-called Bites Gneiss, which is thrusted over Brunovistulian rocks proper (Leichmann et al. 2006). Friedl (2000, 2004) considered Brunovistulicum, based on data by Finger and Steyrer (1995) with Finger et al (1995) as a part of broader tectonic unit – Moravo-Silesicum. However the Brunovistulicum is defined here more closely, and allochtonous units in the hanging wall are classified as Moravicum in accordance with Suess (1912). Main reason for the separation of Brunovistulicum from Moravicum is the presence of slightly metamorphosed Devonian marine

sediments, which are sandwiched between Brunovistulicum and Moravicum (Jaroš and Mísař 1976; Schulmann et al. 1991). The high ages indicating the South America affinity are unknown from the Brunovistulian granites yet. However it is necessary to point out that the age of metasedimentary enclaves in Brunovistulian granites remains unconstrained.

The third model (Finger et al 1995, 1997) invoked again a Gondwanan affinity of the Brunovistulicum, and correlated this unit with the northern Africa margin. The petrological characteristics of Brunovistulicum given in this paper enable closer lithological correlation with the rocks from northern Africa margin in the Eastern Desert in Egypt.

El-Gaby (1975, 1984), El-Gaby et al (1984), Stern and Hedge (1985), Stern and Gottfried (1986), as well as Shackleton (1994) defined several intrusion events in the central and northern parts of the Eastern Desert in Egypt. The oldest one is the Abu Ziran Group, which includes, among other rock types, dismembered ophiolites with a back-arc affinity. Intrusion of tonalites to granites, and the eruption of Dokhan volcanics, manifested the younger phase. The general structure in the northern part of the Eastern Desert (ophiolites surrounded by younger granites) strongly resembles the structure observed in the Brno Batholith. Other strong evidence for a close relation between northern Gondwana and the Brno Batholith is the geochronology. The age of the ophiolites from Brno Batholith (725 ± 15 Ma after Finger 2000b) is very close to the ages observed in the Panafrican ophiolites in the Eastern Desert (Shackleton 1994). The intrusion ages of granites and Dokhan volcanics from the Eastern Desert range between 620 and 550 Ma (El-Gaby et al. 1984; Stern and Hedge 1985; Stern and Gottfried 1986; Shackleton 1994). These values are almost identical with the intrusion ages reported from various granites and diorites in the Brno Batholith (van Breemen et al. 1982; Dallmeyer et al. 1994).

Although it is necessary to take into account that it is difficult to compare a local geological unit of outcrop size ~ 1 200 km^2 with a huge craton several 10 000 km^2 in size, some important analogies in the geological structure and geochronology between the Brno Batholith and northern Gondwana margin could be found.

6. Conclusions

The Brno Batholith, and consequently whole Brunovistulicum, consists of three independent magmatic complexes. They are from West to East: the Western Granitoid Complex (part of the Thaya Terrane), the central Ophiolite Belt (formerly termed Metabasite Zone or Central Basic Belt), and the Eastern Granitoid Complex (part of the Slavkov Terrane). These complexes differ in petrology, chemistry, and post-magmatic evolution.

Three suites of magmatic rocks – Rena, Tetčice and Hlína – were distinguished in the Western Granitoid Complex. The amphibole-biotite granodiorites to biotite granites of the Rena suite represent differentiated I-type granitoids with a strong volcanic-arc affinity. The biotite-bearing, S-type granodiorites of the Tetčice suite originated most likely via partial anatexis of metasedimentary crust. It could have been a consequence of elevated heat flow, induced by an intrusion of dioritic magma at depth, followed by mixing between the primary mafic and secondary granitic melts. The granodiorites of both suites have undergone local late-stage alteration manifested by strong replacement of plagioclase by white mica and albite, and the formation of epidote, carbonate, and palygorskite veinlets. Dykes, or small bodies of highly differentiated I- to A-type, garnet-bearing granites of the Hlína suite with a strong within-plate affinity, cut through both suites. All three suites have direct equivalents in the Dyje Batholith, which represents a southern continuation of the Brno Batholith.

The ophiolites comprise a full sequence including ultramafic and plutonic rocks, basaltic volcanics, ranging even to acidic composition. Based on the lithology and whole-rock geochemistry of the basalts, the ophiolitic complex can be interpreted, most likely, as supra-subduction zone related.

Our petrological data support the idea of Finger et al. (2000a), who interpreted the Brunovistulicum as an arc (Slavkov Terrane) – continent (Thaya Terrane) collisional zone with relics of ocean floor (Ophiolite Belt) in-between.

The broad fit in the geological structure (older ophiolites surrounded by younger granitoids) and geochronology between Brunovistulicum and the northern part of the Eastern Desert in Egypt may favour a close relation of Brunovistulicum to the northern Gondwana margin during the Panafrican orogeny. Nevertheless, alternative views, searching primary position of Brunovistulicum at South America margin or in an orogen-rimmed Baltica could not be excluded yet.

Acknowledgements: The research was supported by the project MSM 0021622416. The authors thank E. Jelínek and V. Janoušek for editorial handling and two anonymous reviewers for their comments and suggestions.

References

Baker F (ed) (1979) Trondhjemites, Dacites and Related Rocks. Elsevier, Amsterdam, pp 1–283

Barbarin B (1996) Genesis of two main types of peraluminous granitoids. Geology 4: 295–298

Barton M, Sidle SC (1993) Petrological and geochemical evidence for granitoid formation: the Waldoboro Pluton Complex, Maine. J Petrol 35: 1241–1273

Batík P (1984) Geological structure of Moravicum between Bíteš gneiss and Dyje Batholith. Věst Ústř Úst geol 59: 321–330 (in Czech)

Batík P, Čtyroký P (1983) Explanations to the geological map 1: 25 000 sheet Šatov 34-131. Czech Geological Survey, Prague (in Czech)

Best MG, Christiansen (2001) Igneous Petrology. Blackwell Science, Malden, pp 1–458

Clarke DB, (1981) The mineralogy of peraluminous granites: a review. Canad Mineral 19: 3–17

Champion DC, Chappell BW (1992) Petrogenesis of felsic I-type granites: an example from northern Queensland. Trans Roy Soc Edinb, Earth Sci 83: 115–126

Chappell BW, White AJR (1992) I- and S-type granites in the Lachlan Fold Belt. Trans Roy Soc Edinb, Earth Sci 83: 1–26

Dallmeyer DR, Fritz H, Neubauer, F, Urban M (1994): $^{40}Ar/^{39}Ar$ mineral age controls on the tectonic evolution of the southeastern Bohemian Massif. Pre-alpine Crust in Austria, Excursion guide 'Geology of the Moravian Zone', Krems, pp 14–22

Deer WA, Howie RA, Zussman J (1992) An Introduction to the Rock-Forming Minerals. Longman, Essex, pp 1–696

Didier J (1987) Contribution of enclave studies to the understanding of origin and evolution of granitic magmas. Geol Rundsch 76: 41–51

Dirnhofer M (1996): Zur Geologie und Petrographie des kristallinen Untegrundes der Molassezone in Niederösterreich. Unpublished MSc thesis, University of Salzburg, pp 1–157

Dudek A (1980) The crystalline basement block of the Outer Carpathians in Moravia: Brunovistulicum. Rozpr Čs Akad Věd, Ř mat přír Věd, 90: 3–85

EL-Gaby S (1975) Petrochemistry and geochemistry of some Granites from Egypt. Neu Jb Mineral, Abh 124: 147–189

EL-Gaby S (1984) Architecture of the Egyptian Basement Complex. Proc 5th Int Conf on Basement Tectonics, Cairo, pp 1–7

EL-Gaby S, El-Nady O, Khudeir A (1984) Tectonic evolution of the basement complex in the Central Eastern Desert of Egypt. Geol Rundsch 73: 1019–1036

Finger F, Steyrer HP (1995) A tectonic model for the eastern Variscides: indications from a chemical study of amphibolites in the southeastern Bohemian Massif. Geol Carpath 46: 137–150

Finger F, Friedl G (1993): Bericht 1992 über petrographische Untersungen im Moravikum auf Blatt 9 Retz. Jb Geol. B-A 136: 637–638

Finger F, Pin C (1997) Arc-type crustal zoning in the Brunovistulicum, eastern Czech Republic: a trace of the late Proterozoic Euro-Gondwana margin. J Czech Geol Soc 42: 53

Finger F, Frasl, G, Höck V, Steyrer HP (1989) The granitoids of the Moravian Zone of northeast Austria: product of a Cadomian active continental margin? Precambr Res 45: 235–245

Finger F, Frasl G, Dudek A, Jelínek E, Thöni M (1995) Cadomian plutonism in the Moravo-Silesian basement. In: Dallmeyer RD, Franke W, Weber KP (eds) Tectonostratigraphic Evolution of the Central and Eastern European Orogens. Springer-Verlag, Berlin, pp 495–507

Finger F, Hanžl P, Pin C, Quadt A, Steyrer HP (2000a) The Brunovistulicum: Avalonian Precambrian at the eastern end of the Variscides. In: Franke W, Altherr R, Haak W, Oncken O, Tanner D (eds) Orogenic Processes: Quantification and Modelling in the Variscan Belt of Central Europe. Geological Society London Special Publication 179: pp 103–112

Finger F, Tichomirowa M, Pin C, Hanžl P (2000b) Relics of an early-Panafrican metabasite-metarhyolite formation in the Brno Massif, Moravia, Czech Republic. Int J Earth Sci 89: 328–335

Fišera M, Patočka F (1989) Geochemistry of Variscan blastomylonites of the Vidly pod Pradědem locality, the Hrubý Jeseník Mts.: paleotectonic implications. Věst Ústř Úst geol 64: 301–312

Frasl G, (1963): Die mikroskopische Untersuchung der akcesorischen Zirkone als eine Routinearbeit des Kristallingeologen. Jb Geol B-A 106: 405–428

Friedl G, Finger F, McNaughton NJ, Fletcher IR (2000) Deducing the ancestry of terranes: SHRIMP evidence for South America-derived Gondwana fragments in central Europe. Geology 28: 1035–1038

Friedl G, Finger F, Paquette JL, von Quadt A, McNaughton NJ, Fletcher IR (2004) Pre-Variscan geological events in the Austrian part of the Bohemian Massif deduced from U-Pb zircon ages. Int J Earth Sci 98: 802–823

Garcia D, Pascal, M. L, Roux J (1996) Hydrothermal replacement of feldspars in igneous enclaves of the Valey granite and the genesis of myrmekites. Eur J Miner 8: 703–717

Gee D (2001) Overview of the Timanide Orogen along the Eastern Margin of the East European Craton. Joint meeting of EUROPROBE, TESZ, TIMPEBAR, URALIDES & SW Iberia Projects, Ankara 30 September–2 October, 2001. Abstracts, pp 19–20

Geofyzika (2000): Gravimetrical map of the Czech Republic, 1: 500 000. Geofyzika Ltd., Brno

Glassmacher UA, Reynold P, Alekseyev A, Puchkov VN, Taylor K, Gorozhanin V, Walter R (1999) $^{40}Ar/^{39}Ar$ thermochronology west of the Main Uralian fault, southern Urals, Russia. Geol Rundsch 87: 515–525

Goodwin AM, (1996) Principles of Precambrian Geology. Academic Press, London, pp 1–280

Gregerová M (1982) The ultramafic rocks of the Brno Massif. Folia Fac Sci Nat Univ Purk 21: 3–34 (in Russian)

Hanžl P (1994) The correlation between the Nectava gneisses and granodiorites of the northern part of the Brno Massif. Věst Czech Geol Úst 69: 73–80

Hanžl P, Melichar R (1997): Brno Massif: a section through the active continental margin or composed terrane? Krystalinikum 23: 33–58

Höck V (1975) Mineralzonen in Metapeliten und Metapsamiten der Moravischen Zone in Niederöstrreich. Mitt Österr Geol Ges 66–67: 49–60

Höck V, Leichmann J (1994) Exkursion C: Das Moravikum der Thayakuppel. Mitt Österr Miner Ges 139: 407–427

Jaroš J, Mísař Z (1976) Nomenclature of the tectonic and lithostratigraphic units in the Moravian Svratka dome. Věst Ústř úst geol 51: 113–122

Jelínek E, Dudek A (1993) Geochemistry of subsurface Precambrian plutonic rocks from the Brunovistulian complex in the Bohemian Massif, Czechoslovakia. Precambr Res 62: 103–125

Janoušek V, Hanžl P (2000) Nd isotopic composition of metabasalts from the metabazite Zone, Brno Massif – geochronological and genetic implications. In: Abstracts of the Conference Moravskoslezké Paleozoikum, February 3, 2000, Brno, pp 8 (in Czech)

Kalvoda J, Bábek O, Fatka O, Leichmann J, Melichar R, Nehyba S, Špaček P (2008) Brunovistulian Terrane (Bohemian Massif, Central Europe) from late Proterozoic to late Paleozoic: an overview. Int J Earth Sci 97: 497–518

Leichmann J (1987) Petrology of the western part of the Dyje Massif. Unpublished MSc thesis. University of J. E. Purkyně, Brno, pp 1–66 (in Czech)

Leichmann J (1994) Trondhjemites of the Brno Massif. Geol výzk Mor a Slez v r 1993: 82–85 (in Czech)

Leichmann J (1996) Geologie und Petrologie des Brünner Massivs. Unpublished PhD thesis, University of Salzburg, pp 1–118

Leichmann J, Novák M, Sulovský, P (1999) Peraluminous whole-rock chemistry versus peralkaline mineralogy of highly fractionated, garnet-bearing granites from the Brno Batholith. Ber Deutsch Miner Ges 1: 144

Leichmann J, Kapinus A, Pivnička L, Weber R (2006) Želetice Group: very low-grade Palaeozoic sequence at the base of Moravicum, Czech Republic. J Czech Geol Soc 51: 189–199

Le Maitre RW (ed) (1989) A Classification of Igneous Rocks and Glossary of Terms. Blackwell Scientific Publications, Oxford, pp 1–193

Melichar R (1995) Tectonic significance of the Boskovice Furrow. Geol Výzk Mor Slez 1994: 64–66 (in Czech)

Mittrenga P, Rejl L (1993) Brno Massif. In: Přichystal A, Obstová V, Suk M (eds) Geology of Moravia and Silesia. Moravian museum, Brno, pp 1–168

Mittrenga P, Weiss J, Rejl L (1976) New results about the geological structure of the southern part of the Brno Massif. Výzk Práce Ústř Úst Geol 13: 33–39 (in Czech)

Novák M, Filip J (2002) Ferroan magnesioaxinite from hydrothermal veins at Lažany, Brno Batholith, Czech Republic. Neu Jb Miner, Mh 7: 385–399

Pearce JA, Cann JR (1973) Tectonic setting of basic volcanic rocks determined using trace element analysis. Earth Planet Sci Lett 19: 290–300

Pearce JA, Harris NBW, Tindle AG (1984) Trace element discriminations diagrams for the tectonic interpretation of the granitic rocks. J Petrol 28: 956–983

Pharaoh TC (1999) Palaeozoic terranes and their lithospheric boundaries within the Trans-European Suture Zone (TESZ): a review. Tectonophysics 314: 17–41

Pitcher WS (1997) The Nature and Origin of Granite. Chapman & Hall, London, pp 1–387

Přichystal A (1999) K-Ar age determination of a basaltic dyke from Želešice (Brno Massif). Geol Výzk Mor Slez 1993: 60–62 (in Czech)

Pupin JP (1980) Zircon and granite petrology. Contrib Mineral Petrol 73: 207–220

Pupin JP (1985) Magmatic zoning of Hercynian granitoids in France based on zircon morphology. Schweiz Mineral Petrogr Mitt 65: 29–56

Riegler G (2000) Chemischen und Th-U-Pb Modelalter akzessorischen Monazite aus kristallinen Bohrkernen des Weinviertels und ihre Bedeutung für das Verständnis der geologischen Situation am Ostrand der Böhmische Masse. Unpublished MSc thesis, University of Salzburg, pp 1–72

Scarrow JH, Pease V, Fleutelot C, Dushin V (2001) The late Neoproterozoic Enganepe ophiolite, Polar Urals, Russia: an extension of the Cadomian arc? Precambr Res 110: 255–275

Shackleton RM (1994) Review of the Late Proterozoic sutures, ophiolitic mélanges and tectonics of the eastern Egypt and north-east Sudan. Geol Rundsch 83: 537–547

Schulmann K, Ledru P, Autran A, Melka R, Lardeaux JM, Urban M, Lobkowicz M (1991) Evolution of nappes in the eastern margin of the Bohemian Massif: a kinematic interpretation. Geol Rundsch 80: 73–92

Skácelová D, Weiss J (1978) A model of the development of the Brno Massif based on geophysical data (in Czech). Čas Mineral Geol 23: 409–415

Stern RJ, Gottfried D (1986) Petrogenesis of a late Precambrian (575–600 Ma) bimodal suite in Northeast Africa. Contrib Mineral Petrol 92: 492–501

Stern RJ, Hedge CE (1985) Geochronologic and isotopic constrains on Late Precambrian crustal evolution in the Eastern Desert of Egypt. Amer J Sci 285: 97–127

Suess FE (1903) Bau und Bild der Böhmischem Masse. Tempsky, Wien. pp 1–290

Suess FE (1912) Die Moravischen Fenster und ihre Beziehung zum Grundgebirge des Hohen Gesenke. Denkrsch K Akad Wiss, math Naturwiss, pp 1–91

Sulovský P (1975): The accessory minerals from the Metabasite Zone of the Brno Massif. Unpublished MSc thesis, University of J. E. Purkyně, Brno, pp 1–78

Šmejkal V (1964): The absolute age of some igneous and metamorphic rocks determined using K-Ar method. Věst ÚÚG 35: 441–449 (in Czech)

Štelcl J, Weiss J (eds) (1986) The Brno Massif. University of J. E. Purkyně, Brno, pp 1–255 (in Czech)

van Breemen O, Aftalion A, Bowes D, Dudek A, Mísař Z, Povondra P, Vrána S (1982) Geochronological studies of the Bohemian Massif, Czechoslovakia, and their significance in the evolution of Central Europe. Trans Roy Soc Edinb, Earth Sci 73: 89–108.

Williamson BJ, Downes H, Thirlwall MF (1992) The relationship between crustal magmatic underplating and granite genesis: an example from the Velay granite complex, Massif Central, France. Trans Roy Soc Edinb, Earth Sci 83: 235–245

Żelaźniewicz A, Buła Z, Jachowicz M, Żaba J (1997) Crystalline basement SW of the Trans-European Suture Zone in Poland: Neoproterozoic Cadomian orogen. Terra Nostra 11: 167–171

Żelaźniewicz A, Seghedi A, Jachowicz M, Bobinski W, Buła Z, Cwojdzinski S (2001) U-Pb SHRIMP data confirm the presence of Vendian foreland flysch basin next to the East European Craton. Joint meeting of EUROPROBE, TESZ, TIMPEBAR, URALIDES & SW Iberia Projects, Ankara 30 September–2 October, 2001. Abstracts vol, pp 98–100

Original paper

Geochemical and isotopic (Sr, Nd and O) constraints on sources of Variscan granites in the Western Carpathians – implications for crustal structure and tectonics

Milan KOHÚT[1*], Peter I. NABELEK[2]

[1] *Dionýz Štúr State Institute of Geology, Mlynská dolina 1, 817 04 Bratislava, Slovakia; milan.kohut@geology.sk*
[2] *Department of Geological Sciences, University of Missouri-Columbia, Columbia, MO 65211, USA*
[*] *Corresponding author*

A Sr, Nd, and O isotopic study of Variscan granitoid rocks from the Western Carpathians reveals the dominance of heterogeneous crustal sources for the most of the granitic rocks. Their neodymium crustal index (NCI) is 0.4 to 1.0 (mainly 0.6–0.8). Initial $(^{87}Sr/^{86}Sr)_{350}$ of 0.7053 to 0.7078 and $\varepsilon_{Nd}^{(350)}$ of -0.6 to -6.9 preclude a simple mantle and/or crustal origin for most of granitoids and suggest more complex sources, such as vertically zoned lower crust consisting of old metaigneous, amphibolitic and metasedimentary rocks. Apparent crustal residence ages, indicated by two-stage depleted-mantle Nd model ages ranging from 1.6 to 1.1 Ga, are comparable with other segments of the European Variscan belt. The whole rock $\delta^{18}O_{(SMOW)}$ values of the granites are heterogeneous and range from 8.4 ‰ in tonalites to 11.3 ‰ in leucogranites, reflecting source compositions ranging from mafic to silicic. Petrographically, these granites are representative of common crustal anatectic rocks with magmatic muscovite; however, their isotopic signature reflects petrogenesis related to subduction processes at active continental margins. Recent metamorphic, sedimentary and/or structural studies of the Variscan basement of the Western Carpathians suggest a continental collisional rather than a volcanic arc setting. The Western Carpathian granitic rocks were most likely generated by partial melting of mainly recycled Proterozoic crustal material during subduction-collisional processes of the Variscan orogeny, with possible input of mafic magmas from the mantle. These mafic magmas may have served as a heat source for melting of the lower crust.

Keywords: granite origin, isotope geochemistry, source of rocks, crustal evolution, Western Carpathians
Received: 25 September 2008; accepted 17 December 2008; handling editor: D. Dolejš

1. Introduction

The present-day structure of the Alps and Carpathians, forming part of Stille's (1924) Alpine "Neo-Europa", is mainly the result of convergent processes between the African Plate fragments (Adria–Apulia) and the North European Plate (Eurasia) spanning from the Late Jurassic to the present (Plašienka et al. 1997). Tethian sedimentary rocks dominate this orogenic mobile belt. However, the pre-Mesozoic basement is an important component of the structure of the Carpathians (Petrík and Kohút 1997). Its polyorogenic history is characterised by juxtaposition of various terranes and/or blocks that in most cases originated at the Gondwana margin due to multistage tectonic evolution with large-scale nappe and strike-slip tectonics as part of the European Variscan orogeny (Stampfli and Borel 2002; von Raumer et al. 2002). Although the basement rocks form only discrete fragments in the Alpine Carpathians structure, the granitic rocks dominate at the present erosion level. One of the salient features of the Western Carpathians is a great variety of granitic rocks within small areas (Petrík and Kohút 1997). There exist many similarities between the Variscan granitic rocks of the Alpine "Neo-Europa" and those of the European Variscan belt in the Iberian Massif, the Massif Central, and the Bohemian Massif that represent "Meso-Europa" in sense of Stille (1924). The varieties of granitoid suites include: (a) high-K–Mg, (b) peraluminous, (c) calc-alkaline; (d) ferro-potassic, (e) subalkaline, and (f) anorogenic – alkaline (Bonin et al. 1993; Finger et al. 1997; Schaltegger 1997; Bussy et al. 2000; Kohút 2002, among others). These suites were generated during main and late-Variscan orogenic stages. However, distribution of these series within particular basement blocks is not uniform and is still a matter of debate. The aim of this paper is to present Sr-Nd-O isotopic data from Western Carpathian granitic rocks that place constraints on their sources, petrogenesis, as well as the Variscan crustal evolution and tectonics.

2. Geological setting

Similarly to the Pyrenees and Alps, the Carpathian Mountain chain is a typical Alpine collisional fold belt. However, its pre-Mesozoic basement rocks were part of the Variscan orogenic belt. During the Alpine orogeny, the Carpathian part of the Variscan belt was disrupted and sliced into nappe and terrane blocks that were variously

uplifted (Andrusov 1968; Plašienka et al. 1997). This polyorogenic history makes reconstruction of the Variscan structures rather difficult but provides excellent exposure of various levels of the Variscan crust. The Western Carpathians form a direct eastern continuation of the Eastern Alps. The pre-Alpine crystalline basement crops out mainly in the Central Western Carpathians (CWC) which consist of three principal crustal-scale superunits (from north to south): the Tatricum, the Veporicum and the Gemericum. In addition there are several cover-nappe systems, including the Fatricum, the Hronicum and the Silicicum, also generally emplaced in sequence from north to south (Plašienka et al. 1997). The Variscan granitoid rocks occur in all three superunits of the CWC (Fig. 1; a more detailed geological map of the Western Carpathians can be found at *http://www.geology.sk*).

In the **Tatricum** the granitoids along with pre-Mesozoic metamorphic rocks build backbones of the so-called "core mountains". Both rock types are overlain by Mesozoic cover sediments and/or nappes. The basement rocks were only weakly affected by Alpine metamorphism (Krist et al. 1992). A large composite granodiorite–tonalite body, strongly affected by the Alpine shear tectonics, dominates the **Veporicum**. Other basement rocks include high- to low-grade metamorphic rocks. These are overlain by Upper Paleozoic and Mesozoic cover. Due to complex Variscan and Alpine tectonics, this unit has a very complicated imbricate structure. The degree of penetrative brittle–ductile deformation increases from the northwest to the southeast. The **Gemericum** is dominated by a large hidden granitoid body, which penetrates the overlying Lower Paleozoic rocks in the form of apophyses (Kohút and Stein 2005 and references therein). The Paleozoic rocks are composed of Silurian to Late Carboniferous, mostly low-grade flysch-like metasedimentary rocks and metavolcanics with remnants of an ophiolite complex. Granitoid magmatism dominated in the Variscan orogeny of the Western Carpathians from 360 to 250 Ma (Petrík and Kohút 1997; Finger et al. 2003). In response to variable geotectonic events, different types of granitic magmas have formed during: a) Early Carboniferous crustal thickening, b) Late Carboniferous thermal event, and c) Permian transtension, as recorded by the respective presence of S-, I- and A-type granitic suites (Petrík and Kohút 1997; Broska and Uher 2001; Finger et al. 2003). Available age data (U-Pb, Rb-Sr and Ar-Ar) indicate the main phase of granite magmatism to have been between 360 and 340 Ma (Petrík and Kohút 1997; Kohút 2007); therefore we adopted the age 350 Ma for calculations of initial isotopic compositions.

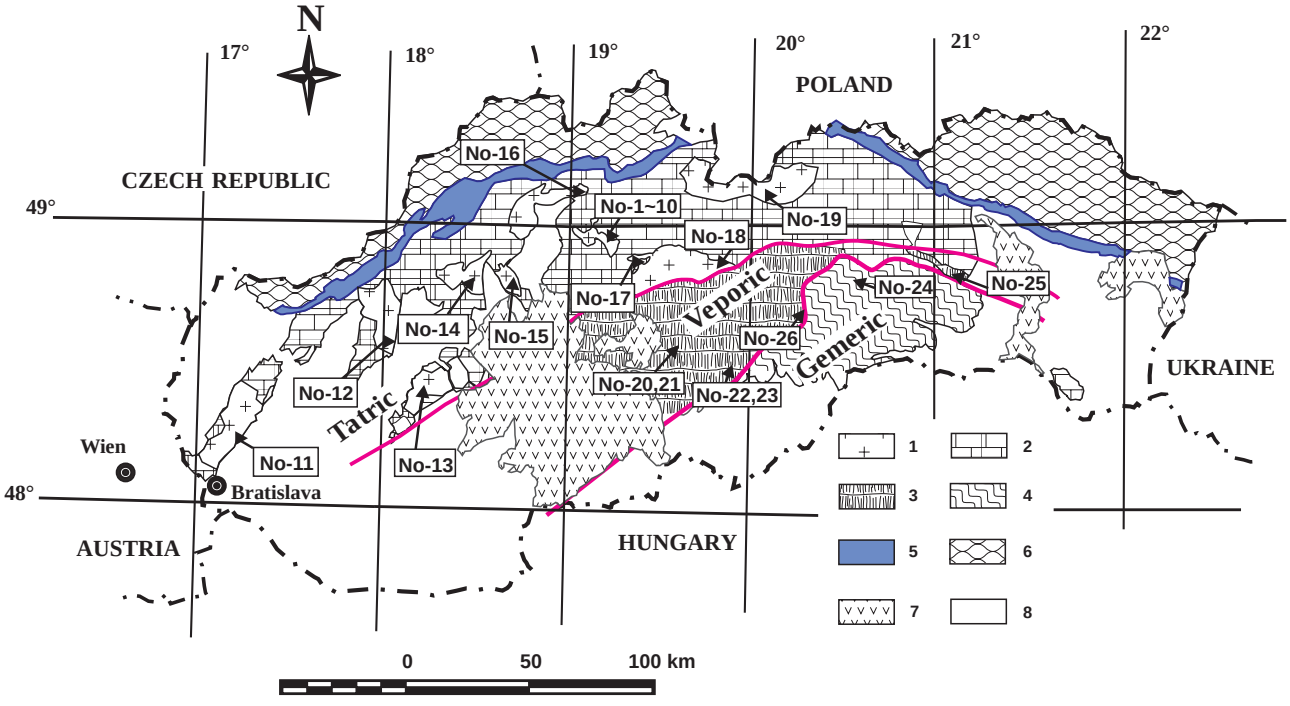

Fig. 1 Simplified tectonic-geological sketch of the Western Carpathians (Slovak part) with location of investigated samples. **1** – Pre-Alpine crystalline basement of Tatric Unit, **2** – Mesozoic sedimentary cover and nappe structures, **3** – Veporic Unit, **4** – Gemeric Unit, **5** – Klippen belt, **6** – Flysch zone, **7** – Neogene to Quaternary Central and East Slovakian neovolcanites, **8** – Neogene to Quaternary sedimentary basins.

3. Analytical methods

Geochemical analyses were performed at the University of Ottawa by X-ray fluorescence and at the Dionýz Štúr Institute of Geology, Bratislava using classical wet chemical techniques. The REE concentrations were analyzed at the Memorial University of Newfoundland, St. John's by ICP-MS (Jenner et al. 1990) and by INAA at MEGA Brno Inc. The measurements were verified against international GM and BM standards. The Sm-Nd isotope analyses were performed at the Institute of Precambrian Geology and Geochronology, Russian Academy of Sciences, St. Petersburg, and Rb-Sr data were acquired in the laboratories of BGR Hannover on a Finnigan MAT 261 mass spectrometer. The powdered whole-rock samples (WR) for Sm-Nd studies were analysed following the method of Richards et al. (1976) and the Rb-Sr analyses were carried out using the method of Wendt (1986). Pulverized samples were spiked with a mixed ^{149}Sm-^{146}Nd or a ^{85}Rb-^{84}Sr solution, respectively, and then dissolved in a mixture of HF + HNO_3 + $HClO_4$. Separation of the relevant elements was done using conventional cation-exchange chromatography, followed, for Nd, by extraction chromatography on HDEHP covered Teflon powder. Total blanks during the measurements were 0.1–0.2 ng for Sm, 0.1–0.5 ng for Nd, 0.03–0.07 ng for Rb and 0.5–0.8 ng for Sr. Accuracy of the measurements of Sm and Nd concentrations at the 2σ level was ±0.5 %, for $^{147}Sm/^{144}Nd$ ±0.5 %, for $^{143}Nd/^{144}Nd$ ±0.005 %, for $^{87}Rb/^{86}Sr$ ±0.5 %, and for $^{87}Sr/^{86}Sr$ ±0.005 %. The weighted average of 31 measurements of the La Jolla Nd-standard yielded 0.511845 ± 4 (2σ) for $^{143}Nd/^{144}Nd$, normalized to $^{146}Nd/^{144}Nd = 0.7219$. For Rb-Sr determinations, internal standards NBS 987 and NBS 607 were used, respectively; all measurements were fractionation corrected to $^{86}Sr/^{88}Sr = 0.1194$. Further details on the analytical techniques were described by Neymark et al. (1993) and Kohút et al. (1996, 1999).

Oxygen isotope analyses were conducted on a Finnigan MAT Delta-E mass spectrometer at the University of Missouri. The samples were reacted with BrF_5 in Ni vessels and the liberated oxygen was converted to CO_2 by reaction with a hot carbon rod (Clayton and Mayeda 1963). All values are reported in permil deviation relative to V-SMOW. Repeated analyses of NBS 28 (quartz) gave a $\delta^{18}O$ value of 9.68 ± 0.21‰.

The εNd(0) values were calculated using $^{147}Sm/^{144}Nd = 0.1967$ and $^{143}Nd/^{144}Nd = 0.512638$ for the Chondritic Uniform Reservoir (CHUR) following Jacobsen and Wasserburg (1980). A linear model with parameters $^{147}Sm/^{144}Nd = 0.2136$ and $^{143}Nd/^{144}Nd = 0.513151$ was used for the Depleted Mantle reservoir (DM) according to Goldstein and Jacobsen (1988). Two-stage apparent crustal residence ages were calculated with a correction for crustal component $^{147}Sm/^{144}Nd_{(CC)} = 0.12$ and the Depleted Mantle parameters $^{143}Nd/^{144}Nd_{(DM)} = 0.513151$ and $^{147}Sm/^{144}Nd_{(DM)} = 0.219$ following the model of Liew and Hofmann (1988). The εSr(0) values were calculated using $^{87}Sr/^{86}Sr = 0.7045$ and $^{87}Rb/^{86}Sr = 0.0816$ for the present-day Bulk Earth (or Uniform Reservoir, UR) composition (DePaolo and Wasserburg 1976; Faure 1986). The values of the neodymium crustal index (NCI) were computed according to the model of De Paolo et al. (1992).

4. Results

The major- and trace-element chemical compositions of the studied samples are given in Tab. 1. The sample set includes ten specimens from one core in the Veľká Fatra Mts. and several representative samples from each of the Western Carpathian granite massifs. The broad sample set, covering all principal granitic types, including tonalites, granodiorites, granites and/or leucogranites (Fig. 2) and hybrid samples from the Veporic Unit, is complemented by one sample of gabbro that is used to constrain the petrogenetic model. The majority of the Carpathian granitoid plutons are composed of several rock types, including tonalites, trondhjemites, granodiorites and leucogranites (granites and granodiorites predominate). Generally, the granitoids have SiO_2 concentrations ranging from *c*. 60 to 77 wt. %, have increasing alkalinity from the more basic to the most acid varieties, but overall they are calc-alkaline. They are metaluminous to peraluminous (A/CNK = 0.7–1.5). Noteworthy is the markedly peraluminous character of hybrid tonalites (A/CNK = 1.4–1.5), in contrast to the subaluminous character of the Veľká Fatra Mts. leucogranites (A/CNK = 0.96–1.04). The prevalence of Na_2O over K_2O is a common feature (K_2O/Na_2O by weight = 0.25–1.15), including the porphyritic "Prašivá" type granite whose alkali ratio is close to 1. The medium- to high-K calc-alkaline character is a common attribute of the European Variscan granitoids (Bonin et al. 1993). Biotite is the dominant ferromagnesian mafic mineral, whereas hornblende occurs only rarely in dioritic enclaves. Accessory mineral assemblages, magnetite + allanite versus monazite + ilmenite, define in some plutons two granite groups (Petrík and Broska 1994) – the occurrence of mafic microgranular enclaves (MME) in magnetite-bearing granites and the presence of metamorphic country-rock xenoliths in magnetite-free granites support division of the Western Carpathian granites into I- and S-type suites. The Sm-Nd, Rb-Sr and oxygen isotopic data are listed in Tab. 2. The Rb-Sr isotopic systematics of the granitoids are shown in Fig. 3. With the exception of two leucogranite samples (ZK-4 and VVM-129), the granitoids fall on a linear array that is in a good agreement with the 350 Ma reference isochron. It is obvious as HT/MP metamor-

Tab. 1 Chemical composition (wt. % and ppm) of the Western Carpathian granites. Symbols: bT – biotite tonalite, mbGD – muscovite-biotite granodiorite, mG – muscovite granite

Number	1	2	3	4	5	6	7	8	9	10	11	12	13
Sample	**VF-43**	**VF-153**	**VF-157**	**VF-283**	**VF-298**	**VF-356**	**VF-417**	**VF-636**	**VF-639**	**VF-700**	**VK-139**	**BGPI-1**	**T-87**
Type	mbG	bT	mG	mbGD	mbG	bT	mbGD	bGD	bGD	mG	mbGD	mbG	bGD
SiO_2	72.66	66.14	74.08	72.27	72.74	68.76	70.69	66.88	66.33	73.94	72.51	72.38	70.01
TiO_2	0.21	0.64	0.11	0.30	0.16	0.51	0.55	0.72	0.58	0.16	0.41	0.17	0.37
Al_2O_3	14.64	16.23	13.09	15.21	15.12	15.59	14.69	15.90	15.70	13.27	14.31	14.86	15.61
Fe_2O_3	0.47	1.79	0.26	0.35	0.33	0.81	0.74	1.33	1.62	0.94	1.00	0.59	1.31
FeO	1.43	2.55	0.89	1.12	0.72	2.33	1.52	1.96	1.93	1.25	1.53	1.60	1.41
MnO	0.03	0.06	0.03	0.05	0.02	0.04	0.05	0.05	0.05	0.02	0.04	0.05	0.04
MgO	0.61	1.35	0.13	0.41	0.37	1.22	0.61	1.32	1.21	0.15	0.81	0.67	0.95
CaO	1.42	2.47	0.49	1.92	1.44	2.83	2.12	2.20	2.89	0.69	1.96	2.88	2.29
Na_2O	3.74	3.93	4.37	4.18	4.24	4.04	4.20	4.51	5.01	4.39	3.23	4.51	3.22
K_2O	3.52	2.79	5.07	2.90	3.83	2.24	3.31	2.83	2.94	3.98	3.19	1.11	2.88
P_2O_5	0.13	0.27	0.48	0.21	0.22	0.21	0.12	0.66	0.24	0.21	0.09	0.17	0.31
H_2O^+	0.75	1.38	0.87	1.02	0.83	0.94	1.07	1.16	1.24	0.76	0.64	0.82	1.60
H_2O^-	0.18	0.26	0.06	0.05	0.06	0.14	0.14	0.12	0.13	0.08	0.22	0.26	0.22
Total	99.79	99.86	99.93	99.99	100.08	99.66	99.81	99.64	99.87	99.84	99.94	100.07	100.22
Sr	259	521	161	179	146	563	302	369	365	103	285	284	482
Rb	110	82	65	117	108	91	105	93	91	177	99	61	92
Ba	864	1110	183	610	534	826	1120	747	641	405	1550	145	575
Zr	112	223	36	78	52	185	139	184	203	40	316	86	156
Y	12.36	8.90	10.89	12.32	11.10	6.98	13.21	13.43	11.50	6.36	16.00	4.69	11.62
Nb	8.79	5.74	10.17	6.53	4.85	8.56	5.87	7.76	8.34	6.00	7.98	9.06	7.41
Ta	0.79	0.28	1.14	0.55	0.46	0.62	0.46	0.51	0.44	0.33	0.63	0.83	0.84
Hf	2.96	4.61	1.36	2.84	1.88	4.30	3.95	4.08	4.62	1.21	3.38	2.27	3.92
Th	6.40	11.75	2.69	5.31	6.52	6.26	10.20	8.56	8.90	2.95	15.40	8.16	8.73
U	2.50	3.25	4.89	2.96	3.70	2.10	4.30	3.05	2.20	3.80	1.70	2.42	2.51
La	20.79	36.07	8.81	16.89	11.82	24.56	28.66	27.41	31.20	5.36	24.20	22.85	25.52
Ce	42.99	76.75	18.12	34.84	26.26	51.11	58.56	54.89	66.34	11.04	54.50	47.47	49.94
Nd	19.73	34.39	8.03	15.38	12.31	23.07	24.18	24.53	29.52	4.84	21.00	20.18	21.15
Sm	4.20	6.03	1.95	3.36	2.80	4.17	4.74	4.82	5.41	1.27	4.00	3.78	3.80
Eu	0.76	1.25	0.67	0.64	0.56	1.19	0.91	0.93	1.09	0.42	0.82	0.84	1.10
Gd	3.32	4.05	1.78	2.43	2.87	2.98	3.06	3.09	3.85	1.22	2.62	2.63	2.84
Tb	0.47	0.45	0.29	0.35	0.38	0.35	0.38	0.40	0.49	0.21	0.37	0.30	0.40
Tm	0.16	0.10	0.11	0.10	0.13	0.08	0.11	0.11	0.15	0.08	0.12	0.06	0.15
Yb	0.94	0.62	0.66	0.74	0.68	0.51	0.79	0.68	0.95	0.51	0.67	0.31	0.95
Lu	0.13	0.09	0.09	0.10	0.09	0.08	0.12	0.10	0.13	0.07	0.11	0.05	0.14

Number	14	15	16	17	18	19	20	21	22	23	24	25	26
Sample	**MM-29**	**Z-164**	**MF-4a**	**NT-401**	**ZK-4**	**TL-117**	**VG-46**	**VG-47**	**V-7312**	**V-9738**	**VVM-129**	**CH-3/72**	**KV-3/622**
Type	mbG	bmG	mbGD	bGD	mG	mbGD	bT	mbGD	bmG	mbG	bmG	bT	Gabbro
SiO_2	72.47	74.19	71.40	69.40	73.31	71.24	68.87	68.95	73.01	71.02	76.09	61.90	48.78
TiO_2	0.18	0.19	0.27	0.49	0.08	0.25	0.46	0.46	0.21	0.32	0.11	0.91	0.78
Al_2O_3	14.55	14.24	14.80	15.16	14.07	14.56	15.64	15.06	14.18	14.45	12.75	16.70	11.22
Fe_2O_3	0.37	0.70	0.40	1.22	0.73	1.24	1.36	1.17	0.56	0.87	0.41	2.69	5.16
FeO	1.50	1.04	1.50	1.50	1.35	1.56	2.21	2.13	0.65	1.82	0.98	5.39	6.12
MnO	0.07	0.02	0.03	0.05	0.06	0.04	0.09	0.04	0.02	0.03	0.03	0.07	0.16
MgO	0.60	0.39	0.59	1.61	0.55	0.77	1.58	1.10	0.44	1.01	0.13	1.94	15.21
CaO	2.09	1.66	1.90	1.96	1.10	2.26	2.37	1.79	1.29	1.97	0.49	2.36	7.44
Na_2O	4.14	4.10	4.15	3.48	4.00	4.48	2.35	3.66	3.60	3.24	2.99	2.16	1.74
K_2O	2.57	2.47	3.49	3.45	3.70	1.87	2.72	3.80	4.52	3.92	4.76	3.06	2.76
P_2O_5	0.12	0.08	0.08	0.23	0.16	0.21	0.18	0.22	0.14	0.17	0.18	0.23	0.34
H_2O^+	0.68	0.51	1.10	1.14	1.32	1.10	1.56	1.31	1.02	0.75	0.78	1.96	0.19
H_2O^-	0.29	0.19	0.14	0.10	0.04	0.18	0.22	0.20	0.16	0.13	0.11	0.16	0.25
Total	99.63	99.78	99.85	99.79	100.47	99.76	99.61	99.89	99.80	99.70	99.81	99.53	100.15
Sr	327	305	473	600	122	449	344	210	120	320	21	464	638
Rb	56	80	65	125	158	88	89	131	240	72	448	102	139
Ba	957	1200	1030	730	316	880	871	851	713	956	60	1040	635
Zr	128	134	124	129	31	159	179	215	96	150	66	268	123
Y	15.23	19.00	10.29	8.75	14.99	7.00	157.59	44.20	24.00	12.00	17.73	40.50	18.00
Nb	5.30	9.00	5.19	12.50	9.19	10.00	17.06	14.35	5.00	7.00	19.65	12.25	4.80
Ta	0.29	0.26	0.37	0.98	1.24	0.29	0.66	0.80	1.10	0.50	5.46	0.59	0.50
Hf	3.53	3.30	3.12	4.46	0.91	4.10	4.44	5.32	3.80	6.80	2.08	4.83	5.10
Th	12.80	10.30	7.20	11.40	5.50	6.30	52.00	14.00	16.90	22.50	9.55	12.05	8.80
U	10.30	3.20	2.80	3.80	3.40	2.60	8.00	3.20	4.80	1.70	6.40	4.30	4.00
La	34.56	31.08	26.87	30.47	6.45	26.67	78.84	31.46	28.52	30.48	7.67	57.20	55.58
Ce	70.83	64.22	55.63	60.26	13.40	54.56	175.60	71.73	58.90	58.14	17.99	120.00	109.70
Nd	29.32	29.10	24.59	27.37	5.81	25.67	84.29	33.97	24.00	29.12	9.51	48.61	45.84
Sm	5.51	5.04	4.72	4.51	1.82	3.91	26.57	8.10	5.23	5.13	2.68	10.20	9.90
Eu	1.24	0.83	0.96	1.01	0.45	0.95	1.37	1.06	0.89	1.13	0.13	1.20	2.05
Gd	4.13	4.12	3.41	3.36	2.05	2.89	32.46	8.22	3.60	3.26	2.20	7.42	4.69
Tb	0.55	0.54	0.44	0.40	0.43	0.36	5.26	1.40	0.71	0.43	0.48	1.27	0.68
Tm	0.26	0.18	0.14	0.16	0.24	0.13	1.81	0.61	0.27	0.17	0.24	0.52	0.27
Yb	1.76	1.04	0.87	1.04	1.65	0.71	9.94	3.74	1.60	0.99	1.34	3.25	1.40
Lu	0.27	0.16	0.13	0.15	0.24	0.12	1.46	0.51	0.25	0.14	0.18	0.41	0.19

Tab. 2 Isotopic composition and related parameters for the studied Western Carpathian granitic rocks

Sample	Rb	Sr	1/Sr	Rb/Sr	$^{87}Rb/^{86}Sr$	$^{87}Sr/^{86}Sr(2\sigma)$	$\varepsilon_{Sr(0)}$	$(^{87}Sr/^{86}Sr)_{350}$	$\varepsilon_{Sr(350)}$	Sm
VF-43	110	259	0.0039	0.42	1.3838	0.71359 ± 21	129.03	0.706695	36.95	3.05
VF-153	82	521	0.0019	0.16	0.4759	0.70856 ± 16	57.56	0.706184	29.69	5.89
VF-157	65	161	0.0062	0.40	1.1644	0.71214 ± 18	108.43	0.706338	31.87	2.26
VF-283	117	179	0.0056	0.65	2.9164	0.71985 ± 22	217.87	0.705318	17.40	3.41
VF-298	108	146	0.0068	0.74	3.0970	0.72220 ± 20	251.24	0.706770	38.01	3.25
VF-356	91	563	0.0018	0.16	0.4330	0.70824 ± 21	53.09	0.706083	28.25	4.73
VF-417	105	302	0.0033	0.35	1.1067	0.71164 ± 20	101.31	0.706123	28.82	4.27
VF-636	93	369	0.0027	0.25	0.5673	0.70962 ± 16	72.65	0.706792	38.32	4.55
VF-639	91	365	0.0027	0.25	0.5255	0.70882 ± 20	61.32	0.706202	29.94	4.72
VF-700	103	177	0.0056	0.58	1.6920	0.71521 ± 16	152.02	0.706780	38.15	2.07
VK-139	99	285	0.0035	0.35	0.9891	0.71240 ± 34	112.14	0.707472	47.98	5.66
BGPI-1	61	284	0.0035	0.21	1.6198	0.71492 ± 22	147.91	0.706850	39.15	3.52
T-87	92	482	0.0021	0.19	0.3500	0.70768 ± 28	45.14	0.705936	26.17	4.82
MM-29	56	327	0.0031	0.17	1.7590	0.71496 ± 24	148.47	0.706196	29.86	5.72
Z-164	80	305	0.0033	0.26	1.5696	0.71403 ± 16	135.27	0.706210	30.05	5.77
MF-4a	65	473	0.0021	0.14	0.4390	0.70848 ± 18	56.49	0.706293	31.24	4.19
NT-401	125	600	0.0017	0.21	0.5644	0.71010 ± 30	79.49	0.707288	45.37	4.19
ZK-4	158	122	0.0082	1.30	3.4260	0.73700 ± 28	461.32	0.719930	224.93	3.57
TL-117	88	449	0.0022	0.20	0.6092	0.70920 ± 20	66.71	0.706165	29.42	3.75
VG-46	89	344	0.0029	0.26	0.5480	0.70800 ± 40	49.68	0.705270	16.71	25.50
VG-47	131	210	0.0048	0.62	1.4660	0.71510 ± 30	150.46	0.707796	52.58	7.96
V-7312	240	120	0.0083	2.00	0.9727	0.71123 ± 28	95.53	0.706384	32.53	5.00
V-9738	72	320	0.0031	0.23	0.7440	0.71005 ± 24	78.78	0.706343	31.95	5.04
VVM-129	448	21	0.0476	21.33	17.4520	0.87094 ± 36	2362.5	0.783988	1134.70	2.58
CH-3/72	102	464	0.0022	0.22	1.0252	0.71110 ± 22	93.68	0.705992	26.97	11.83
KV-3/622	139	638	0.0016	0.22	0.1965	0.70330 ± 20	-17.03	0.702321	-25.17	11.39

$t_{(DM2st)}$ – two-stage apparent crustal residence ages (Liew and Hofmann 1988); NCI – neodymium crustal index (DePaolo et al. 1992)

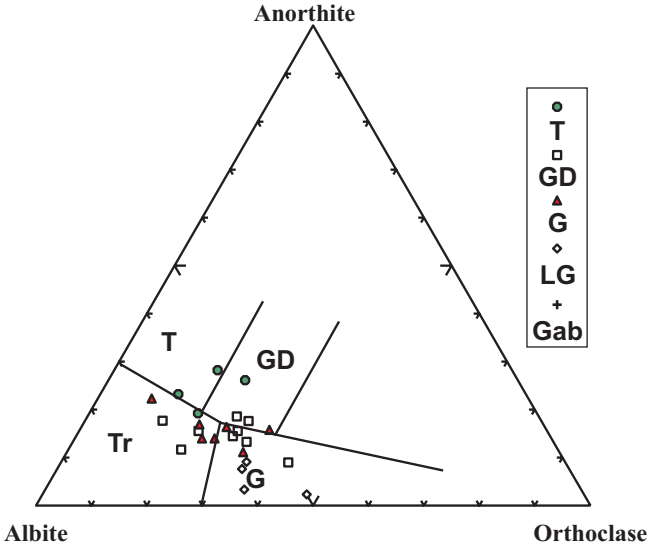

Fig. 2 An-Ab-Or CIPW normative diagram (Barker 1979) showing varied character of the Variscan Western Carpathian igneous rocks. Symbols: circles – tonalites, squares – granodiorites, triangles – granites, diamonds – leucogranites, cross – gabbro.

phism with widespread granitic magmatism is typical of European Variscides, and could have lead partial isotopic homogenization throughout wide areas during Early Carboniferous period or sources could have been isotopically similar *a priori* (F. Finger, personal com-

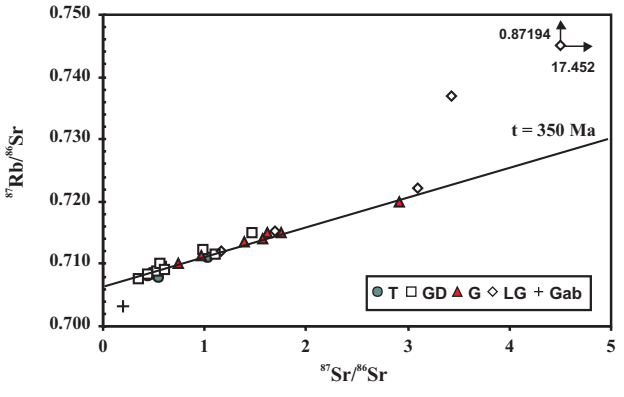

Fig. 3 Whole-rock Rb/Sr isochron (Nicolaysen-type) plot indicating evolution of the Western Carpathian granitic rocks with dominance of studied samples clustering around the reference 350 Ma isochron. Symbols as in Fig. 2.

Nd	Sm/Nd	$^{147}Sm/^{144}Nd$	$^{143}Nd/^{144}Nd$ (2σ)	$\varepsilon_{Nd(0)}$	$(^{143}Nd/^{144}Nd)_{350}$	$\varepsilon_{Nd(350)}$	$t_{(DM2st)}$	NCI	$\delta^{18}O$
15.93	0.19	0.11602	0.512391 ± 5	-4.82	0.512125	-1.21	1155	0.58	9.8
32.25	0.18	0.11636	0.512323 ± 6	-6.14	0.512056	-2.56	1261	0.70	9.3
8.54	0.26	0.13045	0.512284 ± 8	-6.91	0.511985	-3.95	1370	0.77	10.5
15.85	0.22	0.12985	0.512273 ± 10	-7.12	0.511975	-4.14	1385	0.79	11.3
15.45	0.21	0.12768	0.512306 ± 11	-6.48	0.512013	-3.39	1327	0.73	11.0
23.44	0.20	0.12241	0.512346 ± 6	-5.70	0.512065	-2.38	1247	0.66	9.7
23.89	0.18	0.11918	0.512265 ± 9	-7.28	0.511992	-3.81	1359	0.81	10.4
24.47	0.19	0.11444	0.512338 ± 8	-5.85	0.512076	-2.18	1231	0.67	9.6
25.19	0.19	0.11364	0.512347 ± 7	-5.68	0.512087	-1.97	1214	0.66	9.5
8.39	0.25	0.14990	0.512330 ± 13	-6.01	0.511986	-3.92	1368	0.69	9.0
30.80	0.18	0.11135	0.512302 ± 6	-6.55	0.512047	-2.74	1275	0.74	10.2
18.50	0.19	0.11551	0.512235 ± 9	-7.86	0.511970	-4.24	1393	0.86	11.1
27.70	0.17	0.10548	0.512397 ± 7	-4.70	0.512155	-0.62	1109	0.57	10.7
30.60	0.19	0.11346	0.512278 ± 11	-7.02	0.512018	-3.30	1319	0.78	11.2
31.99	0.18	0.10947	0.512298 ± 10	-6.63	0.512047	-2.74	1275	0.75	10.0
22.30	0.19	0.11362	0.512307 ± 11	-6.46	0.512047	-2.75	1276	0.73	9.8
22.66	0.18	0.11216	0.512396 ± 9	-4.72	0.512139	-0.94	1134	0.57	8.6
15.40	0.23	0.14044	0.512156 ± 8	-9.40	0.511834	-6.89	1601	1.00	9.6
21.50	0.17	0.10597	0.512343 ± 4	-5.75	0.512100	-1.70	1194	0.67	9.5
82.10	0.31	0.18865	0.512516 ± 5	-2.38	0.512084	-2.02	1219	0.36	8.4
33.91	0.23	0.14237	0.512354 ± 11	-5.54	0.512028	-3.11	1305	0.65	10.5
22.50	0.22	0.13498	0.512333 ± 14	-5.95	0.512024	-3.19	1311	0.68	8.6
28.50	0.18	0.10717	0.512332 ± 12	-5.97	0.512086	-1.97	1215	0.69	9.3
8.93	0.29	0.17537	0.512364 ± 9	-5.34	0.511962	-4.40	1405	0.63	9.9
52.04	0.23	0.13787	0.512343 ± 9	-5.68	0.512031	-3.05	1299	0.66	9.1
65.68	0.17	0.10515	0.512715 ± 6	1.50	0.512474	5.60	620	0.00	6.6

munication). The $(^{87}Sr/^{86}Sr)_{350}$ ratios in granitoid rocks of the Tatric and Veporic units are low (0.705–0.708), suggesting a mixed lower crustal and mantle source, mixing of more and less radiogenic sources and/or a Rb-poor crustal source (Fig. 4). Granitoids from the Gemeric Unit (VVM-129) have extremely high $(^{87}Sr/^{86}Sr)_{350} \geq 0.725$ (Kovach et al. 1986), which suggests an older supracrustal metasedimentary source.

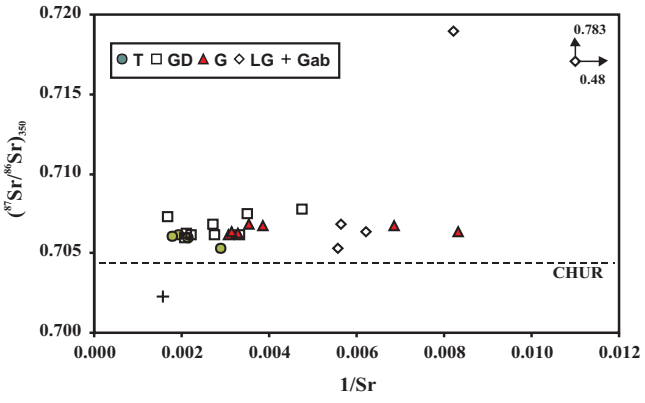

Fig. 4 Initial Sr isotopic ratios at 350 Ma vs. 1/Sr plot documenting nearly balanced and quasi-homogenized isotopic composition during genesis of the Variscan granites in the Western Carpathians. Symbols as in Fig. 2.

The $\varepsilon_{Nd}(0)$ values for the West Carpathian granitoids, ranging from -2.3 to -9.4, are comparable with other data for the Variscan fold belt of Central Europe (Liew and Hofmann 1988), the Massif Central (Pin and Duthou 1990), the Bohemian Massif (Liew et al. 1989; Janoušek et al. 1995; Gerdes 2001) and the Tauern Window (Finger et al. 1993). In contrast to the Rb-Sr isotopic system, no isochron relationship is apparent in the Sm-Nd system at 350 Ma (Fig. 5), and the $(^{143}Nd/^{144}Nd)_{350}$ ratios are more heterogeneous (Fig. 6). Even though, there is an overlap in the Nd isotopic ratios of tonalites, granodiorites, and granites, the leucogranites have systematically less radiogenic Nd. Nevertheless, in comparison to the general broad range of Nd isotope ratios of crustal rocks wordlwide, the range in the CWC granitoids is small. Only the gabbro sample is distinct with the most radiogenic ratio, which reflects its mantle source.The $\delta^{18}O$ values of the granitoids range from 8.4 to 11.3 ‰ (Figs 7 and 8). On average, the tonalites have the lowest $\delta^{18}O$ values of 9.1 ± 0.6 ‰, the granodiorites have 9.9 ± 1.3 ‰, the granites show 10.2 ±

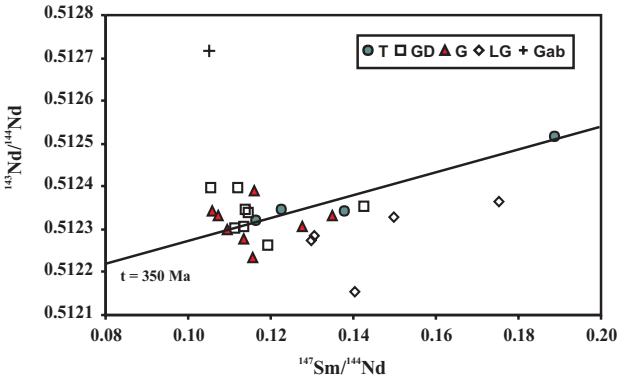

Fig. 5 $^{143}Nd/^{144}Nd$ versus $^{147}Sm/^{144}Nd$ isochron diagram for the Western Carpathian granitic rocks. A reference 350 Ma isochron is drawn for comparison As can be seen, there is no linear relationship reflecting the lack of the regional-scale homogenization. Symbols as in Fig. 2.

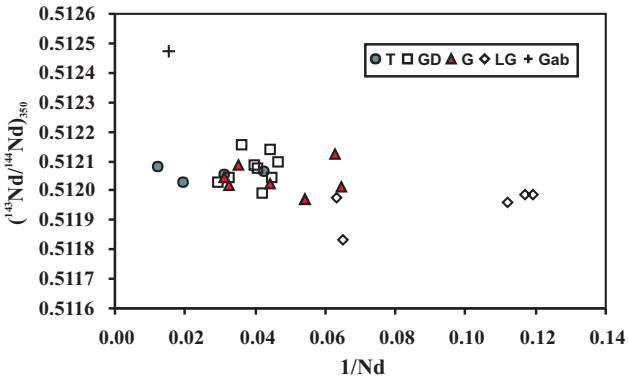

Fig. 6 Initial Nd isotopic ratios at 350 Ma versus 1/Nd ratio diagram. The lack of a linear array rules out simple two-component source mixing and reflects rather heterogeneous sources and/or open-system interactions during genesis of the Carpathian granites.

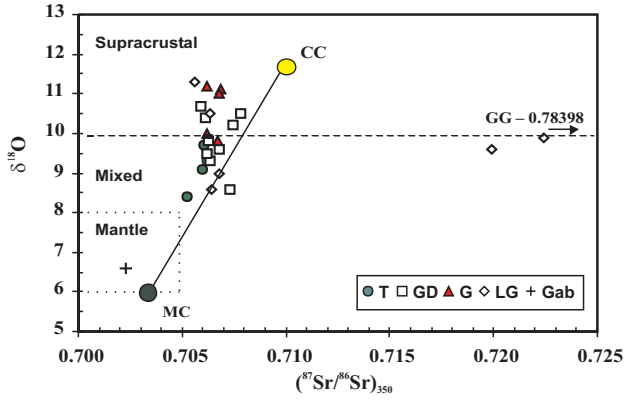

Fig. 7 Diagram $\delta^{18}O$ vs. $(^{87}Sr/^{86}Sr)_{350}$ of the Western Carpathian granites; crustal and mantle components (CC + MC) are taken from James (1981). According this model the CWC granites represent 10–50% assimilation of crustal rocks.

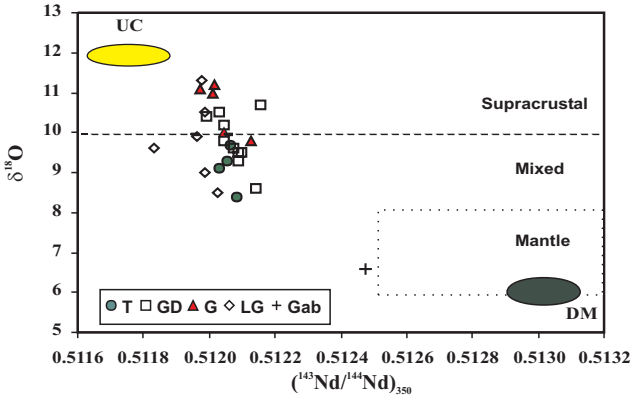

Fig. 8 Plot of $\delta^{18}O$ vs. $(^{143}Nd/^{144}Nd)_{350}$ for granitic rocks of the Western Carpathians. Potential crustal source (upper crust – UC) and depleted mantle component (DM) are shown for comparison.

1.6 ‰, and the leucogranites have 10.0 ± 1.0 ‰. Thus, there is a considerable overlap in the oxygen isotope composition between individual granitoid types. However, with the exception of the leucogranites and one granodiorite sample, there is a fairly good negative correlation of the $\delta^{18}O$ values with $(^{143}Nd/^{144}Nd)_{350}$ (Fig. 8) whereby higher $\delta^{18}O$ values tend to indicate a sedimentary crustal protolith and lower values a mafic protolith (O'Neil and Chappell 1977; Taylor 1988). The gabbro sample has $\delta^{18}O$ value of 6.6 ‰, which is typical of mantle-derived rocks.

5. Discussion

5.1. Sources of granitoids

In spite of the broad range of granitoid types in the Tatric and Veporic superunits, the granitoids have rather narrow ranges of $(^{87}Sr/^{86}Sr)_{350}$ and $(^{143}Nd/^{144}Nd)_{350}$ ratios, particularly in comparison to granitoids of other orogenic belts such as the Lachlan fold belt of Australia (McCulloch and Chappell 1982). The possible source rocks of the Western Carpathian granitoids have previously been discussed (e.g. Cambel and Petrík 1982; Kráľ 1994; Petrík et al. 1994; Kohút and Nabelek 1996; Petrík and Kohút 1997; Petrík 2000; Finger et al. 2003). According to Kráľ (1994), the Tatric and the Veporic granitoids were generated from an isotopically inhomogeneous source by mixing of mantle and crustal material with a low Rb/Sr ratio. Petrík et al. (1994) suggested that S-type granitoids were generated by dehydration melting of peraluminous muscovite- and biotite-bearing metasedimentary rocks with graphitic intercalations because of fairly reduced accessory oxide assemblage. They viewed biotite- and biotite-hornblende plagioclase gneisses as plausible sources for generation of the I-type group. Kohút and Nabelek (1996) suggested for part of the Tatric transitional (I/S) granitoids melting of a vertically zoned lower crust, including a volcanic arc and

crustal metasediments. Petrík and Kohút (1997) preferred a) supracrustal, reduced granulite-facies rocks with minor addition of a mantle-like component as sources for the S-type granites, b) intermediate, oxidized metaigneous rocks in combination with underplated mafic crust as protolith for the I-type group, c) H_2O-poor and F-rich granulite and/or tonalite crust as parental to the A-type group, and d) mature, recycled sedimentary supracrustal rocks, or rocks which experienced sea-floor weathering and were permeated by volcanic (boron) emanations as source lithologies for the Gemeric granites. Petrík (2000), on the basis of previously published data, considered various proportions of at least two contrasting source components – old recycled supracrustal metasediments and a young mafic source with possible addition of assimilants. Presented isotopic data (Sr, Nd and O) preclude a simple mantle (like plagiogranites in ophiolitic complexes) or crustal origin (like Himalayan granites) for most of the Tatric and Veporic granites. Although the lowermost $(^{87}Sr/^{86}Sr)_{350}$ ratio in the Fig. 4 is close to the CHUR composition and thus the mantle limit, most samples have this ratio slightly higher (0.706–0.708). Most of the Western Carpathian granitoids define a well-defined field in a $(^{87}Sr/^{86}Sr)_{350}$ *vs.* $(^{143}Nd/^{144}Nd)_{350}$ plot (Fig. 9) that is characteristic of I-type granitoids (McCulloch and Chappell 1982; Hensel et al. 1985; Liew et al. 1989; Petford and Atherton 1996). Only the Kralička and the Gemer granites have isotopic characteristics that indicate involvement of upper-crustal sources. All granitoid samples lie in quadrant IV, but close to the mantle domain in quadrant II. Magma sources with positive values of both enrichment parameters f_{Sm} and f_{Rb} (quadrant I) are not typical of ordinary felsic igneous rocks (Faure 1986) but old amphibolite/greenstone lower crust shows such enrichment behavior (Keay et al. 1997; Poller et al. 1998). Apparent two-stage Nd crustal residence ages (t_{DM2st}) range from 1.6 to 1.1 Ga, but are mostly between 1.4 and 1.1 Ga (Fig. 10). The 1.6 Ga age is for a leucocratic sample ZK-4 which has the lowest $\varepsilon_{Nd(0)}$ value. Overall, the model ages are comparable with those of the Variscan belt elsewhere in Europe. For example, Nd crustal residence ages in the Central Iberian zone vary between 1.7 to 1.4 Ga (Moreno-Ventas et al. 1995; Villaseca et al. 1998; Castro et al. 1999), in the Bohemian Massif between 1.7 and 1.1 Ga (Liew and Hofmann 1988; Janoušek et al. 1995), in Schwarzwald between 1.6 to 1.4 Ga (Liew and Hofmann 1988) and in Massif Central between 1.8 to 1.1 Ga (Pin and Duthou 1990; Turpin et al. 1990; Williamson et al. 1996; Downes et al. 1997). Analogues of dioritic rocks in the Tatra Mountains are scarce – similar rocks are found in Massif Central (Shaw et al. 1993), Corsica (Cocherie et al. 1994) or Bohemian Massif (Janoušek et al. 1995; Sokol et al. 2000).

The gabbro from the Veporic superunit falls on the mantle array in quadrant II, which demonstrates its mantle origin. The gabbro's model age is 620 Ma, which is in accord with evolution of a hypothetical depleted mantle reservoir in the Carpathian realm during the Pan-African orogeny (700–500 Ma). However, recent U-Pb zircon SHRIMP dating of gabbro from the Branisko Mountains anatectic complex suggests a Late Devonian (370 Ma) age (Kohút et al. in print).

The low $(^{87}Sr/^{86}Sr)_{350}$ ratios might be interpreted in several ways: 1) melting of a relatively young crust, 2) melting of lower crustal rocks with Rb depleted during the ancient granulite-facies metamorphism, 3) melting of a mixture of deep sea sediments with seafloor basalts,

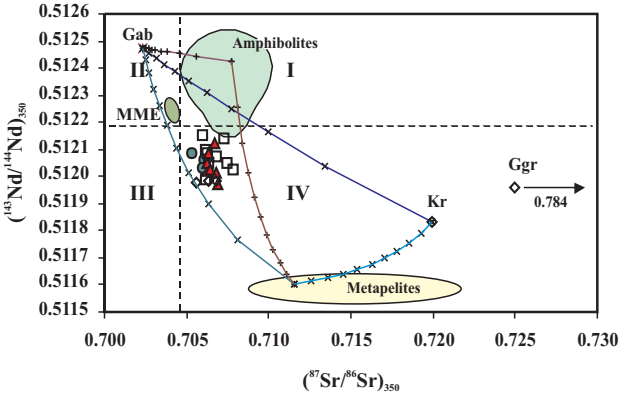

Fig. 9 Initial Nd and Sr isotopic compositions (in relation to CHUR and UR) for granites of the Western Carpathians. Due to extremely high contents of radiogenic Sr in the Gemeric granites (Ggr) the projection point falls beyond the diagram. Quadrants I–IV are indicated according to Faure (1986). Explanations: Kr – Kralička granite, Gab – gabbro, MME – dioritic mafic microgranular enclaves after Poller et al (2001). Symbols as in Fig. 2.

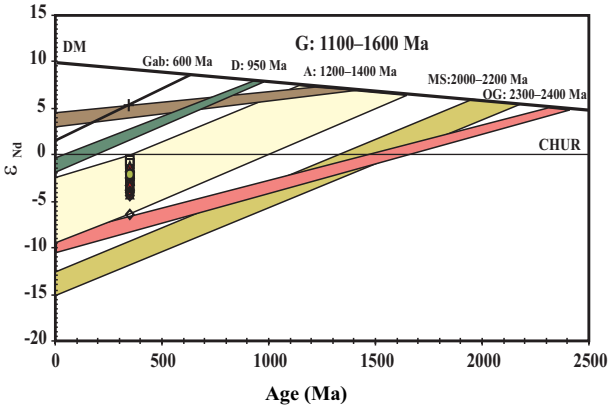

Fig. 10 Diagram of $^{143}Nd/^{144}Nd$ *vs.* time, showing two-stage depleted-mantle (DM) Nd model ages. The evolution curve for DM is after Goldstein et al. (1984). Abbreviations: G – granites and Gab – gabbro of this work in comparison with the fields of D – diorites, A – amphibolites, MS – metasediments and OG – orthogneisses (data taken from Poller et al. 2000, 2001; Kohút et al. 2008).

4) melting of subducted oceanic slab, 5) melting of an underplated basaltic crust, and 6) melting of an old greenstone belt. Given that the European Hercynides are essentially related to subduction and collisional processes (Burg and Matte 1978; Matte 1986, 1991; Pin and Duthou 1990; von Raumer and Neubauer 1993; and/or Petrík and Kohút 1997), one possibility is that the principal source of the Tatric and Veporic granitoids was an underplated volcanic arc below the collisionally thickened continental crust. On the other hand, more mature supracrustal metamorphic rocks and infracrustal igneous rocks were sources for the Gemeric granitoids that have more elevated Sr isotope ratios. From the geochemical point of view, the CWC granitoids seem to be analogues of volcanic-arc granitoids but such a character may have been inherited from products of Early Variscan active margin subduction processes. Similar scenario was described in the Bohemian Massif by Finger and Clemens (1995). The rather broad range of oxygen isotope ratios would then suggest that the arc crust was variably hydrothermally altered prior to underplating.

However, the source region was probably composite and certain portions were perhaps as old as Proterozoic as suggested by the T_{DM} ages of the granitoids. Where exposed by thrusting, the Carpathian basement includes low- to high-grade metamorphic rocks, amphibolites, migmatites, orthogneisses, granites, greenstone rocks and/or Upper Paleozoic sedimentary and volcanic rocks. A heterogeneous source region for the granitoids is inferred by variability of enclave populations, represented by country-rock xenoliths (gneisses, amphibolites, eclogites and granulites), and/or mafic microgranular enclaves (Hovorka and Petrík 1992; Petrík et al. 1994; Janák 1994; Janák et al. 1996, 1999; Petrík and Kohút 1997). An excellent perspective on how the source region may have appeared can be obtained in a new, 4 km long highway tunnel in the Branisko Mountains that exposes a small portion of the Variscan lower crust. The exposed rocks include a greenstone-like granite anatectic complex, composed of various amphibolites alternating with tonalitic gneisses on one side but rather typical greywacke gneisses on the other side of the tunnel. Widespread anatectic phenomena are observed in both lithologies. Stromatic migmatite, metatexite, diatexite and/or dictyonic structure indicate melting and segregation of the melt (Sawyer 1991, 1996; Brown 1994). Salient is the presence of gabbroic enclaves within this anatectic complex and this may indicate input of a juvenile basic magma into the lower crust. It is possible that such a source region yielded the observed spectrum of Variscan granitoids. It is apparent, however, that Sr and Nd isotopes were already fairly homogeneous during the anatectic event as suggested by their narrow ranges in the granitoids.

For better understanding of the nature of the components in the complex source region during the Variscan magmatism, we added fields of amphibolites and metasedimentary rocks from the Tatra Mountains (Poller et al. 1998, Kohút et al. 2008), which represent plausible lower crustal and upper crustal sources, respectively, to the $(^{87}Sr/^{86}Sr)_{350}$ *vs*. $(^{143}Nd/^{144}Nd)_{350}$ diagram (Fig. 9). A prospective mantle source is represented by the gabbro and another upper-crustal component by the Kralička granite (Tab. 3). Although it is possible to construct a simple binary mixing array between a mantle source and the isotopically variable metasedimentary rocks, the occurrence of tonalites indicates that amphibolites were also involved in the melting process. Mixing calculations involving gabbro (mantle source), amphibolites, and metapelites as potential sources yield the following proportions: 25–75 % metasediments, 0–75 % amphibolites and 5–25 % gabbroid rocks, with ranges depending on the assumed isotopic compositions of the metapelites and amphibolites. Mixing calculations involving orthogneisses (represented by the Kralička granite instead of amphibolites) yield 25–75 % metasedimentary rocks, 0–45 % orthogneisses, and 20–35 % mantle-derived melts. In either case, the presence of crustal sources during the generation of the Carpathian granites is evident.

The importance of crustal contribution to the Western Carpathian granitoids is confirmed also by the neodymium crustal index (DePaolo et al. 1992) NCI = 0.4–1.0, mostly between 0.6 and 0.8 (Tab. 2). Furthermore, the $\delta^{18}O$ values of the granitoids are generally elevated relative to mantle values including the gabbro (Figs 7–8), which suggests a significant crustal component in the protolith. This is in accord with the large amount of anatectic granite rocks observed elsewhere within the European Variscides. We note that the two-stage Nd model age for amphibolitic rocks is identical to that of the granitoids and it is in contrast to the Early Proterozoic model ages of metasedimentary rocks and orthogneisses from the Tatra Mountains (Fig. 10). This implies addition of mantle material to the source region that may have initially consisted of more silicic crustal materials. Such an addition is also suggested by the compositions of dioritic MME in the Tatra Mts. granitoids (Poller et al. 2001). The mantle origin of the Tatra Mts. diorites has never been advocated, in accordance with the observation of Pin et al. (1991). However, MME are commonly thought to be products of magma

Tab. 3 Input parameters for individual sources in the mixing models.

	Sr	$(^{87}Sr/^{86}Sr)_{350}$	Nd	$(^{143}Nd/^{144}Nd)_{350}$
Gabbro	638	0.702321	65.7	0.512474
Amphibolite	106	0.707730	13.7	0.512426
Metapelite	95	0.711537	31.9	0.511602
Orthogneiss	122	0.719930	15.4	0.511834

mixing/mingling processes (e.g., Didier 1973; Didier and Barbarin 1991).

5.2. Thermal aspects of melt generation

As is the case for much of the exposed European basement, crystalline products of the Variscan orogeny dominate the present erosion level of the Western Carpathians. Available dates (U-Pb, Rb-Sr and Ar-Ar) support granite-forming events mainly between 360 and 260 Ma. The results of the present study indicate that the source region of the granitoid magmas could have included amphibolites, metasedimentary rocks and orthogneisses, and some mantle-derived material, perhaps in the form of magmas that invaded the source region during anatexis, was probably involved in the petrogenesis. The spectrum of granitoid compositions in the Western Carpathians and their isotopic compositions are consistent with a heterogeneous source region as seen on the exposures in the Branisko Mountains. The source region probably included potentially fertile lithologies, represented by metagreywackes, metapelites and hydrated mafic or intermediate metavolcanics (amphibolites or greenstone-like rocks). The dehydration melting of muscovite, biotite and/or hornblende-bearing rocks has widely been suggested as an anatectic crustal process (Clemens and Vielzeuf 1987; Le Breton and Thompson 1988; Patiño Douce et al. 1990; Skjerlie et al. 1993; Wolf and Wyllie 1994; Singh and Johannes 1996; Montel and Vielzeuf 1997 among others). The continental crust must have been considerably thick (>40 km) and hot enough for melting of a basic metaigneous source to occur. Indeed, the voluminous granitoid production during the Variscan period demonstrates that the pre-Carboniferous crust of the European Variscides was sufficiently thickened by multistage collisional tectonics to become fertile for granite production (Vielzeuf et al. 1990). Although leucogranites can potentially be produced by decompression melting or shear heating of mid-crustal metasedimentary rocks (e.g. Daniel et al. 1987; Nabelek and Barlett 1998; Patiño-Douce and Harris 1998; Nabelek and Liu 1999), these processes are unlikely to result in sufficiently high melt production to explain the volume of the Western Carpathian granitoids. Therefore an enhanced heat flux from mantle or unusually high radioactive heat production is required (e.g. Royden 1993). Supracrustal sedimentary rocks enriched in U, Th and K could potentially sufficiently heat the source region to induce anatexis but a large abundance of such a lithology is not evident in the isotopic composition of the granitoids. The most likely source of heat for anatexis of the Variscan lower crust is an underplated and/or intraplated mantle-derived magma as has been proposed for production of other orogenic granites (e.g. Holland and Lambert 1975; Wells 1981; Huppert and Sparks 1988; Dewey 1988). The gabbro from the Veporicum may represent a product of crystallization from such a magma, although its genetic relationship to the Western Carpathian granitoids is not yet clear. Gabbroic rocks also occur within the Branisko greenstone–granite anatectic complex. Field and petrologic evidence indicates collisionally thickened and inverted structure of the CWC Variscan basement (Janák 1994; Kohút and Janák 1994*)* with intrusion of lens-like granite bodies within the upper unit. Similar structure occurs in the classical Himalayan convergent orogen (Le Fort 1981; France-Lanord and Le Fort 1988; Harrison et al. 1998). It is suggested that melting of heterogeneous crustal sources in the Western Carpathians occurred during subduction of the lithosphere and continental collision in the early Variscan times. Heating through underplating and/or intraplating of mantle-derived magma facilitated partial melting. After the main collisional stage, the thick and thermally weakened crust most probably collapsed due to gravitational instability (Dewey 1988; Hollister 1993), leading to decompression and rapid exhumation at 2–3 mm/year accompanied by rapid cooling of 35–87 °C/Ma (Janák and Kohút 1996; Kohút et al. 1997). Rapid cooling of the hanging wall containing the melt by thrusting onto the colder footwall in the Carboniferous times was followed by gradual cooling attributed mainly to the extensional denudation and concomitant erosion forced by propagation of normal faults in the Permian. Therefore, majority of the crystalline basement terranes of the Western Carpathians have been eroded before the Alpine–Lower Triassic sedimentation.

6. Conclusions

The Western Carpathians belong to the Alpine Neo-Europe. Even though they may have been variably affected by the Alpine orogeny, the granitic rocks in the Variscan basement show many similarities to other European occurrences of granitic rocks within the Variscan orogenic belt. The Sr-Nd-O isotopic compositions of the Variscan granitic rocks in the Western Carpathians indicate a mixed source consisting of Proterozoic and younger crustal and mantle-derived lithologies. It is inferred that the source was vertically-zoned lower crust consisting of felsic and mafic metaigneous and metasedimentary rocks. A contribution of mantle-derived magma is evident in Sr and Nd isotope compositions. Intrusion of such magma may have contributed to homogenization of the isotope ratios of these elements and provided the heat necessary for melting of the lower crust. Although the geochemical features of the Western Carpathian granitoids are typical of volcanic arc igneous suites, the surrounding metamorphic rocks association and their P-T conditions indicate their generation during an intracontinental subduction or conti-

nental collision that involved high-grade metasedimentary and metaigneous rocks in the lower- to mid-crust.

Acknowledgements. We are grateful to Igor Broska, Ľubomír Hraško, Igor Petrík and Vojtech Vilinovič who have kindly donated part of samples for this study and permitted publication of primary chemical data. Petr Černý (The University of Manitoba, Winnipeg) and Pavel Uher (Comenius University, Bratislava) are thanked for major- and trace-element analyses, performed owing to NSERC Grant #311-1727-17. The authors wish to thank to Friedrich Finger and Igor Petrík for constructive reviews. We are grateful to David Dolejš for editorial handling. This work was supported by the Slovak Research and Development Agency under the grant contract Nos APVV-0557-06 and APVV-549-07 as well as GAČR grant No. 205/07/0992. A University of Missouri Research Board grant provided additional funding.

References

Andrusov D (1968) Grundriss der Tektonik der Nördlichen Karpaten, Veda Publishing House of SAV, Bratislava, pp. 1–188.

Barker F (1979) Trondhjemite: definition, environment and hypotheses of origin. In: Barker F (ed) Trondhjemites, Dacites and Related Rocks. Elsevier, Amsterdam, pp 1–12

Bonin B, Brändlein P, Bussy F, Desmond J, Eggenberger U, Finger F, Graf K, Marro C, Mercolli I, Oberhänsli R, Ploquin A, von Quadt A, von Raumer J, Schaltegger U, Steyrer HP (1993) Late Variscan Magmatic Evolution of the Alpine Basement. In: Von Raumer JF, Neubauer F (eds) Pre-Mesozoic Geology of Alps. Springer Verlag, Berlin, pp 171–201

Broska I, Uher P (2001) Whole-rock chemistry and genetic typology of the West-Carpathian, Variscan granites. Geol Carpath 52: 79–90

Brown M (1994) The generation, segregation, ascent and emplacement of granite magma: the migmatite-to-crustally-derived granite connection in thickened orogens. Earth Sci Rev 36: 83–130

Burg JP, Matte Ph (1978) A cross-section trough the French Massif Central and the scope of its Variscan geodynamic evolution. Z Dtsch geol Gesell 109: 429–460

Bussy F, Hernandez J, von Raumer J (2000) Bimodal magmatism as a consequence of the post-collisional readjustment of the thickened Variscan continental lithosphere (Aiguilles Rouges – Mount Blanc Massif, Western Alps). Trans Roy Soc Edinb, Earth Sci 91: 221–233.

Cambel B, Petrík I (1982) The West Carpathian granitoids: I/S classification and genetic implications. Geol Zborn Geol Carpath 33: 255–267

Castro A, Patiño Douce AE, Corretgé LG, de la Rosa JD, El-Biad M, El-Hmidi H (1999) Origin of peraluminous granites and granodiorites, Iberian Massif, Spain: an experimental test of granite petrogenesis. Contrib Mineral Petrol 135: 255–276

Clayton RN, Mayeda TK (1963) The use of bromine pentafluoride in the extraction of oxygen from oxides and silicates for isotopic analysis. Geochim Cosmochim Acta 23: 43–52

Clemens JD, Vielzeuf D (1987) Constraints on melting and magma production in the crust. Earth Planet Sci Lett 86: 287–306

Cocherie A, Rossi Ph, Fouillac AM, Vidal Ph (1994) Crust and mantle contributions to granite genesis – an example from the Variscan batholith of Corsica, France, studied by trace element and Nd-Sr-O isotope systematics. Chem Geol 115: 173–211

Daniel C, Vidal P, Fernandez A, Le Fort P, Peucat JJ (1987) Isotopic study of the Manaslu granite (Himalaya, Nepal): inferences on the age and source of Himalayan leucogranites. Contrib Mineral Petrol 96: 78–92

DePaolo DJ, Wasserburg GJ (1976) Nd isotope variations and petrogenetic models. Geophys Res Lett 3: 249–252

DePaolo DJ, Perry FV, Baldridge SW (1992) Crustal versus mantle sources of granitic magmas: a two parameter model based on Nd isotopic studies. Trans Roy Soc Edinb, Earth Sci 83: 439–446

Dewey JF (1988) Extensional collapse of orogens. Tectonics 7: 1123–1139

Didier J (1973) Granites and Their Enclaves. Elsevier, Amsterdam, pp 1–393

Didier J, Barbarin B (eds) (1991) Enclaves and Granite Petrology. Elsevier, Amsterdam, pp 1–625

Downes H, Shaw A, Williamson BJ, Thirlwall MF (1997) Sr, Nd and Pb isotopic evidence for the lower crustal origin of Hercynian granodiorites and monzogranites, Massif Central, France. Chem Geol 136: 99–122

Faure G (1986) Principles of Isotope Geology. Wiley, New York, 2nd ed, pp 1–589

Finger F, Clemens JD (1995) Migmatization and "secondary" granitic magmas: effects of emplacement and crystallization of "primary" granitoids in Southern Bohemia, Austria. Contrib Mineral Petrol 120: 311–326

Finger F, Frasl G, Haunschmidt B, Lettner H, von Quadt A, Schermaier A, Schindlmayr AO, Steyrer HP (1993) The Zentralgneise of the Tauern Window (Eastern Alps): insight into an intra-Alpine Variscan batholith. In: Von Raumer JF, Neubauer F (eds) Pre-Mesozoic Geology of the Alps, Springer Verlag, Berlin, pp 375–391

Finger F, Roberts MP, Haunschmid B, Schermaier A, Steyrer HP (1997) Variscan granitoids of Central Europe: their typology, potential sources and tectonothermal relations. Mineral Petrol 61: 67–96

Finger F, Broska I, Haunschmid B, Hraško L, Kohút M, Krenn E, Petrík I, Riegler G, Uher P (2003) Electromicroprobe dating of monazites from Western Carpathian basement granitoids: plutonic evidence for an important Permian rifting event subsequent to Variscan crustal anatexis. Int J Earth Sci 92: 86–98

France-Lanord C, Le Fort P (1988) Crustal melting and granite genesis during the Himalayan collision orogenesis. Tran Roy Soc Edinb, Earth Sci 79: 183–195

Gerdes A (2001) Magma homogenization during anatexis, ascent and/or emplacement? Constraints from the Variscan Weinsberg granites. Terra Nova 13: 305–312

Goldstein SJ, Jacobsen SB (1988) Nd and Sr isotopic systematic of rivers water suspended material: implications for crustal evolution. Earth Planet Sci Lett 87: 249–265

Goldstein SJ, O'Nions RK, Hamilton PJ (1984) A Sm-Nd isotopic study of atmospheric dusts and particulates from major river systems. Earth Planet Sci Lett 70: 221–236

Harrison TM, Grove M, Lovera OM, Catlos EJ (1998) A model for the origin of Himalayan anatexis and inverted metamorphism. J Geophys Res 103: 27 017– 27 032

Hensel HD, McCulloch MT, Chappell BW (1985) The New England Batholith: constraints on its derivation from Nd and Sr isotopic studies of granitoids and country rocks. Geochim Cosmochim Acta 49: 369–384

Hollister LS (1993) The role of melt in the uplift and exhumation of orogenetic belts. Chem Geol 108: 31–48

Holland JG, Lambert RSJ (1975) The chemistry and origin of the Lewisian gneisses of Scottish mainland: the Scourie and Inver assemblages and sub-crustal accretion. Precambr Res 2: 161–188

Hovorka D, Petrík I (1992) Variscan granitic bodies of the Western Carpathians – the backbone of the mountain chain. In: Vozár J (ed) The Paleozoic Geodynamic Domains of the Western Carpathians, Eastern Alps and Dinarides. Spec. Vol. IGCP Project 276, Bratislava, pp 57–66

Huppert HE, Sparks RS (1988) The generation of granitic magmas by intrusion of basalt into continental crust. J Petrol 29: 599–624

Jacobsen SB, Wasserburg GJ (1980) Sm-Nd isotopic evolution of chondrites. Earth Planet Sci Lett 50: 139–155

James DE (1981) The combined use of oxygen and radiogenic isotopes as indicators of crustal contamination. Ann Rev Earth Planet Sci 9: 311–344

Janák M (1994) Variscan uplift of the crystalline basement, Tatra Mts., Central Western Carpathians: evidence from $^{40}Ar/^{39}Ar$ laser probe dating of biotite and P-T-t paths. Geol Carpath 45: 293–300

Janák M, Kohút M (1996) Cordierite-bearing migmatites from the Veľká Fatra Mts., Western Carpathians: geothermobarometry and implications for Variscan decompression. Geol Carpath 47: 359–365

Janák M, O'Brien PJ, Hurai V, Reutel C (1996) Metamorphic evolution and fluid composition of garnet-clinopyroxene amphibolites from the Tatra Mountains, Western Carpathians. Lithos 39: 57–79

Janák M, Hurai V, Ludhová L, O'Brien PJ, Horn EE (1999) Dehydration melting and devolatilization of high-grade metapelites: the Tatra Mountains, Western Carpathians. J Metamorph Geol 17: 379–395

Janoušek V, Rogers G, Bowes DR (1995) Sr-Nd isotopic constraints on the petrogenesis of the Central Bohemian Pluton, Czech Republic. Geol Rundsch 84: 520–534

Jenner GA, Longerich HP, Jackson SE, Fryer BJ (1990) ICP-MS – a powerful new tool for high precision trace element analysis in the earth sciences: evidence from analysis of selected USGS standards. Chem Geol 83: 133–148

Keay S, Collins WJ, McCulloch MT (1997) A three-component Sr-Nd isotopic mixing model for granitoid genesis, Lachlan Fold Belt, eastern Australia. Geology 25: 307–310

Kohút M (2002) The Hercynian granitic rocks of the Western Carpathians in the frame of European Hercynides. Geol Carpath 53 (Spec Issue): 219–221

Kohút M (2007) Orogenic granitic magmatism in the Western Carpathians – 500 Ma history: a review. Mineral Pol 31: 30–39

Kohút M, Janák M (1994) Granitoids of the Tatra Mts., Western Carpathians: field relations and petrogenetic implications. Geol Carpath 45: 301–311

Kohút M, Nabelek PI (1996) Sources of the Veľká Fatra granitoid rocks, Slovakia: isotopic constraints or contradiction? Polish Miner Soc Spec Pap 7: 47–50

Kohút M, Stein HJ (2005) Re-Os molybdenite dating of granite-related mineralisation from Hnilec, Gemeric Unit, Slovakia. Mineral Petrol 85: 117–129

Kohút M, Carl C, Michalko J (1996) Granitoid rocks of the Veľká Fatra Mts. – Rb/Sr isotope geochronology (Western Carpathians, Slovakia). Geol Carpath 47: 81–89

Kohút M, Todt W, Janák M, Poller U (1997) Thermochronometry of the Variscan basement exhumation in the Veľká Fatra Mts. (Western Carpathians – Slovakia). TERRA Abstracts, 9/1, EUG 9, Strasbourg, pp 494

Kohút M, Kovach VP, Kotov AB, Salnikova EB, Savatenkov VM (1999) Sr and Nd isotope geochemistry of Hercynian granitic rocks from the Western Carpathians – implications for granite genesis and crustal evolution. Geol Carpath 50: 477–487

Kohút M, Poller U, Gurk Ch, Todt W (2008) Geochemistry and U-Pb detrital zircon ages of metasedimentary rocks of the Lower Unit, Western Tatra Mountains (Slovakia). Acta Geol Pol 58: 371–384

Kohút M, Uher P, Putiš M, Sergeev S, Antonov A (in print) Dating of the Western Carpathians Lower Carboniferous granitic rocks by SHRIMP – new zircon U-Pb data. Miner Slov (in Slovak)

Kovach A, Svingor E, Grecula P (1986) Rb-Sr isotopic ages of granitoid rocks from the Spišsko-gemerské Rudohorie Mts. Miner Slov 18: 1–14

Kráľ J (1994) Strontium isotopes in granitic rocks of the Western Carpathians. Mitt Österr Geol Ges 86: 75–81

Krist E, Korikovsky SP, Putiš M, Janák M, Faryad SW (1992) Geology and petrology of metamorphic rocks of the Western Carpathian metamorphic complexes. Comenius University Press, Bratislava, pp 7–342

Le Breton N, Thompson AB (1988) Fluid-absent (dehydration) melting of biotite in metapelites in the early stage of crustal anatexis. Contrib Mineral Petrol 99: 226–237

Le Fort P (1981) Manaslu leucogranite: a collision signature of the Himalaya. A model for its genesis and emplacement. J Geophys. Res 86: 10 545–10 568

Liew TC, Hofmann AW (1988) Precambrian crustal components, plutonic associations, plate environment of the Hercynian fold belt of Central Europe: indications from a Nd and Sr isotopic study. Contrib Miner Petrol 98: 129–138

Liew TC, Finger F, Höck V (1989) The Moldanubian granitoid plutons of Austria: chemical and isotopic studies bearing on their environmental setting. Chem Geol 76: 41–55

Matte Ph (1986) Tectonics and plate tectonics model for the Variscan Belt of Europe. Tectonophysics 126: 329–374

Matte Ph (1991) Accretionary history and crustal evolution of the Variscan belt in Western Europe. Tectonophysics 196: 309–337

McCulloch MT, Chappell BW (1982) Nd isotopic characteristic of S- and I-type granites. Earth Planet Sci Lett 58: 51–64

Montel JM, Vielzeuf D (1997) Partial melting of metagreywackes, Part II. Compositions of minerals and melts. Contrib Mineral Petrol 128: 176–196

Moreno-Ventas I, Rogers G, Castro A (1995) The role of hybridization in the genesis of Hercynian granitoids in the Gredos Massif, Spain: inferences from Sr-Nd isotopes. Contrib Mineral Petrol 120: 137–149

Nabelek PI, Bartlett CD (1998) Petrologic and geochemical links between the post-collisional Proterozoic Harney Peak leucogranite, South Dakota, USA and its source rocks. Lithos 45: 71–85

Nabelek PI, Liu M (1999) Leucogranites in the Black Hills of South Dakota: the consequence of shear heating during continental collision. Geology 27: 523–526

Neymark LA, Kovach VP, Nemchin AA, Morozova IM, Kotov AB, Vinogradov DP, Gorochovsky BM, Ovchinikova GV, Bogomolova LM, Smelov AP (1993) Late Archaean intrusive complexes in the Olekma granite–greenstone terrain (Eastern Siberia): geochemical and isotopic study. Precambr Res 62: 453–472

O'Neil JR, Chappell BW (1977) Oxygen and hydrogen isotope relations in the Berridale Batholith. J Geol Soc, London 133: 559–571

Patiño Douce AE, Harris N (1998) Experimental constraints on Himalayan anatexis. J Petrol 39: 689–710

Patiño Douce AE, Humphreys ED, Johnston AD (1990) Anatexis and metamorphism in tectonically thickened continental crust exemplified by the Sevier hinterland, western North America. Earth Planet Sci Lett 97: 290–315

Petford N, Atherton M (1996) Na-rich partial melts from newly underplated basaltic crust: the Cordillera Blanca Batholith, Peru. J Petrol 37: 1491–1521

Petrík I (2000) Multiple sources of the Western Carpathian Variscan granitoids: a review of Rb/Sr and Sm/Nd data. Geol Carpath 51: 145–158

Petrík I, Broska I (1994) Petrology of two granite types from the Tríbeč Mountains, Western Carpathians: an example of allanite (+magnetite) versus monazite dichotomy. Geol J 29: 59–78

Petrík I, Kohút M (1997) The evolution of granitoid magmatism during the Hercynian orogen in the Western Carpathians. In: Grecula P, Hovorka D, Putiš M (eds) Geological Evolution of the Western Carpathians. Miner Slov Monograph, Bratislava, pp 235–252

Petrík I, Broska I, Uher P (1994) Evolution of the Western Carpathian granite magmatism: age, source rock, geotectonic setting and relation to the Variscan structure. Geol Carpath 45: 283–291

Pin C, Duthou JL (1990) Sources of Hercynian granitoids from the French Massif Central: inferences from Nd isotopes and consequences for crustal evolution. Chem Geol 83: 281–296

Pin C, Binon M, Belin JM, Barbarin B, Clemens JD (1991) Origin of microgranular enclaves in granitoids: equivocal Sr-Nd evidence from Hercynian rocks in the Massif Central (France). J Geophys Res 95 B11: 17 821–17 828

Plašienka D, Grecula P, Putiš M, Hovorka D, Kováč M (1997) Evolution and structure of the Western Carpathians: an overview. In: Grecula P, Hovorka D. Putiš M (eds) Geological Evolution of the Western Carpathians. Miner Slov Monograph, Bratislava, pp 1–24

Poller U, Janák M, Kohút M, Todt W (1998) Pre-Variscan evolution of the Western Tatra Mts (Slovakia): a Sm-Nd, Rb-Sr and Pb-Pb isotope study. The IXth ICOG meeting Beijing, Chinese Science Bull 43: 103

Poller U, Janák M, Kohút M, Todt W (2000) Early Variscan magmatism in the Western Carpathians: U-Pb zircon data from granitoids and orthogneisses of the Tatra Mountains (Slovakia). Int J Earth Sci 89: 336–349

Poller U, Todt W, Kohút M, Janák M (2001) Nd, Sr, Pb isotope study of the Western Carpathians: implications for Palaeozoic evolution. Schweitz Mineral Pertrogr Mitt 81: 159–174

Richards P, Shimizu N, Allègre CJ (1976) $^{143}Nd/^{144}Nd$, a natural tracer: an application to oceanic basalts. Earth Planet Sci Lett 31: 269–278

Royden LH (1993) The steady state thermal structure of eroding orogenic belts and accretionary prisms. J Geophys Res 98: 4487–4507

Sawyer EW (1991) Disequilibrium melting and the rate of melt-residuum separation during migmatitization of mafic rocks from the Grenville Front Quebec. J Petrol 32: 701–738

Sawyer EW (1996) Melt segregation and magma flow in migmatites: implications for the generations of granite magmas. Trans Roy Soc Edinb, Earth Sci 87: 85–94

Schaltegger U (1997) Magma pulses in the Central Variscan Belt: episodic melt generation and emplacement during lithospheric thinning. Terra Nova 9: 242–245

Shaw A, Downes H, Thirlwall MF (1993) The quartz diorites of Limousin: elemental and isotopic evidence of Devono–Carboniferous subduction in the Hercynian belt of the French Massif Central. Chem Geol 107: 1–18

Singh J, Johannes W (1996) Dehydration melting of tonalites. Part II. Composition of melts and solids. Contrib Mineral Petrol 125: 26–44

Skjerlie KP, Patiño Douce AE, Johnston AD (1993) Fluid-absent melting of a layered crustal protolith: implications for the generation of anatectic granites. Contrib Mineral Petrol 114: 356–378

Sokol A, Domečka K, Breiter K, Janoušek V (2000) The underground storage near Příbram - a source of new information about granitoids of the Central Bohemian Pluton. Věst Čes geol úst 75: 89–104

Stampfli GM, Borel GD (2002) A plate tectonic model for the Paleozoic and Mesozoic constrained by dynamic plate boundaries and restored synthetic oceanic isochrons. Earth Planet Sci. Lett 196: 17–33

Stille H (1924) Grundfragen der vergleichenden Tektonik. Borntraeger, Berlin, pp 1–443

Taylor HP Jr (1988) Oxygen, hydrogen, and strontium isotope constraints on the origin of granites. Trans Roy Soc Edinb, Earth Sci 79: 317–338

Turpin L, Cuney M, Friedrich M, Bouchez JL, Aubertin M (1990) Meta-igneous origin of Hercynian peraluminous granites in N.W. French Massif Central: implications for crustal history reconstructions. Contrib Mineral Petrol 104: 163–172

Vielzeuf D, Clemens JC, Pin Ch, Moinet E (1990) Granites, granulites and crustal differentiation. In: Vielzeuf D, Vidal Ph (eds) Granulites and Crustal Evolution. Kluwer, Dordrecht, pp 59–85

Villaseca C, Barbero L, Rogers G (1998) Crustal origin of Hercynian peraluminous granitic batholiths of Central Spain: petrological, geochemical and isotopic (Sr, Nd) constraints. Lithos 43: 55–79

von Raumer JF, Neubauer F (1993) Late Proterozoic and Paleozoic evolution of the Alpine basement – an overview. In: von Raumer JF, Neubauer F (eds) Pre-Mesozoic Geology of Alps. Springer Verlag, Berlin, pp 625–639

von Raumer JF, Stampfli GM, Borel GD, Bussy F (2002) Organization of pre-Variscan basement areas at the north-Gondwanan margin. Int J Earth Sci 91: 35–52

Wells PRA (1981) Accretion of continental crust: thermal and geochemical consequences. Philos Trans Roy Soc London A301: 347–357

Wendt I (1986) Radiometrische Methoden in der Geochronologie. Ellen Pigler Verlag, Clausthal Zellerfeld, pp 80–86

Williamson BJ, Shaw A, Downes H, Thirlwall MF (1996) Geochemical constraints on the genesis of Hercynian two-mica leucogranites from the Massif Central, France. Chem Geol 127: 25–42

Wolf MB, Wyllie PJ (1994) Dehydration-melting of amphibolite at 10 kbar: effects of temperature and time. Contrib Mineral Petrol 115: 369–383

Appendix: Sample description and location

Sample number		Rock type, location	Longitude (°E)	Latitude (°N)	Altitude (m)
1	VF- 43	muscovite-biotite granite, natural outcrop Vyšná Krivá	49°01′23″01	19°11′33″20	1 035.0
2	VF-153	biotite tonalite, natural outcrop Vyšné Matejkovo	48°59′48″10	19°13′35″46	1 130.0
3	VF-157	muscovite granite, natural outcrop Stupecké Valley	49°46′45″24	19°10′49″47	820.0
4	VF-283	muscovite-biotite granodiorite, natural outcrop, Matejkov Ridge	48°59′53″05	19°16′02″20	831.5
5	VF-298	muscovite-biotite granodiorite, natural outcrop, Vyšné Matejkovo	48°59′44″21	19°15′57″02	705.0
6	VF-356	biotite tonalite, quarry Vyšné Matejkovo	48°59′47″22	19°15′03″59	812.0
7	VF-417	muscovite-biotite granodiorite, natural outcrop Javorisko	49°02′34″56	19°10′27″18	905.0
8	VF-636	biotite granodiorite, natural outcrop Blatná Valley	49°00′29″39	19°09′05″16	685.0
9	VF-639	biotite granodiorite, natural outcrop Blatná Valley	49°00′17″11	19°09′29″40	742.0
10	VF-700	muscovite granite, natural outcrop Nižné Matejkovo	49°00′09″26	19°15′54″23	825.0
11	VK-139	biotite granodiorite, natural outcrop Malý Javorník	48°15′31″20	17°08′57″10	545.0
12	BGPI-1	biotite granodiorite, natural outcrop Hradná Valley	48°36′31″04	18°00′59″50	290.0
13	T-87	biotite granodiorite, natural outcrop Krnča	48°31′36″00	18°15′58″50	250.0
14	MM-29	muscovite-biotite granite, natural outcrop Poruba Valley	48°50′48″02	18°33′11″54	665.0
15	Z-164	biotite-muscovite granite, quarry Veľká Valley	48°49′27″03	18°46′27″30	590.0
16	MF-4a	muscovite-biotite granodiorite, quarry Bystrička	49°10′24″12	19°06′34″44	575.0
17	NT-401	biotite granodiorite, natural outcrop Liptovská Lúžna	48°57′41″50	19°20′19″13	960.0
18	ZK-4	muscovite granite, natural outcrop Vyšná Boca	48°55′28″56	19°44′28″57	1 045.0
19	TL-117	muscovite-biotite granodiorite, natural outcrop, Prostredný Ridge	49°11′24″19	20°01′31″23	1 920.0
20	VG-46	biotite granodiorite, quarry Klementka	48°40′12″41	19°37′30″52	870.0
21	VG-47	muscovite-biotite granodiorite, quarry Chorepa	48°35′43″17	19°51′31″50	555.0
22	V-7312	biotite-muscovite granite, natural outcrop České Brezovo	48°29′13″21	19°48′33″32	340.0
23	V-9738	muscovite-biotite granite, natural outcrop Solisko	48°42′31″53	20°09′48″11	660.0
24	VVM-129	biotite-muscovite granite, drill well Peklisko	48°48′40″58	20°33′39″49	596.9
25	CH-3/72	muscovite-biotite granodiorite, quarry near Ružín dam	48°51′48″42	21°05′28″30	360.0
26	KV-3/622	gabbro, Rochovce borehole	48°42′04″06	20°17′39″21	408.5

Journal of Geosciences, 53 (2008), 323–334 DOI: 10.3190/jgeosci.031

Original paper

Accessory columbite to tantalite, tapiolite and zircon: products of extreme fractionation in highly peraluminous pegmatitic granite from the Považský Inovec Mountains, Western Carpathians, Slovakia

Peter CHUDÍK[1,*], Pavel UHER[1], Milan KOHÚT[2], Peter BAČÍK[3]

[1] *Department of Mineral Deposits, Comenius University, Mlynská dolina, 842 15 Bratislava, Slovakia; chudik@fns.uniba.sk*
[2] *Dionýz Štúr State Geological Institute, Mlynská dolina 1, 817 04 Bratislava, Slovakia*
[3] *Department of Mineralogy and Petrology, Comenius University, Mlynská dolina, 842 15 Bratislava, Slovakia*
[*] *Corresponding author*

Accessory Fe-rich columbite-group minerals, tapiolite and Hf-rich zircon occur in Hercynian pegmatitic leucogranite near Duchonka, Považský Inovec Mts., western Slovakia. The host rock represents highly peraluminous and fractionated S-type pegmatitic leucogranite with ASI = 1.27, Eu_N/Eu^*_N = 0.16, Rb/Sr = 7.2, Ta/Nb = 1.1 and Zr/Hf = 21, but not enriched in Li, B, Be or P. Columbite–tantalite, tapiolite and hafnian zircon form discrete crystals, 30 to 350 μm in size, in association with quartz, plagioclase, K-feldspar, muscovite, sillimanite, almandine–spessartine and fluorapatite. Columbite–tantalite crystals show coarse oscillatory zoning, usually with border parts enriched in Ta. Locally, there is a reversal trend of zoning (decrease of Ta towards the border parts), or irregular convoluted zoning as a result of late-magmatic to subsolidus dissolution-reprecipitation. The composition of columbite–tantalite shows a relatively constant Mn/(Mn + Fe) ratio (0.20–0.27, locally 0.35–0.40), but extreme variations of the Ta/(Ta + Nb) ratio (0.18–0.72). Ratios higher than 0.63 plot inside the tantalite–tapiolite miscibility gap. Ferrotapiolite is mainly homogenous and shows relatively consistent compositions with Mn/(Mn + Fe) = 0.03–0.04 and Ta/(Ta + Nb) = 0.88–0.97. Metamict zircon (5 to 120 μm in size) exhibits tiny uraninite inclusions, high Hf contents (6 to 23 wt. % HfO_2, 0.06–0.23 Hf apfu), and locally elevated P, As and U contents, whereas Y and REE concentrations are low. Unusually widely variable and high Ta/Nb and Hf/Zr ratios in the accessory minerals are probably the product of extreme local Nb-Ta and Zr-Hf fractionation in highly peraluminous granite-pegmatite system.

Keywords: ferrocolumbite, ferrotantalite, ferrotapiolite, hafnian zircon, Hercynian pegmatitic leucogranite, Považský Inovec Mountains, Western Carpathians
Received: 1 October 2008; accepted 5 December 2008; handling editor: M. Novák

1. Introduction

Although uncommon, Nb-Ta oxide minerals and Hf-rich zircon belong to the most characteristic accessory phases in evolved granitic rocks. They can reveal important information about the degree of melt fractionation and are useful tools for interpreting the P-T-X conditions of formation of their host rocks. The Nb-Ta oxide minerals and hafnian zircon are usually found in highly evolved, specialized granites, commonly rich in volatile elements (F, B, P), and their greisenized cupolas, in association with cassiterite, wolframite, topaz, Li-silicates and other characteristic minerals (e.g., Johan and Johan 1994; Raimbault et al. 1995; Huang et al. 2002; Breiter et al. 2007). However, our knowledge of accessory Nb-Ta and Zr-Hf phases in non-specialized, "barren" granites without Li, Be, B or P enrichment and Sn ± W mineralization is still very scarce in comparison to the specialized granites or rare-element granitic pegmatites.

In this article we describe accessory Nb-Ta oxide minerals and Hf-rich zircon in such non-specialized S-type pegmatitic leucogranite near Duchonka, the Považský Inovec Mountains, Western Carpathians, Slovakia as an example of unusual Nb-Ta and Zr-Hf fractionation in highly peraluminous environment.

2. Geological setting

The Považský Inovec Mountain range represents the north-western part of the core mountain belt of the Inner (Central) Western Carpathians, a typical Miocene mega-anticlinal horst that originated before 18–13 Ma (Danišík et al. 2004). It is elongated in the NNE–SSW direction. Maheľ (1986) distinguished three particular blocks of the Považský Inovec: northern – the Selec block, situated north of the Hrádok line, middle – the Bojná block, which extends between the Hrádok and the Koplotovce tectonic

lines, and southern – the Hlohovec block, situated south of the Koplotovce line. The studied locality occurs in the eastern part of the Bojná block. Based on differences in the lithological and metamorphic setting, the crystalline basement in the Bojná block was divided into a Lower and an Upper structural level. The Lower structure of the crystalline basement consists of a relatively high-grade metamorphosed (T > 550 °C, P > 350 MPa) gneissic-amphibolitic complex with intrusions of two generations of granitic rocks (Ivanička et al. 2007). The protolith of the Lower metamorphic complex is Ordovician to Upper Silurian, and shows polymetamorphosed character. The upper structural level of the crystalline basement is formed by the younger, Devonian volcano-sedimentary Hlavinka Complex (Kohút et al. 2006), which is metamorphosed in lower grade (T ≤ 500 °C, P ≤ 300 MPa) and without intrusive contacts with the Hercynian granitic rocks.

The acid magmatic rocks of the Bojná block are represented by the older granitoids of S-type (Lower Ordovician age), which were sheared to orthogneisses during the Hercynian orogeny, as well as the younger unsheared Meso-Hercynian granitoids of S-type (Lower- to Middle-Carboniferous age), which consist of biotite and muscovite-biotite granodiorites to granites, "non-homogenized – immature" hybrid granitoids – diatexites, as well as muscovite and biotite-muscovite leucocratic granites (Kamenický 1956; Broska and Uher 1988; Kohút et al. 2004).

The pegmatitic leucogranite examined in this study belongs to the younger, Meso-Hercynian suite. It occurs in a granite body situated between Podhradie and Duchonka, at the ridge between Lipová and Soľnisko Hill, about 13 km NNW of the town Topoľčany (Fig. 1),

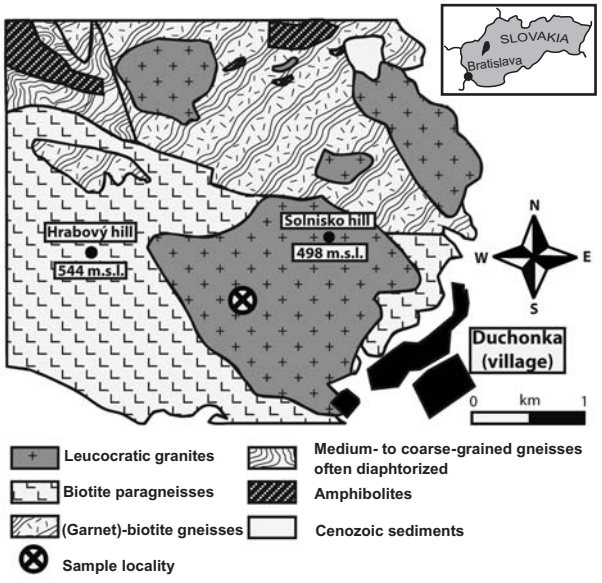

Fig. 1 Simplified geological map of the Duchonka region, Považský Inovec Mountains (modified from Ivanička et al. 2007).

western Slovakia. The main body of biotite-muscovite (leuco-) granite is commonly cut by apophyses and dikes of pegmatitic leucogranite to granite pegmatite, usually 1 to 5 m thick. The studied sample represents an example of such pegmatitic leucogranite apophysis/dike.

3. Analytical methods

Electron-microprobe analyses (EMPA) were carried out in the wavelength-dispersion mode using the Cameca SX-100 electron-microprobe at the State Geological Survey of Slovak Republic, Bratislava (Nb-Ta and silicate minerals) and an analogous instrument at the Institute of Geological Sciences, Masaryk University, Brno (zircon and apatite).

The following analytical conditions were used: accelerating voltage of 15 kV, a sample current of 20 nA, beam diameter of 1–3 μm and a counting time of 20 to 40 s. For the Nb-Ta minerals, the following standards were applied: metallic W (W *Lα*), $LiNbO_3$ (Nb *Lα*), $LiTaO_3$ (Ta *Lα*), TiO_2 (Ti *Kα*), SnO_2 (Sn *Lα*), $ZrSiO_4$ (Zr *Lβ*), ThO_2 (Th *Mα*), UO_2 (U *Mβ*), $ScPO_4$ (Sc *Kα*), YPO_4 (Y *Lα*), Sb (Sb *Lα*), fayalite (Fe *Kα*), rhodonite (Mn *Kα*), MgO (Mg *Kα*), wollastonite (Ca *Kα*), ZnS (Zn *Kα*), and PbS (Pb *Mα*). For zircon, metallic W (W *Lα*), apatite (P *Kα*, Ca *Kα*), InAs (As *Lα*), ferrocolumbite (Nb *Lα*), titanite (Si *Kα*, Ti *Kα*), zircon (Zr *Lα*), metallic Hf (Hf *Mα*), cheralite (Th *Mα*), metallic U (U *Mβ*), sanidine (Al *Kα*), $ScVO_4$ (Sc *Kα*), YAG (Y *Lα*), $CeAl_2$ (Ce *Lα*), Dy and Er glass (Dy *Lα*, Er *Lα*), YbP_5O_{14} (Yb *Lα*), andradite (Fe *Kα*), rhodonite (Mn *Kα*), topaz (F *Kα*), and vanadinite (Cl *Kα*) standards were used. All data were reduced using the PAP routine (Pouchou and Pichoir 1985).

The rock was analyzed in the ACME Analytical Laboratories Ltd., Vancouver. Total abundances of the major oxides and several minor elements were analysed by ICP-emission spectrometry following a lithium metaborate/tetraborate fusion and dilute nitric digestion. Loss on ignition (LOI) is by weigh difference after ignition at 1000 °C. Rare earth and refractory elements were determined by ICP mass spectrometry following a lithium metaborate/tetraborate fusion and nitric acid digestion of a 0.1 g sample. In addition a separate 0.5 g split was digested in aqua regia and analysed by ICP mass spectrometry. For other details see *www.acmelab.com*.

4. Results

4.1. Mineral and chemical composition of the host pegmatitic leucogranite

The pegmatitic leucogranite studied (sample PI-457b) is an equigranular, coarse-grained rock with the granitic

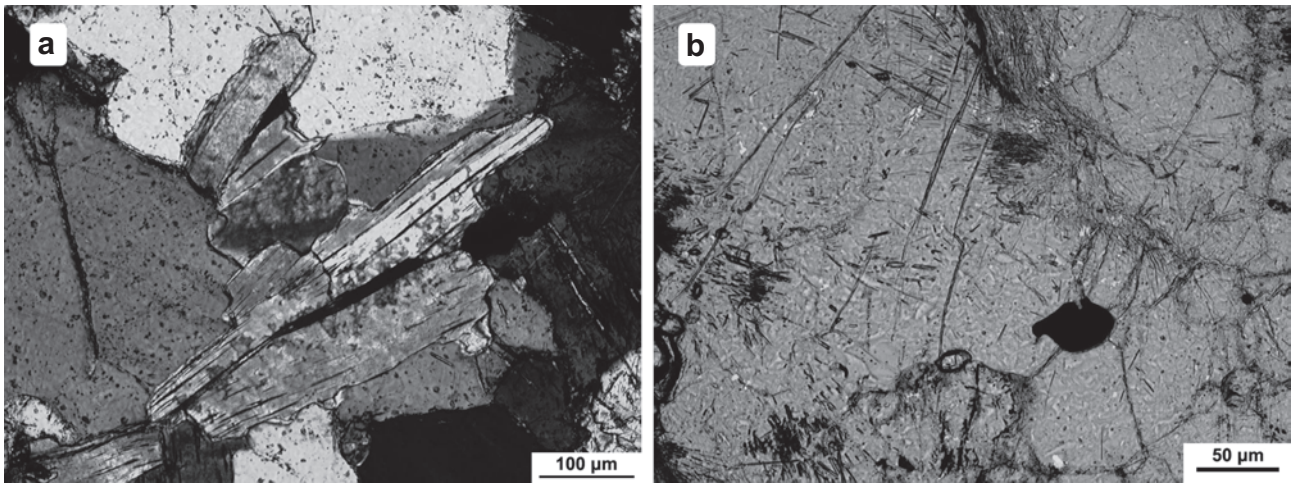

Fig. 2 Optical photomicrographs (transmitted light) of the Duchonka pegmatitic leucogranite (sample PI-457b) with Nb-Ta oxide minerals: **a** – Prismatic acicular crystal of columbite–tantalite (black inclusion in centre) in muscovite associated with quartz (left part) and plagioclase (right part). Crossed nicols. The length of columbite–tantalite is ~0.1 mm. **b** – Tapiolite inclusion (black) in quartz with fibrolitic sillimanite aggregate (upper and left part). Parallel nicols. The size of tapiolite is ~0.07 mm.

lepido-granoblastic texture. Its main mineral constituents are anhedral quartz, plagioclase ($An_{04–28}$), rare K-feldspar and muscovite (Fig. 2a). The muscovite shows usual composition with low Rb and F contents (*c.* 0.1 wt. % Rb_2O and 0.1–0.2 wt. % F, respectively). Common aggregates of fibrolitic sillimanite are intergrown with muscovite and quartz (Fig. 2b). Garnet forms euhedral to subhedral crystals (up to 3 mm in size), in association with quartz, alkali feldspar, muscovite and apatite. It shows almandine–spessartine composition with a small admixture of the pyrope and grossular end-members ($Alm_{52–61}Sps_{31–44}Prp_{03–06}Grs_{00–03}$), locally a slight Mn/Fe enrichment in rim parts and up to 0.6 wt. % P_2O_5 (0.04 P apfu). Apatite occurs as anhedral inclusions in the garnet (100–150 µm in size) or widespread discrete prismatic crystals (up to 400 µm across) in association with quartz, plagioclase, muscovite, garnet and zircon. It shows relatively homogeneous fluorapatite composition with 0.78–0.94 F apfu, up to 0.6 wt. % MnO (≤ 0.04 Mn apfu) and up to 0.3 wt. % FeO (≤ 0.02 Fe apfu). An accessory Ti-phase in muscovite (probably rutile), a Fe-phase (probably magnetite), a Fe-S mineral (probably pyrite), thorianite and barite were identified by EMPA occasionally, besides zircon and Nb-Ta oxide minerals.

The studied rock is geochemically characterized as relatively strongly peraluminous and highly fractionated pegmatitic leucogranite with S-type characteristics. High Si, Al, Na, moderate K and P, and low Ti, Fe, Mg and Ca contents are typical features of the rock (Tab. 1). The aluminium saturation index (ASI, or molar Al/(Ca + Na + K)) of the rock attains a value of 1.27 and indicates its relatively strong peraluminous character (Fig. 3). Concentrations of index trace elements show elevated Ta and Nb,

Tab. 1 Chemical composition of the Duchonka pegmatitic granite (sample PI-457b)

	wt. %		ppm
SiO_2	74.05	Li	35
TiO_2	0.17	Rb	173
Al_2O_3	15.16	Cs	6.0
Fe_2O_3	0.53	Sr	24
FeO	0.28	Ba	45
MnO	0.04	Be	2.5
MgO	0.09	B	8.0
CaO	0.34	Ga	18
Na_2O	4.76	Sn	3.0
K_2O	3.23	Zr	21
P_2O_5	0.16	Hf	1.0
LOI	0.71	Nb	18.5
H_2O^-	0.19	Ta	21.0
Total	99.71	Mo	0.8

	ppm		ppm
As	0.75	Ce	4.55
Cr	5.0	Pr	0.55
V	5.5	Nd	2.20
Ni	0.5	Sm	0.65
Co	6.0	Eu	0.04
Zn	16	Gd	0.90
Cu	4.0	Tb	0.15
Pb	11	Dy	0.95
Th	3.0	Ho	0.20
U	3.0	Er	0.45
Sc	1.0	Tm	0.07
Y	5.75	Yb	0.05
La	2.15	Lu	0.06

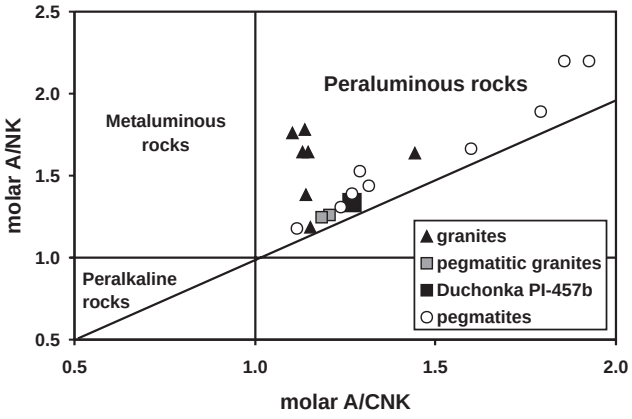

Fig. 3 The A/NK vs. A/CNK diagram for the Duchonka pegmatitic leucogranite (sample PI-457b) in comparison to the adjacent granites, pegmatitic granites and granitic pegmatites of the Bojná and Soľnisko massifs, Považský Inovec Mountains (unpublished analyses of the authors). A/NK = Al/(Na + K), A/CNK = Al/(Ca + Na + K) (millications).

moderate Li, Rb, Cs, Be, Ga, Sn and U, as well as low Sr, Ba, B, REE, Zr, Hf and Th contents (Tab. 1). Moreover, high Rb/Sr = 7.2, and especially unusually high values of Ta/Nb = 1.1 and low Zr/Hf = 21, together with distinctly negative Eu-anomaly (Eu_N/Eu^*_N = 0.16) provide an evidence for a relatively high degree of magmatic fractionation of the investigated pegmatitic leucogranite compared to other granitic rocks in the Považský Inovec Mountains (Fig. 4).

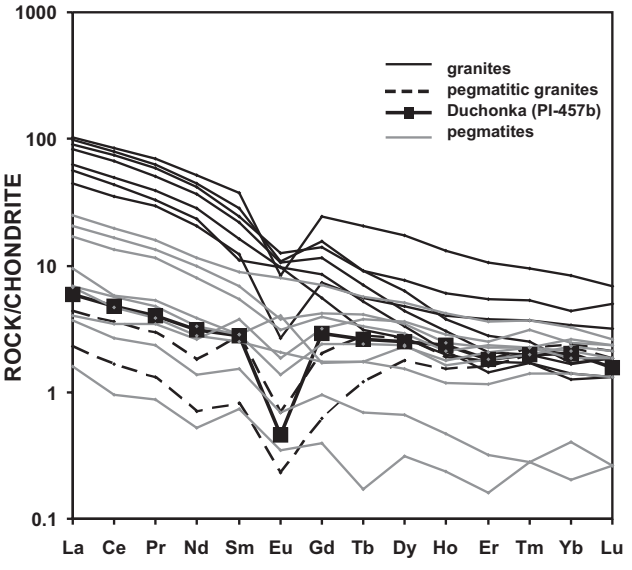

Fig. 4 The chondrite-normalized REE diagram for the Duchonka pegmatitic leucogranite (sample PI-457b). For comparison are plotted adjacent granites, pegmatitic granites and granitic pegmatites of the Bojná and Soľnisko massifs, Považský Inovec Mountains (unpublished analyses of the authors). Chondrite values after Taylor and McLennan (1985).

4.2. Niobium–tantalum oxide minerals

Columbite-group minerals form discrete tabular crystals 30–350 μm in size, in association with quartz, alkali-feldspar, muscovite and sillimanite (Figs 2a, 5a–b). The grains commonly show prograde zoning with central parts enriched in Nb (ferrocolumbite) and rims enriched in Ta (ferrotantalite). However, an irregular convoluted zoning of border parts, as a result of late-magmatic to subsolidus dissolution-reprecipitation processes is also present (Figs 5c–d), or a reversed trend of zoning with decrease of Ta towards the border parts of the crystals was detected (Fig. 5e). The composition of columbite–tantalite shows a relatively constant Mn/(Mn + Fe) = 0.20–0.27 (locally 0.35–0.40), but an extreme range of Nb-Ta fractionation (Ta/(Ta + Nb) = 0.18–0.72). Moreover, some analyses in the rim of the tantalite crystals show a Ta/(Ta + Nb) ratio above 0.63 and plot in the field of the miscibility gap between tantalite and tapiolite (Tab. 2, Figs 5f, 6). Contents of Ti, W, Sn, Mg and other elements in studied columbite to tantalite are low. Titanium attains mostly about 0.5 wt. % TiO_2 and a slight decrease of Ti with increasing values of Ta/(Ta + Nb) was recorded. Locally slightly elevated Zr and Pb contents were noted (≤ 0.6 wt. % ZrO_2 and ≤ 1.2 wt. % PbO) but they represent only up to 0.02 apfu and do not influence significantly crystal chemistry of the columbite–tantalite.

Ferrotapiolite forms discrete irregular or shortly prismatic crystals, *c.* 15–75 μm in size, in association with quartz and sillimanite (Figs 2b, 7a). The ferrotapiolite displays slightly irregular compositional zoning in a BSE image with Mn/(Mn + Fe) = 0.03–0.04 and Ta/(Ta + Nb) = 0.88–0.97 (Figs 7b–c, Tab. 2). The Ti and Sn contents are slightly higher than in the co-existing columbite-group minerals (SnO_2 ≤ 0.8 wt. % and TiO_2 ≤ 1.3 wt. %).

In view of the low contents of W, Ti, Sn, Zr, Mg, Pb and other elements, we conclude that only the single $TaNb_{-1}$ and $MnFe_{-1}$ substitutions, separately or in combination, are relevant to compositional changes for both the columbite–tantalite and the tapiolite.

4.3. Hafnian zircon

Accessory zircon forms euhedral to subhedral, columnar prismatic crystals, 5 to 120 μm long, included in quartz or muscovite (Fig. 7a). In BSE, zircon usually displays a slightly diffuse zoning with a darker center and a brighter rim zone (Fig. 7d), probably mainly due to variations in Hf and U concentrations and/or different metamictization degree. The central parts commonly contain numerous oval inclusions of uraninite, *c.* 0.7 to 2 μm across (Fig. 7d). Zircon shows distinct Hf enrichment, HfO_2 concentrations vary between 6 and 23 wt. %, 0.06–0.23 Hf

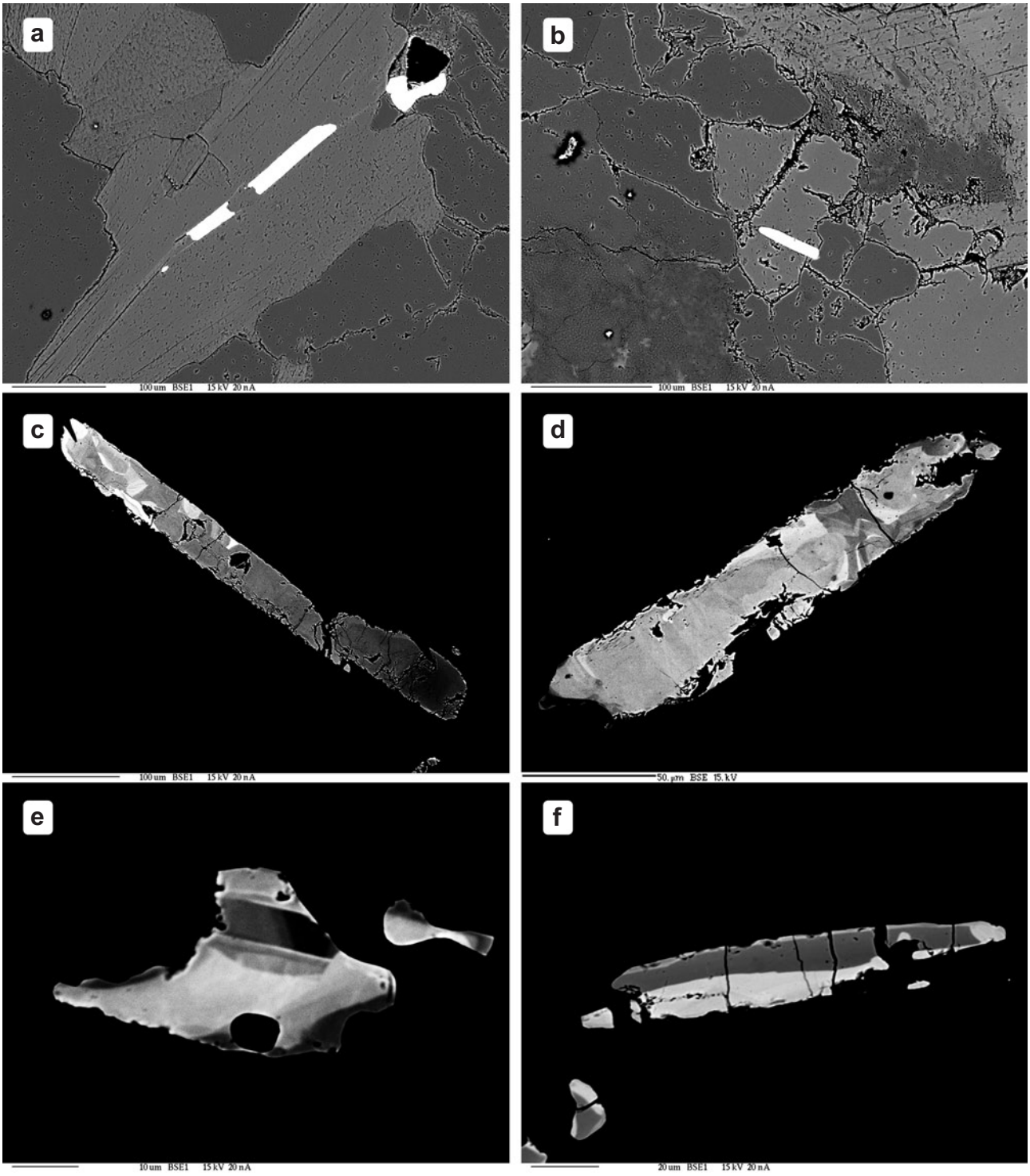

Fig. 5 Back-scattered electron (BSE) images of columbite–tantalite from the Duchonka pegmatitic leucogranite. **a** – columbite–tantalite crystals (white) in muscovite (light grey) in association with quartz (dark grey). **b** – columbite–tantalite crystal (white) in plagioclase (light grey) in association with quartz (dark grey) and muscovite (medium grey, right part). **c** and **d** – columnar columbite–tantalite crystals with irregular zoning caused by late-magmatic to subsolidus partial dissolution-reprecipitation processes. **e** – combination of concentric progressive zoning (dark Nb-rich core and light Ta-rich intermediate zone) with late reverse zoning (Nb-rich rim zone) of columbite–tantalite crystal. **f** – columnar crystal with a core of ferrocolumbite (grey) surrounded by younger (white) rim of ferrotantalite composition falling into the tantalite–tapiolite miscibility gap (see text).

Tab. 2 Representave compositions of ferrocolumbite (Fe-Col), ferrotantalite (Fe-Tan), ferrotantalite in the miscibility gap field (Fe-Tan X) and ferrotapiolite (Fe-Tap) from the Duchonka pegmatitic leucogranite (in wt. %)

	Fe-Col	Fe-Tan	Fe-Tan	Fe-Tan X	Fe-Tan X	Fe-Tan X	Fe-Tap	Fe-Tap
WO_3	0.25	0.10	0.00	0.15	0.05	0.00	0.12	0.17
Nb_2O_5	41.66	25.36	20.83	21.79	17.94	15.88	6.14	1.58
Ta_2O_5	39.81	58.90	63.45	62.44	66.56	68.18	78.91	83.22
TiO_2	0.07	0.09	0.04	0.46	0.16	0.44	1.28	0.83
SnO_2	0.07	0.00	0.18	0.17	0.00	0.13	0.46	0.45
ZrO_2	0.25	0.06	0.24	0.24	0.05	0.24	0.21	0.12
Sc_2O_3	0.00	0.03	0.00	0.00	0.01	0.00	0.00	0.00
Y_2O_3	0.00	0.00	0.04	0.02	0.04	0.00	0.00	0.00
Sb_2O_3	0.06	0.10	0.00	0.03	0.00	0.04	0.10	0.05
Fe_2O_3 calc.	0.00	0.00	0.00	0.00	0.00	0.00	0.00	0.00
FeO	11.73	10.57	9.22	10.65	9.89	10.14	12.31	11.90
MnO	4.22	3.81	5.22	3.05	3.66	2.90	0.48	0.41
MgO	0.16	0.19	0.02	0.28	0.23	0.26	0.00	0.00
CaO	0.02	0.02	0.02	0.01	0.04	0.00	0.01	0.00
PbO	0.58	0.21	0.23	0.43	0.36	0.27	0.00	0.02
Total	98.31	99.22	99.26	99.31	98.63	98.21	100.07	98.73
Formulae based on 6 oxygen atoms and valence calculation								
W	0.004	0.002	0.000	0.003	0.001	0.000	0.002	0.004
Nb	1.275	0.844	0.712	0.735	0.626	0.561	0.225	0.061
Ta	0.733	1.179	1.304	1.268	1.397	1.450	1.740	1.925
Ti	0.004	0.005	0.002	0.026	0.009	0.026	0.078	0.053
Sn	0.002	0.000	0.005	0.005	0.000	0.004	0.015	0.015
Sum *B*	2.019	2.030	2.023	2.037	2.033	2.041	2.061	2.058
Zr	0.008	0.002	0.009	0.009	0.002	0.009	0.008	0.005
Sc	0.000	0.002	0.000	0.000	0.001	0.000	0.000	0.000
Y	0.000	0.000	0.002	0.001	0.002	0.000	0.000	0.000
Sb	0.002	0.003	0.000	0.001	0.000	0.001	0.003	0.002
Fe^{3+}	0.000	0.000	0.000	0.000	0.000	0.000	0.000	0.000
Fe^{2+}	0.664	0.651	0.583	0.665	0.638	0.663	0.835	0.846
Mn	0.242	0.237	0.334	0.193	0.239	0.192	0.033	0.029
Mg	0.016	0.021	0.002	0.031	0.026	0.031	0.000	0.000
Ca	0.002	0.002	0.002	0.001	0.004	0.000	0.001	0.000
Pb	0.011	0.004	0.005	0.009	0.007	0.006	0.000	0.000
Sum *A*	0.944	0.922	0.936	0.909	0.919	0.902	0.880	0.882
Sum *A*+*B*	2.963	2.952	2.959	2.946	2.952	2.943	2.942	2.940
Mn/(Mn+Fe)	0.267	0.267	0.364	0.225	0.272	0.225	0.038	0.033
Ta/(Ta+Nb)	0.365	0.583	0.647	0.633	0.691	0.721	0.885	0.969

Contents of Th, U and Zn are below the detection limit.

⇨

Fig. 7 BSE photomicrographs of ferrotapiolite and hafnian zircon from the Duchonka pegmatitic leucogranite. **a** – ferrotapiolite (larger white) and zircon (smaller white) inclusions in quartz (dark grey) in association with plagioclase (medium grey) and muscovite (light grey). **b** and **c** – irregularly zoned ferrotapiolite crystals. The zoning reflects slight Ta–Nb compositional variations. **d** – columnar metamict, slightly zoned hafnian zircon with numerous uraninite inclusions (white).

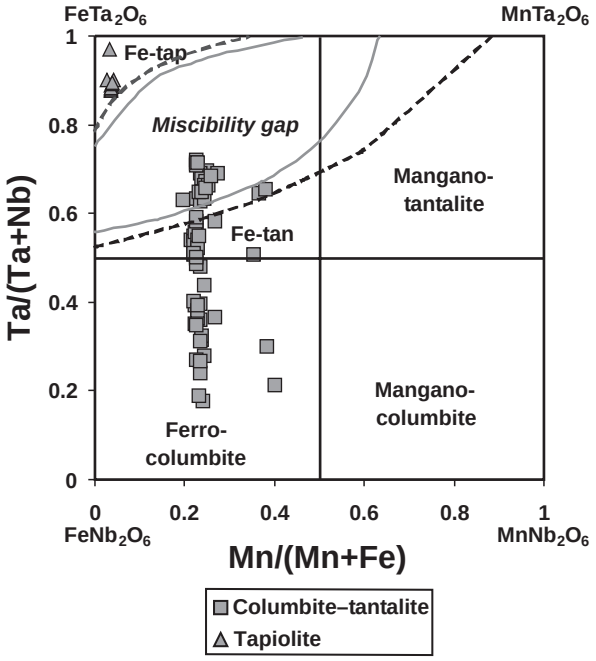

apfu (Tab. 3). Therefore, $HfZr_{-1}$ is the principal substitution in the hafnian zircon (Fig. 8). However, increased contents of P ($P_2O_5 \leq 0.9$ wt. %), As ($As_2O_5 \leq 0.7$ wt. %) and U ($UO_2 \leq 1.4$ wt. %), together with slightly elevated amounts of Fe and Ca were detected locally (Tab. 3). On the other hand, concentrations of Y, REE and Al are usually negligible to low. The apparent discrepancy between the presence of pentavalent cations (P and As) and paucity of trivalent cations (such as Y, REE, Al and Sc) could be explained by partial leaching of some elements during metamictization and structural degradation of the zircon and/or analytical errors of EMPA at low elemental concentrations.

⇦

Fig. 6 Quadrilateral diagram of columbite–tantalite and tapiolite from the Duchonka pegmatitic leucogranite. The boundaries of the tantalite–tapiolite miscibility gap are taken for single-phase, non-paired compositions of tantalite and tapiolite (grey solid line, after Černý and Ercit 1989) and coexisting tantalite–tapiolite pairs (black dashed line, after Černý et al. 1992a). Abbreviations: Fe-tan – ferrotantalite, Fe-tap – ferrotapiolite.

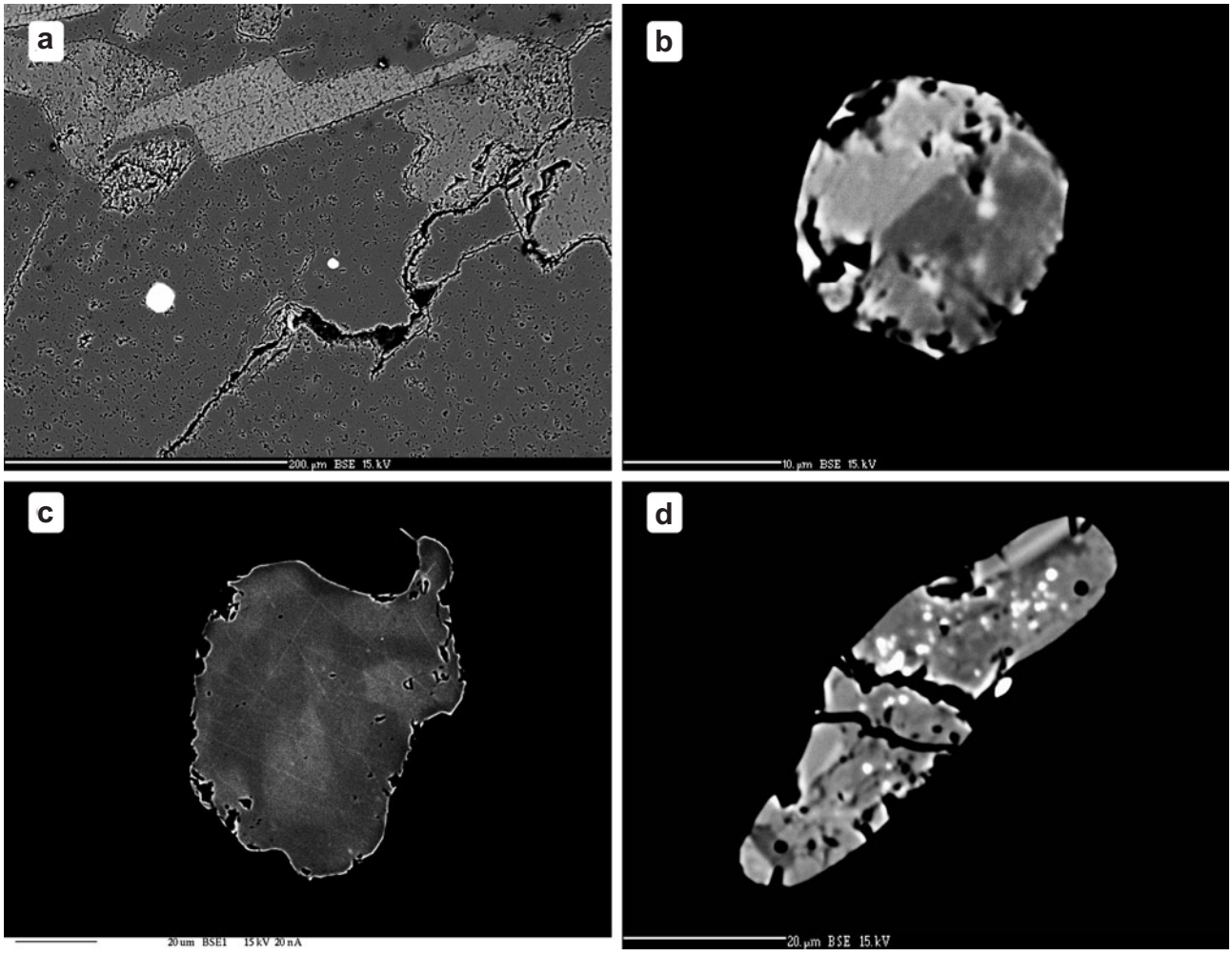

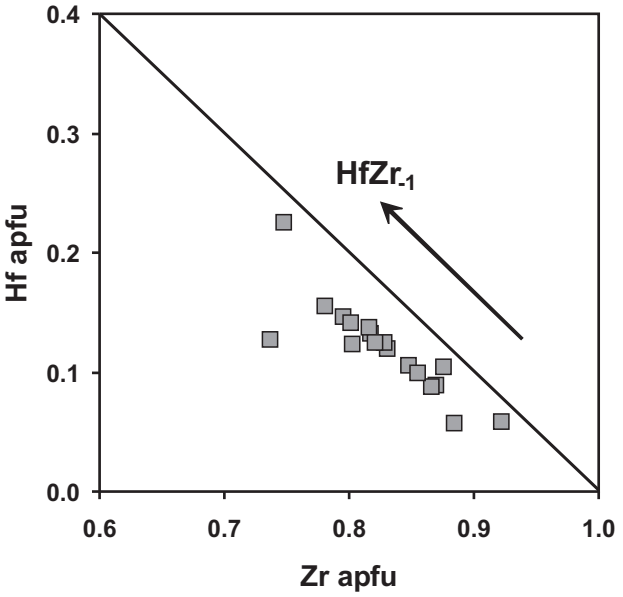

Fig. 8 The Hf vs. Zr substitution diagram for hafnian zircon from the Duchonka pegmatitic leucogranite (atomic proportions).

5. Discussion and conclusion

5.1. Regional importance of Nb-Ta and Zr-Hf mineralization

The disseminated Nb-Ta and Zr-Hf mineralization, which occurs in the fractionated, peraluminous sillimanite-bearing pegmatitic leucogranite apophysis/dike at Duchonka, represents a new genetic type of mineralization in the Považský Inovec Mountains, as well as in the whole West Carpathian area. The occurrence of fibrolitic sillimanite intergrown with primary muscovite and garnet of the almandine–spessartine composition documents the strongly peraluminous character of the host pegmatitic leucogranite (ASI = 1.27; Tab. 1, Figs 2b, 3). Similar occurrences of fibrolitic sillimanite were documented in different granodioritic to leucogranitic rocks in the Považský Inovec Mountains (Broska and Uher 1988). Apparently, the Nb-Ta oxides and other accessory minerals did not suffer any strong post-Hercynian metamorphic overprint and, consequently, they represent primary magmatic to early

Tab. 3 Representative compositions of zircon from the Duchonka pegmatitic leucogranite (in wt. %)

	Crystal 1	Crystal 2	Crystal 3	Formulae based on 4 oxygen atoms			
P_2O_5	0.94	0.01	0.25	P	0.026	0.000	0.007
As_2O_5	0.19	0.35	0.73	As	0.003	0.006	0.013
SiO_2	30.65	31.49	28.61	Si	0.982	1.006	0.982
ZrO_2	56.60	56.26	44.67	Sum *B*	1.011	1.012	1.002
HfO_2	6.19	11.51	23.00				
UO_2	1.26	0.13	1.41	Zr	0.884	0.876	0.748
Al_2O_3	0.18	0.02	0.06	Hf	0.057	0.105	0.225
Y_2O_3	0.92	0.00	0.00	U	0.009	0.001	0.011
Ce_2O_3	0.06	0.05	0.00	Al	0.007	0.001	0.002
Dy_2O_3	0.30	0.04	0.14	Y	0.016	0.000	0.000
Er_2O_3	0.04	0.13	0.24	Ce	0.001	0.001	0.000
FeO	0.39	0.04	0.04	Dy	0.003	0.000	0.002
MnO	0.14	0.00	0.08	Er	0.000	0.001	0.003
CaO	0.23	0.02	0.01	Fe	0.010	0.001	0.001
F	0.00	0.00	0.00	Mn	0.004	0.000	0.002
Cl	0.04	0.00	0.11	Ca	0.008	0.001	0.000
O=F	0.00	0.00	0.00	Sum *A*	0.999	0.987	0.994
O=Cl	-0.01	0.00	-0.02				
Total	98.12	100.05	99.33	Sum *A*+*B*	2.010	2.000	1.997
ZrO_2/HfO_2	9.14	4.89	1.94	Cl	0.002	0.000	0.006
Zr/Hf weight	8.48	4.53	1.80	O	3.998	4.000	3.994
100Hf/(Hf + Zr) at.	6.06	10.70	23.12				

Contents of W, Ti, Th, Sc, Yb, Bi and F are below the detection limit.

post-magmatic textural and compositional features rather than relicts of any progressive metamorphic overprint. On the contrary, effects of a prograde, sillimanite-grade metamorphism on an older granitic pegmatite are known for example from Maršíkov, Czech Republic (Černý et al. 1992b), where took place extensive compositional and structural re-equilibration of the Nb-Ta oxide minerals and breakdown of beryl to chrysoberyl.

In the Považský Inovec Mountains, rare-element mineralization containing Nb-Ta oxide minerals (columbite to tantalite, tapiolite, pyrochlore to microlite and fersmite), in association with beryl, almandine–spessartine, gahnite, and hafnian zircon was described only in a large granite pegmatite dike at Moravany nad Váhom, in the Strieborníca Ridge (Uher 1991; Uher et al. 1994; Novák et al. 2000). Accessory Nb, Ta-rich rutile with exsolved titanian ixiolite occurs in the (biotite-) muscovite leucogranite at Malá Kurňa Hill near Kovarce, in the adjacent Tribeč Mountains (Uher and Broska 1992). However, this mineralization is Ti, Nb-rich and Ta-poor, and represents a different geochemical type in comparison to the Ta-rich and Ti-poor assemblage at Duchonka. Moreover, occurrences of disseminated Nb, Ta-mineralization (W-rich columbite, W-rich ixiolite, qitianlingite?, Nb-rich ferberite, Nb, Ta-rich rutile and pyrochlore to microlite, in association with cassiterite) are known from Permian highly evolved, specialized S-type topaz-albite granites and adjacent greisenized and albitized rocks at Dlhá Valley near Gemerská Poloma, Hnilec, Betliar and Poproč in the Gemeric Superunit, Central Western Carpathians (e.g. Malachovský et al. 2000). However, this mineralization is connected with specialized ore-bearing granites distinctly enriched in Li, B, F, and with Nb, Ti, W, Sn > Ta feature of the Nb-Ta oxide minerals, as opposed to the Duchonka Ta > Nb >> Ti, Sn, W pattern.

5.2. The tantalite–tapiolite association

The Duchonka pegmatitic leucogranite revealed the presence of accessory columbite to tantalite, tapiolite and hafnian zircon with unusually wide and up to extremely high Ta/Nb and Hf/Zr fractionation level. Chemical composition of the host leucogranite indicates its distinctive peraluminous character (ASI = 1.27) and relatively high fractionation degree (Tab. 1). Nevertheless, tantalite and especially tapiolite are restricted to the strongly evolved, rare-element granitic pegmatites of the LCT-family (according to the classification of Černý and Ercit 2005), where extreme magmatic fractionation enables the production of volatile- and alkali-rich residual melts, essentially enriched in Ta, Hf, Li, Rb, B and other rare lithophile elements (e.g., Černý et al. 1985; London 1990, 2005). The tantalite plus tapiolite assemblage is typical of all types of rare-element granitic pegmatites of the LCT-family; the association of ferrotapiolite with Fe-rich columbite–tantalite is mostly characteristic of more primitive beryl type populations (e.g., Černý et al. 1986; Černý 1989; Novák et al. 2000). The tapiolite + Mn-rich columbite–tantalite pairs occur in the most fractionated beryl and especially complex Li, Cs, Ta, F-rich granitic pegmatites worldwide (e.g., Černý et al. 1986, 1992a; Černý 1989; Novák et al. 2000, 2003; van Lichtervelde et al. 2007).

On the other hand, Fe-rich tantalite and ferrotapiolite are scarce in highly evolved, specialized leucogranites, connected with Sn ± W ± Nb-Ta ± Li mineralization, where W-(Ti)-rich columbite and ixiolite, Nb, Ta-rich rutile, Nb, Ta-bearing cassiterite, Nb-rich ferberite–hübnerite and locally pyrochlore-group minerals occur (e.g., Johan and Johan 1994; Raimbault et al. 1995; Uher 1998; Breiter et al. 2007). Rare exceptions are found in Ta-rich, specialized rare-element granites in China, where tantalite (Yichun, Suzhou granite) and also tapiolite (Suzhou granite) were reported (Wang et al. 1997; Huang et al. 2002). Accessory tapiolite is present also in the Sn-bearing granite at Rudolfstein, Fichtelgebirge Mountains, Germany (Bernard and Hyršl 2004). In contrast to the above-mentioned tantalite and tapiolite occurrences, the Duchonka pegmatitic leucogranite represents a relatively highly fractionated but still common, non-specialized rock without apparent enrichment in Li, Rb, Cs, B, P, Sn or other elements, typical of rare-element pegmatites and ore-bearing granites.

The Fe-rich tantalite compositions with Ta/(Ta + Nb) = 0.63–0.72 and Mn/(Mn + Fe) = 0.20–0.27, which enter the empirically defined natural miscibility gap between tantalite and tapiolite (Černý et al. 1992a), is a particularly striking feature of the Duchonka leucogranite. Despite lack of a XRD determination, the phase very likely belongs to ferrotantalite, and not ferrotapiolite. These anomalous compositions are connected with external parts of the columbite to tantalite crystals (Fig. 5f) and these phases represent a part of the same columbite to tantalite evolutionary trend with a rapid increase of Ta/Nb and a stable Mn/Fe ratio (Fig. 6). On the contrary, ferrotapiolite occurs as separate grains with different textural pattern and chemistry (Figs 6–7). Such tantalite or tapiolite compositions are exceptional and are considered as metastable in pegmatitic environments (Černý et al. 1992a). However, some "hyper-ferrotantalite" compositions with Ta/(Ta + Nb) between 0.62 and 0.97 were described from some rare-element granitic pegmatites in Africa (von Knorring and Fadipe 1981; Baldwin 1989) and the Separation Rapids pegmatite group, Ontario, Canada (Tindle and Breaks 1998). Moreover, W, Ti, Fe-rich tantalites from the Suzhou and Yichun specialized granites, China, show Ta/(Ta + Nb) ratios from 0.50 to 0.73 and from 0.14 to 0.95, respectively (Wang et

al. 1997; Huang et al. 2002). All the presented Fe-rich tantalite compositions lie within the field of the tantalite–tapiolite miscibility gap, or even in the tapiolite compositional field (such as ferrotantalite from the Rubicon Mine, Namibia; Baldwin 1989). However, such data are commonly based solely on EMPA without precise XRD identification, and must be taken with a large caution. On the other hand, an empirically determined field of the tantalite–tapiolite miscibility gap (*sensu* Černý et al. 1992a) is based only on known data from granitic pegmatites, and it can be entered by some natural (stable or metastable) compositions as a consequence of specific P-T-X conditions. Based on experimental works, boundaries of the tantalite–tapiolite miscibility gap are controlled by temperature, oxygen fugacity, and phase structural state. The temperature is probably the key factor but the experimental data show inconsistent results (see discussion in Černý et al. 1992a). However, it is reasonable to suggest that the Duchonka pegmatitic leucogranite crystallized at higher temperature compared to classical granitic pegmatites. The tantalite–tapiolite miscibility gap shrinks at such conditions, like in other natural systems of solid solutions or related phases (e.g. Fe-Ti oxide minerals, pyroxenes, feldspars). Moreover, variations of Ta/Nb ratios in Nb-Ta oxide minerals strongly depend on pH of the host pegmatitic melt. The decrease in pH (increase in acidity) causes an increase in the Ta/Nb ratio of the solution and precipitation of Nb-Ta phases (Alexandrov et al. 1985). Similarly, Ta/Nb ratio and the span of the tantalite–tapiolite miscibility gap are possibly controlled also by the ASI (molar Al/(Ca + Na + K) ratio) of the host granite or pegmatite melt. Experimental data show a higher solubility of manganotantalite relative to that of manganocolumbite in silicate melts as well as decrease in columbite and tantalite solubility with Al/(Na + K) ratio. This explains the Ta/Nb enrichment during fractionation and lower saturation level of columbite–tantalite in a peraluminous melt compared to a peralkaline one (Linnen and Keppler 1997; Linnen and Cuney 2005). The Duchonka pegmatitic granite represents such example, where possible synergy of relatively high solidus temperature (compared to common granitic rare-element pegmatites) with an increased fractionation level and strongly peraluminous composition caused precipitation of ferrotapiolite and exceptionally Ta-rich ferrotantalite.

5.3. Occurrence of hafnian zircon

Hafnium concentration in accessory zircon, together with the progressive host-rock Hf/Zr enrichment, represent well-known indicators of magmatic fractionation (see e.g., Černý et al. 1985). Hafnium-rich zircon is characteristic of leucocratic, highly peraluminous crustal granites with S-type affinity in contrast to the metaluminous mantle-crustal I-type, and especially (per-) alkaline mantle-derived granite of A- or M-type suites (Pupin 2000; Uher 2007). However, the most effective Zr–Hf fractionation was observed in the rare-element granitic pegmatites and highly evolved, specialized granites. Generally, the most fractionated granitic pegmatites contain the most Hf-rich zircon, e.g., Tanco, Canada (Černý and Siivola 1980), Mixeriquera, Brazil (Cassedanne et al. 1985), up to exceptional presence of hafnon ($HfSiO_4$) at the Muiane pegmatite, Mozambique (Correa Neves et al. 1974). The Hf concentration in the Duchonka pegmatitic leucogranite shows wide variations and unusually high maximum values: from 6 to 23 wt. % HfO_2 (0.06–0.23 Hf apfu; Tab. 3). Analogous variations and high Hf concentrations in zircon (~5 to 40 wt. % HfO_2) were described from the specialized granites, e.g. Beauvoir, France (Wang et al. 1992), Suzhou and Laoshan, China (Wang et al. 1996, 2000), Podlesí, Czech Republic (Breiter et al. 2006) and several other rare-metal bearing granites (Kempe et al. 1997). Wide Hf variations in zircon (5–22 wt. % HfO_2) are also known from the moderately fractionated, granitic pegmatite of the columbite-beryl subtype at Kamzík Hill in Bratislava, Slovakia (Uher and Černý 1998). This trend is supported by experimental data, whereby zircon/hafnon solubility ratio in a metaluminous melts at 800 °C is *c.* 0.2 and similar behaviour could be suggested also for peraluminous melts (cf. Linnen and Keppler 2002; Linnen and Cuney 2005). The solubility of zircon is strongly dependent on temperature and melt composition, ranging from several wt. % Zr levels in peralkaline melts to less than 100 ppm in siliceous peraluminous melts (Watson and Harrison 1983; Linnen and Cuney 2005). The experimental data explain the Hf/Zr enrichment coherent with the magmatic fractionation degree in metaluminous to peraluminous systems and relatively low zircon saturation level and temperature in peraluminous, silica-rich granitic to pegmatitic melts. However, the above mentioned Hf/Zr trend is relatively rough and irregular due to the presence of other important factors, for example post-magmatic processes (albitization, fluid-driven alteration, metamictization). Therefore, the Hf/Zr ratio in zircon as an index of magma fractionation should be used with caution (Kempe et al. 1997; Pérez-Soba et al. 2007). In the case of the Duchonka pegmatitic leucogranite, the wide Hf/Zr variations and high Hf enrichment in zircon could be explained by a coupled effect of high fractionation and a specific, strongly peraluminous local environment. Consequently, the precipitation of the studied Hf-rich zircon is connected with the same specific environment, as the columbite to tantalite and tapiolite crystallization.

Acknowledgements. The authors thank R. Škoda and I. Holický for the electron-microprobe assistance. Valuable comments of both reviewers, M. van Lichtervelde

and A. Pieczka, as well as M. Novák, a handling editor, improved the quality of the manuscript. This work was supported by the Slovak Research and Development Agency under the contract No. APVV-0557-06.

References

Alexandrov IV, Krasov AM, Kochnova LN (1985) On the effect of potassium, sodium and fluorine on associations of rock-forming minerals and formation of Ta-Nb ore mineralization in the rare-metal granite pegmatite. Geokhim 5: 620–629 (in Russian)

Baldwin JR (1989) Replacement phenomena in tantalum minerals from rare-metal pegmatites in South Africa and Namibia. Mineral Mag 53: 571–581

Bernard JH, Hyršl J (2004) Minerals and Their Localities. Granit, Prague, pp 1–808

Breiter K, Förster HJ, Škoda R (2006) Extreme P-, Bi-, Nb-, Sc-, U- and F-rich zircon from fractionated perphosphorous granites: the peraluminous Podlesí granite system, Czech Republic. Lithos 88: 15–34

Breiter K, Škoda R, Uher P (2007) Nb-Ta-Ti-W-Sn-oxide minerals as indicators of a peraluminous P- and F-rich granitic system evolution: Podlesí, Czech Republic. Mineral Petrol 91: 225–248

Broska I, Uher P (1988) Accessory minerals of granitoid rocks of Bojná and Hlohovec blocks, the Považský Inovec Mts. Geol Zbor Geol Carpath 39: 505–520

Cassedanne JP, Baptista A, Černý P (1985) Zircon hafnifère, samarskite et columbite d`une pegmatite du Rio Doce, Minas Gerais, Brésil. Canad Mineral 23: 543–567

Correa Neves JM, Lopes Nunes JE, Sahama ThG (1974) High hafnium members of the zircon-hafnon series from the granite pegmatites of Zambézia, Mozambique. Contrib Mineral Petrol 48: 73–80

Černý P (1989) Characteristics of pegmatite deposits of tantalum. In: Möller P, Černý P, Saupé F (eds) Lanthanides, Tantalum and Niobium. Springer-Verlag, Berlin, pp 195–239

Černý P, Ercit TS (1989) Mineralogy of niobium and tantalum: crystal chemical relationships, paragenetic aspects and their economic implications. In: Möller P, Černý P, Saupé F (eds) Lanthanides, Tantalum and Niobium. Springer-Verlag, Berlin, pp 27–79

Černý P, Ercit TS (2005) The classification of granitic pegmatites revisited. Canad Mineral 43: 2005–2026

Černý P, Siivola J (1980) The Tanco pegmatite at Bernic Lake, Manitoba XII. Hafnian zircon. Canad Mineral 18: 313–321

Černý P, Meintzer RE, Anderson AJ (1985) Extreme fractionation in rare-element granitic pegmatites: selected examples of data and mechanisms. Canad Mineral 23: 381–421

Černý P, Goad BE, Hawthorne FC, Chapman R (1986) Fractionation trends of the Nb- and Ta-bearing oxide minerals in the Greer Lake pegmatitic granite and its pegmatite aureole, southeastern Manitoba. Amer Miner 71: 501–517

Černý P, Ercit, TS, Wise MA (1992a) The tantalite–tapiolite gap: natural assemblages versus experimental data. Canad Mineral 30: 587–596

Černý P, Novák M, Chapman R (1992b) Effects of sillimanite-grade metamorphism and shearing on Nb–Ta oxide minerals in granitic pegmatites: Maršíkov, Northern Moravia, Czechoslovakia. Canad Mineral 30: 699–718

Danišík M, Dunkl I, Putiš M, Frisch W, Kráľ J (2004) Tertiary burial and exhumation history of basement highs along the NW margin of the Pannonian Basin – an apatite fission track study. Austrian J Earth Sci 95/96: 60–70

Huang XL, Wang RC, Chen XM, Hu H, Liu CH (2002) Vertical variations in the mineralogy of the Yichun topaz-lepidolite granite, Jiangxi province, southern China. Canad Mineral 40: 1047–1068

Ivanička J, Havrila M, Kohút M, Kováčik M, Madarás J, Olšavský M, Hók J, Polák M, Filo I, Elečko M, Fordinál K, Maglay J, Pristaš J, Buček S (2007) Geological map of the Považský Inovec Mts. 1 : 50 000. Slovak Geological Survey, Bratislava

Johan V, Johan Z (1994) Accessory minerals of the Cínovec (Zinnwald) granite cupola, Czech Republic Part 1: Nb-, Ta- and Ti-bearing oxides. Mineral Petrol 51: 323–343

Kamenický J (1956) Report on geological investigation and mapping of northern part of the Považský Inovec Mts. crystalline basement. Geol Práce Zpr 8: 110–124 (in Slovak)

Kempe U, Gruner T, Renno AD, Wolf D (1997) Hf-rich zircon in rare-metal granites: magmatic or metasomatic origin? In: Papunen H (ed) Mineral Deposits. Balkema, Rotterdam, pp 643–646

Kohút M, Kumar S, Határ J (2004) New results of the Považský Inovec Mts. granitic rocks study. In: Geochémia 2004. Slovak Geological Survey, Bratislava, pp 57–59 (in Slovak)

Kohút M, Konečný P, Siman P (2006) The first finding of the iron Lahn-Dill mineralization in the Tatric unit of the Western Carpathians. Mineral Polon Spec Pap 28: 112–114

Linnen RL, Cuney M (2005) Granite-related rare-element deposits and experimental constraints on Ta-Nb-W-Sn-Zr-Hf mineralization. In: Linnen RL, Samson IM (eds) Rare-element Geochemistry and Ore Deposits. Geol Assoc Canada Short Course Notes 17: 70–102

Linnen RL, Keppler H (1997) Columbite solubility in granitic melts: consequences for the enrichment and fractionation of Nb and Ta in the Earth's crust. Contrib Mineral Petrol 128: 213–227

Linnen RL, Keppler H (2002) Melts composition control of Zr/Hf fractionation in magmatic processes. Geochim Cosmochim Acta 66: 3293–3301

London D (1990) Internal differentiation of rare-element pegmatites; a synthesis of recent research. In: Stein HJ, Hannah JL (eds) Ore-Bearing Granite Systems; Petrogenesis and Mineralizing Processes. Geol Soc Amer Spec Paper 246: 35–50

London D (2005) Granitic pegmatites: an assessment of current concepts and directions for the future. Lithos 80: 281–303

Maheľ M (1986) Geological Structure of the Czechoslovak Carpathians. Part 1: Paleoalpine Units. Veda, Bratislava, pp 1–510 (in Slovak)

Malachovský P, Uher P, Ďuďa R (2000) Nb-W minerals in rare-element granites from Dlhá Valley, the Spiš-Gemer Ore Mountains. Natura Carpat 41: 7–14 (in Slovak)

Novák M, Uher P, Černý P, Siman P (2000) Compositional variations in ferrotapiolite + tantalite pairs from the beryl-columbite pegmatite at Moravany nad Váhom, Slovakia. Mineral Petrol 69: 295–306

Novák M, Černý P, Uher P (2003) Extreme variation and apparent reversal of Nb-Ta fractionaction in columbite-group minerals from the Scheibengraben beryl-columbite granitic pegmatite, Maršíkov, Czech Republic. Eur J Mineral 15: 565–574

Pérez-Soba C, Villaseca C, Tánago JG, Nasdala L (2007) The composition of zircon in the peraluminous Hercynian granites of the Spanish Central System batholith. Canad Mineral 45: 509–527

Pouchou JL, Pichoir F (1985) "PAP" (phi-rho-z) procedure for improved quantitative microanalysis. In: Armstrong JT (ed) Microbeam Analysis. San Francisco Press, San Francisco, pp 104–106

Pupin JP (2000) Granite genesis related to geodynamics from Hf-Y in zircon. Trans Roy Soc Edinb, Earth Sci 91: 245–256

Raimbault L, Cuney M, Azencott C, Duthou JL, Joron JL (1995) Chemical evidence for a multistage magmatic genesis of Ta-Sn-Li mineralization in the granite at Beauvoir, French Massif Central. Econ Geol 90: 548–576

Taylor SR, McLennan SM (1985) The Continental Crust: Its Composition and Evolution. Blackwell, Oxford, pp 1–312

Tindle AG, Breaks FW (1998) Oxide minerals on the Separation Rapids rare-element granitic pegmatite group, northwestern Ontario. Canad Mineral 36: 609–635

Uher P (1991) Be-Nb-Ta pegmatites – a new type of rare-element mineralization in the Western Carpathians. Geol Carpath 42: 331–339

Uher P (1998) Composition of Nb, Ta, Ti, Sn-bearing oxide minerals from the Homolka phosphorus-rich granite, Czech Republic. Acta Univ Carol, Geol 42: 169–172

Uher P (2007) Zircon in pre-Alpine granites and pegmatites of the Western Carpathians: Zr/Hf and Y variations. Bull mineral–petrogr Odd Nár Muz (Praha) 14–15: 187–191 (in Slovak)

Uher P, Broska I (1992) Ti-Nb-Ta minerals in the Tríbeč leucogranite. Miner Slov 24: 271–277 (in Slovak with English abstract)

Uher P, Černý P (1998) Zircon in Hercynian granitic pegmatites of the Western Carpathians, Slovakia. Geol Carpath 49: 261–270

Uher P, Černý P, Novák M, Siman P (1994) Niobium–tantalum minerals from granitic pegmatites in the Malé Karpaty, Považský Inovec and Žiar Mountains, Western Carpathians, Slovakia. Miner Slov 26: 157–164

van Lichtervelde M, Salvi S, Beziat D, Linnen RL (2007) Textural features and chemical evolution in tantalum oxides: magmatic versus hydrothermal origins for Ta mineralization in the Tanco Lower Pegmatite, Manitoba, Canada. Econ Geol 102: 257–276

von Knorring O, Fadipe A (1981) On the mineralogy and geochemistry of niobium and tantalum in some granite pegmatites and alkali granites of Africa. Bull Minéral 104: 496–507

Wang RC, Fontan F, Monchoux P (1992) Minéraux disséminés comme indicateurs du caractère pegmatitique du granite de Beauvoir, Massif d`Échassières, Allier, France. Canad Mineral 30: 763–770

Wang RC, Fontan F, Xu S, Chen X, Monchoux P (1996) Hafnian zircon from the apical part of the Suzhou granite, China. Canad Mineral 34: 1001–1010

Wang RC, Fontan F, Xu S, Chen X, Monchoux P (1997) The association of columbite, tantalite and tapiolite in the Suzhou granite, China. Canad Mineral 35: 699–706

Wang RC, Zhao GT, Wang, DZ, Lu JJ, Chen XM, Xu SJ (2000) Chemistry of Hf-rich zircons from the Laoshan I- and A-type granites, Eastern China. Mineral Mag 64: 867–877

Watson EB, Harrison TM (1983) Zircon saturation revisited: temperature and composition effects in a variety of crustal magma types. Earth Planet Sci Lett 64: 295–304

Journal of Geosciences, 53 (2008), 335–352 DOI: 10.3190/jgeosci.034

Original paper

Geochemical and structural constraints on the magmatic history of the Chandman Massif of the eastern Mongolian Altay Range, SW Mongolia

Rita C. ECONOMOS[1,*], Pavel HANŽL[2], Kristýna HRDLIČKOVÁ[2], David BURIÁNEK[2], Lkhagva-Ochir SAID[3], Axel GERDES[4], Scott R. PATERSON[1]

[1] *Department of Earth Sciences, University of Southern California, 3651 Trousdale Parkway ZHS117, Los Angeles, CA 90089-0740, USA; economos@usc.edu*

[2] *Czech Geological Survey, Leitnerova 22, 658 69 Brno, Czech Republic*

[3] *School of Geology and Petroleum Engineering, Mongolian University of Science and Technology, Box 520, P.O. 46, Ulaanbaatar, Mongolia 210646*

[4] *Institut für Geowissenschaften, Goethe Universität, Altenhöferallee 1; 60438 Frankfurt am Main; Germany*

[*] *Corresponding author*

In the Mongolian Altay range, immediately south of the Bogd fault zone, the Chandman Massif intruded the Chandman Khayrkhan Crystalline Complex to the NE. This complex consists of migmatized biotite gneisses, orthogneisses and amphibolites. To the south, the Massif cuts the chlorite schists and quartzites of the Tugrug Formation. The Massif mainly consists of diorites to granites with rare gabbro bodies interspersed with metamorphic host rock screens, generally of amphibolite with calc-silicate lenses. Granitoids are further categorized based on petrography and whole-rock geochemical data into peraluminous and metaluminous groups. Granites comprise the peraluminous group, and possess high (71–77 wt. %) silica contents with abundant modal K-feldspar. Metaluminous granitoids span a wide range in silica contents, from diorite to granite. Also their feldspars are compositionally variable. Both these granitoid units are of volcanic-arc character and display a calc-alkaline geochemical trend. Granodiorites of the metaluminous group contain widespread planar rhythmic schlieren layering. Metaluminous units slightly predate the intrusion of peraluminous granites, but the two suites are occasionally co-magmatic. The Al-in-hornblende barometric analysis combined with plagioclase thermometry reveals a depth of emplacement of 11.5–13.7 km and magma temperatures of 725–775 ºC. Chandman Khayrkhan metamorphic foliations strike NNW. Magmatic fabrics in the Chandman Massif roughly E–W and subparallel E–W solid-state foliations overprint magmatic foliations. All foliations are moderately to steeply dipping. Fabric analysis shows a discordance of structures to the north and south of a fault that cross-cuts the field area. This fault is interpreted to be related to motion on the Bogd Fault. Thus, this area experienced 1) amphibolite-facies metamorphism of the Chandman Khayrkhan Crystalline Complex, 2) exhumation to higher crustal levels, 3) juxtaposition against the greenschist-facies Tugrug Formation, 4) intrusion of the Chandman Massif under tectonic strains that continued through the solidification of plutons, and 5) late block-style rotation related to motion on recent faults. These age and geological constraints identify the Chandman Massif as an intrusion of substantially younger age than the "Caledonian" association into which it was previously placed. It is thus far the only arc-type intrusion in the earliest "Hercynian" age range identified in the Gobi-Altay Terrane. Its metamorphic and magmatic history of migmatization followed by intrusion of metaluminous and peraluminous plutons are similar to those of rocks to the west, in the Tseel Terrane, and may represent its easternmost counterpart. The exact juxtaposition mechanism for metamorphic units of different grade and the formation of schlieren layering in the Chandman Massif granodiorites remain enigmatic.

Keywords: Mongolian Altay, Al-in-hornblende barometry, Gobi-Altay Terrane, magmatism, arcs, granite, Chandman Massif
Received: 15 April 2008; accepted 19 December 2008; handling editor: J. Žák
The online version of this article (doi: 10.3190/jgeosci.034) contains supplementary electronic material.

1. Introduction

The Mongolian Altay is a young intraplate transpressional orogen developed during the Late Cenozoic uplift of central Mongolia (Cunningham 2005). Although it is morphologically young, an important boundary between the northern and southern geological domains of Mongolia occurs in this mountain range. The northern domain is usually classified as belonging to the Caledonian orogen and the southern domain to the Hercynian orogen (Marinov et al. 1973). Although the terms of Caledonian or Hercynian are inappropriate for the complicated geological collage of Central Asian Orogenic Belt, the basic two-fold subdivision for Mongolia into northern and southern domains is still applicable (Badarch et al. 2002). The so-called Main Mongolian Lineament sepa-

rates dominantly Proterozoic and Lower Paleozoic rocks to the north from Lower to Upper Paleozoic rocks in the south (Fig. 1, inset).

The area we discuss below lies immediately to the south of the recently active Cenozoic Bogd fault zone (Molnar and Tapponnier 1975). The area is situated in the surroundings of the Chandman town (Fig. 1) (Govi Altay Aymag, SW Mongolia), approximately 750 km SW of Ulaanbaatar at the junction of south-eastern Mongolian Altay with western Gobi Altay.

This area has been identified by several workers as the transition zone between the "Caledonian" and "Hercynian" provinces (Dergunov 2001; Badarch et al. 2002, references therein). The transition between these phases of magmatism is proposed to represent the collision and consolidation of Caledonian and Hercynian magmatic arcs and the reinitiation of subduction beneath the amalgamated continental margin (e.g. Kovalenko et al. 2004, Table 1). The study area lies in the heart of this transitional zone, and has thus drawn recent attention and attracted detailed studies (Kovalenko et al. 2004; Kozakov et al. 2007; Kröner et al. 2007).

In this paper, we will present new mapping, structural and petrographic data to describe temporal and geochemical relationships between magmatic rocks of the Chandman Massif and its metamorphic host rocks. Magmatic rocks of the Chandman Massif are further characterized into metaluminous and peraluminous units based on field evidence, geochemistry, and petrography. The timing and conditions of intrusion are constrained by previous geochronology (Hrdličková et al. 2008) and new geothermobarometry. These data are combined to create a model of the metamorphic and intrusive history of the area.

2. Geological setting

2.1. General geological and tectonic setting

Mongolia consists of a number of tectonic zones that form the part of the extensive Central Asian Orogenic Belt (CAOB) (Mossakovsky et al. 1994) known also as the Altaid Tectonic Collage (Sengör et al. 1993). This belt occurs between the Siberian Craton in the north, the Tarim Craton in the southwest and the Sino-Korean Craton in the south. It is characterized by a collage of various terranes of different origin (Sengör et al. 1993; Windley et al. 2002; Jahn et al. 2004) and evolved in the time span of 1000–250 Ma (Windley et al. 2007). The CAOB is characterized by an abundance of Paleozoic and Mesozoic granitic intrusions as well as basaltic to rhyolitic volcanics (e.g. Jahn et al. 2000), and is known as an important site of Late Precambrian to Phanerozoic juvenile crustal growth (Sengör et al. 1993; Hu et al.

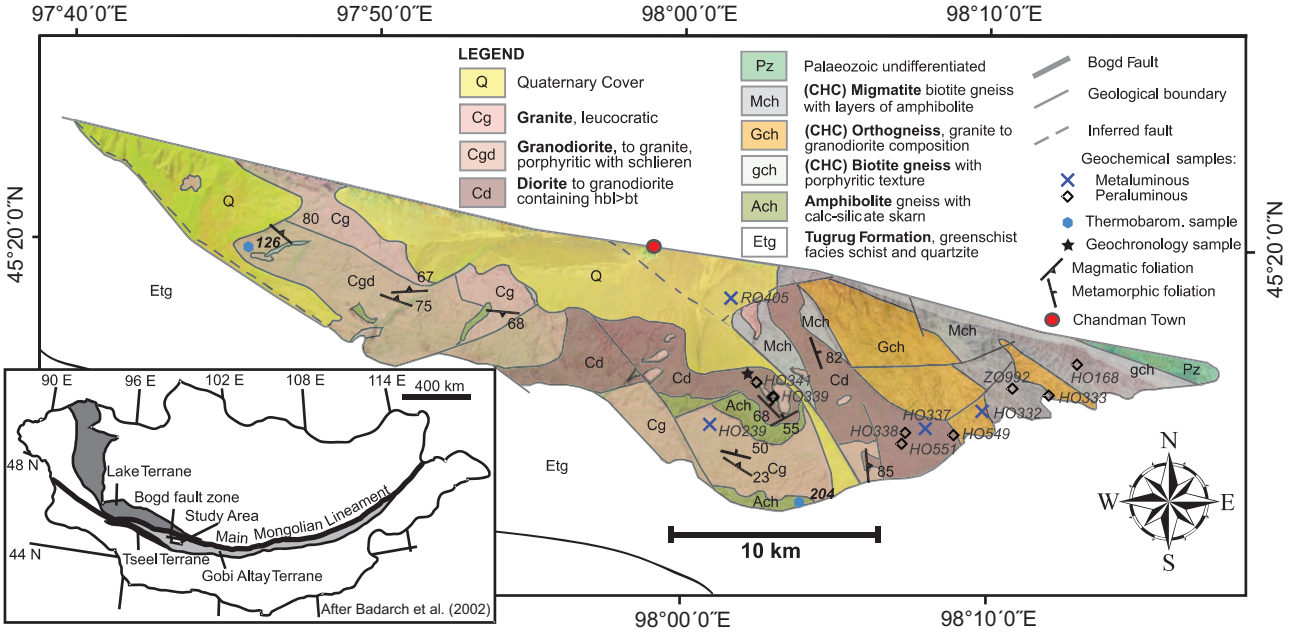

Fig. 1 Geologic map of the Chandman Massif and adjacent metamorphic host rocks. CHC – Chandman Khayrkhan Crystalline Complex. Locations of samples for geochemistry and thermobarometry detailed. Foliation data are selected as representative averages for magmatic and metamorphic foliations. Inset map is modified after Badarch et al. (2002).

2000; Jahn et al. 2000; Jahn et al. 2004). Granitoids have a wide range of compositions and show a temporal evolution from calc-alkaline and alkaline to peralkaline series. The emplacement of most granitic plutons falls between 500 and 120 Ma (Jahn et al. 2000).

In the terrane division of Mongolia by Badarch et al. (2002), the studied area is situated within the Gobi Altay Terrane at its northern margin, near the boundary with the Lake Terrane. The boundary between these two units coincides here with the Chandman strand of the Bogd fault zone (Baljinnyam et al. 1993).

The Gobi-Altay Terrane most likely represents the southwestern continental margin of the Siberian Plate. According to Badarch et al. (2002), it forms a long narrow belt rimming the northern margin of the southern domain of Mongolia. It is composed of Cambrian (?) marine sediments and volcaniclastic rocks metamorphosed under greenschist-facies conditions accompanied by Paleozoic sediments, volcanic and volcaniclastic rocks of a forearc/backarc character. The sequence was intruded mainly by Carboniferous to Permian granite plutons.

The Lake Terrane is composed of slightly metamorphosed volcanosedimentary sequences of Neoproterozoic to Lower Paleozoic ages, which alternate with highly metamorphosed rocks in the Zamtyn Nuruu and Alag Khadny Crystalline Complexes and with relics of oceanic crust (Hanžl and Aichler eds. 2007). The Permian volcanic and volcaniclastic sequences covering the Lower Paleozoic units are tectonically incorporated into the structure of the Lake Terrane along its southern boundary.

The study area occurs spatially in the "Caledonian" province (generally of Cambrian to Ordovician age) of Kovalenko et al. (2004) where Nd model ages of ~900 Ma of felsic igneous rocks indicate the incorporation of older crustal material in their generation. Kozakov et al. (2007) also referred to this area as falling into the Caledonides of the north Asian continental margin, while the adjacent Tseel Terrane to the west (also of Badarch et al. 2002), has been characterized as the northernmost representation of "Hercynian" (generally of Ordovician to Early Carboniferous age) tectonic and magmatic activity. Kröner et al. (2007) similarly described the study area as being built by Ordovician metavolcanics and plutonics. According to map patterns (Kröner et al. 2007, fig. 17), the area represents a sliver of older material bounded to the south by younger Devonian granites, metavolcanics and metasedimentary sequences, and to the north (across the Bogd fault zone) by Permian volcanics and granites. These interpretations, however, are inconsistent with geochronological findings and the geological character of the Chandman Khayrkhan Crystalline Complex, as described below, in Hrdličková et al. (2008) and in geological maps (Hanžl and Aichler 2007).

2.2. Geology of the Chandman Massif and adjacent metamorphic units

The *Chandman Massif* is located in the eastern part of the Mongolian Altay Mountains. It is exposed in an E–W elongated, oval-shaped body in the region of the Chandman Khayrkhan Mountain near the town of Chandman (Fig. 1). Plutons of the Chandman Massif span a wide compositional range, from diorite to granite. A variety of preserved magmatic structures are overprinted by mild to moderate solid-state deformation. The Massif intruded migmatites of the Chandman Khayrkhan Crystalline Complex in the northeast. The contact between metamorphic rocks and the Chandman Massif is disrupted by NW–SE trending faults on the SW slopes of the Chandman Khayrkhan Mountain. The boundary with the Paleozoic volcanosedimentary sequence in the NW is overprinted by mylonite zones associated with the Chandman rupture of the Bogd Fault. The southern, intrusive contact with the moderately metamorphosed volcanosediments of the Tugrug Formation of supposed Cambrian age (Rauzer et al. 1987) is commonly obscured by faults. The eastern termination of the Massif is covered by Quaternary alluvial fans. The Tugrug Formation and the Chandman Khayrkhan Crystalline Complex are never observed in contact, always being separated by granitoids of the Chandman Massif.

The *Chandman Khayrkhan Crystalline Complex* consists of migmatites, orthogneisses, gneisses and amphibolites with lenses of skarn-like rocks. Reconstruction of the metamorphic evolution of this unit is also complicated due to overprinting by HT-LP metamorphism related to the intrusion of the Chandman Massif. The main mineral assemblages indicate amphibolite-facies metamorphism. The mentioned rocks are affected by extensive migmatitization which was likely dominantly related to a pre-intrusive metamorphic event (based on data presented below). Lit-par-lit intrusion by Chandman Massif granites suggests that partial melting caused by high temperatures and fluid flow during granite emplacement also contributed to local migmatization. Discrimination between the magmatic products of migmatization of the Chandman Khayrkhan Crystalline Complex and the peraluminous granites of the Chandman Massif was made on subtle field relationships, which are discussed at length below. For example, structural relationships of cm thick pegmatite dikes of the mineral composition identical to the migmatite leucosomes indicate that these dikes were mainly related to the emplacement of the Chandman Massif.

The *Tugrug Formation* is exposed along the southern and western contact of the Massif. The formation is composed of siliceous, green-gray chlorite-sericite schists with intercalations of light gray quartzites. Layers of

metabasalts and tuffaceous sandstones are minor. Units with greenschist-facies assemblages grade into biotite gneiss and amphibolite towards the Chandman Massif. Bedding is not preserved here, and the dominant structure is the NW–SE oriented crenulated foliation with a prevailing dip (moderate to steep) toward the SW. The sequence is folded by close to tight overturned folds with amplitudes of up to 1 m and a NW–SE orientation of fold axes.

Intrusive boundaries between the Tugrug Formation and Chandman Massif are frequently disrupted by faults. Equivalents of Tugrug Formation are preserved as remnants of metamorphic wall rocks of the Chandman Massif. Rauzer et al. (1987) interpreted crystalline rocks of the Chandman Khayrkhan Mountain situated towards the north as a part of the Tugrug Formation. However, the lithology and character of metamorphism enable us to separate these rocks from the Tugrug Formation proper.

The Chandman Massif includes plutonic suites of both metaluminous and peraluminous character. Metaluminous plutons span a wide compositional range from diorite to granite. Dioritic units were grouped in the field based on proportions of both feldspars, the occurrence of hornblende, the presence of microgranitoid enclaves, and a characteristic rhythmic planar schlieren layering. Some granites of the Chandman Massif were grouped with these units based on their spatial association and common gradational contacts with granodiorites. Porphyritic biotite granodiorite forms the southern part of the Massif, whereas the biotite to biotite-amphibole granodiorite and tonalite units are situated in the northern part (Fig. 1). The boundary is commonly marked by a discontinuous belt of amphibolites and gneisses in roof pendants of the Massif.

Peraluminous granites were identified based on the presence of primary muscovite, color index, and their common occurrence in the vicinity of the Chandman Khayrkhan Crystalline Complex. Compositions of these rocks represent a narrow range from biotite to leucocratic biotite granite and they have a monotonous macroscopic appearance. These units were intruded into granodiorites and diorites in the northern part of the Chandman Massif and in some cases display mutually intrusive relationships with these rocks.

All plutonic units in the Chandman Massif display magmatic fabrics, defined by the statistical alignment of minerals with high axial ratios. These fabrics are presumed to represent strain in plutons during the final stages of crystallization (Paterson et al. 1998). In more mafic units, internal heterogeneities such as schlieren layering and elongate mafic enclaves are aligned parallel to this fabric. Granitoids also display a solid-state foliation in many localities, defined in the field by stretched quartz crystals and in thin section by the presence of subsolidus microstructures. The intensity of this deformation increases towards the northeast where granitic rocks grade into orthogneisses. The contact between orthogneisses of the Chandman Khayrkhan Crystalline Complex and the Chandman Massif is gradational.

3. Petrography

3.1. Petrography of metamorphic rocks

3.1.1. Tugrug Formation

The Tugrug Formation (Etg – *index used in Fig. 1*) is dominated by siliceous, chlorite-sericite schists, with layers of greenschists and quartzite. The composition of rocks varies from sericite phyllite to greenschist. Chlorite schists are fine-grained, banded with lepidoblastic microstructure and a mineral association of quartz + albite + sericite + chlorite ± epidote ± biotite ± carbonate. Opaque minerals and tourmaline appear as accessories. Metabasalts, tuffaceous green–gray, slightly metamorphosed sandstones, greenschists, and quartzite form elongate lenses in the schists, typically with gradational contacts. The metabasalts are fine-grained, massive rocks, locally with relics of tabular phenocrysts of altered feldspars and chloritized amphibole. The groundmass consists of actinolite, chlorite, epidote and opaque minerals. Titanite is accessory. Fine-grained, banded amphibolite with calc-silicate lenses form a narrow, morphologically prominent range exposed together with gneisses near the contact with the Chandman Massif. Amphibolites have poikiloblastic texture and are composed of amphibole, plagioclase, epidote and rare quartz. Titanite is accessory. The amphibolite contains lenses of calc-silicate rocks composed of epidote, quartz and plagioclase.

Fine-grained, laminated quartzites are exposed in thin layers, forming resistant ridges in the chlorite-sericite schist. They are fine- to very fine-grained rocks composed of elongated quartz grains and sericite oriented in the foliation. The trend of the layers is parallel with the foliation. Biotite to chlorite-biotite schists are exposed together with amphibolites in two belts. They also are exposed in the marginal part of the unit near the contact with the Chandman Massif. Main phases are plagioclase, quartz, biotite, sometimes muscovite and locally cordierite.

3.1.2. Chandman Crystalline Complex

Orthogneiss (Gch) forms bodies in migmatites on the SE slopes of the Chandman Khayrkhan Mountain. It is a medium-grained rock of granodiorite to granite composition

with locally porphyroblastic texture. It is composed of K-feldspar, plagioclase, interstitial quartz, minor biotite and muscovite. Interstitial quartz is often recrystallized to very fine-grained mosaics, and K-feldspars are partially recrystallized.

Fine-grained metagranite, locally garnet-bearing, alternated with meta-aplite, metapegmatite, and gneiss forms discontinuous dikes and small lenticular bodies in migmatites and granites on the SE slopes of the Chandman Khayrkhan Mountain. The rocks have a granular texture that gives them a massive appearance. This fine-grained character is accentuated by homogeneous distribution of the major mineral components (K-feldspar, plagioclase, quartz and biotite). Quartz forms grains with sutured contacts and exhibit undulatory extinction. Accessory minerals are apatite, zircon and occasionally garnet.

Red porphyritic metagranites are fine- to medium-grained equigranular rocks with plagioclase and biotite phenocrysts. The groundmass consists of plagioclase (30–40 %), K-feldspar (20–30 %), quartz (15–20 %) and biotite (10–15 %). Accessory minerals include muscovite, epidote, apatite and zircon.

Metagranodiorite to metadiorite are the prevailing rocks in the central part of the Chandman Khayrkhan Crystalline Complex. Microscopic examination reveals that the protolith was similar to granodiorite and diorite of the Chandman Massif. Granular texture is typical, occasionally with a distinct subsolidus fabric defined by thin flakes of biotite and alternating domains of recrystallized feldspar and deformed quartz. Average grain size is up to 1 mm, often with plagioclase or microcline sericitized. Quartz and perthitic microcline form subhedral or elongate grains, mostly or partially recrystallized. Accessory minerals are apatite, zircon, epidote, magnetite and titanite.

Biotite-amphibolite gneiss to amphibolite to hornblende gneiss with skarn and metagabbro lenses (Ach) form layers surrounded by migmatites or metaigneous rocks. The largest bodies are exposed in migmatites on the eastern slope of the Chandman Khayrkhan Mountain. These medium- to fine-grained, commonly banded rocks have varied amphibole content (30–70 modal %). Amphibolites also usually contain anorthitic plagioclase ($Ab_{7–11}$), quartz, and secondary chlorite. Minor biotite, ore minerals and titanite are locally present. Amphibolites are often migmatized or interlayered with migmatites. The metagabbro is composed of prevailing amphibole (more than 60 %), minor plagioclase, rare biotite and titanite, secondary epidote, calcite and sericite. The skarns consist mainly of garnet and pyroxene accompanied by interstitial quartz and plagioclase.

Biotite migmatite to pearl gneiss with anatectic textures, layers of amphibolite (Mch) surrounds metagranodiorite and metadiorite in the central part of the Chandman Khayrkhan Crystalline Complex. The grain size is medium to coarse; biotite is common in both mafic and felsic lithologies. Plagioclase is often present as porphyroblasts. Layers of migmatized amphibolite are up to several dm thick and contain mainly hornblende and plagioclase, with minor quartz, biotite, epidote and titanite. The migmatites also contain layers of calc-silicate rock up to 30 cm thick. The calc-silicate rocks are composed mainly of biotite, plagioclase and quartz, and occasionally muscovite, sillimanite and garnet. Tourmaline occurs only locally in the migmatites, namely on the boundary between melanosome and leucosome.

Biotite gneiss and porphyroblastic gneiss (gch) occurs in the belt in the northernmost part of the unit along the Ikh Bogd Fault. The gneiss is a medium-grained rock, composed of plagioclase, biotite, quartz and sometimes K-feldspar or muscovite, accessory zircon and apatite. Chloritization of biotite is common, and local melting occurs in rare localities in this unit.

Additional information on the described units, including mineralogical compositions determined by electron microprobe, is available in Hrdličková et al. (2008).

Metamorphic host-rock septa within the Chandman Massif include amphibolites, calc-silicate rocks, biotite schists, and rare quartzites. Very fine grained amphibolites are the most common and consist almost entirely of equigranular, stubby hornblende and plagioclase. Some amphibolites contain hornblende porphyroblasts up to 3 mm across with mottled textures and a very dark brown to dark green appearance. Calc-silicate rocks are dominated by calcite with extensive deformation twinning and grain size reduction. Biotite schists are rare and are mostly found near the contact with the Tugrug Formation. Blocks of this composition have undergone a small amount of partial melting, possibly associated with their engulfment in plutons. All host-rock blocks have undergone metamorphism and moderate temperature deformation before their integration into the massif, with quartz, where present, displaying grain size reduction and core and mantle structures.

3.2. Petrography of plutonic rocks

Diorite units are found throughout the Chandman Massif and are characterized by the profusion of long, lath-like plagioclase crystals (Fig. 2a), and large euhedral titanite crystals that can be observed in hand specimen. K-feldspars are rare to absent in these rocks. Mafic minerals include biotite and hornblende in varying proportions; hornblende crystals are subhedral and stubby. Prismatic epidote crystals are common and microstructural relationships confirm that it is a primary magmatic mineral (Fig. 2b). Apatite and magnetite are present as accessory phases.

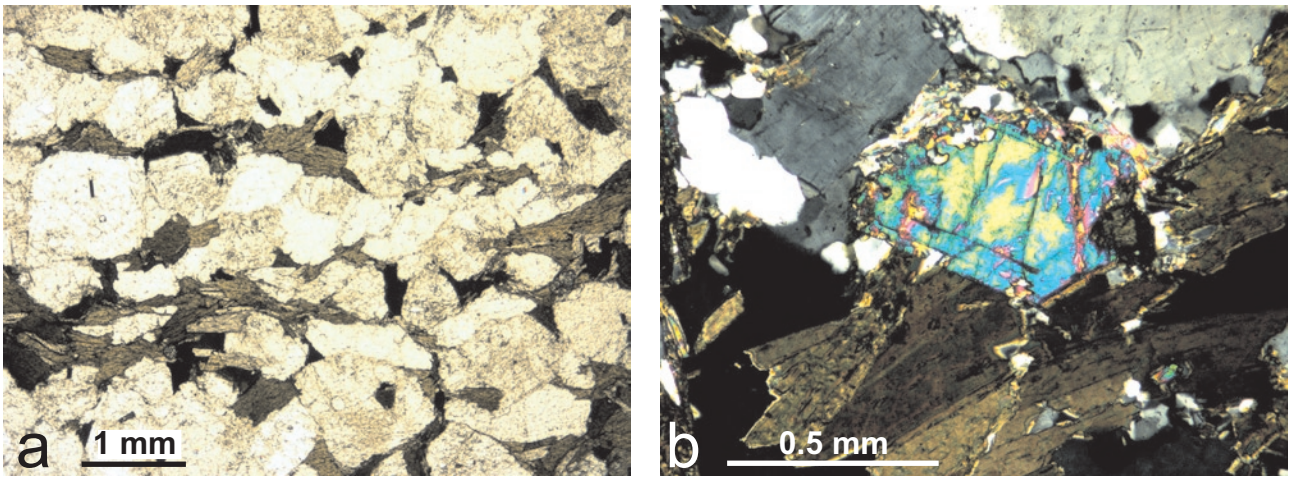

Fig. 2a – Photomicrographs of a biotite-rich schlieren layering characteristic of granodiorites in the Chandman Massif, and **b –** a subhedral epidote crystal situated between plagioclase and biotite demonstrating its magmatic origin.

Granodiorites with extensive planar schlieren layering are found in the southern portions of the massif. Petrographic observations support the interpretation that these rocks are petrologically related to the diorite units. Granodiorites share with diorites long subhedral plagioclase crystals, an abundance of euhedral gold-colored titanite, and accessory magnetite. The major petrologic difference between these two units is the presence of macroscopically perceptible K-feldspar grains. The schlieren distinctive to this unit appear as concentrations of aligned biotite books in thin section, but their matrix is otherwise of the granodioritic composition (Fig. 2a).

Granitic to leucogranitic units are peppered throughout the complex. They consist dominantly of K-feldspar and quartz crystals with plagioclase and biotite. K-feldspars sometimes form phenocrysts. While it is difficult to discern between metaluminous and peraluminous granites in the field, they can be subdivided geochemically and have some distinctive microstructural characteristics. Upon petrographic inspection, peraluminous granites are finer grained and display ubiquitous grain boundaries with a sutured appearance. All crystals are sub- to anhedral, and quartz is polycrystalline. Metaluminous granites tend to have larger grain sizes and more euhedral grains.

4. Geochemistry and thermobarometry

4.1. Whole-rock geochemistry

Samples from the main lithological types of at least 2–4 kg in mass were used for whole-rock geochemical analyses. Major and trace elements were determined at ACME Laboratories, Canada (Tab. 1a–b). Igneous rocks of the Chandman Massif range from diorite to granite (Fig. 3d). Three types can be distinguished according to SiO_2 content: granites (71–77 wt. %), granodiorites with tonalites, (61–71 wt. %) and diorites (55–59 wt. %). Plutonic rocks are calc-alkaline (Fig. 3b), with potassium abundances corresponding to the high-K series for granites and medium-K series for tonalites to granodiorites (Fig. 3a). Analyzed plutonic samples can be separated into peraluminous and metaluminous suites based on A/CNK values and Eu anomaly magnitudes (Fig. 3c, 4a).

Peraluminous samples are acid (SiO_2 = 72–77 wt. %) and display trace-element ratios K/Rb of 145–265 and Rb/Sr of 1–11. The total REE contents are low (49–166 ppm). LREE are slightly to moderately fractionated (La_N/Sm_N = 2.1–5.5) and the HREE trends in chondrite-normalized patterns are flat (Gd_N/Yb_N = 0.9–1.4). These rocks also have a pronounced negative Eu anomaly, demonstrated by Eu/Eu* ratios of 0.2–0.6 (Fig. 3f). In the NMORB-normalized spider diagram, there is depletion in Ba, Nb, Sr, P and Ti, slight depletion in Zr and enrichment in Cs, Rb, Th, K, Pb and MREE (Fig. 3e). Samples fall mainly within the Volcanic Arc Granite (VAG) field, and two samples into the Within Plate Granite (WPG) field of the classification by Pearce et al. (1984) (Fig. 4b–c). A shallow trend is also observed in the CaO/Na_2O vs. Al_2O_3/TiO_2 binary plot, with most peraluminous samples having $CaO/Na_2O < 0.3$ (Fig. 4e). In addition half of peraluminous rocks sampled fall into the strongly peraluminous categorization, having A/CNK values of 1.1 to 1.3 (Fig. 3c) (Sylvester 1998). This suggests a pelitic source according to Sylvester (1998) and references therein.

Metaluminous rocks demonstrate a greater variety, including a wide range in SiO_2 content, from 55 to 77 wt. % (Fig. 3a). Samples show higher and much more variable K/Rb ratios (142–519) than granite units. They are also

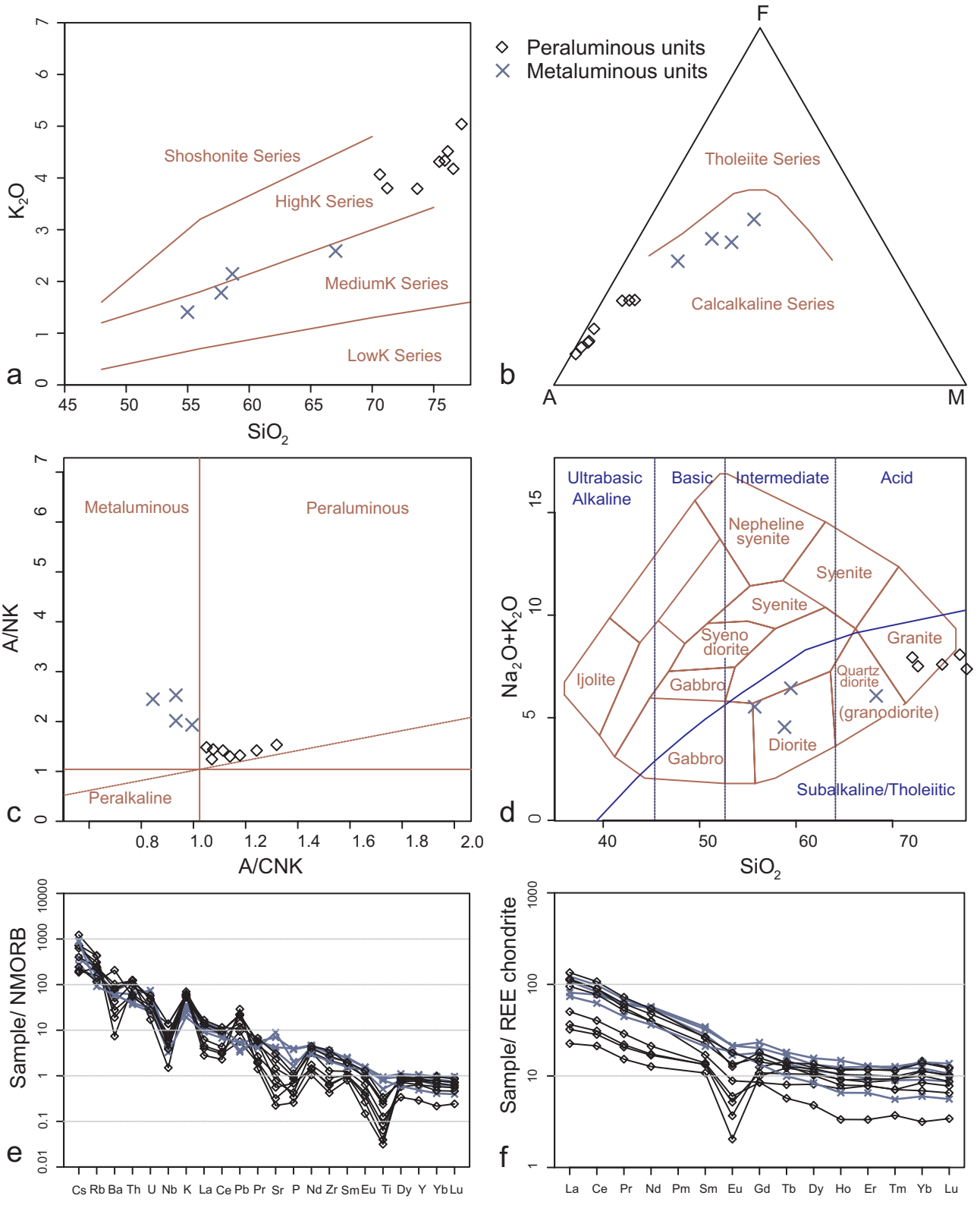

Fig. 3 Geochemistry of the Chandman Massif. **a –** SiO_2 vs. K_2O plot (Peccerillo and Taylor 1976), **b –** AFM diagram (Irvine and Baragar 1971), **c –** A/NK vs. A/CNK plot (Shand 1943), **d –** $Na_2O + K_2O$ vs. SiO_2 (TAS) plot (Cox et al. 1979), **e –** Spider diagram normalized to NMORB (Sun and McDonough 1989), **f –** Rare earth element patterns normalized to chondrite (Boynton 1984).

Tab. 1a Whole-rock major-element analyses (wt. %) for igneous rocks of the Chandman Massif

Sample	H0168	H0239	H0332	H0333	H0337	H0338	H0339	H0341	H0549	H0551	R0405	Z0992
Sheet_no	L-47-101A										L-47-89A	L-47-101A
E_coord. (°)	98.22329	98.02093	98.16809	98.19587	98.13047	98.11511	98.05684	98.03772	98.15180	98.11545	98.01052	98.17676
N_coord. (°)	45.27573	45.25558	45.26511	45.26924	45.25467	45.25046	45.26844	45.27135	45.25055	45.24709	45.31053	45.27202
Rock	granite	granite	diorite	granite	diorite	granite	granite	diorite	granite	granite	diorite	granodiorite
SiO_2	75.48	58.63	57.72	76.12	67.06	76.58	73.67	71.19	77.29	75.94	54.99	70.64
Al_2O_3	14.00	17.44	15.43	13.43	15.20	12.99	13.31	14.11	11.49	13.22	19.48	14.16
Fe_2O_3	1.05	6.87	8.39	1.15	4.29	1.20	2.64	2.84	1.59	0.85	6.44	2.92
MgO	0.13	2.69	4.14	0.19	1.42	0.21	0.50	0.81	0.18	0.09	3.36	0.69
CaO	0.66	5.55	6.63	0.68	4.10	0.74	1.30	2.16	0.76	0.54	7.33	1.78
Na_2O	3.45	4.07	2.82	2.63	3.27	3.54	3.50	3.50	2.52	3.54	3.95	3.56
K_2O	4.32	2.15	1.78	4.51	2.59	4.17	3.80	3.79	5.05	4.34	1.41	4.07
TiO_2	0.05	1.10	1.20	0.08	0.65	0.11	0.30	0.35	0.16	0.04	1.01	0.43
P_2O_5	0.08	0.44	0.46	0.08	0.19	0.04	0.10	0.11	0.05	0.03	0.24	0.13
MnO	0.10	0.09	0.13	0.04	0.06	0.05	0.05	0.04	0.02	0.07	0.07	0.03
Cr_2O_3	0.00	0.00	0.01	0.00	0.00	0.00	0.00	0.00	0.00	0.00	0.00	0.01
LOI	0.60	0.50	0.80	0.90	0.80	0.20	0.60	0.80	0.70	1.20	1.40	1.40
TOT_C	0.01	0.01	0.01	0.01	0.01	0.01	0.01	0.01	0.03	0.04	0.03	0.10
Total	99.92	99.54	99.52	99.81	99.63	99.83	99.77	99.70	99.81	99.86	99.69	99.82

Abundances of the major oxides were analysed by ICP-emission spectrometry in ACME Laboratories, Canada. Loss on ignition (LOI) was calculated by weight difference after ignition at 1000 ºC.

far less enriched in Rb, with Rb/Sr ratios of 0.06–0.60; only one sample has Rb/Sr = 1.3. The REE concentrations are similar to granites in their low values, from 86 to 180. The LREE are moderately fractionated (La_N/Sm_N = 2.3–6.7). The HREE show a weak fractionation (Gd_N/Yb_N = 1.4–2.7). The Eu anomalies in these rocks are weak or absent (Fig. 3f). In NMORB-normalized spider diagrams, there is a distinct depletion in Nb and P, and a slight depletion in Ti. This diagram also indicates a pronounced enrichment in Cs and K, and a slight enrichment in Th and Nd. The Ba, Pb and Sr show complex trends for felsic and intermediate rocks (Fig. 3e). Rocks of the metaluminous group fall into the Volcanic Arc Granite (VAG) field in the Pearce et al. (1984) classification scheme (Fig. 4b–c).

4.2. Mineral composition and thermobarometric analysis

Analysis of mineral major oxide composition for the aluminum-in-hornblende igneous barometer (Hammastrom and Zen 1986; Hollister et al. 1987) was conducted on a JEOL JXA-8200 electron microprobe at the University of California, Los Angeles. Samples were analyzed in spot mode with a beam current of 15 nA and accelerating voltage of 15 kV. One σ analytical error is 1 %. Two samples from dioritic units were selected based on the presence of the appropriate mineral assemblage, including amphibole, quartz, K-feldspar, titanite, and magnetite. These samples were doubly polished, cleaned and sputter coated with graphite. Major oxides were analyzed for plagioclase, hornblende, biotite and Fe-Ti oxide minerals. Plagioclase and hornblende analyses were used to apply the Al-in-Hbl barometer and the plagioclase-hornblende thermometer (Blundy and Holland 1990) in order to constrain conditions of crystallization of dioritic plutons (Fig. 5a–b). Analysed were conducted on adjacent plagioclase and hornblende grains that were each touching a quartz grain to ensure silica saturation at the last phase of crystallization (Fig. 5d). Transects from core to rim of both the plagioclase and hornblende grains were conducted, and additional analyses of each crystal on its rim against quartz were also obtained. The goal of these transects was to constrain both the crystallization history of the sample and the thermobarometric conditions at the final stages of crystallization, represented by analyses on sample rims. To constrain secular variation, three plagioclase–hornblende pairs were analyzed for each sample. Pressures stated are corrected for temperature according to the formulation of Anderson and Smith (1995).

Sample 204 displays complexly zoned hornblende crystals that yield an average rim crystallization of 2.9 ± 0.5 kbars (1σ combined analytical and statistical errors) (Fig. 5a). Based on a pressure gradient of 3.7 km per kbar (based on a crustal density of 2.7 g/cm^3), these rocks crystallized at *c.* 11 km. Anorthite content of plagioclase in this sample varies from 30 to 40 %. Rim crystallization temperatures are calculated as 756 ± 23 ºC.

Tab. 1b Whole-rock trace-element analyses (ppm) for igneous rocks of the Chandman Massif

Sample	H0168	H0239	H0332	H0333	H0337	H0338	H0339	H0341	H0549	H0551	R0405	Z0992
Rock	granite	granite	diorite	granite	diorite	granite	granite	diorite	granite	granite	diorite	granodiorite
Ba	119.2	419.6	404.4	174.3	457.1	264.9	524.4	648.6	472.5	46.6	369.9	1305.0
Co	0.8	18.0	27.6	1.0	9.2	1.3	4.0	5.8	2.4	0.6	21.9	5.5
Cs	8.6	6.4	1.9	4.4	2.7	1.3	2.8	5.0	1.4	5.1	6.2	1.7
Ga	21.4	23.7	20.8	17.8	19.1	16.2	17.6	17.9	12.6	21.2	23.4	15.7
Hf	2.4	6.6	5.4	1.9	5.2	3.1	5.9	4.9	2.9	2.1	4.1	6.8
Nb	32.0	12.2	14.9	19.1	12.5	16.4	13.5	10.1	3.5	32.2	7.6	9.0
Rb	244.9	93.9	66.9	173.3	100.0	131.6	136.4	132.8	88.0	240.8	51.0	65.1
Sn	2	2	3	2	2	1	3	2	1	6	1	1
Sr	28.6	628.0	382.1	50.3	316.5	95.8	131.3	204.5	67.5	20.1	798.5	278.0
Ta	3.8	1.7	0.9	2.5	1.1	1.8	1.3	1.0	0.3	7.9	0.4	0.6
Th	6.7	7.3	4.4	7.2	13.5	12.7	15.1	14.6	14.8	10.6	4.8	6.5
U	1.3	3.5	1.2	1.6	2.6	1.5	2.2	2.3	0.8	2.7	1.4	1.3
V	–	114	173	6	74	10	22	37	10	7	158	29
W	0.5	0.4	0.1	2.4	0.1	0.3	0.1	0.1	0.2	1.3	0.5	0.2
Zr	48.6	265.5	226.7	45.5	185.5	66.4	201.9	162.7	94.5	31.3	153.8	267.9
Y	25.8	29.7	29.0	21.9	21.9	17.7	24.5	23.4	8.1	21.5	13.7	17.9
Mo	0.2	0.2	0.3	0.2	0.3	0.2	0.3	0.3	0.3	0.2	0.2	0.2
Cu	6.3	32.2	53.0	6.9	19.6	4.6	5.8	6.8	15.2	4.4	47.8	6.1
Pb	1.7	1.0	1.1	2.8	1.6	6.6	6.4	4.3	6.7	8.7	1.6	3.2
Zn	9	68	61	13	49	21	40	38	17	4	45	35
Ni	2.2	17.5	49.9	2.1	6.9	2.8	4.8	8.0	4.1	2.2	17.0	4.4
As	0.5	0.5	0.8	0.6	–	–	0.8	0.6	0.9	–	0.8	0.5
Cd	0.1	–	–	–	–	–	–	–	–	–	–	–
Sb	–	–	–	–	–	0.1	0.1	–	–	–	–	–
Bi	0.1	0.1	–	0.2	–	–	–	–	0.1	0.1	–	–
Au	1.4	–	1.1	0.9	–	0.7	–	0.7	2.1	3.1	1.2	4.3
La	10.0	33.4	25.2	11.3	37.8	15.6	34.5	29.5	35.5	7.0	22.9	41.7
Ce	22.9	66.9	62.5	25.1	79.5	32.5	72.5	62.8	72.5	17.2	50.3	86.7
Pr	2.52	7.46	7.55	2.68	8.44	3.52	7.51	6.33	6.81	1.86	5.44	8.83
Nd	10.1	33.0	34.3	10.4	31.7	12.7	28.4	23.7	23.9	7.6	21.7	32.5
Sm	2.6	6.3	6.7	2.6	5.5	2.7	5.2	4.4	3.3	2.1	4.1	5.1
Eu	0.27	1.57	1.57	0.38	1.24	0.44	0.93	0.99	0.65	0.15	1.36	1.32
Gd	3.23	5.22	6.02	2.80	4.63	2.19	4.67	4.08	2.21	2.57	3.50	3.69
Tb	0.69	0.79	0.86	0.50	0.65	0.38	0.66	0.60	0.27	0.58	0.47	0.61
Dy	3.97	4.29	5.03	3.35	3.69	2.61	4.34	3.86	1.54	3.55	2.70	3.26
Ho	0.86	0.89	1.06	0.66	0.76	0.52	0.83	0.74	0.24	0.65	0.47	0.57
Er	2.46	2.64	2.70	1.80	1.97	1.64	2.47	2.14	0.70	1.93	1.37	1.64
Tm	0.38	0.41	0.39	0.29	0.29	0.23	0.37	0.32	0.12	0.30	0.18	0.23
Yb	3.04	2.94	2.54	2.35	1.90	1.76	2.90	2.39	0.66	2.10	1.25	1.44
Lu	0.40	0.44	0.34	0.33	0.28	0.25	0.39	0.32	0.11	0.28	0.18	0.21
REE	63.42	166.25	156.76	64.54	178.35	77.04	165.67	142.17	148.51	47.87	115.92	187.80

The rare earth and most remaining trace elements were analysed in ACME Laboratories, Canada by INAA and ICP-MS following a $LiBO_2$ fusion; the precious and base metals were analysed by aqua regia digestion/ICP-MS.

Sample 126 displays an average rim pressure of 3.7 ± 0.5 kbars (Fig. 5b), representing a crystallization depth of 13.7 km. An average of core analyses yields 2.8 ± 0.2 kbars. This pattern is antithetical to the simple scenario where, in an ascending magma, the crystal rims preserve the lowest pressures. This may suggest that hornblende crystals grew at the expense of pyroxene or indicate that core compositions are not representative of equilibrium

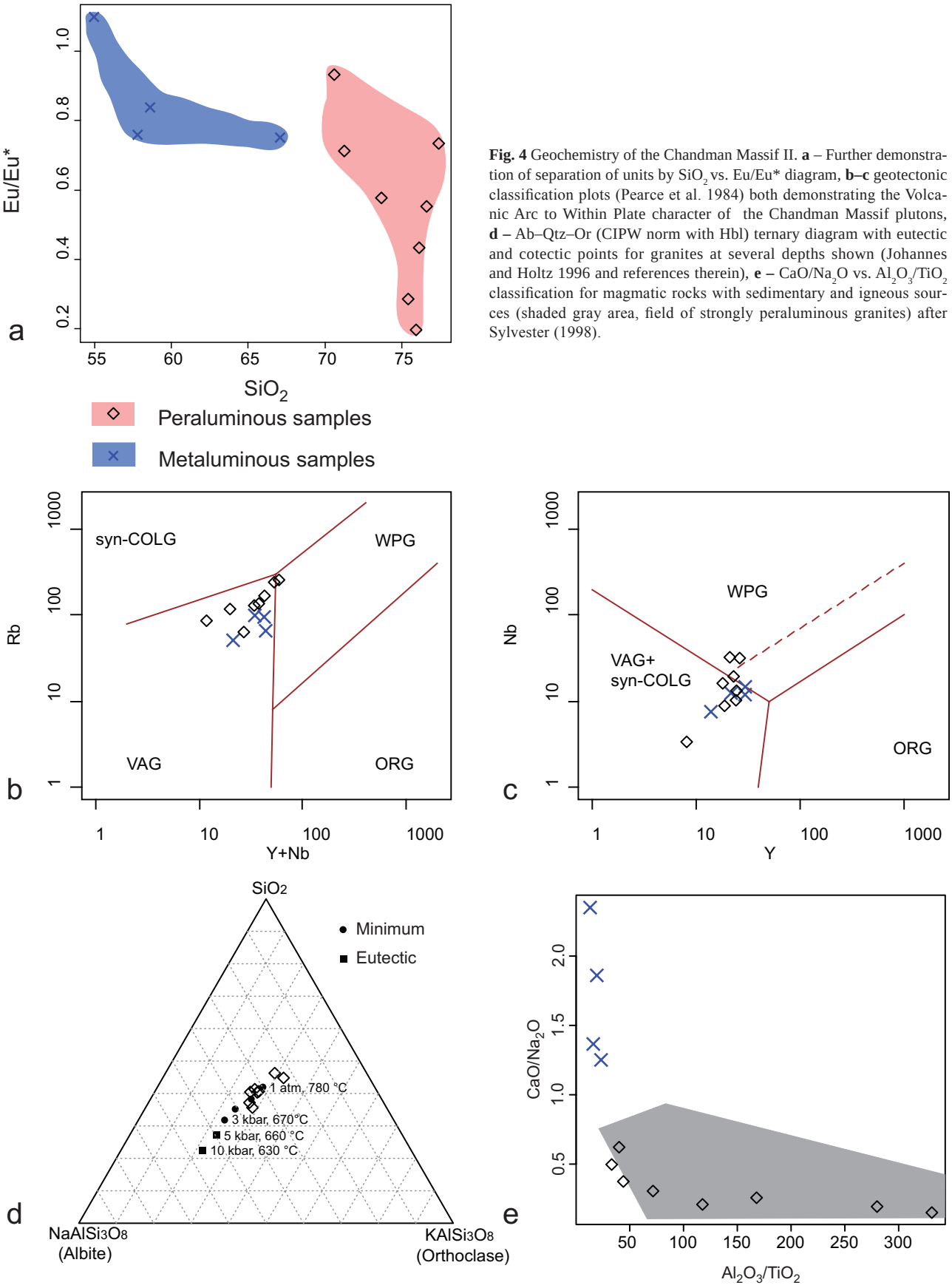

Fig. 4 Geochemistry of the Chandman Massif II. **a** – Further demonstration of separation of units by SiO_2 vs. Eu/Eu* diagram, **b–c** geotectonic classification plots (Pearce et al. 1984) both demonstrating the Volcanic Arc to Within Plate character of the Chandman Massif plutons, **d** – Ab–Qtz–Or (CIPW norm with Hbl) ternary diagram with eutectic and cotectic points for granites at several depths shown (Johannes and Holtz 1996 and references therein), **e** – CaO/Na_2O vs. Al_2O_3/TiO_2 classification for magmatic rocks with sedimentary and igneous sources (shaded gray area, field of strongly peraluminous granites) after Sylvester (1998).

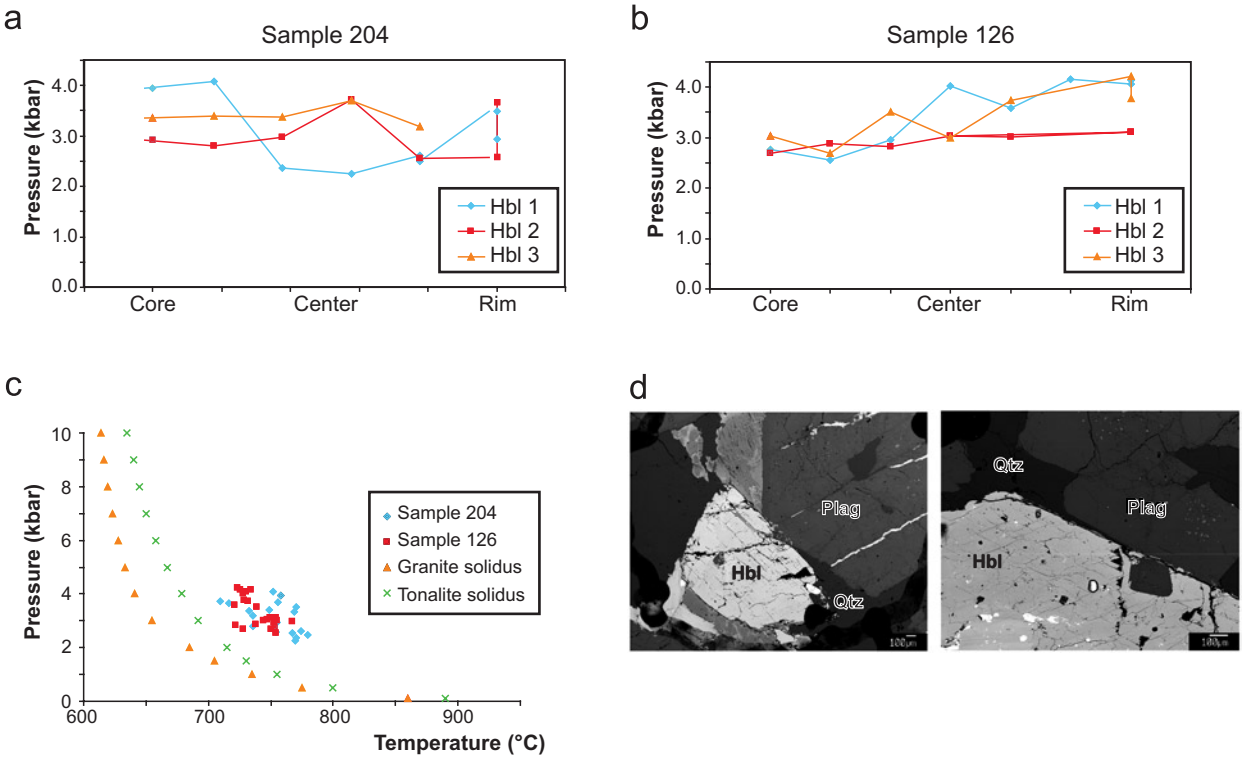

Fig. 5 Thermobarometric analysis of two samples: **a–b** results of Al-in-hornblende geobarometry (Holland and Blundy 1994 calibration). Transects from cores to rims of companion feldspars and hornblendes demonstrate relatively homogeneous composition and show a slight reverse zoning of sample 126, **c** – P-T conditions based on Al-in-hornblende barometry (Holland and Blundy 1994; Anderson and Smith 1995) and plagioclase–hornblende thermometry (Blundy and Holland 1990 calibration) compared to the granite and tonalite solidi (Luth et al. 1964; Piwinskii 1968), and **d –** backscattered electron images of analyzed companion feldspar and hornblende grains in contact with quartz.

crystallization. Estimated temperature for this sample is 740 ± 14 ºC. In P-T space, these samples plot well above the tonalite solidus (Fig. 5c). Anorthite content of plagioclase in this sample varies from 25 to 32 %.

Further barometric constraint is provided by several dioritic and granodioritic samples that contain magmatic epidote. Igneous epidote has been shown to exist at a minimum pressure of 4–6 kbars (Schmidt 1983; Zen and Hammastrom 1984; Schmidt and Poli 2004). Magmatic epidotes are found in the northern portion of the field area, near the contact between diorites and the Chandman Khayrkhan Crystalline Complex. This stability field translates to a minimum of 15–20 km for emplacement of diorites based on a barometric gradient of 3.7 km per kbar.

4.3. U-Pb LA-ICP-MS zircon dating

Zircons from a dioritic sample were analyzed for U-Pb geochronology (Hrdličková et al. 2008). Thirty-two U-Pb spot analyses were carried out on 26 grains by LA-ICP-MS at the Institute of Geosciences, Johann-Wolfgang-Goethe-University, Frankfurt. Zircons displayed igneous textures including long prismatic crystal habit. Cathodoluminescence images revealed fine igneous oscillatory crystal zoning: no discordant cores were identified. Continuous zoning from core to rim documents only one phase of zircon growth, which is in line with the U-Pb analyses. Twenty-five spot analyses yielded concordant results with a concordia age of 345 ± 2 Ma (2σ). Additional analytical details are available in Hrdličková et al. (2008).

5. Structural data

5.1. General structure

Satellite images of the Chandman Massif reveal a fault that trends ~330º that dissects the Chandman Massif into a northern and southern section (Fig. 1). Orientations of structures display a marked difference to the north and south of this fault (Fig. 6).

Metamorphic foliation in host rocks, rafts and blocks is the oldest foliation in the complex and displays some variation. The northern domain of the complex displays strikes toward ~345º while the southern domain has strong maxima towards ~330º. Both foliations are moderately to steeply dipping towards the NNE (Fig. 6a).

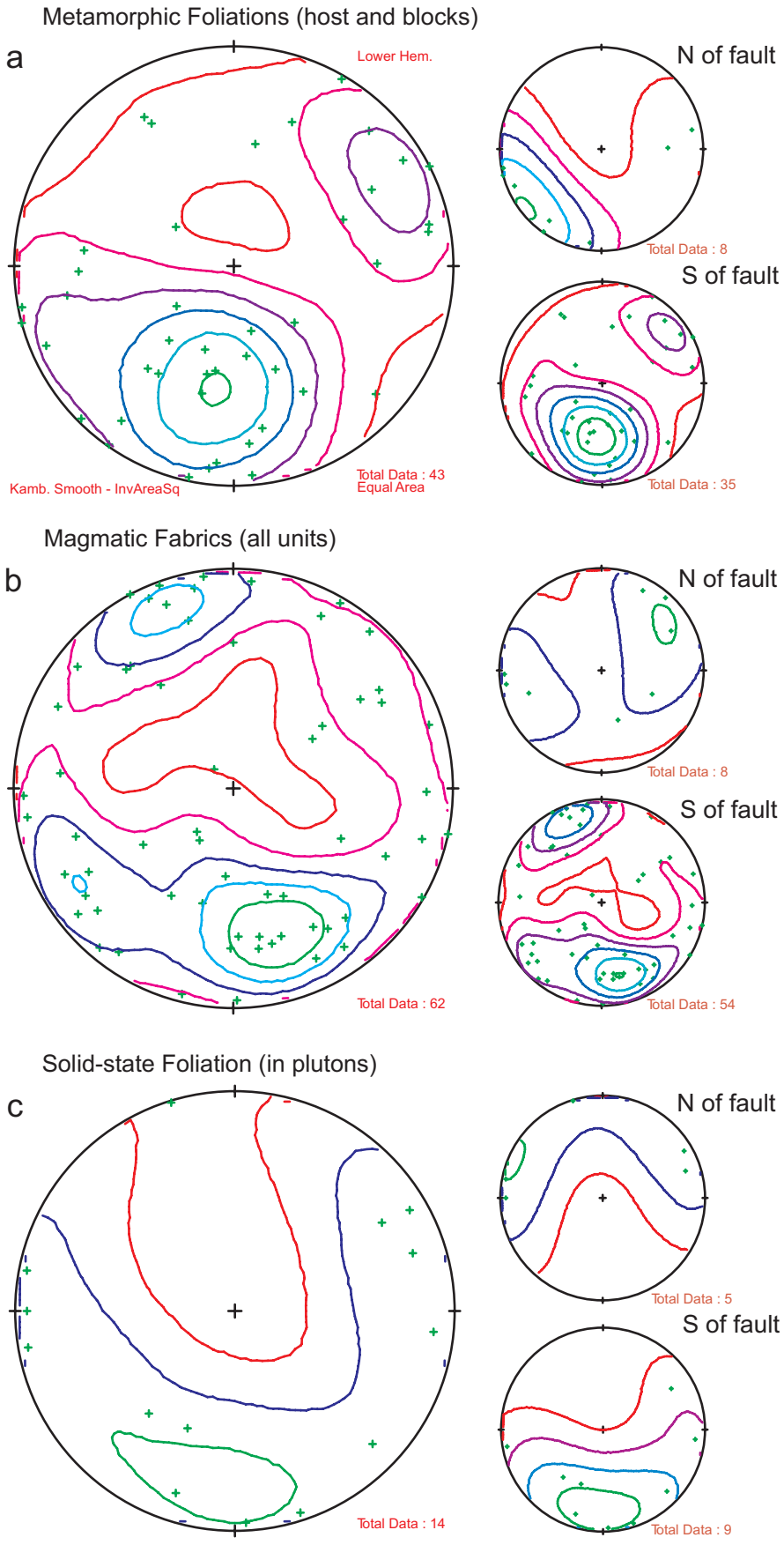

Cross-cutting relationships throughout the field area indicate that peraluminous granitic intrusions are generally younger than dioritic intrusions. Dikes of granite cross-cut granodioritic units. Granitic contacts cross-cut internal structures in the dioritic units, including schlieren layering and magmatic fabrics. While these contacts are generally sharp, occasional cuspate-lobate margins can be observed between the granite and diorite units. Furthermore, granitic intrusions, such as dikes, rarely fine toward their margins or display quench textures that would indicate intrusion into a cold host. Finally, at one locality granites and diorites are mutually intrusive with blocks of granites enclosed in diorites and dikes of granites cutting diorites (Fig. 7c–d). Metaluminous granodiorite and granite plutons display multiple varieties of schlieren. The most common are conspicuous, planar, rhythmic schlieren, best defined adjacent to contacts with schists, but common throughout the complex south of the fault. These schlieren are parallel to the magmatic mineral foliation and are repeated on the cm to dm scale. Individual layers have a thickness on the mm scale and can be continuous for several meters. Where these schlieren are present, layers are in groups that are several meters thick and continuous for 10 to 50 meters. While these schlieren are sometimes concordant to earlier metamorphic layering, suggesting a "ghost stratigraphy" type origin, such as that described by Pitcher (1970)

Fig. 6 Structural data plotted on lower hemisphere stereonet projections with Kamb contouring. Left side figures display all data for **a** – metamorphic foliations, **b** – magmatic foliations, and **c** – solid-state foliations in plutons. Right side shows identical data separated to the north and south of the fault that runs through the center of the pluton.

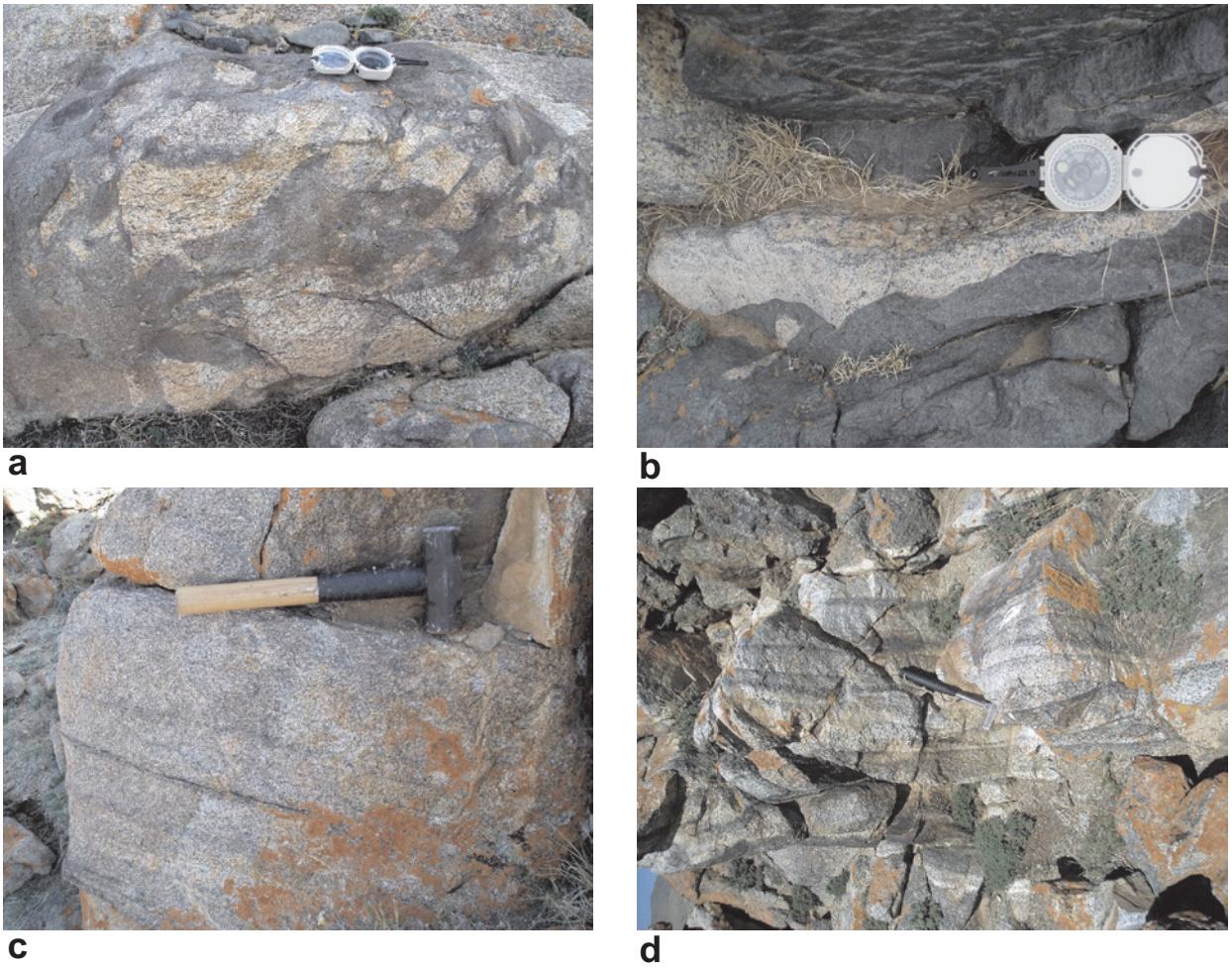

Fig. 7 Field photographs of magmatic structures in plutons: **a–b** field evidence for the coeval intrusion of granites and diorites, **c–d** enigmatic rhythmic schlieren layering common in granodioritic units.

for the Main Donegal Pluton, there are no minerals with metamorphic textures in these layers. Petrographically, these layers consist of accumulation of only biotite and apatite. Thus, the mechanism for formation of these structures remains enigmatic.

Magmatic fabrics were defined by the statistical alignment of minerals with high axial ratios, particularly biotite in granites and biotite and hornblende in granodiorites to diorites. In granodioritic and dioritic units, elongate mafic enclaves are often aligned with the magmatic foliation. Magmatic foliation represents strain potentially caused by several processes, including margin effects, local flow, and strain from tectonic forces (Paterson et al. 1998). Thus, it is not surprising that measured magmatic foliations show a moderate amount of scatter. However, clear differences in maxima are seen to the north and south of the fault. North of this structure, steeply dipping, roughly N-S oriented magmatic fabrics are observed. To the south of the fault, magmatic foliations are oriented roughly E–W and are also steeply dipping (Fig. 6b).

Dioritic units also contain schlieren, but this layering is rarer and more complex in geometry. Discontinuous schlieren are found particularly along contacts with metamorphic host-rock blocks. This layering displays trough-like structures with crystal size sorting along trough bottoms, similar in appearance to sedimentary graded bedding. These structures suggest, according to Barrière (1981), that crystal deposition and magmatic scouring and flow-sorting occurred during magmatic flow (Fig. 7b).

Solid-state foliations in plutons were defined in the field by observable elongation of quartz grains and occasionally folding of earlier magmatic foliations (Fig. 8a). In the southern portion of the complex, solid-state foliations are found only at scattered outcrops spaced over several tens to several hundreds of meters. Effects of solid-state deformation become more widespread toward the north, and are ubiquitous on the SW slopes of the Chandman Khayrkhan Mountain. As the foliation becomes more pervasive, it also increases in intensity.

These foliations again show distinct orientations in northern and southern portions of the Massif. These orientations are in excellent agreement with magmatic fabrics, with those to the north striking roughly N–S and those to the south striking roughly E–W (Fig. 6c).

5.2. Structures in migmatites

Migmatites throughout the Chandman Khayrkhan Crystalline Complex display a wide range of structures. Lit-par-lit style migmatization is defined by leucosome and melanosome layering, for example in the core of the Chandman Khayrkhan Mountain (Fig. 8b–c). Here, leucosomes form discontinuous elongate bodies, generally cm to dm in length, and all structures are parallel to the foliation in metamorphic rocks. These concordant stromatic migmatites grade into a more diatectic structural style, where leucosomes cross-cut and disrupt schist foliation (Fig. 8c). Here leucosomes comprise a larger total percentage of rocks and form continuous interconnected melt networks. In outcrops where leucosome dominates, melanocratic material becomes highly disrupted and can achieve a rounded or ellipsoidal shape.

Near the margins of the Chandman Khayrkhan Mountain, where schists are intruded by diorites and granites, leucosomes make up approximately 20 % of the rock. Gradational contacts with granites in these localities suggest that migmatitic material contaminated granite intrusions. Such localities often display gradational contacts with adjacent granodiorites and granites where physical contamination of granitoids is observed in the form of small fragments of melanosome/restite encased in the intruding bodies. In many instances, dikes with sharp contacts are observed cross-cutting these structures. However, in some localities, leucosomes grade into intruding magmas at fine scales. While these structures do not rule out that migmatization occurred prior to the intrusion of the Chandman Massif, they do indicate that, at least in part, the heat of these intrusions contributed to local melting and contamination of the magmas.

6. Discussion

Intrusive relationships indicate that units of the peraluminous and metaluminous suites of the Chandman Massif formed (nearly) contemporaneously. While the majority of cross-cutting relationships show the Chandman granites as younger than granodiorites, rare outcrops with cuspate–lobate margins and mutually intrusive contacts suggest that these units are nearly co-magmatic. However, even in these areas, no effects of mixing or

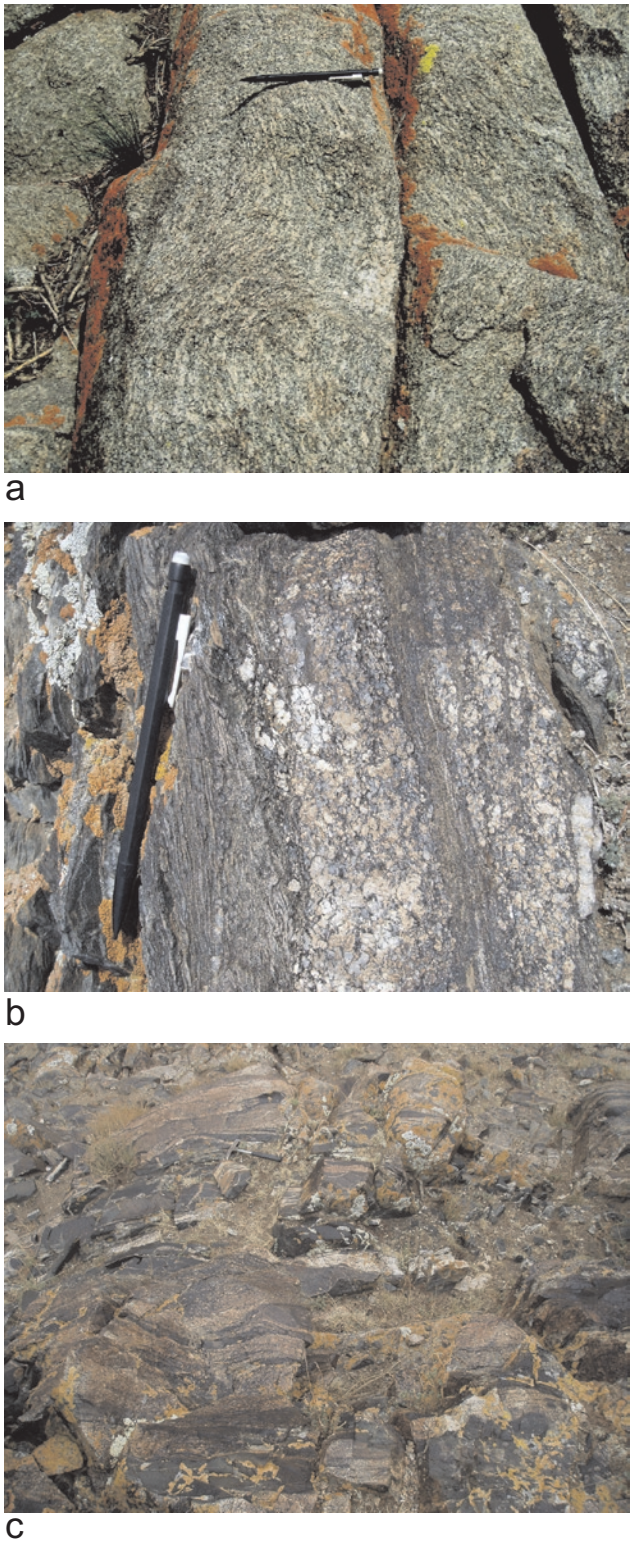

Fig. 8 Field photographs of post-magmatic structures in plutons and wall rocks, **a –** solid-state foliation folding of the earlier magmatic fabrics, **b –** lit-par-lit or stromatic migmatites, **c** – diatectic migmatites.

hybridization are observed. Compositional variation at the intrusive contacts between these two magma types suggests a significant viscosity contrast, which could have prevented hybridization.

While peraluminous granites are closely spatially related to migmatites, it is unlikely that migmatites at the level of exposure were the main source material for these plutons. At the relatively shallow level of intrusion of these granites, only a very small percent of partial melting would be possible without a significant input of a surplus heat. Based on hornblende-plagioclase thermometry and the presence of magmatic epidote, melting of fertile materials at the emplacement level would be likely, but the large amount of schist needed to generate voluminous peraluminous plutons is lacking in the Chandman Khayrkhan Crystalline Complex. Thus, contamination from local migmatites could account for only a small portion of the volume of Chandman granites exposed here. In addition, in Qtz-Or-An space (Fig. 4d), Chandman granites are evolved away from eutectic compositions for melting at 3–3.5 kbars, which could be evidence of fractionation during ascent. These data are consistent with the bulk of Chandman peraluminous granites having a source below the level now exposed. Thus, although the Chandman Massif peraluminous granites have some connection to the adjacent migmatite terrane, a larger body, not presently exposed, must be responsible for the bulk of the peraluminous material seen in the Chandman Massif.

Metaluminous rocks of the Chandman Massif display calc-alkaline geochemical trends and are of magnetite series, indicating crystallization from highly oxidized magmas (Ishihara 1977). They contain a high percentage of hydrous minerals, particularly hornblende, and fall within the volcanic arc geochemical field. Based on this evidence, we suggest that these plutons were generated in a subduction regime. The temporally overlapping, but slightly delayed, emplacement of peraluminous granites with respect to the metaluminous magmas suggests that the intrusion of more mafic units could have initiated partial melting of country rock during their ascent and/or emplacement.

Finally, the excellent agreement of magmatic and solid-state foliations suggests that the tectonic forces responsible for generating the strong magmatic fabric in the massif continued to influence these rocks after crystallization – we are unsure as to the cause of increased pervasiveness of solid-state foliation toward the Chandman Khayrkhan Mountain. The present discordance of metamorphic foliations, magmatic foliations, and solid-state fabrics to the north and south of the central fault suggests that it was active late in the evolution of the complex, possibly as a secondary Riedel Fault related to recent motion on the Bogd Fault along the northern margin of the massif.

Compilation of all available datasets suggests that this area experienced amphibolite-facies metamorphism of the Chandman Khayrkhan Crystalline Complex, exhumation to mid-crustal levels, and juxtaposition against the greenschist-facies Tugrug Formation. The Crystalline Complex was then intruded by metaluminous and peraluminous plutons of the Chandman Massif. These data correlate well with the findings of Hrdličková et al. (2008), where a similar sequence of events (early migmatite generating metamorphism and later peraluminous granitic intrusion) was identified in the Unegt Uul Crystalline Complex. As no geochronological constraints on the age of migmatization are currently available for the Chandman Khayrkhan Crystalline Complex, a possibility of a shared evolution of the complexes cannot be assessed.

The Chandman Massif is shown here to be unique among the complexes presented in Hrdličková et al. (2008), in that it consists of dominantly metaluminous, amphibole-bearing units that fall clearly into the volcanic-arc field. These data thus indicate that the generation of the massif could not be due to crustal thickening and geothermal heating alone, but was mainly related to the subduction-related magmas. The Chandman Massif represents the first recognition of a volcanic-arc magmatism of Mississippian age in the western Gobi-Altay Terrane. The onset of Hercynian magmatism is suggested to be as early as 370 Ma, based on rocks from the Tseel Terrane (immediately to the west of the Chandman Massif area), which bear striking resemblance to those studied here. Kozakov et al. (2007) described plutons of mafic to plagiogranite compositions as well as granites and migmatites intruding biotite schists in many areas in the Tseel Terrane. Additional study is required in order to identify whether there is a relationship between Tseel Terrane units and the Chandman Massif, which may represent the easternmost extremity of the Hercynian arc.

Furthermore, the relationship between the Chandman Khayrkhan Crystalline Complex and Chandman Massif may be a direct evidence for the integration of pre-existing Caledonian materials into magmas of the Hercynian arc, suggested by isotopic evidence (Kovalenko et al. 2004). This situation calls for further work on the age of metamorphism within the crystalline complex and the isotopic systematics of both metamorphic and plutonic rocks. Such studies of central Mongolian granites, in concert with data presented here and by Hrdličková with her co-workers, will further our understanding of the complex transition from collision and crustal amalgamation to renewed magmatism (345 Ma) in Early Carboniferous times.

7. Conclusions

Recent mapping of the Chandman Massif and its country rocks has led to the recognition of the Chandman Khayrkhan Crystalline Complex as having a separate protolith and metamorphic history from the Tugrug Formation. Structural, geochemical and thermobarometric evidence presented here suggests that the Chandman Khayrkhan Crystalline Complex is related to, but not representative for the entire source region of, the peraluminous granites in the Chandman Massif. The granitic rocks were classified into metaluminous and peraluminous units with distinctly different chemistries and subtly distinct petrographic characteristics. Our preferred interpretation of the two, roughly coeval, units is that they represent an evolution of volcanic-arc magmas, from diorite to granite, and partial melting of fertile sedimentary materials, triggered by their thermal input.

Mapping, petrography, geochemical and thermobarometric analyses all suggest a multi-phase history to migmatization of the Chandman Khayrkhan Crystalline Complex migmatites. Thermobarometry places constraints on the conditions of pluton emplacement to 11.5–13.7 km in the south, at least 15–20 km in the north and temperatures of 725–775 °C. These estimates provide the necessary conditions for migmatization of gneisses of the Chandman Khayrkhan Mountain. However, field observations, geochemistry and petrography suggest that additional processes below the level of exposure largely contributed to migmatization and the generation of peraluminous plutons. The barometry and magmatic history also place constraints on the exhumation history of this migmatite terrane.

Our data point to a few local problems that require additional attention. For instance it remains unclear what mechanism juxtaposed of the Chandman Khayrkhan high-grade metamorphic rocks with greenschist-facies rocks of the Tugrug Formation. Any structure that would have accommodated this movement is now obscured by the Chandman Massif, but mapping of even greater detail of common host-rock septa in the complex could yield important constraints on such a structure. In addition, the mechanism for the formation of repetitive schlieren layering is enigmatic, but additional study could yield insights into internal processes that occurred during the construction of the Chandman Massif. Further geochronological and isotopic work in the area would supplement the available data that suggest that the evidence for initiation of Hercynian magmatism in Mississippian times is preserved in the Gobi-Altay Terrane.

Acknowledgements. Fieldwork was done during the project *Geological survey of the Mongolian Altay on the scale 1: 50,000,* which was performed in the framework of the Program of the Development Cooperation Project of the Czech Republic. We are grateful to Mongolian staff of the expedition for participating in the fieldwork. We are indebted to J. Holák and Z. Novotný for the technical backing of geological survey. Funding was also provided by the Department of Earth Sciences at the University of Southern California. Our thanks extend to Viktor Kovach and an anonymous reviewer for their contributions to the manuscript.

Electronic supplementary material. The table with whole-rock geochemical data (Tab. 1), tables with geobarometric determinations by the Al-in-hornblende method, as well as GPS coordinates of the studied samples, are available online at the Journal web site (http://dx.doi.org/10.3190/jgeosci.034).

References

Anderson JL (1996) Status of thermobarometry in granitic batholiths. Trans Roy Soc Edinb, Earth Sci 87: 125–138

Anderson JL, Smith DR (1995) The effects of fO_2 on the Al-in-hornblende barometer. Amer Miner 80: 549–559.

Badarch G, Cunningham WD, Windley BF (2002) A new terrane subdivision for Mongolia: implications for the Phanerozoic crustal growth of central Asia. J Asian Earth Sci 20: 87–100

Baljinnyam I, Bayasgalan A, Borisov BA, Cisternas A, Dem'yanovich MG, Ganbaatar L, Kochetkov VM, Kurushin RA, Molnar P, Philip H, Vashchilov YY (1993) Ruptures of major earthquakes and active deformation in Mongolia and its surroundings. Geol Soc Am Memoir 181: pp 1–62

Barrière M (1981) On curved laminae, graded layers, convection currents and dynamic crystal sorting in the Ploumanac'h (Brittany) subalkaline granite. Contrib Mineral Petrol 77: 214–224

Blundy JD, Holland TJB (1990) Calcic amphibole equilibria and a new amphibole-plagioclase geothermometer. Contrib Mineral Petrol 104: 208–224

Boynton WV (1984) Cosmochemistry of the rare earth elements: meteorite studies. In: Henderson PE (ed) Rare Earth Element Geochemistry. Elsevier, Amsterdam, pp 63–114

Cox KG, Bell JD, Pankhurst RJ (1979) The Interpretation of Igneous Rocks, George Allen & Unwin, London, pp 1–450.

Cunningham D (2005) Active intracontinental transpressional mountain building in the Mongolian Altai: defining a new class of orogen. Earth Planet Sci Lett 240: 436–444

Dergunov, AB (2001) Tectonics, Magmatism, and Metallogeny of Mongolia. Routledge, London, pp 1–288

Hammarstrom JM, Zen E (1986) Aluminum in hornblende: an empirical igneous geobarometer. Amer Miner 71: 1297–1313

Hanžl P, Aichler J (eds) (2007) Geological Survey of the Mongolian Altay at a scale 1 : 50,000 (Zamtyn Nuruu – 50). Final report of the International Development Cooperation project of the Czech Republic. Czech Geological Survey, Brno & MPRAM, Ulaanbaatar, pp 1–376

Holland TJB, Blundy JD (1994) Non-ideal interactions in calcic amphiboles and their bearing on amphibole-plagioclase thermometry. Contrib Mineral Petrol 116: 433–447

Hollister LS, Grissom GC, Peters EK, Stowell HH, Sisson VB (1987) Confirmation of the empirical correlation of Al in hornblende with pressure of solidification of calc-alkaline plutons. Amer Miner 72: 231–239

Hrdličková K, Bolormaa K, Buriánek D, Hanžl P, Gerdes A, Janoušek V (2008) Petrology and age of metamorphosed rock in tectonic slices inside the Palaeozoic sediments of the eastern Mongolian Altay, SW Mongolia. J Geosci 53: 139–165

Hu A, Jahn BM, Zhang G, Chen Y, Zhang Q (2000) Crustal evolution and Phanerozoic crustal growth in northern Xinjiang: Nd isotopic evidence. Pt 1. Isotopic characterization of basement rocks. Tectonophysics 328: 15–51

Irvine TN, Baragar WR (1971) A guide to the chemical classification of the common volcanic rocks. Can J Earth Sci 8: 523–548

Ishihara, S (1977) The magnetite-series and ilmenite-series granitic rocks. Mining Geology 27: 293–305

Jahn BM, Wu F, Chen B (2000) Massive granitoid generation in Central Asia: Nd isotope evidence and implication for continental growth in the Phanerozoic. Episodes 23: 82–92

Jahn BM, Wu F, Chen B (2001) Granitoids of the Central Asian Orogenic Belt and continental growth in the Phanerozoic. Trans Roy Soc Edinb, Earth Sci 91: 181–193

Jahn BM, Capdevila R, Liu D, Vernon A, Badarch G (2004) Sources of Phanerozoic granitoids in the transect Bayanhongor–Ulaan Baatar, Mongolia: geochemical and Nd isotopic evidence, and implications for Phanerozoic crustal growth. J Asian Earth Sci 23: 629–653

Johannes W, Holtz, F (1996) Petrogenesis and Experimental Petrology of Granitic Rocks. Springer-Verlag, Berlin, pp 1–335

Kovalenko VI, Yarmolyuk VV, Kovach VP, Kotov AB, Kozakov IK, Salnikova EB, Larin AM (2004) Isotope provinces, mechanisms of generation and sources of the continental crust in the Central Asian mobile belt: geological and isotopic evidence. J Asian Earth Sci 23: 605–627

Kozakov IK, Kovach VP, Bibikova EV, Kirnozova TI, Zagornaya NY, Plotkina YV, Podkovyrov VN (2007) Age and sources of granitoids in the junction zone of the Caledonides and Hercynides in southwestern Mongolia: geodynamic implications. Petrology 15: 126–150

Kröner A,Windley BF, Badarch G, Tomurtogoo O, Hegner E, Jahn BM, Gruschka S, Khain EV, Demoux A, Wingate MTD (2007) Accretionary growth and crust formation in the Central Asian Orogenic Belt and comparison with the Arabian-Nubian shield. In: Hatcher RD, Carlson MP, Mcbride JH, Martinez Catalan JR (eds) 4-D Framework of Continental Crust. Geol Soc Am Memoir 200: pp 181–209

Luth WC, Jahns RH, Tuttle OF (1964) The granite system at pressures of 4 to 10 kilobars. J Geophys Res 69: 759–773

Marinov NA, Zonenshain LP, Blagonravov VA (eds) (1973) Geologija Mongolskoi Narodnoi Respubliky. Nedra, Moscow, pp 1–582 (in Russian)

Molnar P, Tapponnier P (1975) Cenozoic tectonics of Asia: effects of a continental collision: features of recent continental tectonics in Asia can be interpreted as results of the India–Eurasia collision. Science 189: 419–426

Mossakovsky AA, Ruzhentsev SV, Samygin SG, Kheraskova TN (1994) Central Asian fold belt; geodynamic evolution and formation history. Geotectonics 27: 445–474.

Paterson SR, Fowler TK, Schmidt KL, Yoshinobu AS, Yuan ES, Miller RJ (1998) Interpreting magmatic fabrics in plutons. Lithos 44: 53–82

Pearce JA, Harris NW, Tindle AG (1984) Trace element discrimination diagrams for the tectonic interpretation of granitic rocks. J Petrol 25: 956–983

Peccerillo A, Taylor SR (1976) Geochemistry of Eocene calc-alkaline volcanic rocks from the Kastamonu area, Northern Turkey. Contrib Mineral Petrol 58: 63–81

Pitcher WS (1970) Ghost stratigraphy in intrusive granites: a review. In: Newall G, Rast N (eds) Mechanisms of Igneous Intrusion. Geol J Special Publication 2: 123–140

Piwinskii AJ (1968) Experimental studies of igneous rock series: Central Sierra Nevada Batholith, California. J Geol 76: 548–570

Rauzer AA, Zhanchiv DI, Golyakov VI, Yhhina IF, Ivanov IG, Tsukernik AB, Afonin VV, Smirnov IG, Bykhover VI, Kravtsev AV, Baatarkhuyag A, Skoryukin MI, Khodikov, IV, Mantsev NV, Okaemov SV, Mischin VA, Enkhsajkhan T (1987) Report on results of geological mapping on scale 1:200,000 in the south-western part of Mongolian Altay in 1983–1983, Mongolian National Republic. Tekhnoexport, Moscow, pp 1–352 (in Russian)

Schmidt MW (1983) Phase relations and compositions in tonalite as a function of pressure: an experimental study at 650 ºC. Am J Sci 293: 1011–1060

Schmidt MW, Poli S (1983) Magmatic epidote. In: Liebscher A, Franz G (eds) Epidotes. Mineralogical Society of America and Geochemical Society Reviews in Mineralogy and Geochemistry 56: 399–430

Sengör AC, Natal'in BA, Burtman VS (1993) Evolution of the Altaid tectonic collage and Paleozoic crustal growth in Eurasia. Nature 364: 299–306

Shand SJ (1943) Eruptive Rocks. Their Genesis, Composition, Classification, and Their Relation to Ore-Deposits with a Chapter on Meteorite. 2nd Edition. John Wiley & Sons, New York, pp 1–444

Sun S-s, McDonough WF (1989) Chemical and isotopic systematics of oceanic basalts: implications for mantle composition and processes. In: Saunders AD, Norry MJ (eds) Magmatism in the Ocean Basins, Geol Soc London Spec Pub 42: 313–345

Sylvester PJ (1998) Post-collisional strongly peraluminous granites. Lithos 45: 29–44

Windley BF, Kröner A, Guo J, Qu G, Li Y, Zhang C (2002) Neoproterozoic to Paleozoic geology of the Altai orogen, NW China: new zircon age data and tectonic evolution. J Geol 110: 719–737

Windley BF, Dmitriy A, Wenjiao X, Kröner A, Badarch G (2007) Tectonic models for accretion of the Central Asian Orogenic Belt. J Geol Soc, London 164: 31–47

Zen E, Hammastrom JM (1984) Magmatic epidote and its petrologic significance. Geology 12: 515–518